UNIVERSITY OF CALIFORNIA

Los Angeles

Mitigation of Mineral Scaling and Fouling of RO Desalination via Self-adaptive Operation

A dissertation submitted in partial satisfaction of the

requirements for the degree Doctor of Philosophy

in Chemical Engineering

by

Han Gu

2017

ABSTRACT OF THE DISSERTATION

Mitigation of Mineral Scaling and Fouling of RO

Desalination via Self-adaptive Operation

by

Han Gu

Doctor of Philosophy in Chemical Engineering

University of California, Los Angeles, 2017

Professor Panagiotis D. Christofides, Co-Chair

Professor Yoram Cohen, Co-Chair

Dwindling fresh water supplies from traditional sources, such as surface and ground water, coupled with rapid population growth in developing countries and frequent drought conditions across the globe, have intensified the need for developing alternative and sustainable potable water supplies. In recent years, seawater and brackish water desalination and water reuse technologies have been implemented in various regions of the U.S. and around the globe as part of the movement to diversify the portfolio of available water resources. Generation of the above non-traditional water resources often involves reverse osmosis and nanofiltration membrane technology for desalination and as a barrier against multiple contaminants. However, membrane fouling and scaling are major impediments for robust and effective operation of membrane

desalination. Membrane scaling is the result of surface crystallization of sparingly soluble mineral salts and/or the deposition of bulk-formed mineral salt crystals onto the membrane surface. Membrane surface scaling leads to water permeate flux decline and potential membrane damage, thereby limiting recovery and increasing water production cost. Membrane fouling by particulate, colloidal matter, organic, and biofoulant results in reduced membrane permeability and thus result in increased applied pressure requirement for a given target flux, decreased permeate quality, increased frequency of required chemical cleaning and consequently shortening of membrane longevity and as a consequence increased water treatment cost.

In order to alleviate the adverse impact of membrane fouling and mineral scaling, the present work focused on developing a novel approach of self-adaptive operation of reverse osmosis (RO) membrane desalination (including pretreatment). The goal of the approach is to enable effective self-adaptive RO desalination and feed pretreatment operation even when confronted with temporal variability of source feed water quality. In this approach fouling and scale indicators are quantified in real time and the desalination plant autonomously adjust its operating conditions (e.g., triggering of cleaning cycles, coagulant dose setting, feed pretreatment operational strategy).

In order to mitigate mineral scaling, a self-adaptive operation of spiral-wound RO desalting in a cyclic mode of feed-flow reversal (FFR) was evaluated for desalting of brackish water of high mineral scaling potential. Self-adaptive operation was enabled by triggering of FFR once the onset of mineral scaling was detected via a novel ex-situ membrane scale monitoring system. Subsequently, in order to ensure effective RO feed pretreatment the use of ultrafiltration (UF) was explored in a uniquely integrated UF-RO system whereby the RO concentrate was utilized for enhanced UF backwash. The RO concentrate stream was utilized (as both a continuous stream and a high flux pulse achieved using hydraulic accumulators) for UF backwash, with backwash triggering based on by thresholds levels of fouling indicators. The applicability of different fouling indicators for real time performance assessment of UF feed pretreatment and optimization of UF operating conditions (e.g., backwash duration and coagulant dosing strategy) in RO seawater desalination was explored in an extensive field study using an integrated seawater UF-RO desalination pilot plant. Fouling indictors were evaluated with respect to quantification of UF backwashability, unbackwashed fouling resistance and UF fouling rate.

The dissertation of Han Gu is approved.

Jennifer Ayla Jay

Yoram Cohen, Committee Co-Chair

Panagiotis D. Christofides, Committee Co-Chair

University of California, Los Angeles

2017

This work is dedicated to my parents.

Thank you for your love and support.

TABLE OF CONTENTS

PAGE

LIST OF TABLES

LIST OF FIGURES

ACKNOWLEDGEMENTS

I would like to thank my PhD advisors Prof. Yoram Cohen and Prof. Panagiotis Christofides for their guidance and support with my research and for providing me a rewarding academic experience. The support of the fellow graduate students in their research groups is also greatly appreciated. I would also like to thank my colleagues Drs. Anditya Rahardianto, John Thompson, Tae Lee, Larry Gao, Michal Uchymiak, Alex Bartman, Richard Zhu, Xavier Pascual Caro, and Sirikarn Surawanvijit for their help with various aspects of my research works, including. I especially want to thank Dr. Rahardianto for his role as project coordinator in our PolySep Research Group and I am grateful for the constructive comments and suggestions he provided. My work would not have been possible without the support and collaboration from the U.S. Navy Office of Navy Research and California Department of Water Resources.

VITA

1983 Born, Beijing, China

2007 BS, Chemical Engineering, University of California, Los Angeles

2010 MS, Chemical Engineering, University of California, Los Angeles

2008-10 Teaching Assistant, Department of Chemical and Biomolecular Engineering,

University of California, Los Angeles

2014-16 Teaching Fellow, Department of Chemical and Biomolecular Engineering,

University of California, Los Angeles

2017- Scientist/Process Specialist, Orange County Water District, Fountain Valley, CA

SELECTED PUBLICATIONS AND PRESENTATIONS

Gu, H., A. Rahardianto, L. X. Gao, P. D. Christofides and Y. Cohen, *Ultrafiltration with Self-Generated RO Concentrate Pulse Backwash in a Novel Integrated Seawater Desalination UF-RO System* J. Membrane Sci., 520, 111-119, 2016

Gu, H, Bartman, A Uchymiak, M, Christofides, P.D. and Cohen Y., *Self-Adaptive Feed Flow Reversal Operation of Reverse Osmosis,* Desalination 308 (2013) 63–72

Gu, H, L. Gao, X. Pascual Caro, A. Rahardianto, P. D. Christofides and Y. Cohen, *Online Fouling Quantification for Self-adaptive UF-RO System* (submitted to Desalination, September 2017)

Gao, L., **H. Gu**, A. Rahardianto, P. D. Christofides and Y. Cohen, "Self-Adaptive Cycle-to-Cycle Control of In-line Coagulant Dosing in Ultrafiltration for Pre-Treatment of RO Feed Water," *Desalination*, **401**, 22-31, 2017.

Gao, L., A. Rahardianto, **H. Gu,** P. D. Christofides and Y. Cohen, *Novel Design and Operational Control of Integrated Ultrafiltration - Reverse Osmosis System with RO Concentrate Backwash,* Desalination, 382, 43-52, 2016.

Gao, L., **H. Gu**, A. Rahardianto, P. D. Christofides and Y. Cohen, *Energy-Optimal Control of RO Desalination, Ind. & Eng. Chem. Res.,* **53**, 7409–7420, 2014.

Pascual Caro, X., **H. Gu**, A.Bartman, A.Zhu, A. Rahardianto, J.Giralt, R. Rallo, P. Christofides*, Y. Cohen, Fault Detection and Isolation in a Spiral-Wound Reverse Osmosis (RO) Desalination Plant, Ind. Eng. Chem. Res. 53 (2014) 3257.*

Pascual Caro, X., **H. Gu**, A. Bartman, A. Zhu, A. Rahardianto, J. Giralt, R. Rallo, P.D. Christofides and Y. Cohen*, Data-driven models of steady state and transient operations of spiral-wound RO plant*, Desalination 316 (2013) 154–161

J. Thompson, **H. Gu**, M. Uchymiak, A. Bartman, A. Rahardianto, P. Christofides, W.J. Kaiser, J.I. Faria, Y. Cohen, *Rapid field assessment of RO desalination of brackish agricultural drainage water*, Water Res. 2013 May 15;47(8):2649-60.

Gu, H., A. Rahardianto, L. Gao, P. D. Christofides and Y. Cohen, "Self-Generated RO Concentrate Pulse Backwash of Ultrafiltration Module in an Integrated Seawater Desalination UF-RO Pilot Plant", 2016 AIChE Annual Meeting, November 13-18, 2016, San Francisco, CA

Gu, H., L. Gao, X. Pascual Caro, A. Rahardianto, P. D. Christofides and Y. Cohen, "Field Evaluation of Fouling Quantification Soft Sensors for an Integrated UF-RO Desalination System," *IDA World Congress*, San Diego, California, September 2015.

Gu, H., L. Gao, J. Thompson, A. Rahardianto, P. D. Christofides and Y. Cohen, "Field Deployment of Smart Integrated Membrane Systems Technology For Cooling Tower Water Treatment and Reuse", 2015 WateReuse California Annual Conference, Los Angeles, 2015

Gu, H., M. Uchymiak, A. Bartman, A. Rahardianto , P. Christofides, W. J. Kaiser and Y. Cohen, "Novel System and Field Characterization of Self-Adaptive UF-RO Membrane Desalination of Coastal Seawater", American Institute of Chemical Engineers (AIChE) Annual Meeting, Nov 2013, San Francisco, CA

Gu, H., L. Gao, A. Rahardianto, M. Heijnen, P. Berg, J. Wunram, P. D. Christofides and Y. Cohen, "Self-Adaptive Integrated Ultrafiltration (UF)/Reverse Osmosis (RO) Desalination Systems," North American Membrane Society, New Orleans, LA, May 2012.

PATENTS

Cohen, Y., P. D. Christofides, **H. Gu**, L. X. Gao and A. Rahardianto, "Self-adaptive control and optimization of ultrafiltration", U.S. Provisional Application Serial No. **62/286,735**, filed on **1/25/2016**

Cohen, Y., P. D. Christofides, A. Rahardianto, A. R. Bartman, A. Zhu, **H. Gu** and L. Gao, "Apparatus for integrated filtration and reverse osmosis desalination, comprises filtration skid configured to generate filtrate through microfiltration and ultrafiltration, and a desalination skid fluidly connected to the filtration skid," Patent Number(s): WO2012037274-A2; WO2012037274-A3; US2014048462-A1, 2014.

1 Introduction

1.1 Background

Fresh water shortage is a global problem that our world faces today. The amount of fresh water is fixed and as the world population reaches 7 billion, the demand for fresh water will also increase [1-4]. Today, half of the global population is in countries where groundwater tables are falling in a faster phase than normal [5] and approximately 2.1 billion people globally are affected by water scarcity [6]. It is estimated that by 2025, two-thirds of the world's population will be in water-stressed regions [7]. The amount of water available per capita will decrease unless we recycle, reuse or generate new water supplies. In the United States, states with the least amount of potable water resources (e.g., Texas and California) tend to have a higher level of water consumption compared to less populated states such as Wisconsin and Minnesota, causing an uneven distribution of fresh water resources [8, 9]. In the state of California, in additional to severe drought conditions in recent years [10] , increasing groundwater salinity in agricultural regions (such as the San Joaquin valley) and rising demand due to population growth are two of the main causes of water shortages in that region [11, 12].

In today's world, water usage and energy production are interlinked. Agriculture, energy production, and manufacturing industries all require large amounts of fresh water to maintain productivity. For example, about 201 billion gallons of fresh water are used in the U.S. each day to produce electricity in thermoelectric power plants [13]. By 2035, the world's energy consumption will increase by 35 percent, which in turn will increase water use by 15 percent [8, 14].

At present, reverse osmosis (RO) is the leading technology for brackish and seawater desalination and in water reuse applications for the generation of potable water supplies.

However, widespread implementation of RO technology is impeded by the operational challenges imposed by membrane mineral scaling and fouling, temporal variability of source feed water, and the need for reducing energy consumption. Effective feed water pretreatment in RO membrane desalination is essential to ensure effective plant performance. Microfiltration (MF) and ultrafiltration (UF) systems have been widely incorporated as part of RO feed pretreatment processes. While the concept of MF/UF integration with RO is appealing and has met with a reasonable level of success, there remain technical challenges, particularly in situations where feed water quality fluctuates temporally, and where it is desired to reduce both the frequency of membrane cleaning and the use of both membrane cleaning chemicals and chemical feed additives (e.g., coagulants), for the purpose of both cost reduction and minimizing environmental impact.

The goal of the present work is the develop effective means of mitigation both RO membrane mineral scaling and fouling. Accordingly, a multipronged approach was undertaken in the present study whereby: (a) RO operation in the mode of self-adaptive feed flow reversal was implemented in a spiral-wound RO system as facilitated by a unique membrane scale monitor, (b) UF treatment of RO feed was developed whereby optimal UF backwash was achieved in a self-adaptive mode that responds to temporal changes in feed water quality (**Figure 1-1**). UF operation was evaluated in a novel integrated UF-RO system whereby UF backwash was achieved with the RO concentrate. In order to achieve the above goals, membrane mineral scaling and fouling indicators were evaluated and utilized to arrive at effective operation of RO and UF operations so as to reduce the progression of RO mineral scaling and irreversible UF fouling as described in **Section 3-6** and summarized in **Figures 1-1 and 1-2**.

1.2 Mitigation methods for fouling

Feed filtration, as part of feed pretreatment in RO desalination, is commonly used for prevention and mitigation of RO fouling. Although various methods have been proposed for feed filtration, ultrafiltration (UF) has emerged as one of the more effective means of preventing RO membrane fouling [6, 15] in a wide range of RO applications including, for example, desalting of seawater, brackish water and in water reuse. UF systems are highly effective for removing macromolecules, colloids and particles from the source water to be treated [16]. However, UF membranes can be fouled by macromolecules such as proteins and bacteria due to surface adsorption, pore plugging and gel/cake layer formation [17]. Since UF pretreatment of RO feed water is typically accomplished in a dead-end filtration mode, UF membranes are backwashed periodically in order to avoid excessive buildup of a cake layer and irreversible fouling [16, 18, 19]. Current state-of-the-art UF systems are designed to perform hydraulic backwash and chemically enhanced treatment to restore membrane performance. It is important to note that uncontrolled UF fouling can result in the passage of small particles (in the micron range) and organic materials (low molecular weight), which can then lead to fouling of the downstream RO membranes. In order to restore the performance of fouled RO membranes chemical cleaning is required which the lead to increased maintenance cost [16, 20] , while both fouling and membrane cleaning can ultimately result in permanent membrane damage [21].

Conventional RO feed filtration methods are ineffective with respect to mitigation of mineral scaling which is prevalent particularly at high recovery RO operation [4, 22]. Currently, mitigation of mineral scaling is accomplished via feed water pH adjustment (for scalants whose solubility is pH dependent such as calcium carbonate [23] and silica [24]) and via addition of antiscalants [25]. Under certain conditions (e.g., where the RO feed is sufficiently undersaturated with respect to the mineral scalants of concern) it may also be possible to operate the RO system in the mode of feed flow reversal (FFR) [26].

Mineral scaling is largely the result of surface mineral crystallization, which is a function of nucleation (a stochastic process) and crystal growth [22, 27] and is governed by the feed water chemistry (e.g., degree of saturation with respect to sparingly soluble mineral salts). Surface crystallization is governed by feed water chemistry and level of saturation with respect to the sparingly soluble salts. Given that water composition can vary temporally, mineral scale mitigation approaches would greatly benefit from real time monitoring of mineral scaling. Mineral scale monitoring requires: (a) early detection of mineral scaling, and (b) membrane performance monitoring (e.g., membrane permeability, salt rejection) in order to assess both the impact of scaling and the degree by which it is averted via the utilized scale mitigation strategy.

Feed filtration as part of feed pretreatment serves to remove various foulants (particles, bacteria and colloidal matter) from the RO feed in order to avert or reduce the level of RO fouling. Although UF membrane (typically having pore size of 0.1 - 0.005 μm) technology has emerged as one of the more effective means of RO feed pretreatment, these membranes tend to foul (both reversibly and irreversibly) by a variety of colloids, organics and biological matter [15, 28]. Therefore, effective periodic cleaning of UF membrane modules (e.g., via backwash) is critical for robust UF operation. A critical element of UF backwash in most systems is the use of coagulants that serve to flocculate fine particles and form a cake layer on the membrane surface. The cake layer of larger particles can then be more effectively backwash and also provides a protective layer to avoid pore plugging by small particles. However, since the feed water quality (represented by salinity, organic content, pH, turbidity, temperature, etc.) and possibly required water processing capacity may vary over time, ensuring optimal coagulant dose is critical.

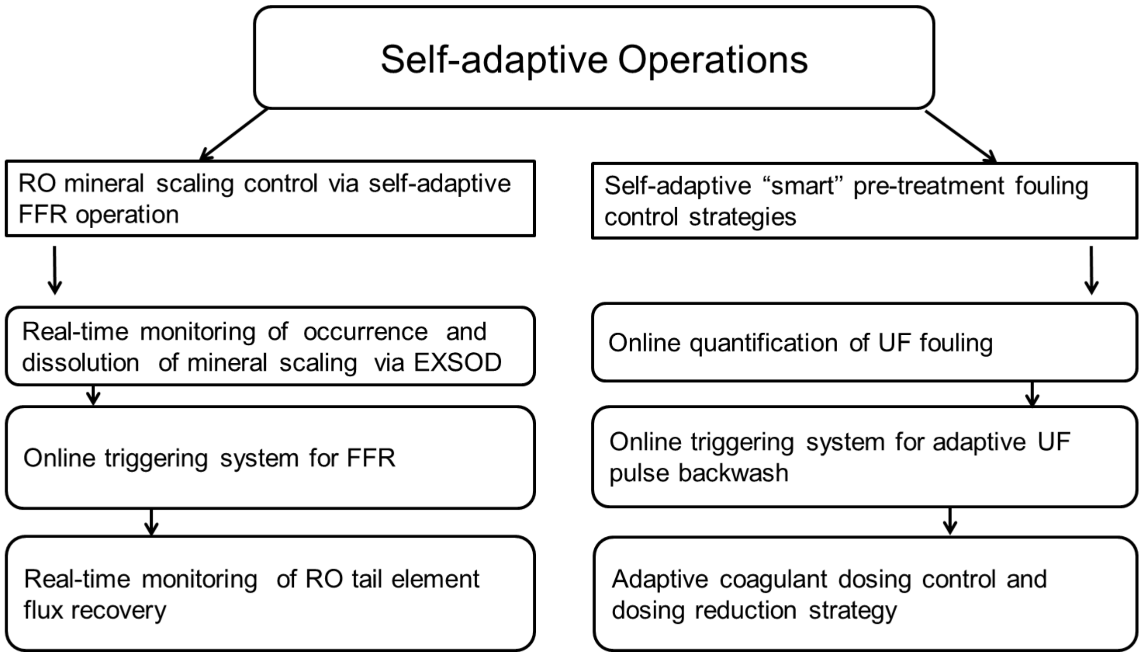

Figure 1-1 Components of self-adaptive operations in RO mineral scaling control and UF fouling control

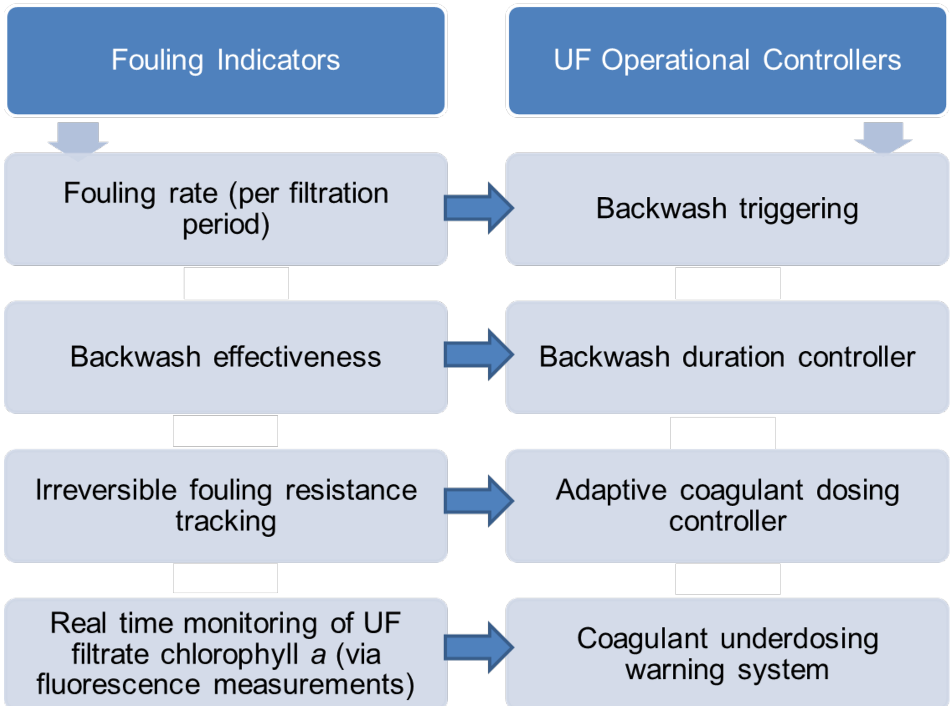

Figure 1-2 Relationships between fouling quantification indictors and UF operational controllers

1.3 Research Objectives

The major goals of this dissertation were to develop self-adaptive smart operation of UF and RO systems that can: a) adjust the UF operational parameters such as coagulant dose, filtration duration and backwash strategy (e.g., intensity and flux) based on advanced sensing that considers the variability of the feed water fouling propensity, and b) mitigate mineral scaling in a high recovery RO operation via feed flow reversal that is triggered by threshold level of mineral scaling as detected via membrane scale monitoring. The above goals are rooted in the hypothesis that real time cycle-to-cycle quantification of UF fouling and RO scaling can form the basis for UF-RO performance forecasting and thereby form the foundation for developing self-adaptive UF and RO operation.

The specific dissertation research objectives are listed below:

1. Develop and demonstrate am approach for effective multi-cycle RO feed flow reversal (FFR) operation for mitigation of membrane mineral scaling:

- Integrate real-time mineral scale monitoring technology with feedback process controller to enable automated and self-adaptive FFR triggering.
- Demonstrate high recovery scale-free cyclic FFR operation, without antiscalant addition, for high recovery RO desalting of feed water of high level of gypsum supersaturation.

2. Develop the fundamental basis for UF operation in an integrated UF-RO system with RO concentrate for UF backwash and self-generation of UF pulse backwash:

- Investigate the efficacy of UF operation with inline coagulation.
- Develop and experimentally validate a fundamental model for ta hydraulic accumulator charging/discharging model.
- Investigate the benefit of multiple consecutive backwash pluses via self-adaptive triggering of UF backwash.
- Evaluate the effectiveness of self-adaptive triggering of multiple consecutive backwash pluses in a long-term field operation.

3. Develop and field demonstrate an approach for online quantification of UF fouling indicators:

- Develop a framework for online UF fouling metrics (or indicators) that can be used to track UF cycle-to-cycle fouling progression and backwash effectiveness.
- Assess fouling metrics with respect to the effectiveness of coagulant feed dosing, filtration and filtration, as well as backwash flux and duration.
- Evaluate the change in fouling indicators during variations in water quality in relation to feed water turbidity and chlorophyll-*a* levels in both the UF feed water and filtrate.

4. Develop a novel coagulant dosing strategy with the objective of reducing the dosing amount, preventing both coagulant overdosing and underdose while maintaining sufficient level of organic matter retention by UF RO feed pretreatment.

- Develop and field demonstrate an approach for determining optimal coagulant dose reduction set points based on fouling characteristic and changes in UF chlorophyll-a retention.
- Develop and field demonstrate a coagulant dose reduction strategy for use in conjugation with adaptive UF backwash triggering and a self- adaptive coagulant controller for optimal UF backwash operation for reducing both the frequencies of UF backwash and chemical cleaning in place (CIP).

1.4 Structure of Dissertation

The research objectives were completed through a combination of laboratory and field pilot UF and RO studies using two pilot systems. A full scale RO seawater desalination system integrated with a UF pretreatment skid was designed and constructed for U F fouling characterization and backwash enhancement studies. In addition, a brackish water RO desalination system, equipped with a custom plate-and-frame membrane optical cell, was designed and constructed for feed flow reversal experiments. Field studies enabled realistic assessment of operating conditions that affect UF fouling.

A literature review and relevant background information are provided in Chapter 2. The technical feasibility of cyclic mode of feed-flow reversal (FFR) for high recovery desalting under conditions of high mineral scaling propensity is addressed in the study presented in Chapter 3. Real-time detection of mineral scaling in the external membrane monitoring cell enabled cyclic triggering of FFR operation without interruption of permeate productivity.

In Chapter 4 a study is presented of the effectiveness of a self-generated UF pulse backwash system in a novel integrated UF-RO system for seawater desalination. Pulse backwash, which was added to a continuous UF backwash (directly from the RO brine stream) strategy, enabled peak UF backwash flux up to 4 times higher than the normal filtration flux. The performance of multiple consecutive backwash pulses was assessed with inline coagulation to further enhanced UF backwash.

In Chapter 5, the applicability real-time quantification of UF fouling indicators for real time assessment of the performance of UF pretreatment of seawater RO desalination is presented based on a field study using an integrated seawater UF-RO plant. In the study, the impact of feed water quality and coagulant dose were assessed with respect to both UF fouling rate (during the filtration period) and effectiveness of foulant removal by UF hydraulic backwash.

Chapter 6 presents an evaluation of a novel strategy of variable inline coagulant dosing aimed at reducing the amount of coagulant utilization. The coagulant dose reduction strategy develop id in the present work was shown to be effective in maintaining optimal UF backwash effectiveness while also ensuring UF retention of chlorophyll-*a* retention so as to protect the downstream RO membrane elements.

2 Background and literature review

2.1 Reverse osmosis membrane desalination

Reverse osmosis (RO) desalination is a pressure driven process in which solutes (as small as monovalent ions) are separated from water via a semipermeable membrane. Compared to other desalination methods such as multi-stage flash (MSF) and multi-effect distillation (MED), RO desalination has a lower capital cost (reduced plant footprint and complexity). At the same time, RO desalination provides high product water quality (RO membrane can remove up to 99.9% of the salt ions from the feed water) at lower energy cost compared to thermal-based desalination processes [4, 6, 29]. RO desalination is well established around the world for generation of potable water from brackish and seawater sources. The current total installed capacity of RO membrane desalination plants has reached 86.5 million m^3/day (as of August 2016), which account for about 60% of all desalination plants [30], while the largest plant has the capacity of 624,200 m^3/day (notable examples include the Magta plant in Algeria and the Sorek plant in Israel) [29].

Recent advancements in RO technology include the development of high rejection (~98-99% salt rejection) and low pressure (with net driving pressure about 4-5 bar for brackish water at 1,500 ppm salinity) RO membranes made from composite polyamide materials [31]. These types of membranes have high permeability and thus allow plant design for achieving high recovery (in excess of 80%). High recovery RO is beneficial since it reduces the volume of generated brine and this the associated challenges and costs of brine disposal and management [32, 33].

A reverse osmosis (RO) membrane is a semi-permeable membrane that is able to reject solutes larger than about 10 nanometers in diameters [4]. Typical RO membrane for water desalination consists of a thin film (~200nm thickness) composite of a polyamide active layer, on a porous supportive layer (~40µm) made from polysulfone or polyester. The majority of commercially available RO membranes are in the spiral-wound configuration (**Figure 2-1**) designed to provide a high membrane surface area to volume ratio which enables increased productivity while minimizing plant footprint.

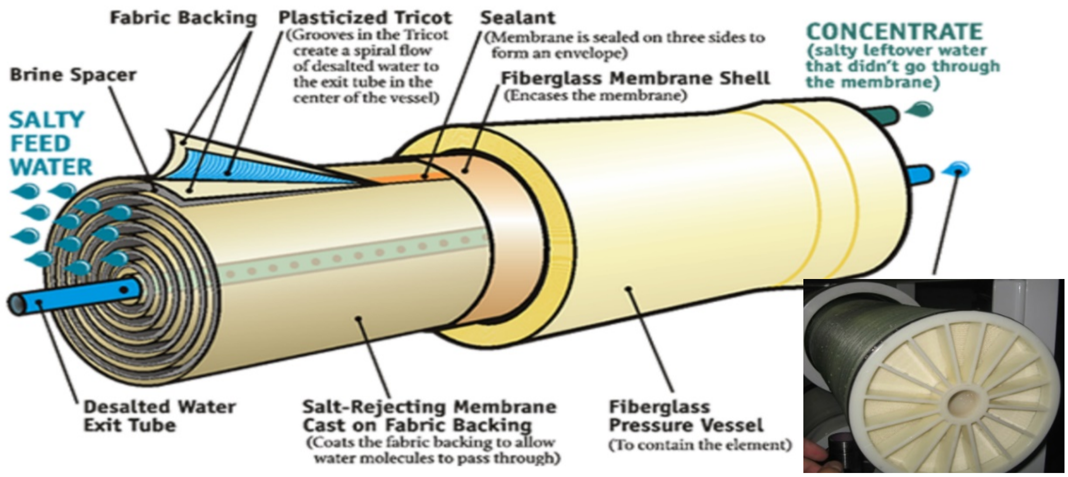

Figure 2-1 An illustration of the major components of a typical spiral wound Reverse Osmosis membrane inside a pressure vessel. Lower right insert: Photo of a 8'' diameter spiral wound Reverse Osmosis Membrane inside a pressure vessel. Adapted from [34]

2.2 Basic principle of RO membrane process

In the simplified cross-flow RO membrane process presented in **Fig. 2-2**, a feed stream enters at flow rate F_f, feed, salt concentration C_f, and pressure P_f. The feed stream flows tangentially across the RO membrane surface and is separated into two streams. The low-salinity permeate stream passes through the membrane with flow rate F_p, salt concentration C_p, and pressure P_p. The second stream is the retentate with a flow rate of F_R, salt concentration C_R, and pressure P_R which exits the membrane feed channel.

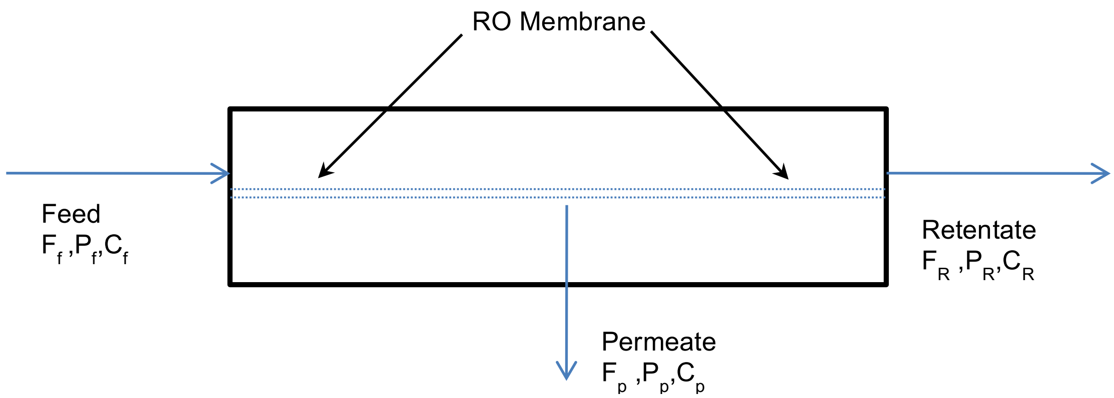

Figure 2-2 Simplified schematic of a cross flow RO membrane process. F: flow rate, P: pressure, C: concentration. Subscripts: f: feed stream, p: permeate stream and R: retentate stream.

Conservation of mass on the salt in the RO system can be shown to lead to a salt concentration increase of the retentate (brine) stream by a factor *CF* as given below [18, 35]:

$$CF = \frac{C_R}{C_f} = \frac{1 - Y(1 - R_o)}{1 - Y} \tag{2.1}$$

in which C_R and C_f are the salt concentrations in the retentate and feed streams, respectively, R_o= 1-C_p/C_f is the observed salt rejection, and Y is the product water recovery by the RO process expressed as:

$$Y = \frac{F_p}{F_f} = \frac{F_p}{F_R + F_p} \tag{2.2}$$

in which F_R, F_p and F_f are the flow rates of the retentate, permeate (product) and feed streams, respectively. The performance of the membrane with respect to salt passage (*SP*) is quantified as:

$$SP = 1 - R_{obs} \tag{2.3}$$

and the intrinsic rejection, defined based on the solute concentration at the membrane surface, C_m, on the retentate side, is given by:

$$R_i = 1 - \frac{C_p}{C_m} \tag{2.4}$$

The volumetric flux (flow rate per membrane area) of product water (permeate) through the membrane is given by the classical flux expression [36]:

$$J_v = L_p \cdot (\Delta P - \sigma \Delta \pi) \tag{2.5}$$

where J_v is the total permeate flux. L_p is the membrane water permeability, σ is the reflection coefficient (for high rejection membranes, the reflection coefficient $\sigma \sim 1$ [37] and $\Delta\pi$ is the difference between the osmotic pressure at the retentate and permeate sides of the membrane surface:

$$\Delta\pi = \pi_m - \pi_p \tag{2.6}$$

As water permeates through the membrane rejected ions and other solutes accumulate next to the membrane surface forming a concentration boundary layer that is higher in concentration relative to the bulk (**Figure 2-3**).

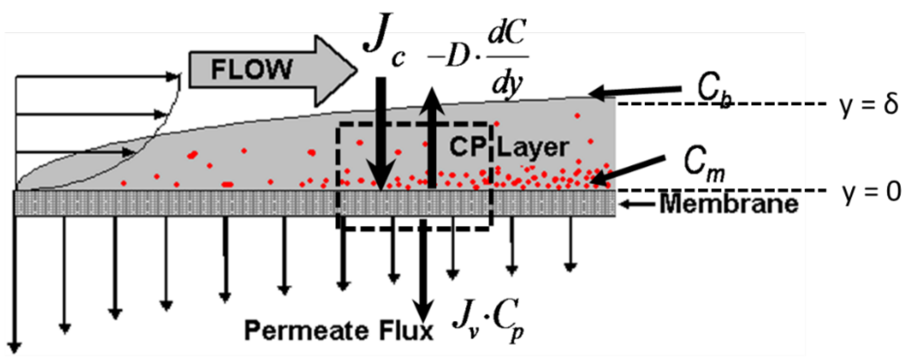

Figure 2-3 Schematic of concentration polarization layer at the membrane surface. The box with a dashed line represents the control volume.

A mass balance on the solute over a control volume (represented by the box with dashed line in **Figure 2-3**), assuming fully developed flow and concentration fields for a steady state operation, results in the following equation:

$$J_v \cdot C = J_v \cdot C_p - D \cdot \frac{dC}{dy} \tag{2.7}$$

where J_v is the permeate flux, C is the solute concentration in the boundary layer (at a distance of y from the membrane surface), D is the solute diffusion coefficient in water, and C_p is the permeate solute concentration. The solution of Eq. (2.7) subject to the boundary conditions of $C = C_m$ at y =0 and $C = C_b$ at y $=\delta_c$:

$$\frac{C_m - C_p}{C_b - C_p} = e^{\frac{J_v \delta_c}{D}} \tag{2.8}$$

where D is the solute diffusivity and δ_c is the boundary layer thickness (above the membrane surface). C_b is the bulk solute concentration, C_m is the solute concentration on the membrane surface. The average feed side mass transfer coefficient $\overline{k_m}$ can be defined as:

$$\overline{k_m} = \frac{D}{\delta_c} \tag{2.9}$$

It is noted that the ratio of C_m/C_b is known as the concentration polarization modulus (CP) for which Eq. (2.8) provides a reasonable average value for the membrane feed channel.

2.3 RO membrane scaling and fouling

RO operation at high recovery is often limited due to the risk of membrane fouling by colloidal, organic, and biological materials, and/or mineral scaling (or precipitate fouling) caused by mineral salts [6, 38, 39]. Membrane fouling refers to the deterioration of membrane performance (reduced permeate flux and hindered salt rejection) due to the accumulation of dissolved and suspended materials on the membrane surface and/or within the membrane pores [40].

2.3.1 RO scaling

RO membrane desalination technology has become a viable approach for the generation of new water supplies from seawater and inland brackish water [4, 9, 41-43], as well as for water reuse [44]. Brackish water typically has total dissolved solids (TDS) contents higher than freshwater and below seawater (>1,000 mg/L and < 30,000mg/L) [22, 26, 38]. Despite the significant progress and growth of inland water desalination, brackish water desalination remains challenging because the recovery levels achievable by RO desalination are typically limited by membrane mineral scaling due to precipitation of sparingly water soluble salts. As product water recovery increases along the RO modules, the concentration of mineral salts on the feed-side and near the RO membrane surface can increase to levels exceeding their solubility limits. As a consequence, crystal nucleation and growth may occur on the membrane surface or in the bulk solution [22] followed by deposition onto the surface. Mineral scale effectively blocks the membrane area for permeation and thus reduces the water flux. **Figure 2-4** shows flux decline due to gypsum scaling and images of gypsum crystal formation on a flat sheet RO membrane [26, 45].

Sparingly soluble mineral salts such as calcium sulfate dihydrate (also known as gypsum, $CaSO_4 \cdot 2H_2O$), calcium carbonate (known as calcite, $CaCO_3$), strontium sulfate (SrSO4), barium sulfate (also known as barite, $BaSO_4$), and silica (SiO_2) are the most problematic scaling species in brackish water desalination [46]. Extensive amount of mineral scale coverage on the membrane surface may cause damage to the active separation layer of the membrane [46], thereby increasing water production cost of the RO system. The supersaturation level of the mineral scalant of concern can be expressed in terms of the saturation indices (SI) defined as:

$$SI_y = IAP_y / K_{sp,y} \tag{2.11}$$

where IAP_y and $KP_{sp,y}$ are the ion activity products and solubility products of mineral scalant y, respectively. The mechanism of mineral salt crystallization can be divided into two phases: crystal nucleation and crystal growth. The induction time for crystal nucleation is defined as the length of time when the first crystal nucleus is observed. These nucleation sites are the foundation for the crystal growth phase [22, 26]. The crystal growth phase is a multi-step process which include: solute diffusion (to the crystal), surface adsorption, surface diffusion, surface reaction, and ion integration into the crystal lattice [22].

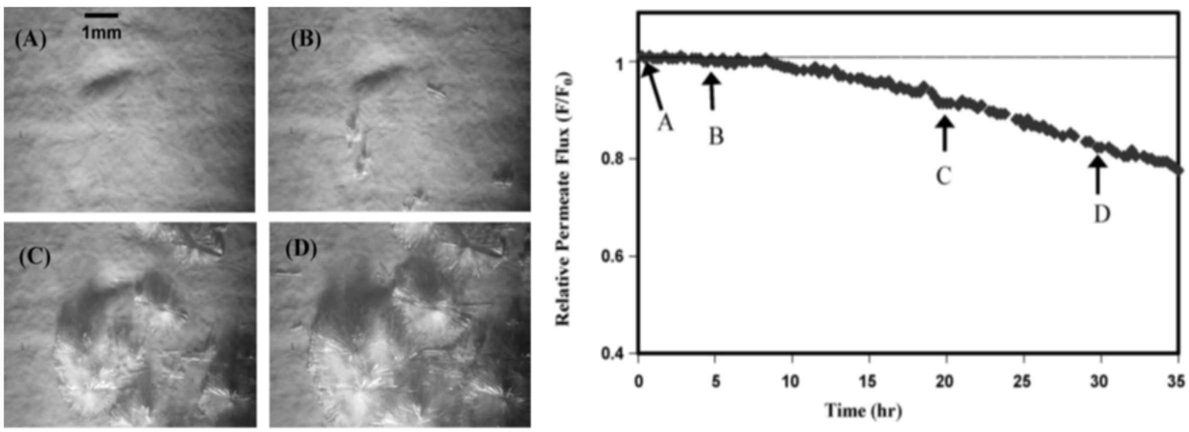

Figure 2-4 Flux decline data and associated images demonstrating early detection of gypsum scale using the approach by Uchymiak et al. [46]. The initial gypsum saturation index at the membrane surface was ~2.09. The first surface crystal was identified at time t = 0.5 h with the second crystal identified at time t=1h. At the point where flux decline was about ~5% (at t = 10 h), 20 crystals were identified on the viewable membrane surface area. Experimental conditions: A model solution of 7,990 mg/L (TDS) was used with a gypsum saturation index (SI) of 0.77. The images from left to right were taken at 0, 5, 20 and 30 h. The system operating pressure is 1.72 MP.

The supersaturation level of mineral salts on the membrane surface is directly related to the composition of the feed water which can vary temporally and geographically. As an example, the salinity of the agriculture drainage water varies significantly at different locations in the San Joaquin Valley (SJV) and the TDS is extremely high in some areas (TDS range 1,500 – 30,000 mg/L). Analysis of available water quality monitoring data from the California Department of Water Resources (DWR) from SJV also revealed substantial seasonal and spatial water quality variations [38]. **Figure 2-5** illustrated the drastic change in water quality over a year in a specific location in the San Joaquin Valley with **Figure 2-6** shows short term time-varying feed salinity of in another location.

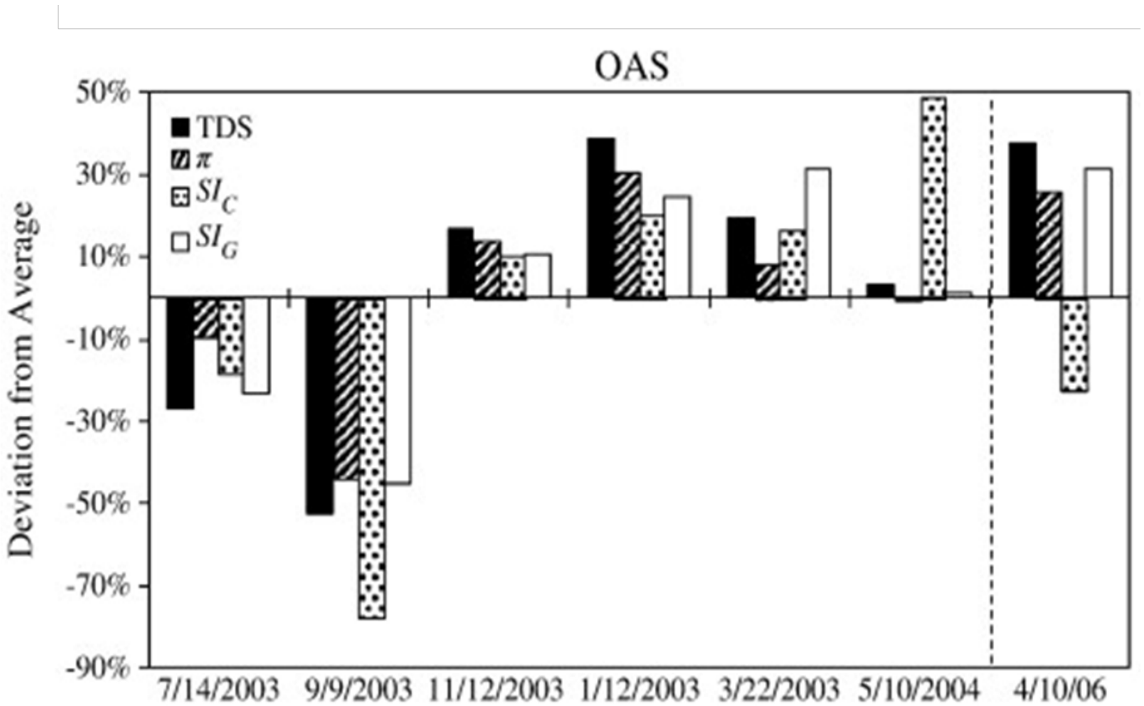

Figure 2-5 Illustration of water quality deviation from the annual average in the DWR database at the OAS site from July 2003 to May 2004. Average TDS: 7,999 mg/L. Average [Ca^{2+}] concentration: 356 mg/L, average [SO_4^{2-}] concentration: 4,810 mg/L, average pH: 7.7. [38]

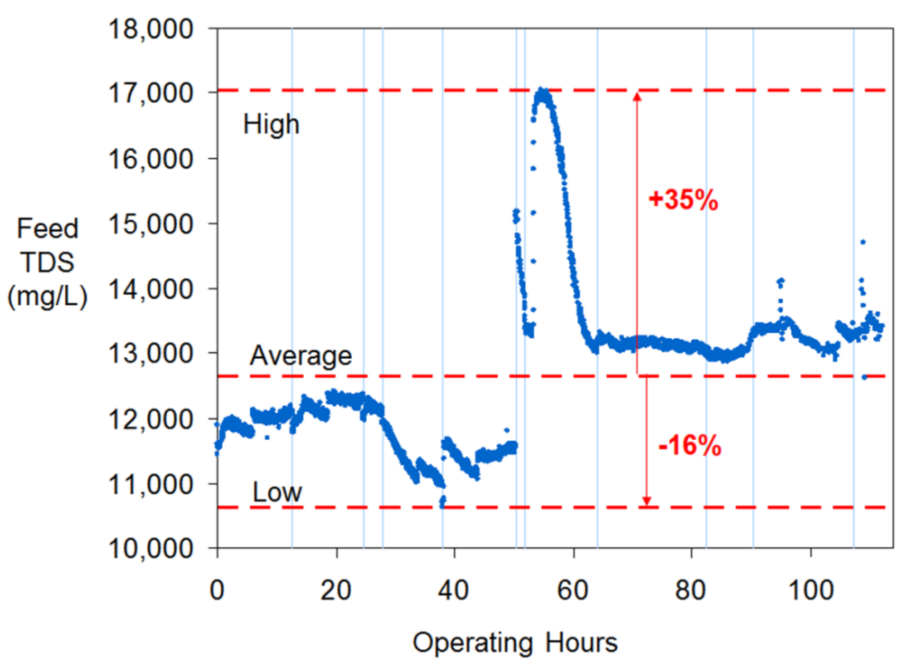

Figure 2-6 Short term time-varying feed salinity of San Joaquin Valley agriculture drainage water DP-25 (Data taken between 5/12/09-5/26/09, adapted from [47])

2.3.2 RO fouling

RO membranes can be easily fouled by small organic, colloids and biological materials present in the feed water. Organic materials such as polysaccharides and proteins can attach to membrane surfaces and promote biofilm growth on the membrane surface and cause biofouling [6] and as a result flux decline. Biofouled RO membranes are difficult to clean, and the fouled membrane module needs to be taken offline for aggressive chemical cleaning to restore its performance [48]. As indicated in the photo of **Figure 2-7** of a biofouled spiral wound RO membrane, physical damage to the module components can occur if fouling is severe; thus, membrane service life may be shortened and system maintenance cost (including membrane replacement) are increased.

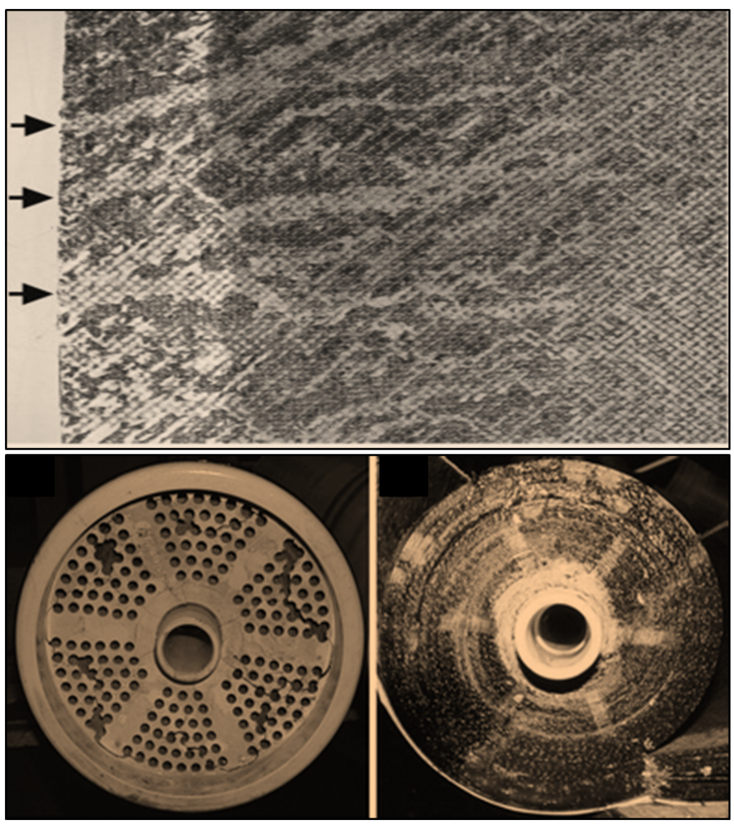

Figure 2-7 Examples of membrane damage due to biofouling. Top: Unwound spiral wound membrane modules from full-scale installations suffering from severe biofouling showing flow channels caused by

biofouling. The flow direction is from left to right. Bottom: Damage to module end cap due to biofouling in feed spacer channel of spiral wound membranes. (adapted from [49]).

RO membrane performance and the tendency to foul by organic, colloidal and biological material are directly related to feed water quality. The water quality of coastal seawater (or littoral water) is temporally variable and water quality is heavily influenced by natural events such as seasonal algal bloom. **Figure 2-8** shows the raw seawater (intake) quality at a seawater desalination facility demonstrating rapid variation of chlorophyll-*a* fluorescence measurements which are indicative of the concentrations of blue and green algae.

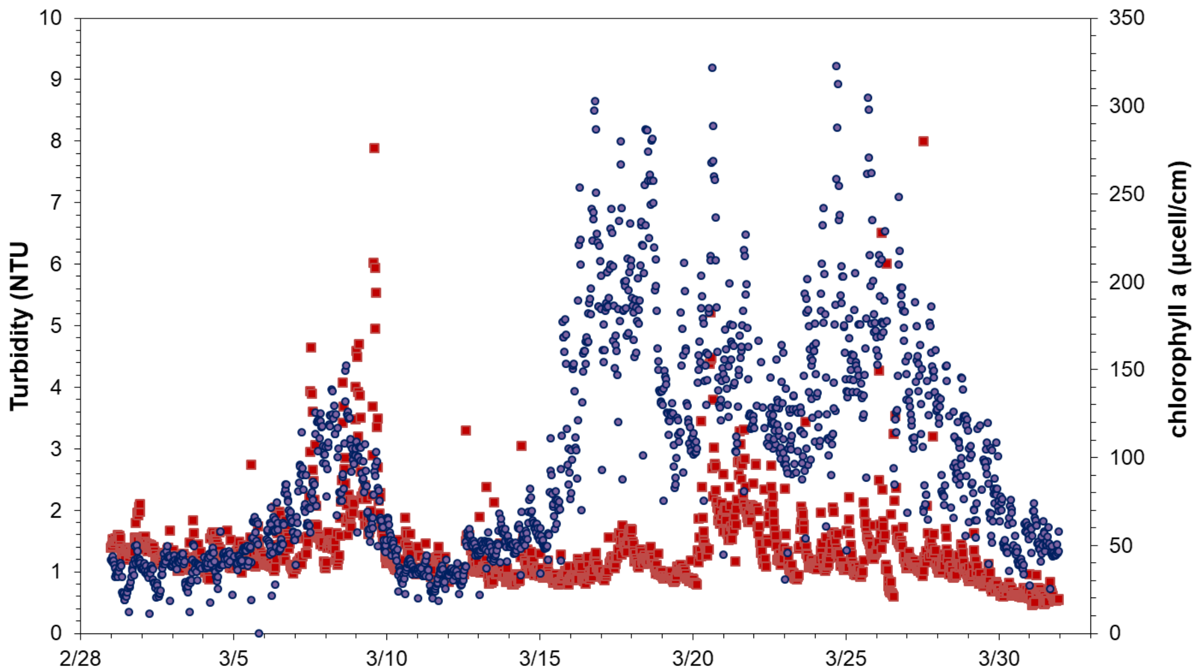

Figure 2-8 Feed seawater intake quality represented by water turbidity, dissolved oxygen and fluorescence measurement over a short testing period. RFU: Relative Fluorescence Unit. LDO: Dissolved oxygen concentration. (2013 data obtained from US Navy seawater desalination facility at Port Hueneme, CA**)**.

2.4 Pretreatment options for RO desalination

2.4.1 UF membrane as pretreatment

Prevention of RO membrane fouling is most effectively achieved through feed pre-filtration. While there are different types of filters (e.g., cartridge and media filters) that can be used, it is essential or the filer elements to have a long service life, element should be easily cleaned and pretreatment should require a low level of treatment and/or cleaning chemicals. Combining existing filtration techniques such as ultrafiltration (UF) and RO have led to major improvement in treating more contaminated RO feed water sources [2, 15]. Ultrafiltration is a separation process that makes use of membranes with pore size in the range of 0.001 to 0.1 micron. Typically, UF membranes are capable of removing high molecular-weight substances, colloidal materials, and organic and inorganic polymeric molecules [2]. However, low molecular-weight organic substances and inorganic ions (e.g., sodium, calcium, magnesium chloride, and sulfate) are not removed by UF membranes. **Figure 2-9** illustrates the range of filtration capabilities of MF, UF, NF and RO membranes. It is noted that since only high-molecular weight species are removed, the osmotic pressure differential across the UF Membrane surface is negligible [17].

There are two modes of feed flow through UF elements which are crossflow and dead-end filtration. Dead-end filtration, where the feed stream is passes perpendicularly through the membrane such that recovery is at a 100% without the generation of a residual stream during the filtration period. Crossflow filtration, where the feed flows tangentially to the membrane surface, enables a lower level of cake formation during the filtration step, but does results in a residual stream. Dead end filtration mode uses less energy (in terms of water pumping requirement) than cross flow filtration, it is widely adapted [2, 36]. UF membrane processes are deployed in a membrane submerged system where they operate such that permeation is under negative pressure (i.e., suction, [2, 50]) or under positive applied pressure [15]. UF membranes are available in various hydrodynamic designs and arrangements such as flat sheet, spiral wound, tubular, capillary, and hollow fibers [2]. Hollow fiber UF membrane consist of many single strand hollow fibers housed within a module or cartridge (**Figure 2-10**). Hollow fiber UF membrane can also be divided into "inside-out" and "outside-in" filtration modes according to the direction of the feed and permeate flows. **Figure 2-10** illustrates the flow paths through a hollow fiber UF membrane cartridge during production (filtration) and backwash modes. In "inside-out" dead-end mode, the feed water travel radially from inside to the outside of the fiber during filtration operation. During backwash operation, the backwash water travel from the outside to the inside of the fiber. The feed flow and backwash patterns in "outside-in" mode are reversed. Modern UF modules also allow alternation of the feed and backwash directions. **Figure 2-11** shows three feasible configurations for a UF module filtration/backwash cycle that has two feed ports and a single filtrate port. It is noted that fouling behavior and associated mechanisms in pressurized (inside out) and submerged (outside in) hollow fibre membrane systems can be very different and thus profoundly affect backwash strategies [51].

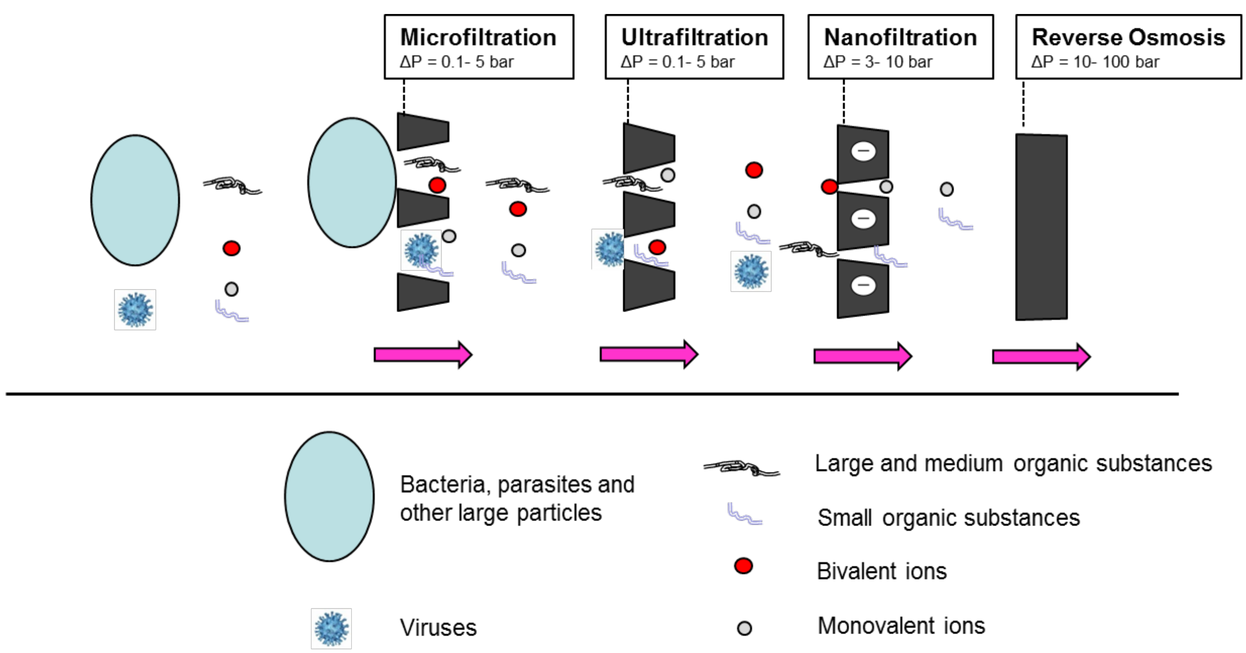

Figure 2-9 Illustration of different membrane filtration techniques and their capability (not drawn to scale, adapted from [4])

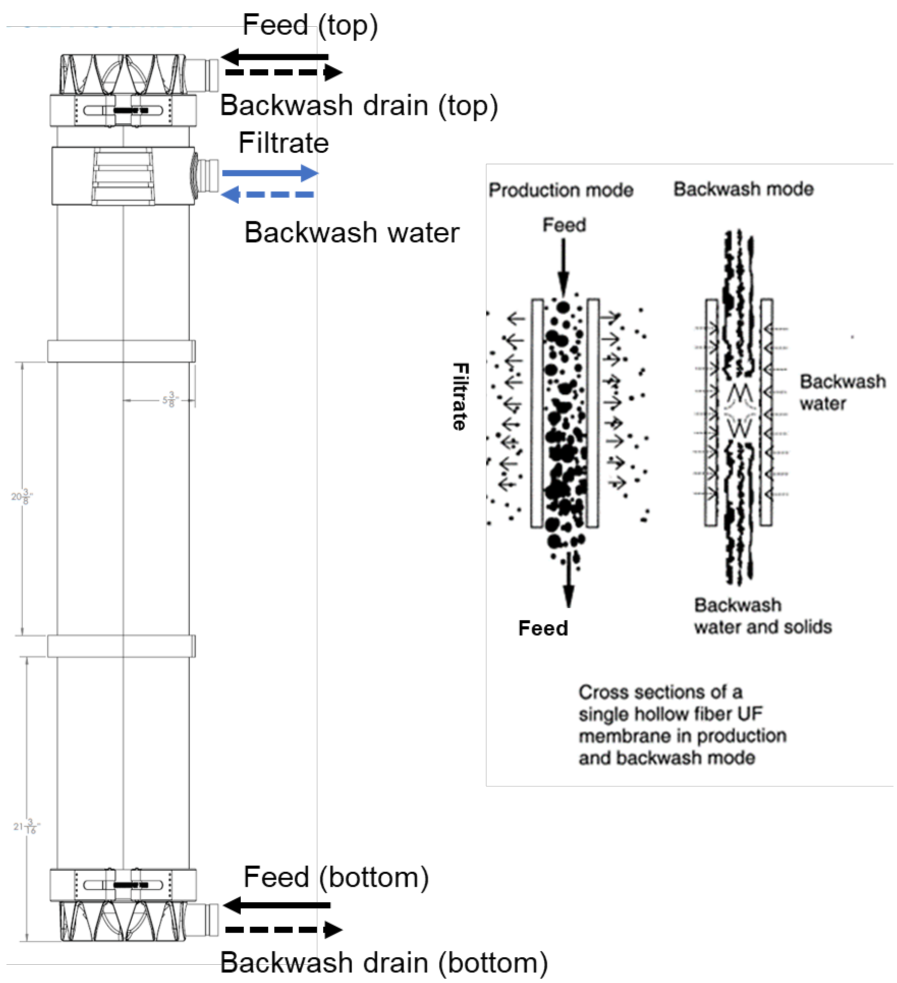

Figure 2-10 Illustration of flow paths through a hollow fiber UF membrane cartridge during production (filtration) mode and backwash mode (Left); Cross section of a single hollow fiber "inside-out" UF in filtration and backwash mode (Right), adapted from [19].

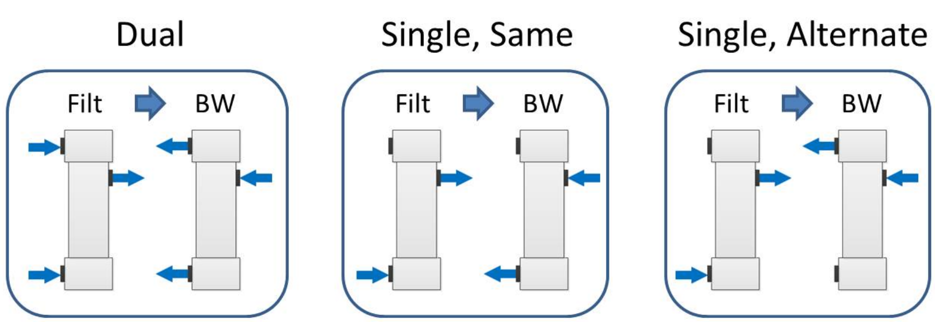

Figure 2-11 Illustration of UF module filtration and backwashing flow configurations for a UF module that has two feed ports and a single filtrate port. "Dual": Feed from both feed ports in filtration mode and allow backwash water drain from both feed ports. "Single, Same": Feed and drain from the same feed port. "Single, Alternate": Feed from one of the feed port, and drain the backwash water from the another feed port.

In recent years, “multi-bore” or “multichannel” UF fibers has been developed to increases the mechanical strength of the fibers [15, 52]. **Figure 2-12** shows the structure of a “multi-bore” UF membrane and membrane module whereby the membrane is with 0.02 μm nominal pore size and an active filtration layer that consisting of Polyethersulfone (PES). As shown in **Figure 2-12**, left), during filtration the feed water travel radially from inside the fiber lumen to the fiber outside zone. This UF module type (**Figure 2-12**, Right) has two feed and filtrate ports. The multi-bore fiber can operate at pressure up to 70 psi [52]. The benefit of the multi-bore UF module is its ability to withstand aggressive backwash without the risk of fiber breakage.

Despite its advantage, UF membrane technology is hampered by membrane fouling which leads to flux reduction and increased cost of system maintenance. However, with automated backwash, UF feed pretreatment can improve overall desalination operation and reduce maintenance requirements.

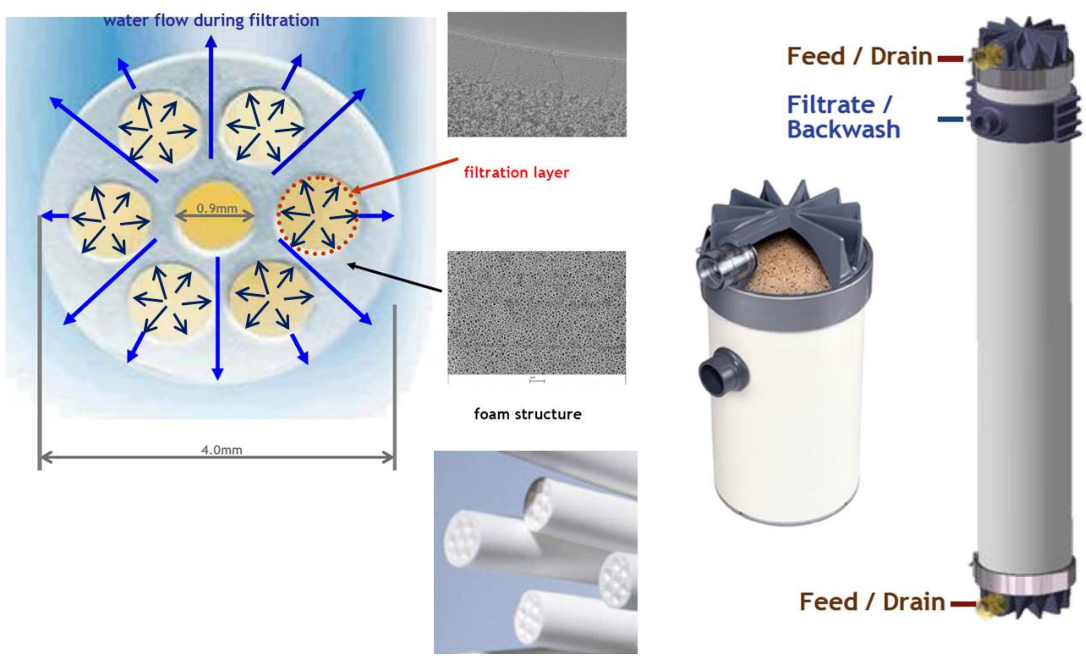

Figure 2-12 Multi-bore Hollow fiber UF membrane modules. Left image: Cross sectional image of a multi-pore hollow fiber UF membrane. Right image: 3D rendering of a UF module with feed/drain and filtrate/backwash ports. Bottom: a photo of several multi-bore hollow fibers. Adapted from [15].

2.4.2 *Inline coagulation*

Smaller, colloidal materials (diameter range of 0.01 - 5 μm) present a major challenge in RO feed pretreatment. Their removal via gravitational settling, typically with the aid of coagulants, is slow (up to hours), requiring large settling basins or tanks [53-55] and is not effective for removal of submicron particles. Coagulants are either metal salts (e.g. ferric chloride or aluminum chlorohydrate) or polyelectrolytes. UF and MF treatment of RO feed also benefits from the use of coagulant addition in inline mode (i.e., coagulant addition to the feed stream to the RO modules).

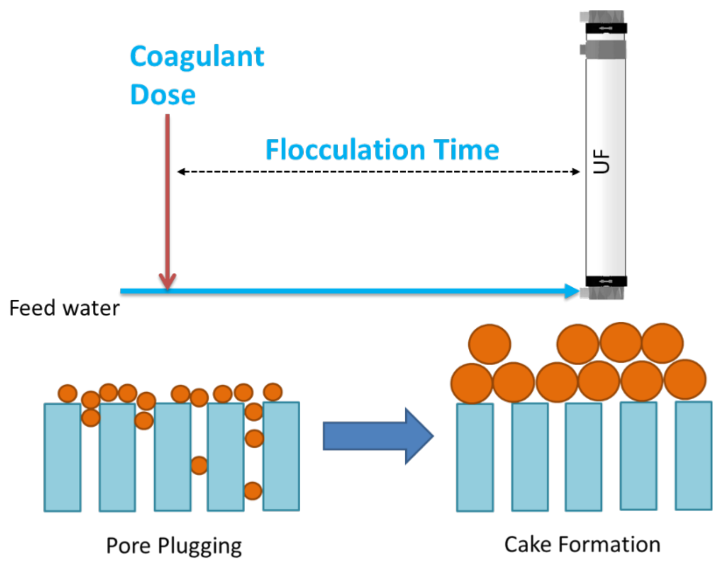

Figure 2-13 Illustration of UF filtration with coagulant dosing.

As depicted in **Figure 2-13** for inline coagulation, flocs formed by coagulation [54] reach the MF/UF membrane surface and form a foulant cake which is periodically removed via backwash. The floc size is governed by both coagulant dose and coagulation residence time. The required optimal coagulant dose is affected by both particle size, and feed water pH and temperature. It has been reported [51] that at an optimal dose and coagulant selection, certain coagulants can be effective in removing dissolved organic matter (DOM). It is emphasized that coagulant overdosing would lead to passage of residual coagulant through the UF/MF membrane which can lead to fouling of the RO membrane.

The behavior of colloidal particles in water is strongly influenced by their electrostatics charges [56]. Colloidal particles are typically negatively charged and their electrostatic repulsion [56] tends to prevent significant agglomeration. Effective agglomeration and flocculation. The use of coagulants can both reduce surface charge, promote aggregation and thus the formation of small aggregates and eventually visible flocs. Sweep flocculation (SW) occurs when a suspension is overdosed in excess of the amount needed to neutralize the charge on the colloid (**Fig. 2-14**). Therefore, a significant fraction of the dispersed colloids or particles may be become enmeshed in the settling hydrous oxide floc [57, 58].

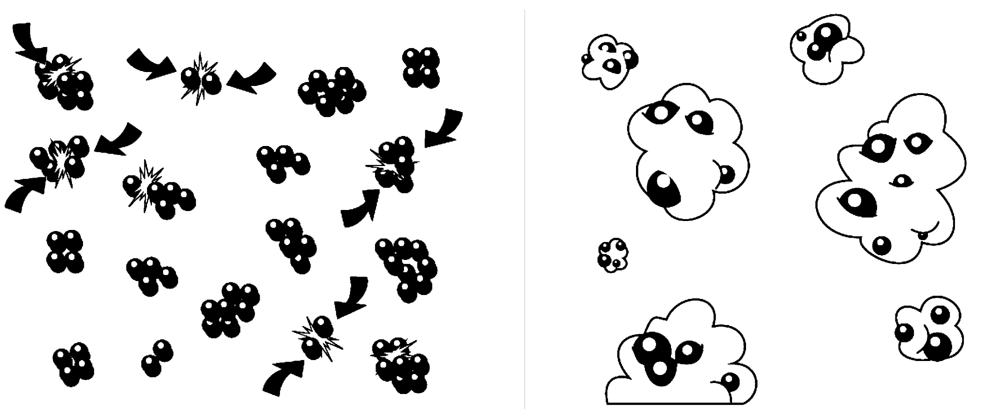

Figure 2-14 Illustration of Charge Neutralization (left) and Sweep Flocculation (right) for coagulation and flocculation process [58].

Charge neutralization (CN) due to coagulation involves adsorption of a positively charged coagulant onto the surface of the colloid. This charged surface coating neutralizes the negative charge of the colloid, resulting in a near zero net charge (zero zeta potential). As a result attractive van der Waals forces will dominate leading to creating of micro-flocs which deposit onto the membrane surface upon filtration; however, the foulant cake is of reduced compaction level which is beneficial for improved backwash efficiency [57]. There is also evidence that dissolved organics maybe adsorbed onto the floc matrix, thereby increasing the level of organics rejection by the UF membrane. It is noted, however, that overdosing can lead to surface charge reversal and could result in redispersion of colloidal matter [41].

The effect of coagulation on improving RO feed pretreatment has been investigated to treat seawater, brackish water and other types of contaminated water [41, 53, 54, 56, 58-61]. Jar tests are typically employed with subsequent filtration tests using small source water feed volumes (usually 1- 5 liters). In jar tests, different coagulant dosages are added to samples of the source water is initially rapidly mixed (for short duration) in a set of jars, with subsequent slow mixing to allow for the formation of flocs of particles, with cessation of mixing that allows for sedimentation [41, 57]. The optimal coagulant dose is usually determined based on the lowest permeate turbidity measurement [3, 59]. The main disadvantages of the jar testing approach are as follows: (a) jar tests are inadequate for simulating the complex hydraulic environment in treatment systems, and (b) fouling and cleaning (backwash) characteristics of filtration systems, particularly where water quality is temporally variable, are not reflected in limited jar tests.

Traditional approaches of applying coagulant for RO feed pretreatment are based on determination of a single optimal coagulant dose which must be determined offline. The potential problem of applying a fixed coagulant dose is that with changing water quality one may encounter the condition of either coagulant overdosing or underdosing. Coagulant overdosing leads to increase chemical cost, increased backwash sludge, passage of coagulant through UF, and potential for RO fouling downstream from UF [62, 63]. On the other hand, coagulant underdosing can result in rapid irreversible fouling and thus decreased backwash efficiency and increased chemical cleaning frequency. Coagulant underdosing can also result in increased passage of "sticky" organic materials such as transparent exopolymer particles (TEP), and other RO fouling pre-cursors to the RO membrane downstream [2, 64-70]. On the other hand, proper coagulant dose can be beneficial not only for improving the removal of particulate matter, but also in removing organic materials in some cases [71, 72].

2.5 UF fouling

UF membranes are also susceptible to adsorptive fouling by macromolecules such as proteins and by bacteria, pore plugging and foulant cake formation [17]. The most common fouling symptoms are flux decline (in a constant pressure operation), transmembrane pressure (TMP) increase (in constant flux operation), and permeate quality changes. **Figure 2-15** illustrates the UF fouling process on a UF membrane surface. The main fouling mechanisms include adsorption, pore clogging/blockage and external cake formation. Adsorption and pore blockage are internal fouling mechanisms that occur for foulants of size equal to or smaller than the pore size. Suspended matters of size smaller than the pore radius can adsorb along the pore walls, as well as the external surface of the membrane leading to pore "narrowing" [73]. When the foulant particle size is about the size of the membrane pore, pore blocking mechanism will be the dominate fouling mechanism. In this case, the fouling particles will plug or block the membrane pores, reduce the total available pore volume and thus reduce permeate flux. Gel or cake layer formation occurs when suspended particles or their agglomerates are larger than the pore size and thus accumulated on the membrane surface during the filtration process.

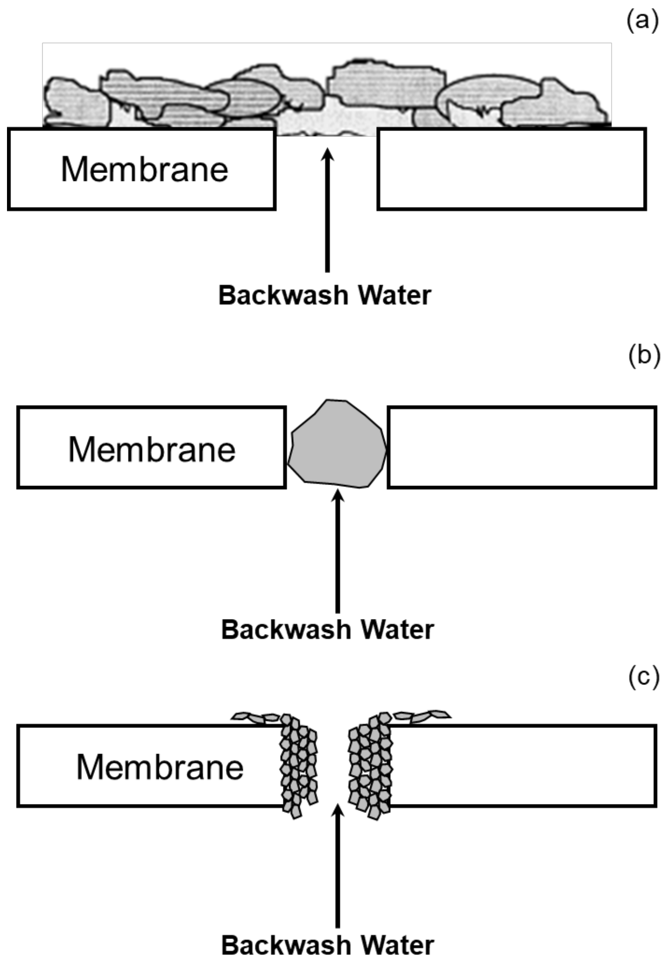

Figure 2-15 Common fouling mechanism for porous membranes: (a) gel/cake formation; (b) pore plugging; and (c) adsorption - pore "narrowing" effect. Adapted from [19].

2.5.1 UF fouling model

Fluid permeation through a porous membrane under applied pressure can be expressed via Darcy's law:

$$J = \frac{1}{A}\frac{dV}{dt} = \frac{\Delta P}{\mu R_t} \tag{2-12}$$

in which J is the permeate flux, A is the membrane surface area, dV/dt is the rate of change of filtered volume, V, with time, t, ΔP is the transmembrane pressure across the cake and membrane, and μ is the fluid dynamic viscosity. The total membrane filtration resistance R_t can be expressed, following the resistance-in-series model as the sum of the membrane resistance (R_m), cake resistance (R_c), and cumulative irreversible resistance (R_i) [74, 75].

$$R_t = R_c + R_m + R_i \tag{2-13}$$

The transmembrane pressure in Eq. 2-12, ΔP, can be expressed as the summation of the contributions of the different resistances to the required transmembrane pressure for a given permeate flux. Accordingly,

$$\Delta P = \frac{\mu R_m}{A}\frac{dV}{dt} + \frac{\mu R_C}{A}\frac{dV}{dt} + \frac{\mu R_i}{A}\frac{dV}{dt} \tag{2-14}$$

The cake resistance can be described as the product of the effectiveness cake thickness (l_c) and the specific cake resistance (m/Kg) (α) as given below [57, 75]:

$$R_C = \alpha l_C = \frac{\alpha\omega V}{A} \tag{2-15}$$

where ω is the solids concentration in the cake per unit filtrate volume (kg/m^3). The filtered volume V can be expressed as $V = AJ/t$ by integrating Eq. (2-14) and substituting the expression for J in Eq. (2-12) which leads to the total transmembrane pressure during filtration:

$$\Delta P = \mu R_m J + \mu\alpha\omega J^2 t + \mu R_i J \tag{2-16}$$

Typically, membrane resistance is determined by determining the pure water flux in the absence of a cake layer as shown in Eq. (2-17); the membrane and accumulated irreversible fouling resistance is related to the transmembrane pressure as given below:

$$J = \frac{\Delta P_0}{\mu R_m} \tag{2-17}$$

$$J = \frac{\Delta P_i}{\mu R_i} \tag{2-18}$$

where ΔP_0 and ΔP_i are the transmembrane pressures for pure water flux for a clean membrane and due to irreversible fouling, respectively.

Combining Eq. (2-17) – Eq. (2-18), the transmembrane pressure can be expressed as:

$$\Delta P = \Delta P_0 + \Delta P_i + \mu\alpha\omega J^2 t \qquad (2\text{-}19)$$

which can be can be rearranged such that the total UF membrane resistance is expressed as:

$$R_t = \frac{\Delta P_0}{J \cdot \mu} + \frac{\Delta P_i}{J \cdot \mu} + \alpha\omega J \cdot t \qquad (2\text{-}20)$$

and for a constant flux and environmental conditions (e.g., temperature), the fouling rate for the filtration process is then given by:

$$\frac{dR_t}{dt} = \alpha\omega J \qquad (2\text{-}21)$$

2.5.2 UF fouling monitoring and quantification

In order to quantify the "fouling potential" of the source water, different fouling indices have been proposed such as the Silt Density Index (SDI) and various forms of Modified Fouling Index (MFI) [76-89]. The above fouling indices are determined based on flux decline measurements for selected membranes in in-situ filtration cells. These fouling indices rely on off-line measurements and thus introduce an inherent lag time relative to the real-time UF system behavior. It is also noted that the majority of the reported studies on fouling indices for UF and MF systems did not consider the impact of coagulation and have relied on the use of synthetic saline, surface water or seawater blended with organic foulants [77, 79-81, 85, 86, 88-92]. Noted are recent investigations of seawater and algal-rich surface water UF fouling potential, associated with green and blue algae, that relied on time fluorometeric measurements of chlorophyll-*a* [60, 64, 93-95]. These studies with laboratory-scale hollow fiber UF membranes demonstrated significant correlation of chlorophyll-*a* with UF membrane flux decline associated with biofilm growth.

Invariably, arriving at effective UF filtration and backwash strategies will require tracking of the extent of UF fouling and assessment of backwash effectiveness. Conventional UF operations rely on tracking of UF fouling via the UF transmembrane pressure (TMP), UF filtration resistance or membrane permeability normalized with respect to their initial value in the filtration step just post CIP [96-102]. Such approaches, however, do not lend themselves to cycle-to-cycle tracking of backwash efficiency nor quantifying the contributions of reversible (i.e., backwashable) and irreversible (i.e., unbackwashable) fouling to progressive UF resistance change over the course of system operation.

2.6 Fouling and scaling control techniques and cleaning methods

2.6.1 Scaling control and cleaning methods

Typical control methods for mineral scaling in brackish water desalination include pH adjustment, reduce concentration polarization effect by lowering water recovery, and antiscalants (e.g., polymer additives) addition. Feed pH adjustment is usually achieved via acid (e.g., H_2SO_4) dosing and is appropriate for retarding the precipitation of mineral salts whose solubility is impacted by pH (e.g. Calcium carbonate). As an illustration, the pH dependence of the saturation indices of calcite, silica, magnesium hydroxide, gypsum and barite are shown in **Fig. 2-16** for a representative water sample from a specific brackish water site (Section 2.2.1) in the California San Joaquin Valley. As shown in **Fig. 2-16**, the saturation indices for barite and gypsum are pH insensitive, while those of calcite, silica and magnesium hydroxide highly pH dependent. It is noted that RO membrane mineral scaling can be averted by operating at a recovery level such the mineral scalants of concern are below their saturation level. However, such an approach may reduce overall water system productivity. **Figure 2-17** contains plots of saturation indices as a function of recovery for calcite, silica and gypsum for a representative water sample from a specific site (Section 2.1) in the SJV. However, this method will limit productivity and it is not optimal in term of energy usage [46].

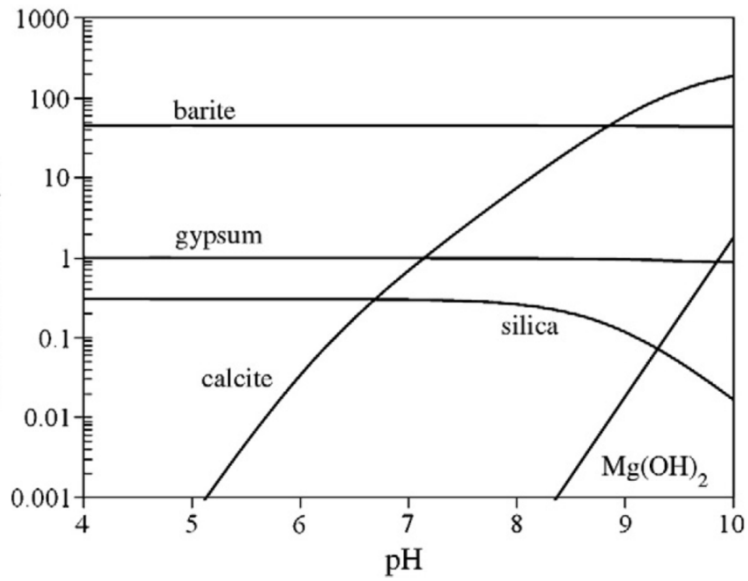

Figure 2-16 Saturation indices as a function of pH for agriculture brackish water (TDS: 11,020 mg/L) [38].

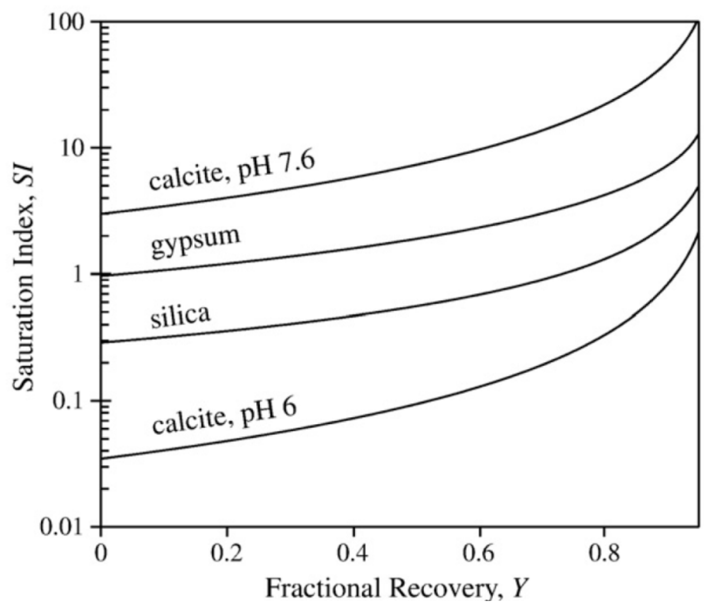

Figure 2-17 Saturation indices as a function of recovery for the brackish water composition corresponding to Figure 2-16 (11,020 mg/L, calculated based on 98% salt rejection).

Mineral scaling can be suppressed using antiscalants additives which can be added to the RO feed to retard mineral salt nucleation and crystal growth [39, 103]. The recommended upper limit of saturation index (SI) values (at the membrane surface) at which antiscalants can be effectively used are $SI_{CaCO_3} \leq 60$, $SI_{SrSO_4} \leq 8$, $SI_{CaSO_4} \leq 2.3$, $SI_{SiO_2} \leq 1$ [25, 39, 104]. The use of antiscalants increases the cost of RO desalination [9, 39, 105] and at high doses nay lead to increased biofouling propensity [39].

Osmotic backwash is an operational approach that has been proposed for periodic cleaning of RO membrane surfaces so as to avoid the buildup of a mineral scale layer [106, 107]. IN this approach, a pulse of high salinity feed (higher than the feed water) is injected into the membrane channel while the feed pressure is reduced, thereby triggering permeate flow from the permeate side to the feed channel [6]. Another proposed approach is that of "Feed Flow Reversal" (FFR) or "Concentrate Backflow" operation mode [27, 108]. In the FFR approach (**Fig. 2-18**), as feed flows in the normal forward flow (NFF) mode; feed water enters the spiral-wound membrane module from its "normal" feed side. Salt concentrations then increase axially along the feed channel at the membrane surface as a consequence of concentration polarization [109]. When the mineral salt scalant concentration exceeds saturation (SI>1), scaling is expected to occur first in the downstream area toward the "brine" exit zone. Once the scaling level reaches a specific threshold, feed flow reversal (FFR) is initiated, whereby the raw feed is redirected to enter through the previously designated outflow end. As the entrance "end" is exposed to the undersaturated raw feed, mineral salts on the membrane surface are dissolved. The above mode of periodic switching of the flow direction disrupts and reverses the CP profile (**Fig. 2-19**) in the RO feed channel and results in cycling scale dissolution/formation. It is noted that, unlike cleaning methods such as osmotic backwash [106] and high-salinity solution direct osmosis (DO) backwash [110], FFR operation does not interrupt permeate production. When used with antiscalant addition in the feed, FFR operation can potentially achieve high RO recovery without permanent mineral scaling.

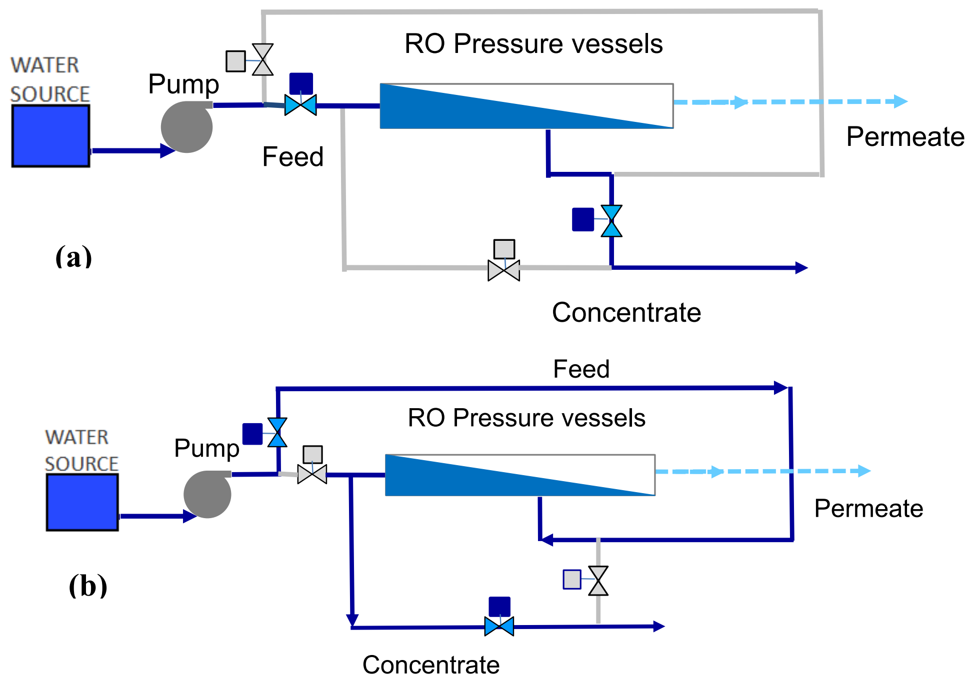

Figure 2-18 RO operation in modes of (a) normal feed flow (NFF), and (b) feed flow reversal (FFR).

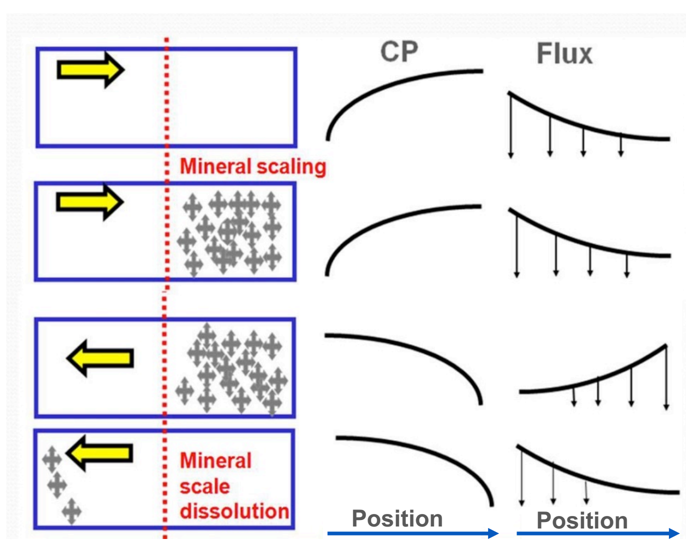

Figure 2-19 Illustrations of the basic concept of feed flow reversal operation. Periodic reversal of the flow direction reverses the CP profile in the RO elements exposing scaled areas to undersaturated solution thereby resulting in dissolution of mineral crystals.

Triggering of FFR using an ex-situ scale observation detector (EXSOD) was previously demonstrated [26, 46] for mitigating gypsum scaling using in a small brackish water RO pilot plant (up to 3 m^3/day capacity). In this approach, a flat sheet RO membrane coupon is placed in a transparent plate-and-frame RO (PFRO) cell for direct real-time membrane surface imaging for monitoring scale formation. It was shown that FFR triggering can be achieved sufficiently early by adjusting the flow through the PFRO cell to achieve the desired level of solution supersaturation at the membrane surface. Improved mineral scale detection and evaluation of the evolution of crystal nucleation, via automated image analysis, was subsequently developed [22] for application of the EXSOD type scale detection system. Also, the use of model-predictive control of FFR operation for RO desalting was later proposed [105] in order to avoid pressure fluctuation and water hammer when reversing the feed flow. It is noted that earlier studies on RO operation in FFR mode have not demonstrated self-adaptive control (i.e., in terms of FFR cycle frequency and duration) over many operational cycles. In addition, FFR operation was not demonstrated at significant scaling level of the RO membranes to unambiguously establish the reversal of mineral scaling (i.e., effective cleaning and restoration of membrane permeability).

2.6.2 Fouling control and cleaning methods

Various fouling control techniques and membrane cleaning methods have been developed in an attempt to increase the operational life of membranes by reducing or mitigating membrane fouling [111-113]. Several approaches can be distinguished: 1. pretreatment of feed solution, 2. hydraulic cleaning, and 3. chemical cleaning.

Methods of averting membrane fouling include the use of complexing agents (EDTA etc.), chlorination of the feed solution, adding pretreatment filtration stages (such as MF/UF, media filtration, active carbon adsorption filter, and coagulation/flocculation) before the RO membrane stage [6, 15, 28, 44, 50, 53, 66, 99, 114-116]. For MF and UF membranes, coagulant dosing into the feed stream of the pretreatment system has shown to be an effective way of reducing fouling of the membrane system downstream [117-119]. The chemistry and mechanism of inline feed water coagulation for UF membrane system has been discussed in section 5.2.2.

There are numerous publications about the concept of "critical flux" for MF and UF membranes which have been developed to enhance or to "optimize" the filtration period in order to prevent irreversible fouling [53, 61, 73, 99, 120-123]. The premise of the above concept is that one can operate the UF/MF system below a critical filtration flux in order to ensure complete permeability recovery after each backwash cycle [120]. However, field studies have revealed irreversible fouling (surface and pore blocking) cannot be completely removed by backwash alone [123]. It is also noted that the "critical flux" approach is applicable to crossflow operation which is typically not practiced in commercial applications.

Hydraulic cleaning methods of UF/MF membranes rely on physical means to dislodge the foulant layer from the membrane surface. For RO membranes, hydraulic cleaning includes periodic shutdown of the feed water for a short period and then flushing the system with low salinity RO permeate water (fresh water flush) [4, 6, 124, 125]. For MF/UF membranes, the most common hydraulic cleaning methods are backwashing, feed flushing, and air sparging [50]. During backwash operation, the backwash water enter the membrane module through the filtrate side, penetrate the membrane pores and dislodge the fouling cake layer into the feed side

(**Figure 2-18 and 19**). Unlike MF/UF membranes, NF and RO membranes typically cannot be subjected to backwash because they have a delicate active separation layer (e.g., polyamide) that may be delaminated in reverse high pressure backwash [6]. Fresh water flush of UF/MF membranes has been shown to provide some level of foulant cake removal. Figure 23 depicts the processes of coagulation with hydraulic cleaning. It is noted that with effectively coagulated flocs, neutral hydrophilic compounds attached to membrane surface can be removed by physical backwash and feed flushing (**Figure 2-20**, top) [115].

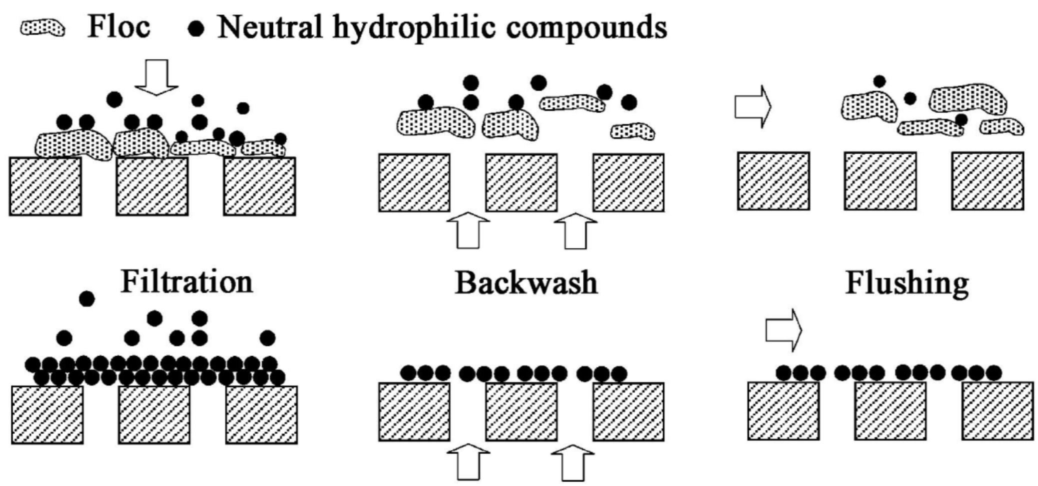

Figure 2-20 A set of cartons illustrate the filtration, backwash and feed flushing process with (top) and without coagulation (bottom) treatment [115].

In order to mitigate UF/MF membrane fouling, backwashing or back-flushing has been widely used for cleaning MF/UF membranes [113, 126-129]. Backwashing disrupts and removes the foulant cake layer of MF/UF membranes via “lift-and-sweep” mechanism [85, 130, 131]. Typically, the MF/UF filtrate water is collected and used as the backwash fluid for backwash over a period of ~30 s to several minutes depending on the fouling condition. In order for backwash to be effective membrane manufacturers typically recommend backwash flux that is 2-3 times the filtration flux [132].

In contrast with low frequency backwash, high frequency (~1-300 backwash instances/min) short duration (0.1-4 s) backwash pulses (typically known as "backpulsing") have been utilized, in particular, to improve filterability of particulate and colloidal suspensions in either crossflow or dead-end filtration [128, 133-137]. Laboratory studies of backpulsing have been reported for polymeric MF/UF polymeric [112, 131, 135] and ceramic and metallic [126, 138-140] membranes, at pressure range of ~21-90 kPa and ~100-600 kPa, respectively. It is noted that in high frequency backpulsing, filtrate recovery (or productivity) is generally in the range of 50-93%. Backpulsing has traditionally relied on backwash fluid delivery from a pressurized reservoir [127, 128, 131, 134, 135, 141, 142], as well as with the use of gas-driven pistons to generate a backwash pulse [140, 143, 144]. It is important to recognize that in large-scale RO feed pretreatment, UF/MF operation is carried out primarily in dead-end filtration in order to maximize filtrate recovery. Therefore, high frequency backpulsing for high throughput RO feed pretreatment for which a steady feed flow is needed would represent a significant operational and equipment challenges [145].

Low frequency backwash is the preferred approach in UF/MF pretreatment of RO feedwater [15, 50, 133, 146], and the addition of low frequency (~2-5 backwash cycles/hr) pulse backwash using hydraulic accumulators has been proposed for improvement of backwash efficiency [147]. It is noted that UF and MF filtration with pulse backwash, actuated with hydraulic accumulators, has been described in the patent literature [148, 149]. The use of hydraulic accumulators has also been reported for pressure stabilization during backwash of microfilters [150]. Hydraulic accumulator typically consist of a gas and liquid chambers separated by a bladder [151, 152], whereby the accumulator is typically charged via a pump that delivers the backwash water from the filtrate product stream [153]. The operational characteristics of such hydraulic accumulators have been analyzed with respect to their application in automobile regenerative braking (energy storage) [151, 152, 154]. Such hydraulic accumulators can in principle be utilized to enhance backwash flux of UF and MF membranes used for RO feedwater pretreatment. Indeed, in a recent seawater desalination study [147], it was shown that UF pretreatment of RO feedwater was improved with the use of pulsed UF backwash. The above was demonstrated in a UF-RO system in which the RO concentrate stream was used directly for UF backwash, thereby eliminating the need for both intermediate storage tanks (for both RO feed and backwash) and UF backwash pump.

Chemical cleaning is one of the most important methods for restoring the permeability of heavily fouled membranes [6, 29, 118]. Chemical cleaning can effectively remove most organic, biological and particulate fouling from the membrane surface and from within membrane pores. Chemical cleaning methods include the use of cleaning solutions that are pumped through the membrane feed channel (i.e., cleaning-in-place or CIP), as well as backflushing from the permeate side of the membrane with a cleaning solution during chemically enhanced backwash (CEB) [116]. The cleaning solution composition, cleaning time and soaking time are important factors that affect the effectiveness of membrane cleaning.

A number of different chemicals are commonly used (separately or in combination) during chemical cleaning. For example, in CIP of UF/MF membranes, a high pH caustic cleaning (pH =12) followed by low pH (pH = 3) acidic cleaning strategy can be used [155]. A strong (e.g., HCl) or weak acid (e.g., citric acid) and NaOH solution are typically used to disperse foulant particles [118]. In CEP of UF membranes, high concentration (20 -200ppm) of disinfectant such as NaOCl and H_2O_2 are mixed with backwash water to backwash the UF membrane. In CIP of RO membranes, alkaline detergent and surfactant can be used to chemically clean the RO membrane. RO membrane have low tolerance for free active chorine exposure; therefore, permanent membrane damage could occur after several minutes of exposure to high chorine concentration (>100ppm). Although chemical cleaning is effective in removing membrane foulants, it is also associated with high chemical cost and high chemical waste disposal cost [6, 28, 99, 156].

2.7 Adaptive operation in integrated UF-RO membrane system

In conventional UF operation, the UF system operates under fixed filtration and backwash durations. If the feed water quality changes and the system cannot cope with this change, membrane fouling in the system will occur quickly. **Figure 2-21** illustrates fouling behavior under fixed filtration and backwash durations. The severity of membrane fouling is typically characterized based on analysis of measurable process parameters such as TMP or membrane permeability or the reciprocal of membrane resistance (i.e., Eq. (2-12)). **Fig. 2-21** provides a schematic illustration of the variation of membrane permeability with time during several filtration and backwash cycles. The permeability decrease during a filtration cycle is attributed to short-term fouling phenomena, such as particle deposition onto the membrane surface or pore blockage in the case of UF or MF applications [123]. For the above example, backwash efficiency can be defined as the ratio of membrane permeability at the beginning of cycle (n) to membrane permeability at the beginning of the previous cycle (n − 1).

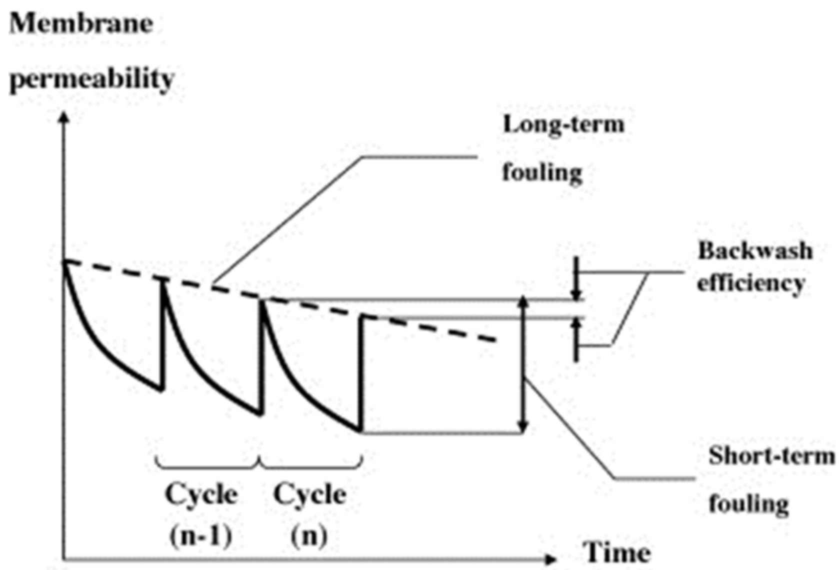

Figure 2-21 Illustration of conventional UF operation with constant filtration and backwash time**.** Characterization of backwash efficiency and fouling [123]

Ultrafiltration operational strategy with a pre-determined threshold of the maximum transmembrane pressure for triggering backwash was proposed in [74]. For each filtration cycle, the TMP of the membrane was tracked and when the maximum threshold value was reached, backwash was triggered. In the above approach the filtration time was found to vary initially until it reach a stable level as indicated by a stable cake property αω value [74]. In another approach, a model-based control was proposed for a membrane bioreactor filtration process [157]. In this approach only TMP measurement was utilized and process operation was optimized on the basis of operational cost, demonstrating energy savings of up to about 50%. In another study with submerged membranes a backwash control strategy was developed whereby the filtration period was maintained constant, but the backwash duration varied depending on the backflush TMP [158, 159]. In a related study, the above researchers introduced a new control system that relies on a cumulative TMP increase as a set-point for initiating backwash [158]. In the above study, the TMP threshold was set as the cycle TMP change within 3% of the maximum allowable resistance, by varying the filtration time. In an attempt to improve UF performance a control system was also introduced for in-line coagulation dose control [160]. As shown in Fig. 2-22, the initial resistance of the last filtration step before chemical cleaning can be controlled within an accuracy of approximately 3% (of the total resistance) or 9% (of the fouling resistance).

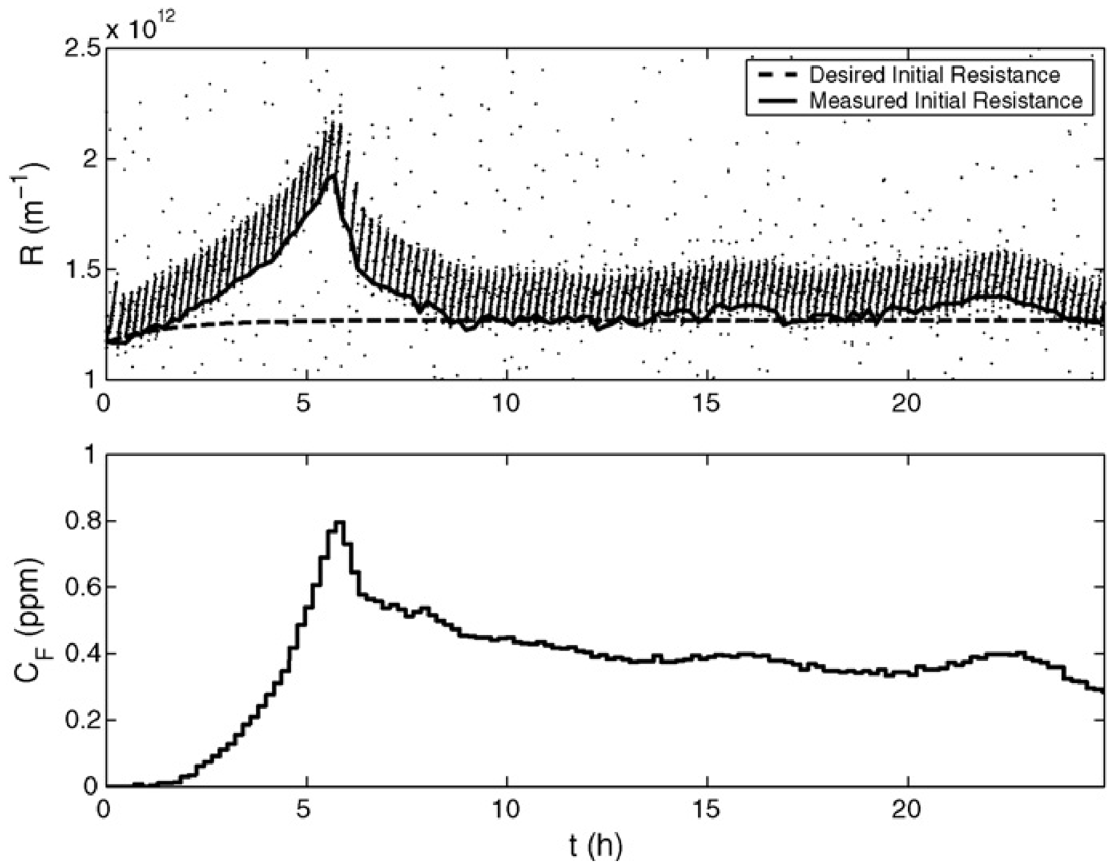

Figure 2-22 Performance of the coagulant controller on a sequence of short filtrations. R: membrane resistance due to fouling, C_F: the coagulant dose. The backwash flux (J = 250 l/(m^2 h)) and the backwash duration (t = 45 s) were kept constant. UF membrane: hollow fiber porous PES/PVP membranes with an internal diameter 0.8mm and an effective length of approximately 1.5 m. filtration surface of 40 m^2 each and a cut-off of approximately 200 kDa were used. Coagulant used: commercially available poly-alumina coagulant (Quadrafloc PUS, CAS 990001-02-9, ViVoChem BV) [160].

In previous work, a backwash triggering controller, based on a maximum allowable filtration resistance change per cycle ($\Delta R_{T,max}$) was proposed and demonstrated as an effective and practical method to control backwash frequency [147]. Subsequent work demonstrated that real-time quantification of backwash efficiency, along with determination of the associated of coagulant dosing, can be utilized for determination of optimal coagulant dose adjustment in response to changing UF fouling as affected by varying feed water fouling potential [161]. The above study presented a real-time self-adaptive approach to in-line UF coagulant dosing and its field demonstration in an integrated UF-RO seawater desalination system. The coagulant controller, which tracks the UF resistance during filtration and backwash, adjusts coagulant dose to the UF feed with the objective of reducing the incremental cycle-to-cycle UF post-backwash resistance change (**Figure 2-23**). Real-time tracking the above UF resistance metrics, as well as the rate of change in post backwash (PB) UF resistance (Δn) with coagulant dose, enabled the controller to quantify the progression of both irreversible fouling and UF backwash effectiveness.

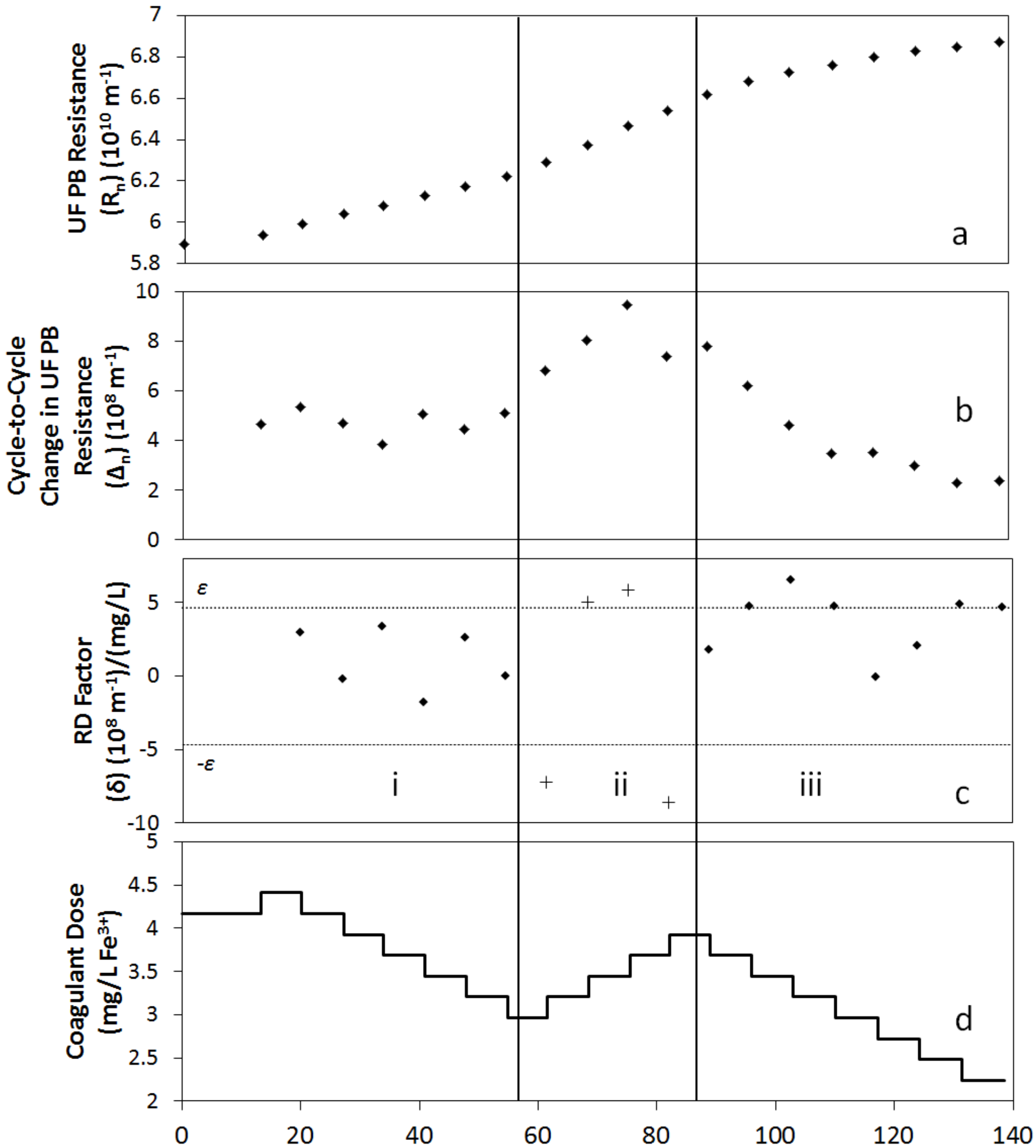

Figure 2-23 UF performance and coagulant controller response demonstrating self-Adaptive cycle-to-cycle control of in-line coagulant dosing (a) UF PB resistance, (b) cycle-to-cycle change in PB UF resistance (Δ_n), (c) Resistance Dose (RD) factor (δ) and (d) coagulant dose, in mg/L of Fe^{3+}. The controller gradually was increased in response to the rise of the change initial UF cycle resistance in period (ii). Adapted from [161].

2.8 Assessment of organic fouling and organic material passage through UF and RO membranes

Organic material passage through UF membranes is of concern because of the potential for fouling of the downstream RO membrane elements. Typical UF membrane can reject 40-70% of dissolved organic substance from the feed stream with the aid of coagulant [69, 70]. EPS (or Extracellular Polymeric Substances), defined as any dissolved or particulate macropolymer organic substances that are excreted by cell external to the membrane [162]. EPS has a high content of gelling agents such as mucopolysaccharides [162] that can be retained on membrane or filter. TEP (or Transparent Exopolymer Particles) are a subcategory of EPS. They are defined as discrete exopolymer particles (typically larger than 0.4μm) that stain with the cationic copper phthalocyanine dye (Alcian Blue) at pH of 2.5. Gel particles such as TEP are generally transparent unless stained by a specific dye. It has been shown that TEP are major contributor of EPS in early stages of RO biofouling [64] Currently, the most effective way of removing EPS from fouled membranes is via chemical cleaning using NaOCl in order to "dissolve" or disrupt the EPS structure. **Figure 2-24** shows TEP fouled RO membranes stained by Alcian blue. It has been shown that RO fouling due to organic material (e.g., TEP) passage through UF can be mitigated via optimal inline coagulation [163]. Also, TEP can be effectively removed by adsorption onto filters composed of nanoalumina fibers [66].

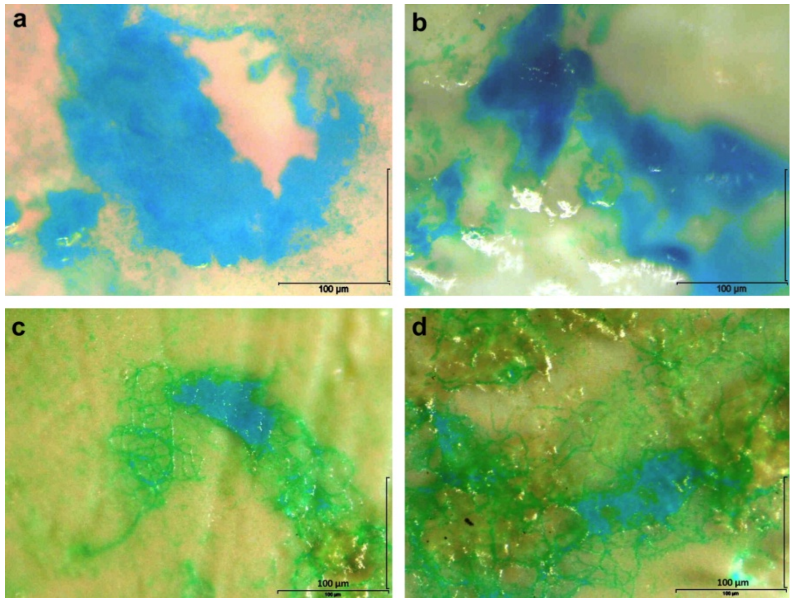

Figure 2-24 TEP detection on RO membrane samples. Visible green to blue color is due to staining using Alcian blue. Staining was done during RO membrane autopsy procedure. Feed water was surface lake water. Images from [70].

3 Self-Adaptive Feed Flow Reversal Operation of Reverse Osmosis Desalination

3.1 Overview

The feasibility evaluation of operating a spiral-wound RO plant in a cyclic mode of feed-flow reversal (FFR) was evaluated for brackish water desalting under conditions of high mineral scaling propensity. Scale-free and continuous permeate productivity was demonstrated, with calcium sulfate as the model scalant, in an automated spiral-wound RO pilot system in which FFR was triggered by scale detection in an external membrane monitor (MeM). Real-time detection of mineral scaling in an external RO membrane monitor (MeM) cell, receiving its feed from the concentrate of the RO plant tail element, enabled cyclic FFR operation in a self-adaptive mode accomplished by feed-back RO plant control in which permeate productivity was maintained. Membrane permeability was restored after each FFR cycle even with the initiation of membrane cleaning (i.e., via FFR) after measurable level of scale formation in the MeM and spiral-wound RO pilot. FFR cycle periods varied in length given the stochastic nature of crystal nucleation on the membranes in both the RO plant and in the MeM RO cell. Scale-free FFR operation was demonstrated, without anticalant addition, with the RO plant operating (up to 81% recovery) such that the gypsum saturation index was up to 3.45 at the tail membrane surface.

3.2 Experimental

3.2.1 Materials and model solutions

Model feed solutions (**Table 3-1**) were prepared using analytical grade calcium chloride dihydrate and anhydrous sodium sulfate (Fisher Scientific, ACS grade, Pittsburgh, PA) in deionized (DI) water, with the solution pH maintained at 7.4. The feed solution had a salinity of 1,779 mg/L total dissolved solids (TDS) and a gypsum ($CaSO_4 \cdot 2H_2O$) saturation index (SI_g) of 0.454. The solution was undersaturated with respect to gypsum to avoid bulk crystallization (**Table 3-1**) in the feed reservoir and in the piping network feeding the RO plant.

The membrane coupons had an active surface area of 26.9 cm^2, average water permeability of 1.56 L/($m^2 \cdot h \cdot bar$) and an observed salt rejection of 92.5% (at 25.8 bar). The spiral-wound membranes utilized in the RO system (Dow Filmtec XLE-2540, The Dow Chemical Company, Midland, MI) were 2.5 inch (outer diameter) elements and 40 inch long with an average surface area of 2.60 m^2. These membranes had water permeability of 4.57 ± 0.11 L/(m^2-h-bar) and an average observed rejection of 97.7% determined at 18.7 bar and 63% recovery for a 11,380 mg/L NaCl solution. Each membrane was loaded into a separate pressure vessel with six membranes connected in series. It is noted that for each set of experiments, newly conditioned flat sheet membrane coupons were used in the membrane surface mineral scale monitor.

Table 3-1 Composition and properties of the RO feed solution

Analytes	**Concentration**	
Ca^{2+}	10	mM
Na^{+}	20	mM

SO_4^{2-}	10	mM
Cl^-	20	mM
TDS (mg/L)	1,779	mg/L
SI_{gypsum} (at 25^{o}C)	0.454	
pH	7.6	

3.2.2 RO pilot system and mineral scale monitor

RO operation in FFR mode was investigated using the UCLA compact and modular (CoMRO) RO system [9, 43] having permeate production capacity of up to 1.2 m^3/h (7,560 gallons/day) for brackish water (5,000 mg/L TDS) operating at 75% recovery and up to 0.64 m^3/h (4,058 gallons/day) for seawater desalination (at recovery of 40%). However, in the configuration used in the present study only six spiral-wound elements (instead of the full capacity of 18 elements) were installed series (each housed in a separate pressure vessel); PV1-PV6 rated up to 68.9 bar (1,000 psi). The system was operated in a total recycle mode with the permeate and concentrate streams returned to the feed tank. A refrigerated recirculator (Model CFT-75 Neslab Instruments Inc. Newington, New Hampshire) was used (along with a 1.27 cm outer diameter cooling coil of 1.7 m linear length) to control the feed temperature to 25°C ±1°C.

Feed water to the RO unit from a 450 liters tank was first directed using low pressure intake pumps (Model JM3460-SRM, Sea Recovery, Carson, CA) through a sequence of cartridge microfilters (5 μm, 0.45 μm and 0.2 μm; 08P GIANT, pleated 177 polypropylene filter cartridges, Keystone Filter, Hatfield, PA). An inline turbidity meter (Micro TOL 20055, HF Scientific, Fort Myers, Florida) was used to monitor the stream exiting the feed pre-filtration system. The feed to the RO is then provided with two positive-displacement high pressure pumps (Danfoss Model CM 3559, 3HP, 3450RPM, Baldor Reliance Motor, Sea Recovery Corp.

Carson, California) controlled by variable frequency drives (VFDs) (Model FM50, TECO Fluxmaster, Round Rock, Texas). The feed and retentate pressures were monitored using two pressure transducers (0-1,000 psig, Model PX409-1.0KG10V Omega, Stamford, Connecticut). An electrically actuated needle valve (valve V-1) (model VA8V-7-0-10, ETI Systems, Carlsbad, California) on the retentate stream of the CoMRO RO system, along with the pump VFD, enabled the control of the retentate flow rate and pressure in the RO unit using a model-based controller [43].

Permeate and retentate streams of the CoMRO were also monitored with in-line via conductivity sensors, and conductivity/resistivity sensor electronics (Signet 2839 to 2842 and Signet 2850, George Fischer Signet, Inc. El Monte, California) and pH sensor (DryLoc pH electrodes 2775, George Fischer Signet, Inc. El Monte, California). Real-time calcium ion concentration in the concentrate stream, for the present feed solution, was determined by correlating calcium ion concentration with the measured conductivity of the RO concentrate, based on simulation results from a multi-electrolyte thermodynamic simulator [164]:

$$[Ca^{2+}] = \left(\frac{EC}{150.7}\right)^{1.265} \tag{3-1}$$

$$SI_g = 59.77[Ca^{2+}] - 0.1289 \tag{3-2}$$

in which EC is the solution conductivity (mS), $[Ca^{2+}]$ is the calcium ion concentration (M), and SI_g is the gypsum saturation index. The above correlations is applicable to the SI range of 0.48 – 5.12 for a calcium ion concentration range of 15 – 80 mM, which covers the range relevant in the present study.

Feed flow reversal through the feed/retentate channel of the RO membranes was facilitated via a series of direct acting two-way solenoid valves (GC valves model HS4GF15A24GC, Simi

Valley, California) (**Fig. 3-1**). The solenoid valve network (valves V-5, V-6, V-7, and V-8) controlled the direction of the feed water flow to allow for feed channel flow reversal. The valve configurations for the normal feed flow (NFF) and FFR modes are provided in **Table 3-2** and details of the operation were provided in **Section 3.2.3.** FFR was triggered by a preset scaling threshold in the MeM scale monitoring system (**Fig. 3-2**). The MeM PFRO cell received as its feed the RO retentate (i.e., concentrate) from the high-pressure side stream (upstream from the retentate valve) of the RO CoMRO system (**Fig. 3-1**), on the exit side of its last (sixth) pressure vessel (PV6 during NFF and PV6 during FFR).

The MeM system was equipped with a semi-transparent plate-and-frame RO (PFRO) flow cell with an optical window and a microscope interfaced with a high resolution digital camera. The active membrane area was 8.1 cm × 3.16 cm with a 0.254 cm feed channel height. Selected areas of the membrane or the entire membrane coupon can be imaged aided with near dark-field illumination to provide high contrast imaging of surface crystals. For the purpose of FFR triggering the imaged area of the membrane monitoring (MeM) flow cell (1.3 cm × 0.95 cm) was set 0.32 cm away from the center line of the viewing window and 6.5 cm downstream from the feed inlet to avoid areas of diminished mass transfer and recirculation eddies [45, 109]. The inlet pressure to the MeM flow cell was monitored by a pressure transducer (PX 303-500G5V Omega, Stamford, Connecticut) and the permeate flow rate was measured using a digital flow meter (Model 1000, Fisher Scientific, Pittsburgh, Pennsylvania). Feed and permeate conductivities were monitored with an on-line conductivity meter (Model WD-35607-30, Oakton Research, Vernon Hills, Illinois). Additional details of the MeM system are provided elsewhere [43, 105].

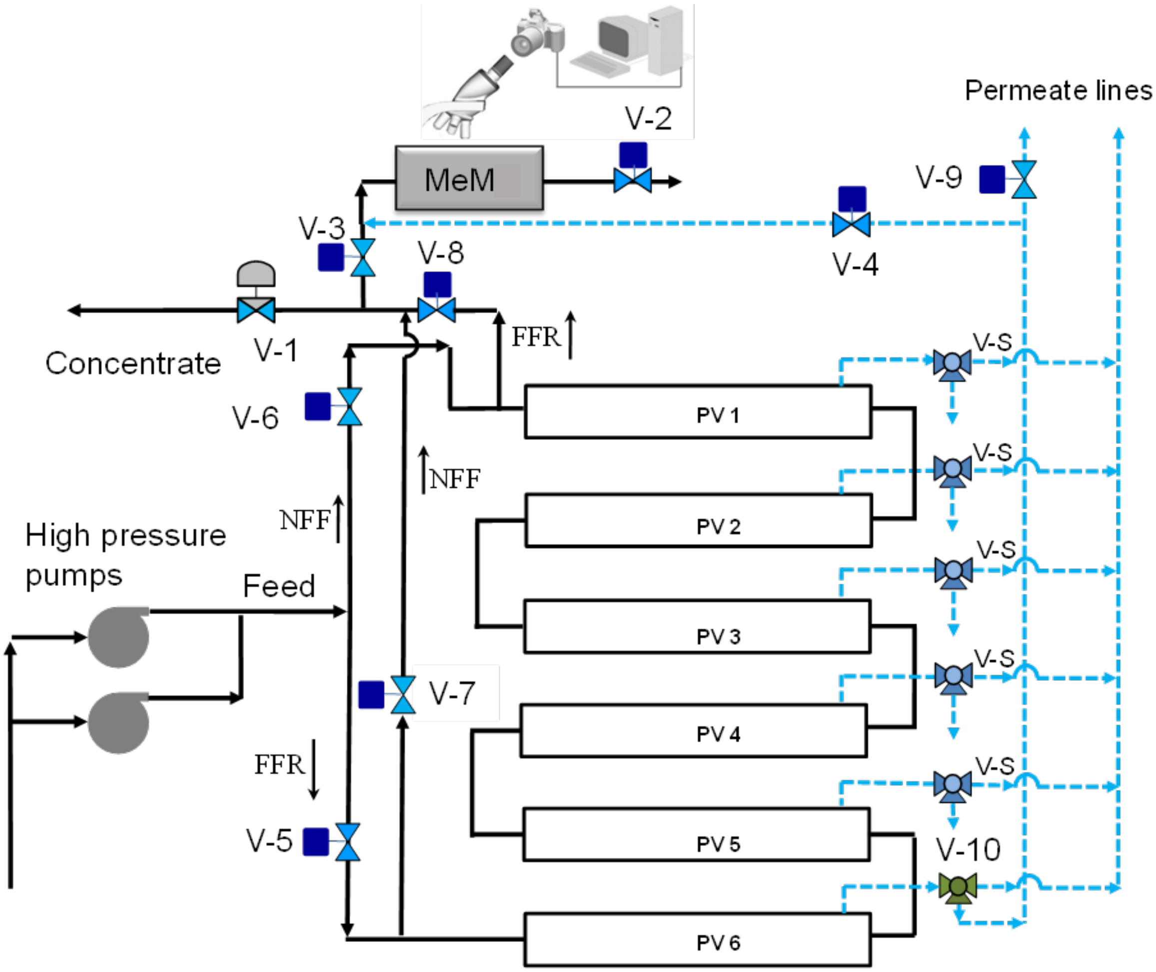

Figure 3-1 Schematic diagram of the CoMRO–MeM flow reversal system showing the location and arrangement of actuated valves, pressure vessels and permeate collection network (dashed lines). NFF and FFR represent normal feed flow and feed flow reversal direction, respectively, with the arrows indicating the corresponding flow directions. (Note: permeate sampling valves are labeled as V-S).

Table 3-2 Valve configuration during RO system operation in normal feed flow and feed flow reversal[(a)]

	V-1	V-2	V-3	V-4	V-5	V-6	V-7	V-8	V-9
Normal Feed Flow	Unchanged	MeM NFF setting	MeM NFF setting	Closed	Open	Closed	Closed	Open	Open
Feed Flow Reversal	Unchanged	MeM cleaning setting	MeM cleaning setting	Open	Closed	Open	Open	Closed	Closed

Note: valves V-4 and V-10 are open when the MeM undergoes cleaning with permeate water (**Fig. 3-1**); (a) Valves V-1, V-2, and V-3 are actuated control valves and are not adjusted during transition between NFF and FFR modes

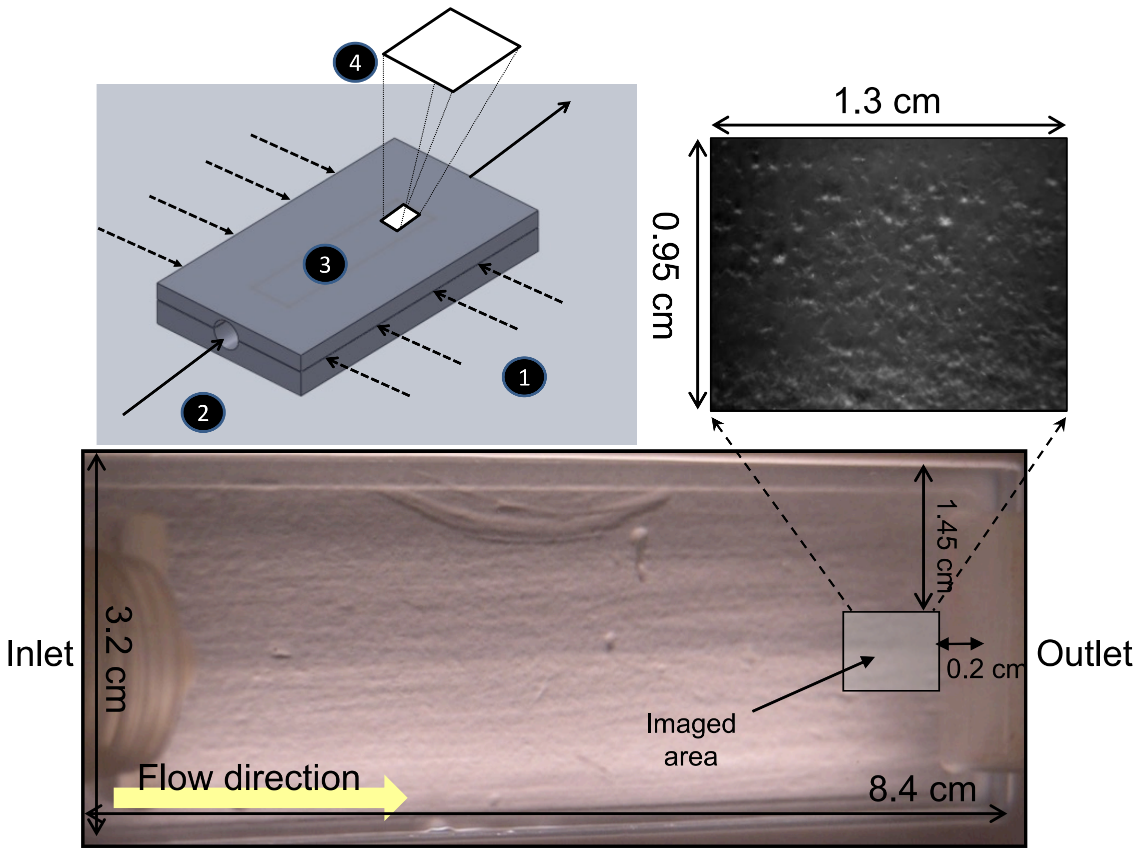

Figure 3-2 Membrane monitor (MeM) cell: 1) Incident light, 2) Feed water stream inlet, 3) Membrane coupon. An example of a scaled image of a small portion of a monitored location near the exit region of the RO cell is shown above the expanded image of the membrane coupon in the MeM cell (adapted from [165]).

The MeM membrane surface was continuously monitored with images recorded at regular time intervals (typically 5 minutes) and subsequently analyzed (online) using specially developed automated image analysis software [26, 165]. Images were analyzed for the fractional mineral scale surface coverage and the crystals count in the observation area [165]. Once the surface scale coverage (or number of crystals) reached the specified threshold value (**Fig. 3-3**), a signal (analog or digital) was transmitted to the RO control system to initiate the FFR mode of operation and MeM cleaning in preparation for scale monitoring in the subsequent

NFF cycle. After a specified period of operation in the FFR mode (**Fig. 3-3**, typically 5 minutes less than the NFF period; [165]), the flow is again reversed to the NFF mode.

Gypsum saturation level at the MeM membrane surface, $SI_{gm,}$ was calculated for the given flow conditions (pressure, inlet velocity, and salinity) from the CP modulus (i.e., $CP=C_m/C_b$, where C_m and C_b are the concentrations at the membrane surface and in the bulk of the flow channel, respectively) for the cell geometry. The CP profile was determined using a previously developed numerical 3-D computational fluid dynamic (CFD) model for the MeM cell geometry [109]. The feed flow rate and transmembrane pressure in the MeM cell were adjusted so as to set the desired SI_{gm} level at the membrane surface relative to the SI_{gm} in the tail spiral wound element (membrane surface at the exit region) in the CoMRO system. Concentrations of the scaling species at the membrane surface in the CoMRO RO tail element were estimated based on the ROSA software [166] approach, where the CP modulus was determined from CP = C_m/C_b = $e^{[k\cdot 2Y/(2-Y)]}$, where Y is the recovery for the spiral wound RO element, k is a proportionality constant that depends primarily on membrane element length (taken to be 0.7 for the 40 inch spiral wound elements used in this study), and C_m and C_b are the concentrations at the membrane surface and in the bulk of the feed channel, respectively [167, 168].

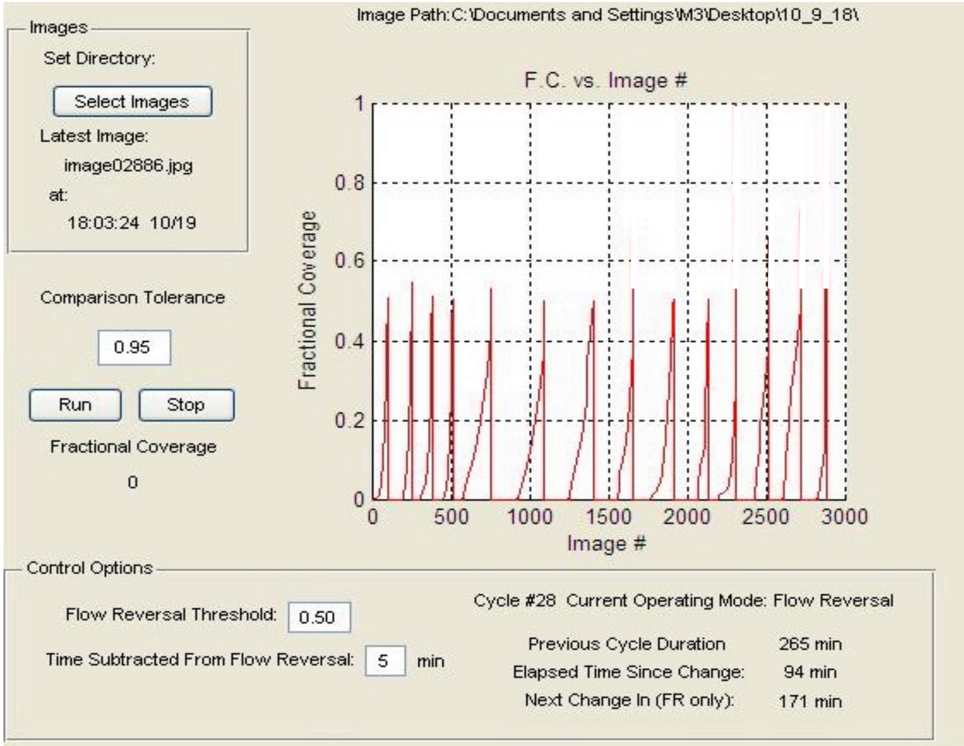

Figure 3-3 Screenshot of the user interface of the online image tracking software during the multi-cycle FFR operation (Test #2) showing the calculated fractional surface scale coverage. The Run and Stop buttons initiate and stop, respectively, the online image analysis program. Control Options include: Flow Reversal Threshold indicates (pre-set fractional coverage for triggering flow reversal), time for NFF (i.e., FFR time reduced by "time subtracted from flow reversal").

3.2.3 Self-adaptive feed flow reversal operation of RO system

In normal feed flow (NFF) (i.e., flow from PV1 to PV6), valves V-5 and V-8 are open, while valves V-4, V-6, and V-7 are closed (**Table 3-2** and **Fig. 3-1**). During this period, the MeM system is at a scale-detection mode and where it is fed with a side stream of RO concentrate from the tail element. It is noted that the pressure and flow rate for the MeM cell feed are adjusted with the aids of valves V-2 and V-3. During the subsequent FFR operation (i.e., feed flow from PV6 to PV1), valves V-4, V-6 and V-7 are open while valves V-5 and V-8 are closed. In this mode, the MeM system is cleaned (i.e., mineral crystals are dissolved) by low pressure permeate water produced by the lead element of the CoMRO system (typically at permeate cross flow rate of ~10 cm/s and pressure~ 0.345 bar). The process of switching from NFF to FFR mode is completed within ~2 seconds after the control system receives the triggering signal. A proportional integral (PI) controller is utilized in the CoMRO system to adjust the retentate valve position (V-1) in order to maintain the feed pressure after the switching of the solenoid valves (**Table 3-2**) to the FFR configuration (and also when switching from FFR back to NFF mode).

Automated RO desalting operation in FFR mode was demonstrated via three distinct operational scenarios (**Table 3-3**) using the spiral-wound COMRO RO pilot plant[105]. In all cases the feed solution was undersaturated with respect to gypsum while being oversaturated (SI_{gm} = 2.74–3.65) at the membrane surface for both the COMRO tail element and at the MeM RO cell. In the first test, the COMRO was operated in normal feed flow at an initial water recovery level of 69% ($SI_{gm,\ COMRO}$ = 2.74). Mineral scaling was monitored with the MeM with the initial conditions set such that $SI_{gm,MeM}$ = 2.87. In this operational scenario the MeM was operated at just slightly above the saturation level encountered in the COMRO tail element (**Table 3-3**); this enabled evaluation of early scale detection relative to the monitored overall and tail element flux decline in the COMRO plant. This test also served to establish a reasonable mineral scaling threshold (in the MeM cell) for triggering the RO plant switch from NFF to FFR mode of operation. At the termination of the above test, the COMRO system was cleaned by pumping DI water in both the forward and reverse directions. Complete scale removal (i.e., permeate flow rate recovered to its original level, and no scale observed within viewable area in the MeM cell) was achieved after 1.5 h.

FFR evaluation in the second test was carried out over a period of 88 hours with the COMRO plant product water recovery set at 69%. The level of gypsum supersaturation at the membrane surface was set as in the first test (**Table 3-3**) with the scaling threshold in the MeM (for triggering FFR) set to surface scale coverage of about 50%; this scaling threshold was equivalent to about 5% flux decline in the COMRO tail element as evaluated from the test without FFR (i.e., Test 1, **Table 3-3**). The membrane cleaning efficiency (i.e., removal of surface scale) via the cyclic FFR process was determined based on the percent flux recovery for the tail element (F_R), at the same initial transmembrane pressure, calculated as $F_R = F_i/F_o$, where F_i and F_o are the normalized permeate flux values at the end of the previous NFF period and the beginning of the cycle (or 1st cycle) for each FFR cycle.

In the subsequent FFR evaluation (Test 3, **Table 3-3**), the COMRO pilot system was operated for a period of 80 hours at a higher water recovery of 81% and thus a higher gypsum saturation index ($SI_{gm,COMRO}$ = 3.45) at the membrane surface of the tail element. For this test, the MeM cell was operated such that $SI_{gm,MeM}$ = 3.65 and the scaling threshold for FFR triggering was increased to 65% surface area scale coverage. The purpose of above scenario was to evaluate the impact of a less stringent FFR triggering threshold on the FFR cycle time and permeate flux recovery.

Table 3-3 Experimental conditions for gypsum RO membrane scaling experiments

Test	COMRO RO system transmembrane pressure in bar (psi)	CoMRO system recovery (%)	Gypsum Saturation Index			FFR triggering threshold (% Surface coverage)	Duration (h)
			Feed (bulk)	COM RO$^{(b)}$	MeM$^{(b)}$		
#1$^{(a)}$	11.6 (168)	69.1	0.44	2.74	2.87	None	4
#2	11.6 (168)	69.1	0.44	2.76	2.87	50	88
#3	13.6 (197)	81.1	0.37	3.45	3.65	65	80

$^{(a)}$ Operation without feed flow reversal; (b) Initial gypsum saturation indices at the membrane surfaces for the CoMRO tail element and for the MeM RO cell.

3.3 Results and Discussion

3.3.1 Evaluation of early scale detection in the CoMRO plant

Adequacy of the MeM scale monitoring for early detection of the onset of mineral scaling in the RO pilot plant was first assessed in Test #1 (**Table 3-3**). The CoMRO operated at 69% recovery such that the level of gypsum saturation at the membrane surface of the CoMRO tail element was above the saturation (SI_{gm} = 2.74). Surface scaling was observed in the MeM cell with rapid buildup of mineral scale in the monitored area (**Figs. 3-4a and 3-4b**) reaching about 100% in 1.5 hours. During the same period the total COMRO permeate flow did not reveal significant flux decline with only up to ~4% flux decline over the 4 h period of Test #1, while significant flux decline was observed for both the CoMRO tail element (PV6) and for the MeM cell. Flux decline for the MeM and for the CoMRO tail element paralleled each other (**Fig. 3-4a**) until a period of 2 hours. At t>2 h, flux decline for the MeM was greater relative to the CoMRO tail element; this was expected since the $SI_{g,m}$ at the MeM was greater than for the CoMRO tail element (**Table 3-3**). With the $SI_{g,m}$ at the MeM being only ~5% above that in the CoMRO system ($SI_{g,m}$ = 2.74), a surface scale coverage of 50% was detected (in the MeM monitored zone) when the CoMRO tail element flux declined by only 5%, with essentially no detectable overall flux decline for the RO pilot. The percent of surface scale coverage in the MeM observation region (**Figs. 3-4a** and **3-4b**) increased to 100% once about 47% flux decline was reached for the tail element. It is noted that only a small portion of the MeM membrane surface (**Section 3.2.2**) was monitored near the membrane exit region; thus, the percent scaled area is significantly higher in this region of higher CP [109] relative to upstream regions of the membrane coupon. Therefore, setting the MeM operation to a level of supersaturation just slightly above that of the tail element was adequate for mimicking the scaling trend in the tail element, thereby enabling early scale detection.

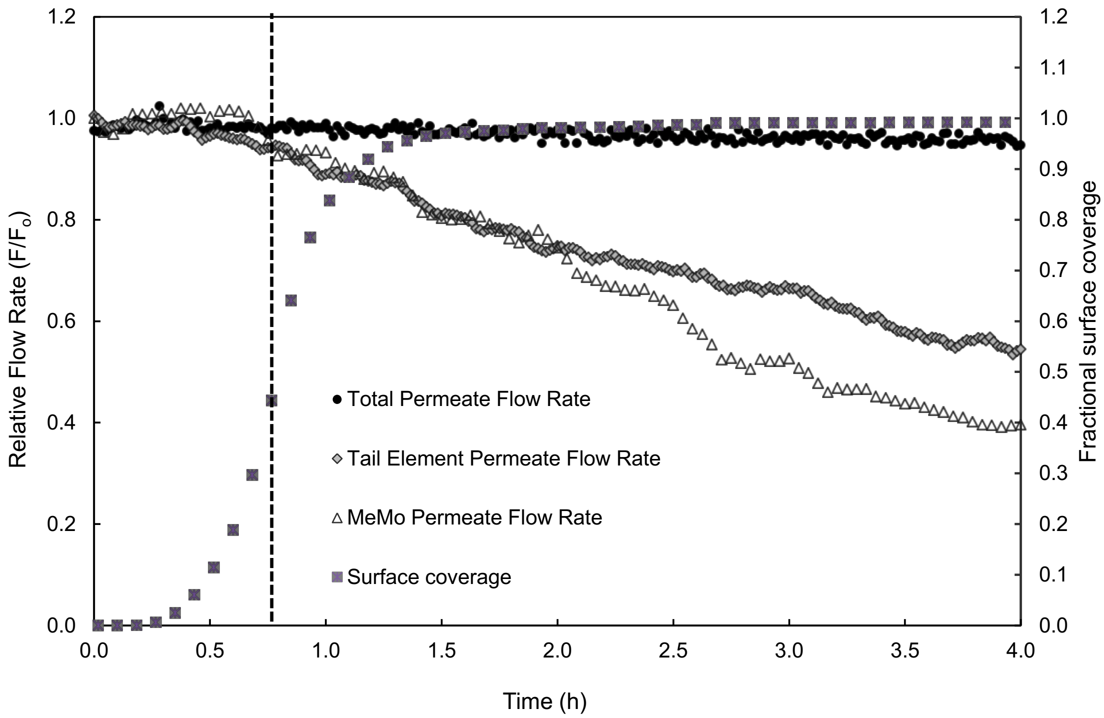

(a)

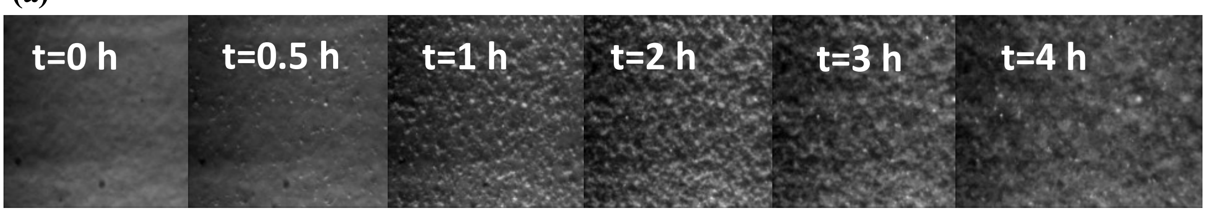

(b)

Figure 3-4 (a) CoMRO operation at 69% recovery, with MeM scale monitoring, in normal feed flow (Test 1; Table 3-3) under mineral scaling conditions, showing the relative permeate flow rates (total and PV6 tail element for the COMRO system and for the MeM cell) along with crystal surface coverage in the MeM cell. (F_o= 6.59, 0.477 and $0.27\text{x}10^{-3}$ L/min for the total COMRO, PV6 and MeM, respectively). The vertical dashed line indicates the time at which the surface coverage in the MeM cell reached 50%. (b) Selected membrane surface images in the monitored area of the MeM cell.

In principle, one could in principle utilize a MeM flux decline threshold for triggering FFR. However, setting of FFR initiation based on direct observation of scaling on the membrane surface would be attained at a higher level of sensitivity, in addition to verifying that FFR triggering is indeed due to membrane scaling. It is also possible to utilize a crystal count density to establish a trigger for FFR since the surface area and crystal count density are correlated as shown in **Fig. 3-5.** Temperature and feed water composition, however, may affect the rate of crystal nucleation as well as crystal growth. Therefore, different levels of surface scale coverage can result for the same crystal number density on the membrane surface. Surface scale coverage is known to closely correlate with flux decline [22] and thus it is more reliable to set a threshold for FFR triggering based on scaled area.

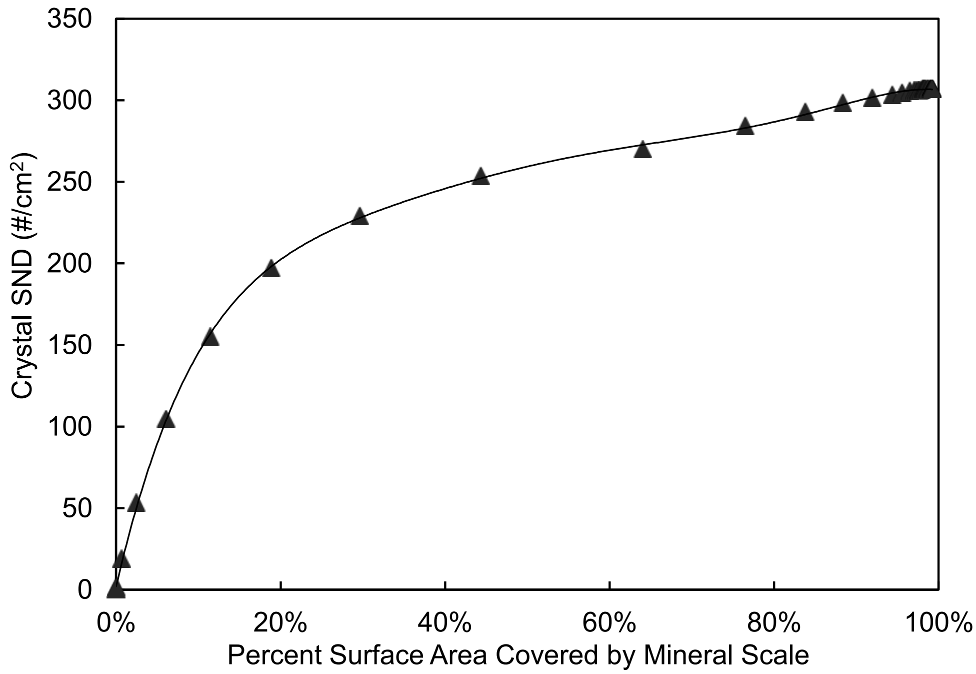

Figure 3-5 Correlation of crystal site number density (SND) with the percent mineral scale coverage in the MeM viewing area for Test #1 (CoMRO operation at 69% recovery, SI_{gm} =2.74, Table 3-3).

3.3.2 Self-adaptive multi-cycle FFR operation

The reliability of the MeM system for mineral scale detection and triggering of FFR was evaluated in Test #2 (**Table 3-3**) with the CoMRO system also operating at 69% recovery (overall permeate productivity of 353 L/h). The MeM scaling threshold for FFR triggering was set to 50% surface scale coverage, which resulted in 15 FFR cycles over the 88 h test period (**Fig. 3-6**). The repeated FFR cycles show that permeate flux for PV6 was higher when it was the lead element (i.e., FFR operation) and lower when it was the tail element (NFF operation). Since the osmotic pressure of the feed water is below that of the RO concentrate, the lower osmotic pressure of the feed to PV6, during each period of FFR, resulted in a sharp permeate flux increase to ~28.0 – 28.4 L/h·m^2 (**Fig. 3-7** - top permeate flux curves). Since PV6 alternated between being the lead (in FFR mode) and tail (in NFF mode) element, permeate quality from this element correspondingly varied from 330 – 590 mg/L TDS to 50 – 230 mg/L TDS in the NFF and FFR modes, respectively. Overall, however, permeate produced by the COMRO system was in the range of 210 – 310 mg/L TDS for both the NFF and FFR modes.

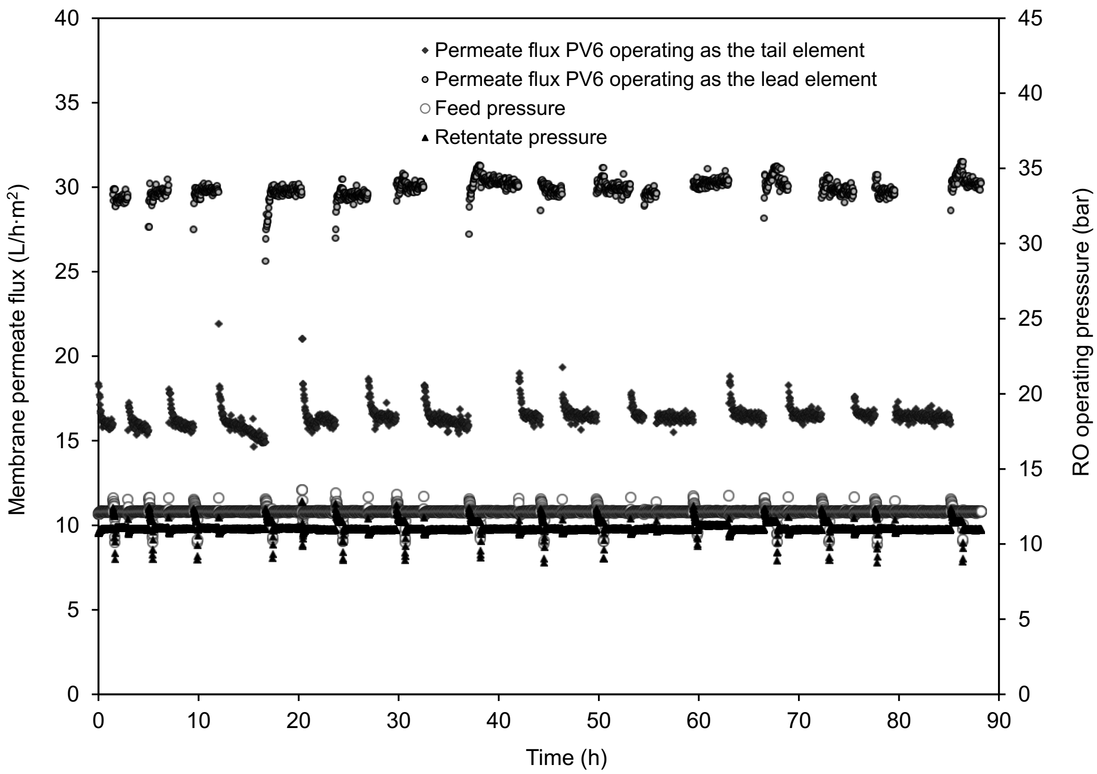

Figure 3-6 Tail membrane element permeate flux (normalized w.r.t pressure) during feed flow reversal and system feed pressure over the course of a multi-cycle FFR test (Test #2, CoMRO operation at 69% recovery, SI_{gm} =2.76; **Table 3-3**). The lower permeate flux time profiles are for PV6 operating as the lead element in normal feed flow (NFF), while the lower permeate flux profiles are for PV6 as the tail element in FFR.

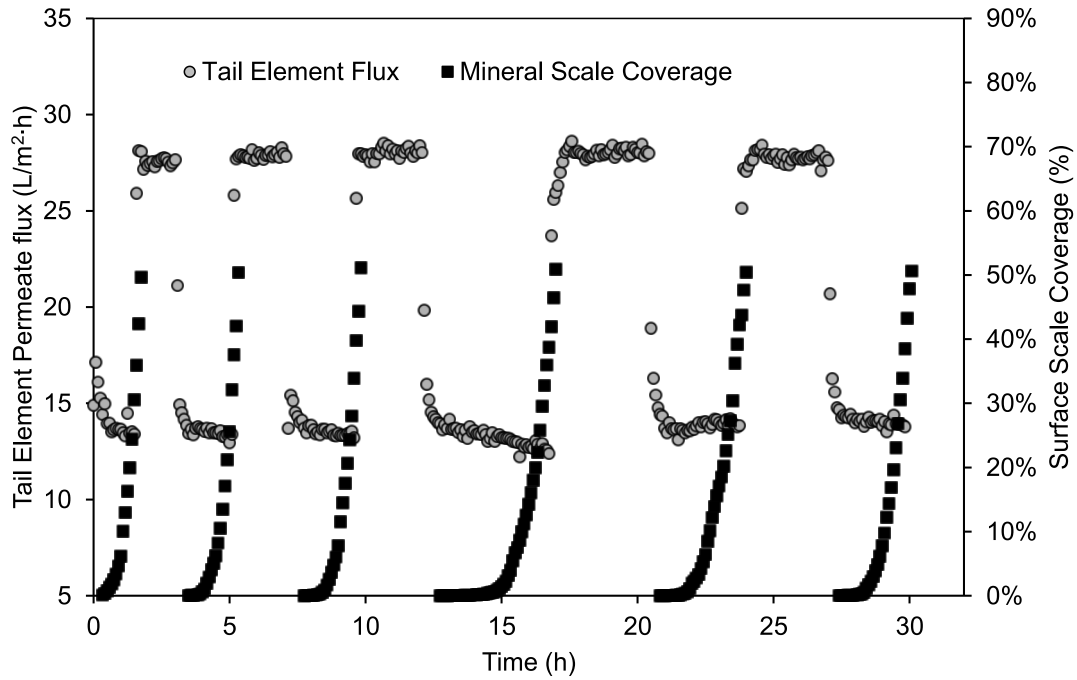

Figure 3-7 Tail element (PV6) permeate flux (normalized w.r.t pressure) and percent mineral surface scale coverage (in the monitored area of the MeM cell) for Test #2 (CoMRO operating at 69% recovery, SI_{gm} =2.76; Table 3-3). The lower permeate curves designate the forward flow operation (i.e. flux of membrane element in PV6) while the top permeate flux curves denote the flow reversal operation (i.e. flux of membrane element in PV1).

A cyclic pattern of mineral scaling was suggested by flux decline and recovery indicated by the initial flux post FFR for each new NFF cycle (**Fig. 3-6**). A more detailed view is provided in **Fig. 3-7** which also shows the progression of scale coverage in the MeM RO cell, along with the FFR cycle duration tracked by the COMRO control system (**Fig. 3-3**). During periods of NFF operation, the normalized permeate flux from the tail element ranged from 18.2 to 17.9 L/h·m^2 at the beginning of the cycles and decreased to values ranging from 16.2 to 14.7 L/h·m^2 (depending on the cycle length). The relatively low level of permeate flux decline (about 6 – 13%), during each operational period in the forward flow direction, indicated that membrane mineral scaling began to occur in the COMRO tail membrane element just before triggering of feed flow reversal. In FFR mode, PV6 which was previously the tail element (when operating in NFF mode) became the lead RO element being exposed to the RO feed water. Toward the end of each FFR period permeate flux from the lead element increased slightly from ~27 – 28.5 L/h·m^2 to ~29 – 30 L/h·m^2. This permeate flux increase is indicative of gypsum crystal dissolution (from PV6 which was previously scaled in the NFF operational period) due to exposure of the PV6 membrane surface to the gypsum undersaturated feed water. As the feed flow reverted to the forward direction (NFF), permeate flux for PV6 (lead element in FFR) recovered toward its initial tail element value at the beginning of the new NFF period (29.1 – 30.2 L/h·m^2). Except for one cycle (#11), permeate flux recovery (based on PV6) was always restored to within 5% of the initial permeate flux which was set as that measured at the beginning of the test (**Fig. 3-8**). Overall, within the accuracy of permeate flux measurements, the cyclic CoMRO system operation was robust without persistent flux decline due to scaling.

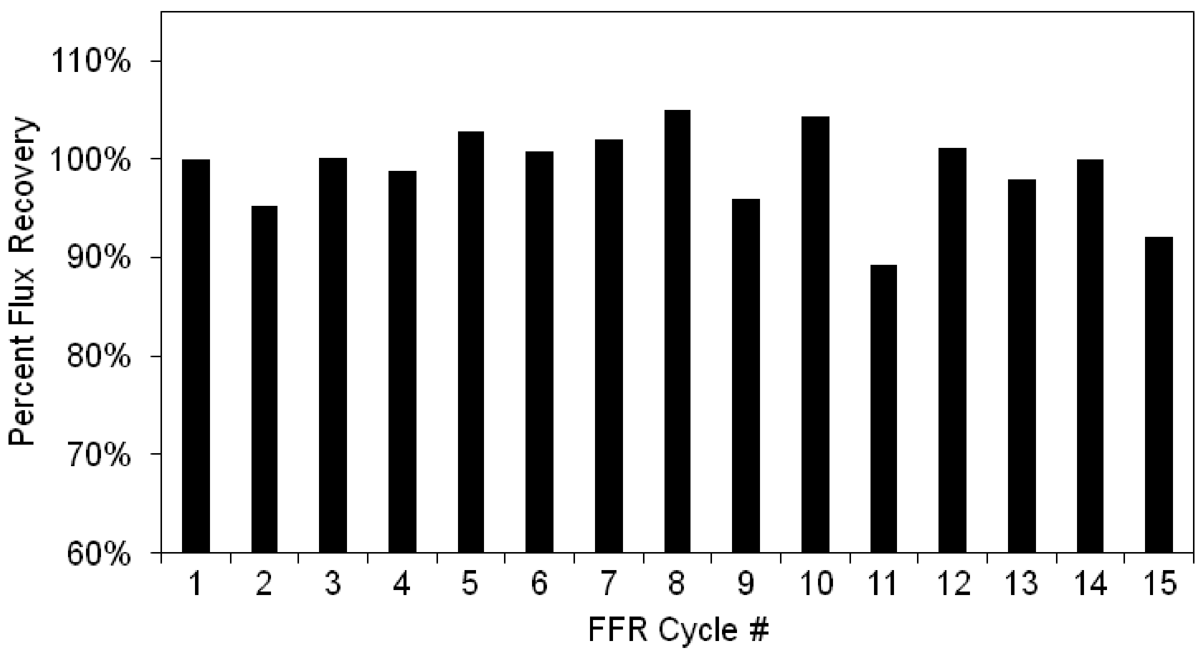

Figure 3-8 Percent recovery for the tail element (PV6) permeate flux for the series of FFR cycles for Test #2 (69% recovery for period of 88 h, SI_{gm} =2.76; Table 3-3).

3.3.3 FFR cycle period and frequency

The FFR cycle time, defined as the sum of the NFF and FFR operating times, varied in Test #2 (**Table 3-3**) from about 3 to 11 hours (the average being 5.58 ± 3.76 h). Variability of the FFR cycle times should be expected since mineral salt nucleation on the membrane surface is a stochastic process [22, 27]. Therefore, the rate of nucleation and seeding of crystals on the membrane surface can vary to some degree even for the same level of solution supersaturation. The above range of cycle period is reasonable as infrequent FFR triggering could lead to rapid progressive membrane scaling and thus loss of performance. Conversely, too frequent FFR triggering may result in pressure fluctuations that are difficult to control in addition to potential increase of valve maintenance cost due to heavy "duty cycle". From a practical viewpoint, variability of the triggering time for each FFR cycle highlights the importance of incorporating feedback control [43, 169]. It also indicates that setting a fixed predetermined triggering time interval for a long-term desalting operation could result in FFR triggering that may occur prematurely or too late. Overall, Test #2 demonstrated that self-adaptive FFR can be effective in mitigating membrane mineral scaling under scaling operating conditions (**Table 3-3**, SI_{gm}= 2.74 for the CoMRO) without antiscalant dosing (**Fig. 3-9**).

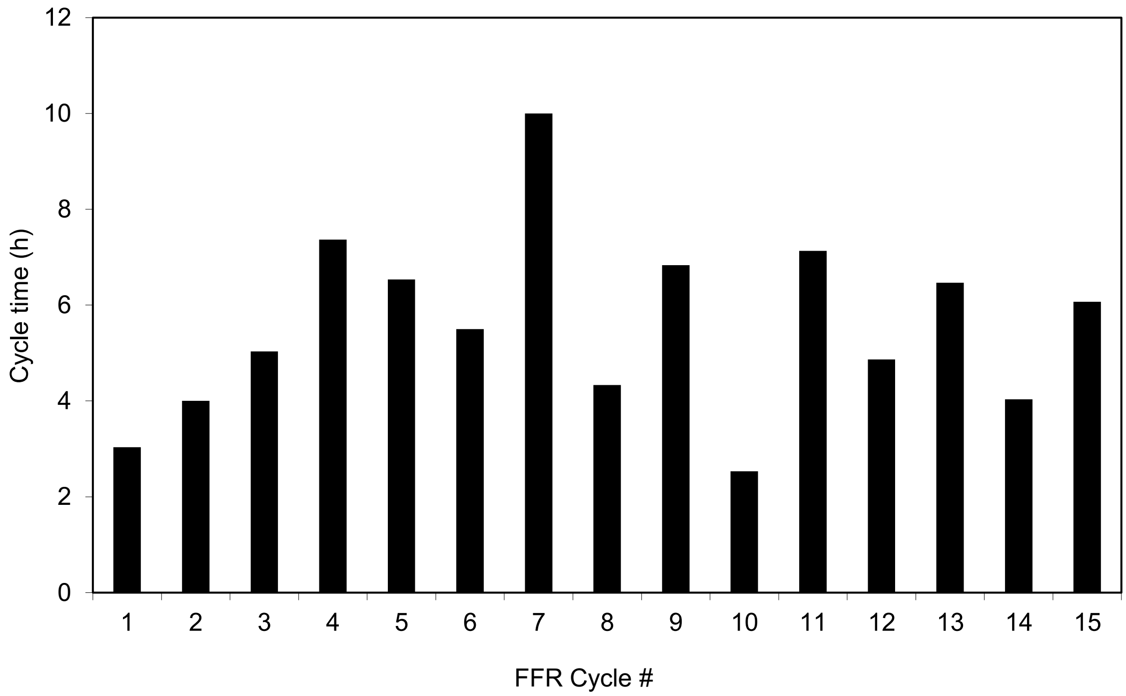

Figure 3-9 FFR Cell cycle periods over the course of Test #2 (CoMRO operation at 69% recovery for 88 h, SI_{gm} =2.76; **Table 3-3**) demonstrating variability of FFR cycle times due the stochastic nature of mineral scaling.

3.3.4 Self-Adaptive FFR at high RO recovery

In order to further evaluate the feasibility of self-adaptive FFR operation at a higher recovery level, and thus greater mineral scaling propensity, the CoMRO pilot was operated at 81% recovery in Test #3. The gypsum saturation index at the membrane surface was 3.45, which is even above the level typically recommended for antiscalant dosing for gypsum scale suppression [166, 167]. At this higher SI_{gm}, the FFR scaling threshold (set in the MeM RO cell) was increased from 50% to 65% surface area scale coverage in the MeM observation zone. The MeM operating conditions were then set to attain $SI_{g,m}$=3.65 (in the observation zone) which was higher by ~6% than in the spiral-wound tail element. The self-adaptive 80 h operation of Test #3 resulted in five cycles (**Figs. 3-10** and **3-11**) with a cycle time of 17.43 ± 8.25 h (**Fig. 3-11**), which (as expected) was significantly higher than in Test #2. The normalized flux for elements PV1 and PV6 (which alternated as being either the lead or tail element; **Fig. 3-10**) indicates repeated cycles where the initial flux of these elements PV6 was recovered (as observed by the initial flux of their respective NFF cycles). The initial tail element permeate flux for PV1 returned to 14.6 – 15.0 L/h·m^2 while the initial tail permeate flux for membrane element in PV 6 returned to flux values of 14.3 – 15.2 L/h·m^2. The initial permeate flux of PV1, when operating as the lead element after each FFR cycle, recovered to ~33 L/h·m^2 while the initial permeate flux for PV6 recovered to 32 – 33 L/h·m^2 when operating as the lead element. The normalized tail permeate flux recovery for PV6 was 98.3% ± 2.4% which was an excellent level of performance considering the fact that the FFR cycles were long. It is noted that FFR triggering was less aggressive than in Test #2 for which the FFR cycles were on the average about a factor of two shorter than in Test #3.

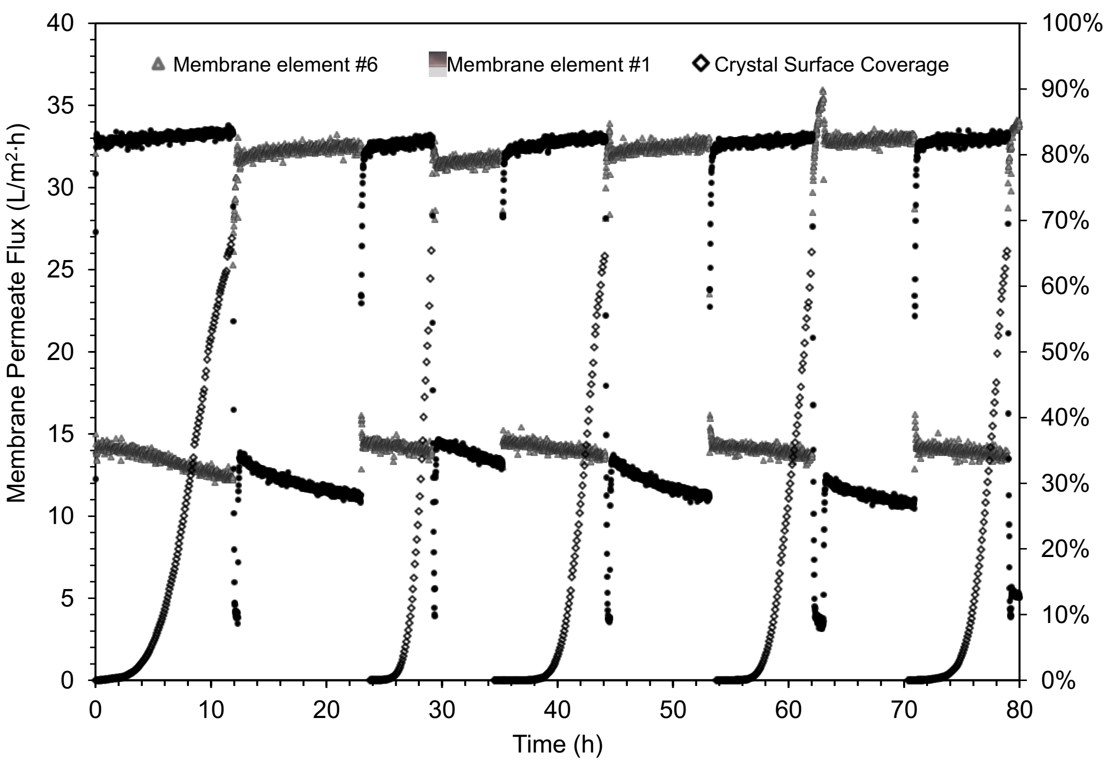

Figure 3-10 Permeate flux (normalized) for membrane elements PV1 and PV6 during NFF and FFR periods, along with percent surface crystal coverage in the MeM cell monitored area (CoMRO operation at 81% recovery with SI_{gm} =3.45, with the FFR trigger set to 65% surface scale coverage in the MeM monitored area, Test # 3, **Table 3-3**).

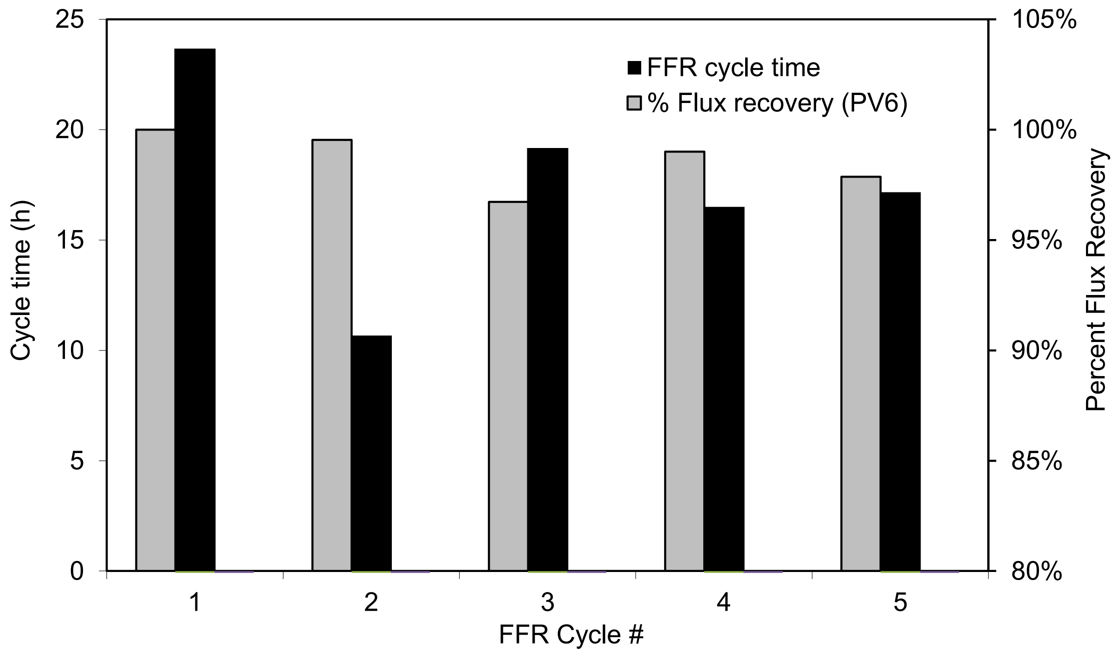

Figure 3-11 FFR Cell cycle periods for Test #3 (CoMRO operating at 81% recovery for 80 h, with the FFR trigger set to 65% surface scale coverage in the MeM monitored area, Test # 3, **Table 3-3**) demonstrating variability of FFR cycle times due the stochastic nature of mineral scaling.

The present study demonstrated that self-adaptive operation of a spiral-wound RO plant, under conditions of high mineral scaling propensity, is technically feasible with the use of advanced mineral scale monitoring and integrated RO FFR plant control. Given that water feed quality may vary (over time), with respect to the concentration of sparingly water soluble mineral salts, self-adaptive FFR operation is essential for scale-free RO plant operation. Although the present study demonstrated that FFR can be effective without antiscalant use, there is merit in exploring FFR operation even with antiscalants use to reduce antiscalant dosage and thus allow higher level of recovery. Admittedly, long-term pilot testing will be required to assess the reliability of the approach under field conditions when scaling can be due to multiplicity of different mineral scalants.

3.4 Conclusions

The technical feasibility of operating a spiral-wound RO desalting process in a cyclic mode of feed-flow reversal (FFR) was evaluated using an automated RO pilot system interfaced with an online external membrane monitor (MeM). Real time detection of mineral scaling enabled self-adaptive FFR operation which was accomplished by feed-back control with FFR triggering based on a threshold level of mineral scaling in the MeM RO cell. Cyclic FFR RO operation at a high permeate product recovery, under conditions of gypsum supersaturation at the membrane surface, was feasible without antiscalant addition while achieving effective scale mitigation without interruption of permeate productivity. FFR operation of spiral-wound RO plant was effective even with the initiation of membrane cleaning (i.e., via FFR) after measurable level of scale formation in the MeM and spiral-wound pilot. Variations in the length of FFR cycles were encountered and attributed to the stochastic nature of crystal nucleation on the membrane surface demonstrating the need for real-time feedback control. Although the adoption of FFR for scale-free RO plant operation is appealing, there are a number of key issues that need to be addressed via systematic studies including: (a) resilience and performance of the membranes in the RO plant and the MeM cell when subjected to extended multi-cycle FFR operation of scaling and scale dissolution; (b) FFR effectiveness under field conditions involving multiplicity of different mineral scalants; and (c) feed-back control of FFR with added redundancy (in the event of failure of online MeM membrane surface image analysis) to allow for triggering of FFR based on permeate flux decline monitoring from both the tail element and the MeM cell.

4 Ultrafiltration with Self-Generated RO Concentrate Pulse Backwash in a Novel Integrated Seawater Desalination UF-RO System

4.1 Overview

A systematic investigation was undertaken of the operability and effectiveness of UF pulse backwash for seawater desalination using an integrated UF-RO system. Direct supply of RO concentrate to the UF module served for UF backwash which was further enhanced with pulse backwash generated using bladder-type hydraulic accumulators. In the first phase of the study the operability of hydraulic accumulator was evaluated using an accumulator charging/discharging model, along with a series of field tests with a directly integrated seawater UF/RO desalination system. Moreover, pulse backwash over a short period (~5 s) which was added to the continuous UF backwash (directly from the RO brine stream), enabled peak UF backwash flux that was up to a factor of 4.2 - 4.6 higher than the normal filtration flux. The above UF pulse backwash analysis served to fine-tune the pulse backwash strategy and assess the benefit of multiple consecutive backwash pulses, while also exploring the benefit of inline coagulation. Subsequently, self-adaptive triggering of UF backwash that combined continuous and multiple UF backwash pulses was evaluated over long-term field operation for eight days. Self-adaptive triggering of UF backwash, whereby the number of consecutive pulses increased when a higher membrane fouling resistance was encountered, was highly effective enabling stable UF operation over a wider range of water quality conditions and without the need for chemical cleaning. These encouraging results suggest that direct UF-RO integration with enhanced pulse UF backwash is an effective approach for dead-end UF filtration without sacrificing water productivity.

4.2 Experimental

4.2.1 Integrated UF-RO Pulse Backwash System

Field studies of UF pulsed backwash were conducted using a seawater UF-RO desalination pilot plant consisted of UF and RO skids integrated as shown schematically in **Fig. 4-1** and described in detail elsewhere [147, 170, 171]. Briefly, the plant was designed with water feed capacity of up to 129.1 m^3/day (i.e., 34,116 gal/day) and permeate product water production of up to 45.2 m^3/day at 35% feed water recovery. The RO unit consisted of three spiral-wound RO elements (Dow Filmtec SW30HRLE-400, The Dow Chemical Company, Midland, MI) each being 8''x 40'' (20.3 cm x 101.6 cm) in size, having a surface area of 37 m^2 per element. The UF system consisted of a skid of three hollow-fiber (inside-out) UF modules (Dizzer 5000+, Inge, Greifenberg, Germany) in parallel. The multi-bore PES (polyethersulfone) hollow fiber UF modules were 182 cm in length and 22 cm in diameter having active membrane area of 50 m^2 per module and permeability of 7.0 ± 0.2 L/m²·h·kPa [15].

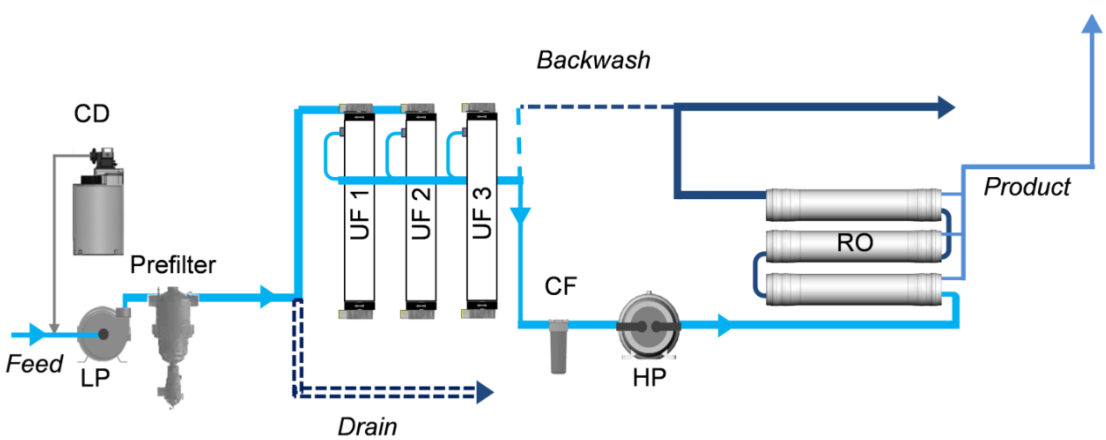

Figure 4-1 Schematic of the integrated UF-RO system. The MF/UF skid consists of a rotating disk microfilter (prefilter) and three hollow-fiber (inside-out) UF modules connected in parallel. Filtrate stream from the UF modules is fed directly to the RO system. The concentrate stream from the RO system (dashed line) is used directly for UF backwash. (CD: Chemical dosing pump, LP: low pressure pump, HP: high pressure pump, CF: cartridge filter.

The UF unit receives its raw water feed via a centrifugal pump (XT100 SS, 5 hp, Price Pump, Sonoma, CA) equipped with a variable-frequency drive (VFD) (VLT AQUA Drive FC 202, Danfoss, Nordborg, Denmark). Prior to the UF, raw seawater feed is passed through a coarse screen then microfiltered via a self-cleaning screen filter (200 micron, TAF-500E, Amiad Filtration Systems, Mooresville, NC). A metering pump (DDA 7.5-16, Grundfos, Bjerringbro, Denmark) is utilized for coagulant dosing at the inlet of the UF feed pump (**Figure 4-1**). Inline coagulation was accomplished using ferric chloride (Technical grade $FeCl_3$, 40.2 wt%, Gallade Chemical, Santa Ana, CA). The UF-RO system was equipped with a network of sensors (conductivity, pH, temperature, turbidity, and chlorophyll *a*), flow meters and pressure transducers interfaced with an embedded controller (cRIO-9022, National Instruments, Austin, TX) and data acquisition system.

In the present UF-RO system configuration the UF module automatically responds to flow demand by the RO unit, whereby the pressure and flow rates are controlled as described elsewhere [147]. The concentrate from the RO unit is then used for direct sequential backwash of the UF modules either only through continuous backwash or in conjunction with a pulse backwash making use of two hydraulic accumulators (**Fig. 4-2**). The RO concentrate stream pressure is throttled down (using a throttle valve) to the level suitable for direct UF backwash and for charging of the hydraulic accumulators (for pulse backwash) with the RO concentrate. The RO concentrate pressure control scheme is described elsewhere [147].

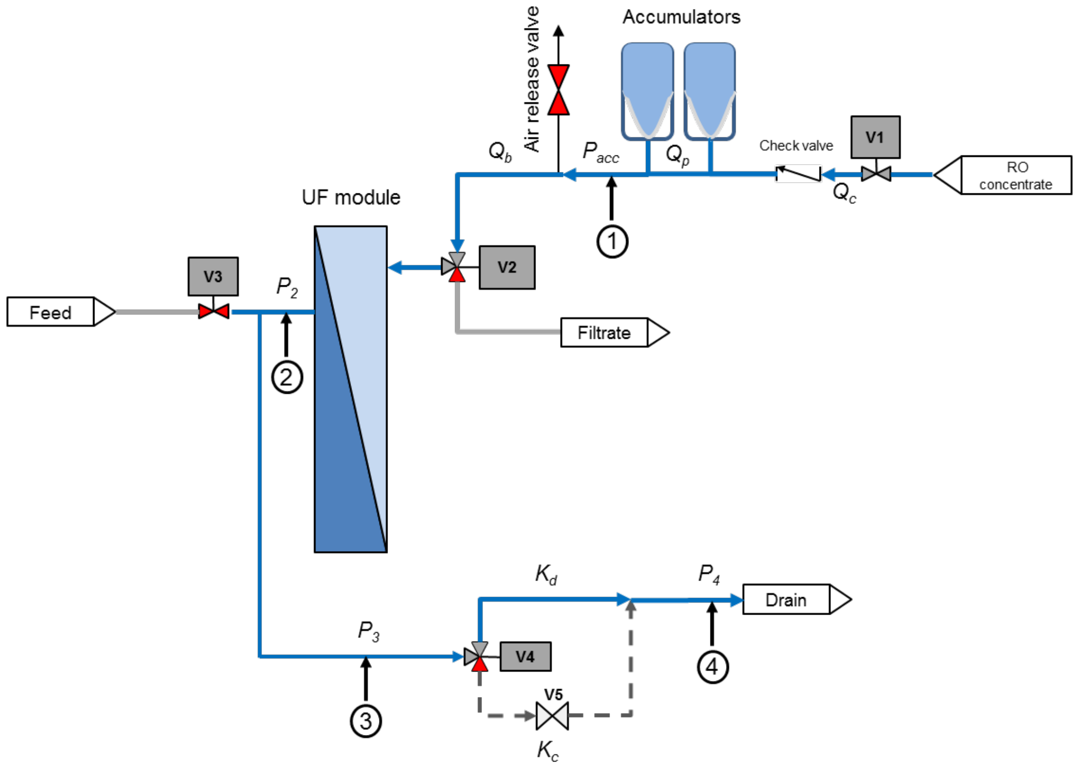

Figure 4-2 Schematic diagram of the integrated pulse backwash (PBW) system (shown for a single UF module). V1: backwash valve, V2: three-way filtrate valve, V3: feed valve, and V4: three-way drain valve. Valves 1-4 are electric actuated ball valves. An adjustable diaphragm valve (V5) serves as a flow regulator in the UF backwash drain line. Q_c: RO concentrate flow rate during backwash. Q_b: backwash flow rate through the UF module. Q_p: flow rate in/out of the accumulators. K_c is the flow coefficient for flow segment between locations 3 and 4 (Valve V4 directs the flow via Valve 5 to drain) during accumulator charging; K_d is the flow coefficient (for the discharge operation) for the same flow section (3→4) with valve V4 facilitating direct flow to the drain (bypassing the segment of Valve 5 indicated by the dashed line).

A series of valves (banks of 2 and 3 ways electric actuated ball valves (Type 107, 2-ways, 1.5'', Georg Fischer LLC, Irvine, CA and TEBVA6-1, 3-ways, Plast-O-Matic Valves, Inc. Cedar Grove, NJ) on the UF skid serve for automated switching of UF operation between filtration and backwash modes while maintaining constant productivity for the RO module. Backwash pressure (AST4000 Industrial P Sensor, 0.5% Acc. 0-517 kPa, American Sensor Technologies, Inc., NJ) and flow rate (Signet Magnetic FM Type 2551, 2", 0-151 L/m, George Fischer Signet, Inc. El Monte, CA) were monitored online during the backwash period.

In the integrated UF-RO system, sequential backwash of the UF modules is accomplished sequentially, whereby as a given UF module is backwashed the remaining two maintain (through filtration at increased flux) the required feed flow to the RO unit. UF backwash is achieved by directing the RO concentrate from the RO modules to the UF backwash line at relatively low pressure (48-50 kPa) for continuous backwash (i.e., without a pulse backwash). It is noted that for the present system [147], at its typical RO operational recovery of ~35%, continuous RO backwash flux would be 1.90 times the normal UF operational filtration flux. The above is below the typical range of manufacturer recommended backwash flux of ~2-3 times the filtration flux. Therefore, the system was designed with a capability for pulse backwash in order to elevate the backwash flux and provide for effective UF operation. The above is accomplished in the present system with self-generation of backwash pulse (i.e., charging of the hydraulic accumulators without the use of auxiliary pumps) and flexibility of triggering multiple pulses during a backwash cycle.

A pulse backwash cycle involves a charging period during which the three-ways drain valve (V4) is opened to the direction of flow regulator V5 (Type 514 diaphragm valve, 1/2" PVC, Georg Fischer LLC, Irvine, CA) and the accumulators (Sentry C111ND, Blacoh Fluid Control, INC., Riverside, CA) are filled with RO backwash water. During the discharge period, valve V4 is set to divert the RO concentrate flow to drain line (**Fig. 4-2**) leading to a rapid (pulse) discharge of the accumulators. The pressure-time profile of the accumulator during charging and discharge is governed by the pressure drop in the flow segment between locations 2 and 4 (**Fig 4-2**). The pressure drop (kPa) for the above flow segment was expressed as $\Delta P = (Q^2 / K_i^2) \cdot SG$, where Q (m^3/h) is the flow rate, SG is the water specific gravity, and where flow coefficients value during accumulator charging is given as $K_i = K_c$, and by $K_i = K_d$

during discharge. The above flow coefficients were determined experimentally from a series of pressure-flow rate measurements for the valve positions set for the above two conditions. These coefficients were essentially constant for the present system and over the range of operating conditions in the study.

In the system configuration utilized in the present study, accumulator charging and discharging can be repeated multiple times during each backwash period. In the present system, the complete backwash cycle (combination of continuous and pulse backwash) was programmed to be autonomous with backwash triggered by a system controller that tracks the UF fouling resistance [147].

Table 4-1 UF feed water and filtrate quality at the field study location

Water Property	UF feed	UF filtrate
Turbidity (NTU)	1.7-14	<0.02
TDS (Total Dissolved Solids) (ppm)	33,440-36,800	33,440-36,800
Chlorophyll *a* (µg/L)	12-400	<0.7
pH	7.5-8.2	7.5-8.2
Temperature °C	11.2-19.7	11.2-19.7

4.2.2 Field Study

The effectiveness of direct UF backwash with RO concentrate and the effectiveness of pulse backwash were evaluated in an integrated UF-RO system at the seawater desalination test facility at the Naval Facilities Engineering and Expeditionary Warfare Center (NAVFAC EXWC) at Port Hueneme, CA. Raw surface ocean water was pumped directly from the port channel through a pumping/distribution facility before delivery to the UF-RO system. The average intake seawater quality is shown in **Table 4-1**.

The influence of the charging flow coefficient, K_c and RO concentrate flow rate (adjusted by changing the RO recovery at fixed RO feed flow rate) on charging and discharge flux- and pressure-time profiles was first evaluated using the accumulator model (**Section 4.3**) in a series of short-term field tests. The minimum K_c value was 1.86 which assured that the charging pressure did not exceed the maximum pressure limit of 480 kPa recommended by the manufacturer for the UF module backwash. During pulse backwash (i.e., rapid discharge of the accumulator volume) the flow coefficient K_d for the drain flow section during the accumulators' discharge (**Fig. 4-2**) was 7.80.

UF backwash performance was first evaluated in short-term tests with and without pulse backwash at a fixed backwash frequency, as well as assessing the added improvement of inline coagulant dosing. Subsequently, the effectiveness of pulse backwash that is self-triggered, based on a UF fouling resistance threshold, was demonstrated in a continuous operation over an eight day period. In this latter test, a secondary UF resistance threshold was utilized for initiating a sequence of either 2 or 4 sequential backwash pulses during a given backwash cycle.

4.3 Pulse backwash model

The hydraulic accumulator used in the present system consists of gas and liquid compartments separated by a rubber type bladder [154]. The hydraulic accumulator is charged with liquid that is pressurized (from the RO concentrate line, **Fig. 4-2**) such that the pressure in the gas chamber (P_g) also increases as its volume (V_g) decreases. The total accumulator volume, V_{acc}, is the sum of the gas (V_g) and liquid (V_l) compartment volumes

$$V_{acc} = V_l + V_g \tag{4-1}$$

The gas volume (V_g) can be assumed to follow adiabatic compression/expansion of an ideal gas [172], i.e., $PV_g^{\gamma} = \mathrm{C}$, where C is a constant and $\gamma = C_p/C_v$ is the ratio of the constant pressure (C_p) and constant volume (C_v) heat capacities, respectively. For ideal gas γ = 1 and for rapid adiabatic expansion γ = 1.4 [172]. The hydraulic accumulator's gas chamber is pre-charged with air and as the liquid compartment is filled with the backwash fluid (i.e., RO concentrate in the present case) V_l increases while correspondingly V_g, decreases while gas chamber pressure increases. The backwash flow rate through the UF module Q_b (L/min) in the integrated RO-UF system (**Fig. 4-2**) is given as:

$$Q_b = Q_c - Q_p \tag{4-2}$$

where Q_c (L/min) and Q_p (L/min) represent the flow rates of concentrate from the RO module and the liquid flowing into/out of the accumulators during the backwash operation, respectively. Q_p can be obtained from the time rate of change of the accumulator liquid volume:

$$Q_p = \frac{dV_l}{dt} = \frac{C^{\frac{1}{\gamma}}}{\gamma \cdot P_{acc}^{\frac{1}{\gamma}+1}} \cdot \frac{dP_{acc}}{dt} \tag{4-3}$$

where t (s) is time and P_{acc} (kPa) is the hydraulic pressure at the accumulator outlet (also designated as P_1 at location 1 in **Fig. 4-2**) that can be determined considering the pressure drop over the flow segment between locations 1-2 and 2-4 as indicated on **Fig. 4-2**. In the present system the pressure drop between the accumulator and the UF module/valve plus piping segment (**Fig. 4-2**, between locations 1 and 4) can be expressed as:

$$P_{acc} - P_0 = (P_{acc} - P_2) + (P_2 - P_3) + (P_3 - P_4) \quad \left(\frac{Q_b}{A \cdot L_p}\right) + \left(\frac{Q_b}{K_i}\right)^2 \tag{4-4}$$

where P_0 (kPa) is the pressure at the UF backwash drain outlet (i.e., location 4, **Fig. 4-2)** which is considered at atmospheric pressure. The pressure drop in the piping section between location 2 and 3 (**Fig. 4-2**) is relatively small such that $\left(P_2 - P_3\right)/(P_{acc} - P_2) < 0.05$; therefore it is reasonable to approximate the pressure difference $\left(P_{acc} - P_0\right)$as the sum of the UF module transmembrane pressure (ΔP_{UF}) and across UF drain section (between locations 1-2 and 3-4,

Fig. 4-2), respectively. ΔP_{UF}, is related to the UF permeation flux, $J_{UF} = L_p \cdot \Delta P_{UF}$, where L_p is the average UF membrane permeability during backwash ($L/m^2 \cdot h \cdot kPa$), A is the UF membrane area (m^2) for a UF module. During the accumulator charging, $K_i = K_c$ and during discharge, $K_i = K_d$ (**Section 4.2.1**). The above flow coefficients are taken as constant when the flow is in the turbulent regime [172, 173].

The discharge (or charge) flow rate, Q_b, can be determined from Eq. (4-4),

$$Q_b = \frac{\sqrt{1+4\cdot\alpha\cdot\beta\cdot(P_{acc}-P_0)}-1}{2\cdot\alpha} \tag{4-5}$$

in which $\alpha = A \cdot L_p / K_i^2$ and $\beta = A \cdot L_p$, and where the pressure term, P_{acc}, can be determined from the differential equation obtained by combining Eq. (4-3) and (4-5),

$$\frac{dP_{acc}}{dt} = Q_c \cdot \frac{\gamma \cdot P_{acc}^{\frac{1}{\gamma}+1}}{C^{\frac{1}{\gamma}}} - \frac{\sqrt{1+4\cdot\alpha\cdot\beta\cdot(P_{acc}-P_o)}-1}{2\cdot\alpha} \cdot \frac{\gamma \cdot P_{acc}^{\frac{1}{\gamma}+1}}{C^{\frac{1}{\gamma}}} \tag{4-6}$$

which can be solved numerically for the pulse back wash charging and discharging periods given the appropriate K_i values and the initial condition for the pressure. The maximum attainable charging pressure P_{max} as determined from Eq. (6) (i.e., by setting $dP_{acc}/dt = 0$) is:

$$P_{max} = \frac{(2\cdot Q_c \cdot \alpha + 1)^2 - 1}{4\cdot\alpha\cdot\beta} \tag{4-7}$$

and the maximum discharge flow rate, Q_{max}, is determined by substituting P_{max} into Eq. (4-5).

4.4 Results & Discussion

4.4.1 UF pulse backwash (PBW) pressure and flux profiles

The pressure- and backwash –flux profiles for the accumulator charging and discharge cycles are illustrated in **Fig. 4-3** for RO concentrate flowrate of 57 L/min and flow coefficients K_c and K_d values of 2.31 and 7.8, respectively. As the hydraulic accumulator is charged with the

RO concentrate its pressure increases up to the maximum value that is reached within ~35 s. During the accumulator charging period, as the RO concentrate fills the accumulator, the continuous RO concentrate backwash flux decreases somewhat (Eq. 4-5). In all cases the total pulse discharged volume is equal to the water volume stored in the accumulator by the end of the charging period. However, the maximum attainable pulse backwash flux is higher when the accumulator discharge is carried out at a higher initial discharge pressure (attained for longer charging periods) as depicted in **Figure 4-3**. Reaching a higher accumulator pressure (and thus higher peak pulse backwash flux) requires a longer charging time and thus there is a tradeoff between the desire to increase the backwash flux and the longest required charging period for attaining the maximum pressure. For example, in order to increase the charging pressure from 183 to 233 kPa (~27% increase), the charging time had to be raised from 14 s to 48 s; correspondingly, the maximum attainable pulse backwash flux increases by only 10.8% upon increasing the maximum accumulator charging pressure by 27%. For the illustration of **Fig. 4-3**, the backwash flux was (for a period of 8-9 s) a factor of 2.5-4.6 above the normal module filtration flux. Also, the peak backwash flux was a factor of 4.2-4.6 above the normal filtration flux. The above backwash flux was well within recommended range (**Section 4.2.1**).

The rate of accumulator pressure increase can be controlled to some degree by adjusting the position of Valve V5 (**Fig. 4-2).** For example, restricting the valve opening lowers the flow coefficient K_c, which then increases the rate of pressure rise leading to a higher maximum attained accumulator pressure. As a consequence a higher pulse backwash flux can be reached. As shown in **Fig. 4-4**, as the flow coefficient, K_c, decreased from a value of 2.64 to 1.86 (i.e. a 29.5% decrease), for the charging period of 33 s, the attained accumulator pressure increased from 167 kPa by about 76% (i.e., to 294 kPa) with the peak backwash flux increasing by 18%

(i.e., from 151 to 177 L/m^2·h). The accumulator model predictions closely matched the experimental data (**Fig. 4-4**) and where the predicted peak flux deviated by 2.21-3.82% from the experimental values.

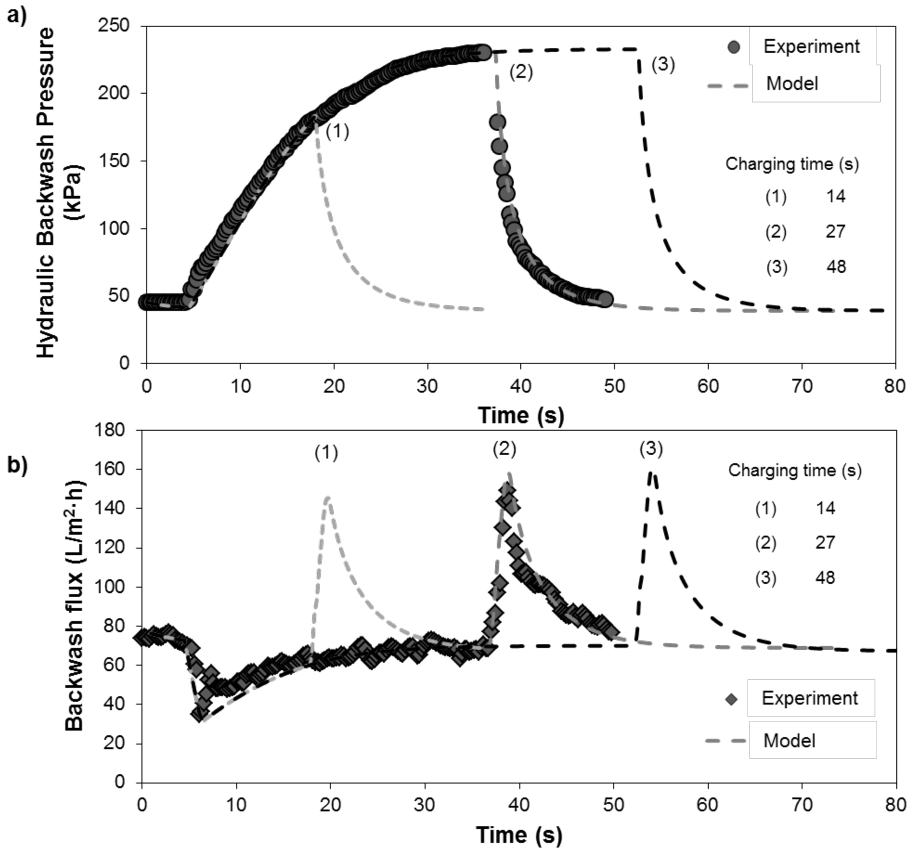

Figure 4-3 Illustration of the PBW model predictions compared with experimental total backwash flux (continuous and pulse backwash) and accumulator pressure profiles. a) Pressure profiles for the PBW charging and discharging cycle. b) Backwash flux profile for the PBW charging and discharging period. UF single module filtration flux: 34.4 L/m^2·h. PBW conditions: RO concentrate backwash flowrate: 57 L/min, K_c: 2.31, K_d: 7.80. Note: The dashed line depicts the model predicted pressure and flux profiles for charging time of 14, 27 and 48 seconds.

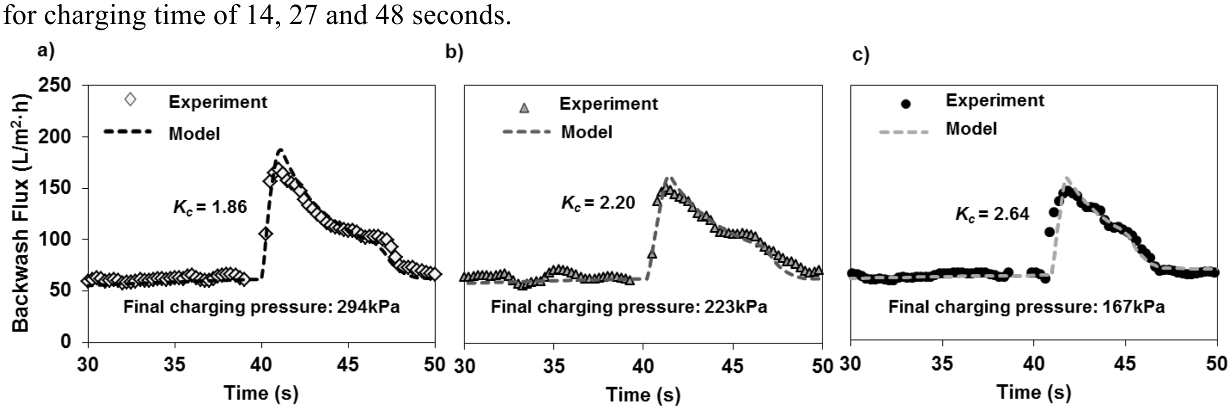

Figure 4-4 Backwash flux profile attained as an outcome of different conditions of accumulator charging for different values of the flow coefficient K_c (**Section 4.3, Eq. 4-4**). Experimental conditions: UF single module filtration flux: 35.0 L/m^2·h. Pulse backwash condition: RO concentrate backwash flowrate: 57 L/min, K_d: 7.80, Charging time was 33s.

Higher RO concentrate flow rate (Q_c) would enable higher accumulator pressure and backwash flux to be attained as can be verified from predictions of the accumulator model (**Eqs. 4-6**, **Section 4.3**; **Fig. 4-5)** which closely match the experimental data (**Figs. 4-5** and **4-6** and **Table 4-2**). As an example of the impact of RO concentrate flow, raising the concentrate flow rate from 58.7 L/min by ~30% (i.e., to 76.5 L/min; achieved by increasing UF filtration flux for the present system) elevated the final charging pressure (**Table 4-2**) from 225 kPa (attained in 37 s) to 402 kPa (attained in 32 s), while the peak pulse backwash flux increased by 31.3% (i.e., from 144.6 to 190.1 L/m^2·h). Clearly, adjustment of Q_c (e.g., diverting part of the RO concentrate to UF backwash) offers additional flexibility in controlling the desirable peak pressure (e.g., to avoid over-pressurizing the UF module during backwash). However, from a practical viewpoint it should be noted that Q_c is more likely to be dictated by the desired level of RO system productivity.

For the present integrated UF-RO system with its capability for direct RO concentrate backwash and its two six liter hydraulic accumulators, the peak backwash flux (i.e., the sum of the pulse backwash and the continuous RO concentrate backwash flows) was in the range of ~4.2-4.4 times the normal filtration flux which was well within the recommended range (**Section 4.2.1**). The use of larger volume accumulators can be useful in attaining a longer backwash pulse, although the peak pulse backwash flux would be unaltered (**Fig. 4-7**). Increasing the peak pulse backwash flux can be achieved via control of Valve 5 (**Fig. 4-2**), so as to increase the accumulator hydraulic pressure upon being filled with the RO concentrate. For example, in the present system, at the maximum allowable UF operational pressure of 480 kPa, the maximum feasible peak backwash flux was about 252 L/m^2·h for RO system operation at a feed flow rate of 62.4 L/min and at recovery of 35%. Finally, it is noted that operation with consecutive backwash pulses is feasible (**Fig. 4-8**) with a consistent charging period and peak pulse backwash flux.

Table 4-2 Effect of varying flow coefficient setting of the UF backwash drain line (K_c) and RO concentrate flowrate on peak charging pressure and peak backwash flux

Effect of varying flow coefficient setting (K_c)[a]							
Flow coefficient during charging K_c	UF filtration flux per module (L/m^2·h)	Accumulator charging time (Δt_c)	Accumulator discharge time (Δt_d)	Final charging pressure[c] (kPa)		Peak pulse backwash flux (L/m^2·h)	
				Theory	Experim ent	Theory	Experiment
1.86	35.0	33.0	10	295	294	181	177
2.20	35.0	33.0	9.5	224	223	162	156
2.64	35.0	33.5	9.8	167	167	157	151
Effect of varying RO concentrate flowrate (Q_c)							
RO concentrat e flowrate, Q_c (L/min)[b]	UF filtration flux per module (L/m^2·h)	Accumulator charging time (Δt_c)	Accumulator discharge time (Δt_d)	Final charging pressure[c] (kPa)		Peak pulse backwash flux (L/m^2·h)	
				Theory	Experiment	Theory	Experiment
57.0	32.6	32.8	12.5	227	225	147.5	144.6
66.0	36.2	33.0	12.5	280	281	168.5	165.6
76.0	42.9	33.5	12.7	403	402	194.9	190.1

[a] K_c = 2.2; RO concentrate backwash flowrate: 57 L/min, K_d: 7.8; RO recovery: 34.4%, [b] RO recovery: 28.8% ; [c] gauge pressure.

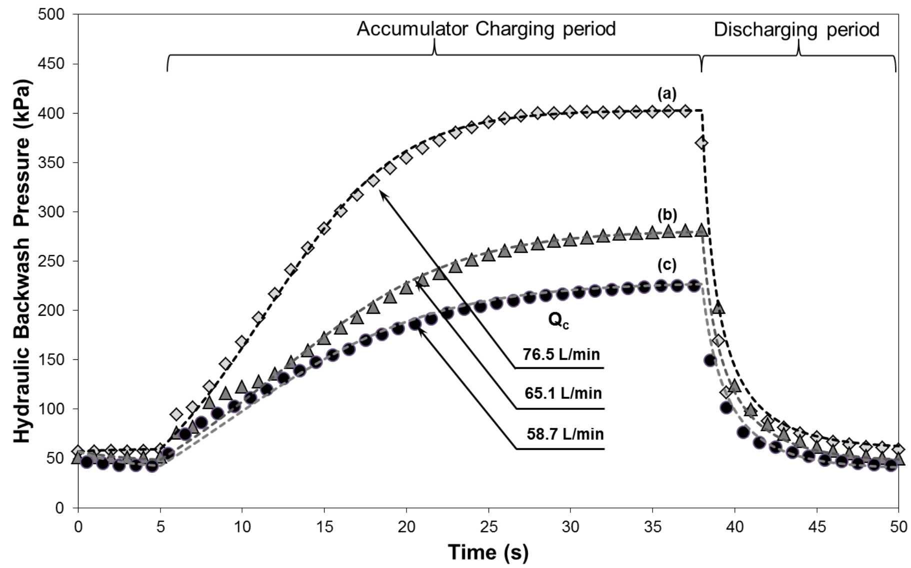

Figure 4-5 Effect of RO concentrate flowrate on pulse backwash pressure profile. The experimental data and model predictions are represented by filled symbols and dashed lines, respectively. Experimental conditions: K_c: 2.20, K_d: 7.80, charging duration: 30s. Note: The accumulator charging pressure (gauge) prior to discharge were: a) 409 kPa; b) 327 kPa; and c) 256 kPa.

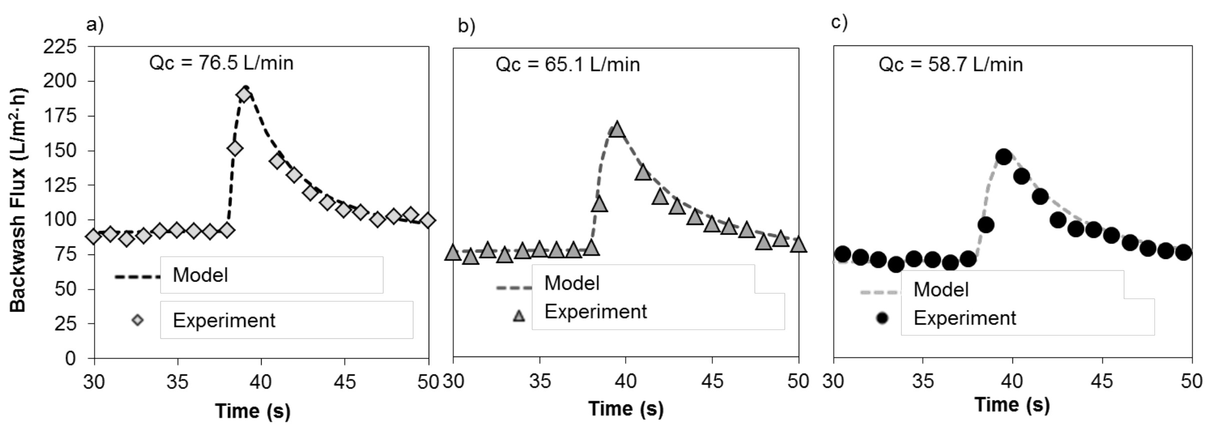

Figure 4-6 Illustration of the **e**ffect of RO concentrate flowrate on pulse backwash flux profile. Experimental conditions: K_c: 2.20, K_d: 7.80, charging duration: 30s. Note: The accumulator charging pressure (gauge) prior to discharge were: a) 409 kPa; b) 327 kPa; and c) 256 kPa.

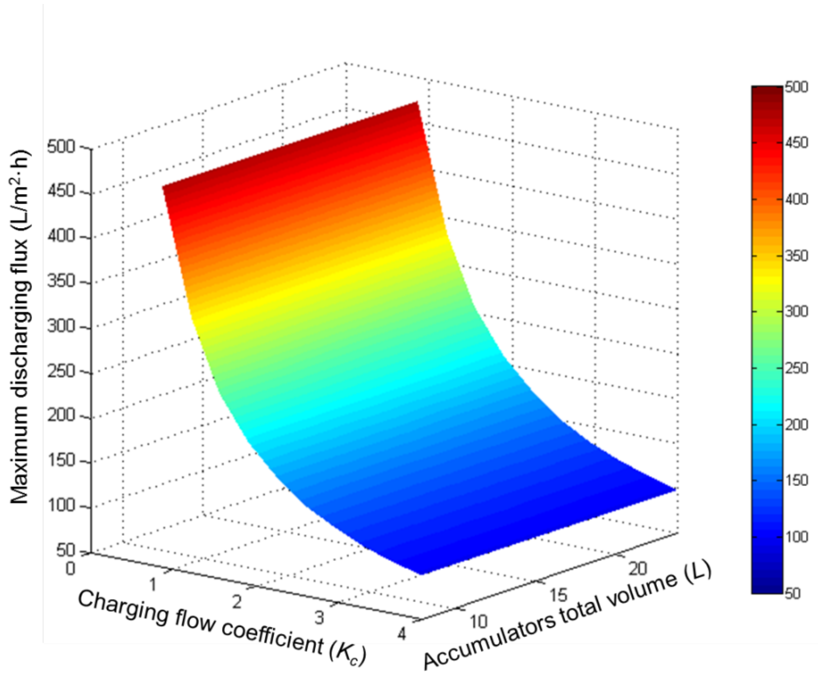

Figure 4-7 Dependence of peak pulse backwash flux (L/m^2·h) on pulse backwash flow coefficient (K_c) and accumulator volume (L). (K_d = 7.80, RO concentrate backwash flowrate = 58.3 L/min).

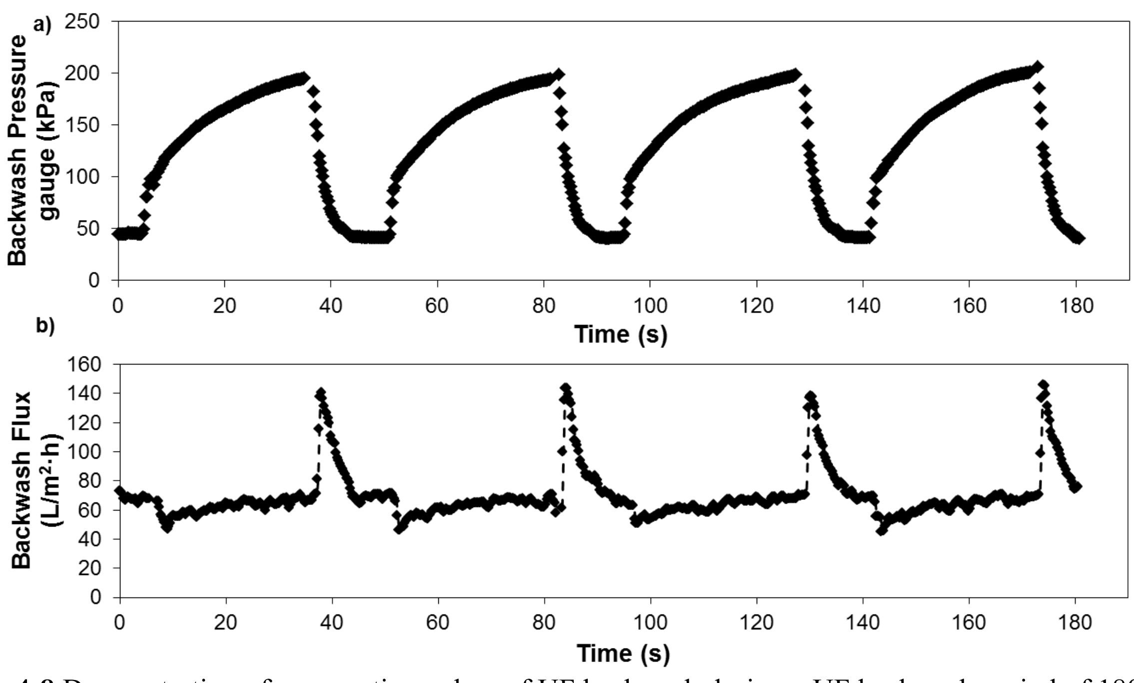

Figure 4-8 Demonstration of consecutive pulses of UF backwash during a UF backwash period of 180s. a) Backwash accumulator pressure profiles, and b) Backwash flux profile (continuous RO concentrate backwash + accumulator pulse backwash). Flow charging and discharge coefficients were set at K_c = 2.21 and K_d = 7.80 with accumulator charging period of ~35s and discharge period of 13 s for a total backwash period per cycle of ~48s and where the continuous RO concentrate backwash flux was ~70 L/m^2·h. UF system filtration flux per module: 34.4 L/m^2·h.

4.4.2 Effectiveness of pulse and continuous RO concentrate backwash

In order to assess the effectiveness of combining continuous RO concentrate backwash with pulse backwash, seawater desalting tests were conducted with the UF-RO pilot under the following conditions: (a) UF operation without coagulation and fixed backwash frequency (every 30 minutes) with continuous RO concentrate backwash flux of 71 L/m^2·h for 45 s, followed by two backwash pulses yielding a peak backwash flux of 141 L/m^2·h; (b) UF operation with inline coagulation (4.01 mg/L Fe^{3+}, [147]) and backwash strategy as above, but with a single backwash pulse yielding a peak backwash flux of 141 L/m^2·h; and (c) UF operation and backwash scheme as in (b) but with two consecutive backwash pulses (each providing peak backwash flux of 142 L/m^2·h) in each backwash cycle. In these tests the normalized UF membrane resistance at the beginning of each filtration cycle was expressed as $R_{UF,i} = (R_i - R_o)/R_o$, where R_i is the overall membrane resistance at the beginning of the *ith* filtration cycle (just after backwash), and R_o is the membrane resistance at the beginning of the filtration test period. Results of the above three tests as depicted in **Fig. 4-9** demonstrate that UF operation without coagulation is less effective even when using two backwash pulses relative to a single one. The rate of fouling in case (a) without coagulation is a about a factor of 3.5 higher than for case (b) with coagulation and only one backwash pulse per backwash cycle. However, when using two consecutive pulses in case (c) instead of a single one as in operation (b), the rate of fouling was lowered by about a factor of 2.4, even though the feed water turbidity was 40% higher (i.e., 2.20± 0.64 NTU) than during the former two tests.

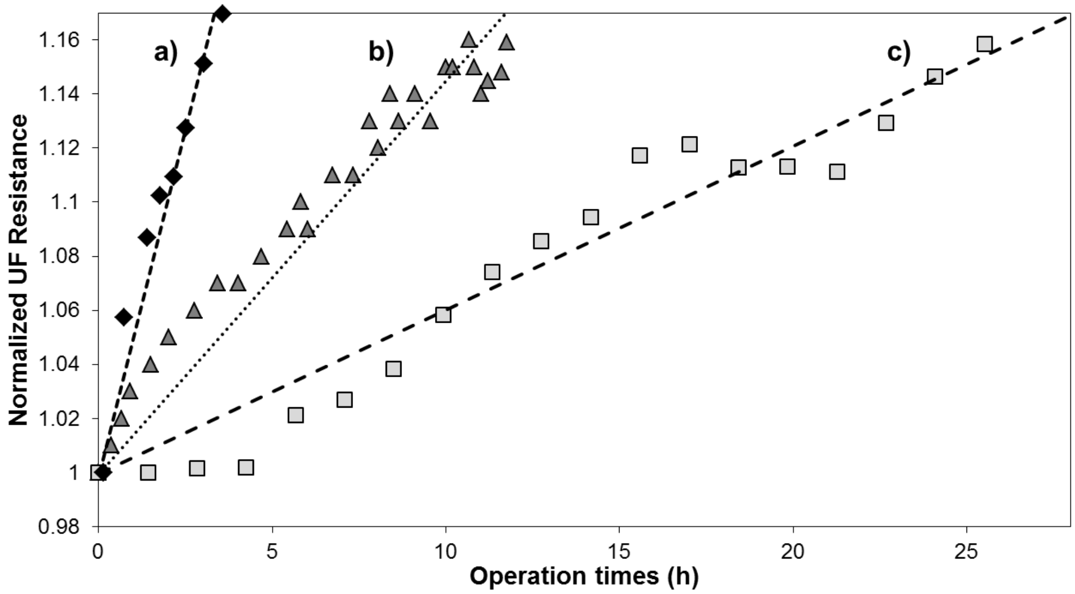

Figure 4-9 Comparison of the progression of UF fouling resistance for the following UF operation and backwash strategies: (a) UF filtration without coagulation with backwash triggered every 30 min with a continuous RO concentrate backwash (71 L/m^2·h) for a period of 45 s, followed by two backwash pulses each yielding a peak backwash flux of 141 L/m^2·h. Raw feed water turbidity = 1.56 ± 0.42 NTU; (b) UF with inline coagulation (dose: Fe^{3+}: 4.01 mg/L) with backwash triggered as in (i) with continuous backwash followed by a single backwash pulse of peak flux of 141 L/m^2·h. UF feed water turbidity: 1.46 ± 0.19 NTU); and (c) UF filtration as in (ii) with a continuous backwash period that is followed by two consecutive backwash pulses each yielding a peak backwash flux of 142 L/m^2·h. UF feed water turbidity: 2.20 ± 0.64 NTU. (Flow charging and discharge coefficients set at K_c = 2.21 and K_d = 7.80, RO feed flow rate= 86.7 L/min, RO recovery: 35.4%).

The short-term UF tests (**Fig. 4-9**) suggested that the backwash strategy as per test (c) would be beneficial. However, it was also of interest to assess if increasing the number of backwash pulses would increase backwash effectiveness. Accordingly, a self-adaptive UF backwash strategy was utilized whereby UF backwash was triggered when the UF resistance reached a level such that $\Delta R_{UF} / R_o \geq \delta$, where ΔR_{UF} is the maximum allowable UF resistance increase per filtration period, and R_o is the initial membrane resistance. Previous studies on self-adaptive UF backwash triggering have indicated that a value of $\delta =$ 0.034 was adequate for the present UF system [147]. Although a higher δ value can be set as threshold to enable longer filtration time, such operation would in turn require a longer backwash period for effective UF operation. Therefore, there is clearly a tradeoff with respect to triggering backwash and in general setting a backwash trigger such that filtration periods are in the range of 30 min - 1hr is regarded as a reasonable approach [146]. Once backwash is triggered, if the UF resistance at the beginning of the given filtration cycles is below a given threshold, i.e., $R_{UF} / R_o < \alpha$, then two consecutive pulses are triggered past the continuous backwash period of 45 s. On the other hand, if at the beginning of the filtration cycle $R_{UF} / R_o \geq \alpha$ then four consecutive backwash pulses are utilized post the continuous concentrate backwash period. The above filtration and backwash strategy, with $\alpha = 1.11$, was evaluated over a period of about 8 days (**Fig. 4-10**) during which the raw seawater turbidity and chlorophyll *a* were in the range of 1.75 - 5.21 NTUs and 31 - 121 µg/L, respectively. While there was no apparent correlation with the UF resistance-time profile, it is accepted that UF fouling is likely to be impacted by multiplicity of water quality parameters; hence, the challenge of establishing a UF operational strategy based on multiple water quality metrics. Therefore, in the present approach, UF backwash strategy was established based on real-time tracking of the UF resistance. As the field test results indicate (**Fig. 4-10**), the UF system fouling rate was high initially but fouling was brought under control despite significant variability of water quality over the course of the field test. Here it is important to note that no attempt was made to optimize the number of backwash pulses. Nonetheless, the results clearly indicates that the combination of continuous backwash with variable backwash pulse frequency can be effective in significantly improving UF operation.

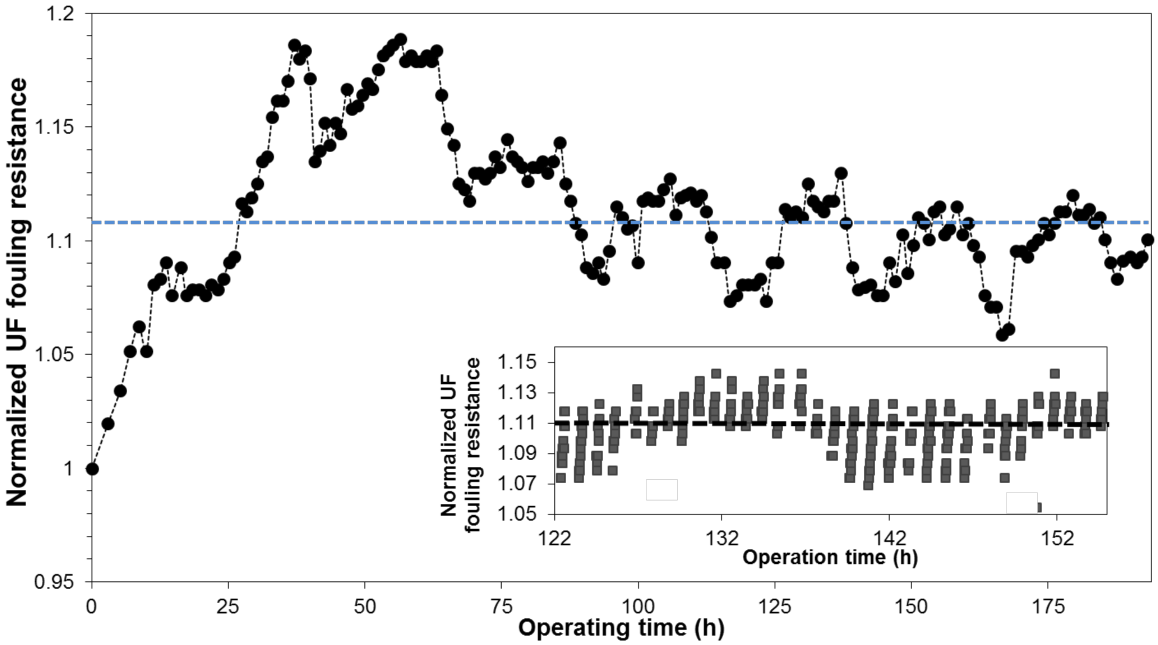

Figure 4-10 Evolution of UF resistance (normalized with respect to initial UF resistance) during UF operation with coagulation (4.01 mg/L Fe^{3+}) and self-adaptive backwash triggering. Backwash with a continuous RO concentrate flow rate (56 L/min for RO operation at 35.4%) was for a period of 45s, followed by either two or four consecutive backwash pulses as determined by a normalized UF resistance threshold (indicated by the dashed line in the main and inset Figures). The inset Figure illustrates a trace of filtration cycles. (UF system filtration flux per module= 34.4 L/m^2·h, K_c= 2.21, K_d =7.80, charging duration= 35s).

4.5 Conclusions

The integration of continuous UF backwash with direct supply of RO concentrate along with pulse backwash using hydraulic accumulators was evaluated in a novel integrated UF-RO seawater desalination system. Model analysis of the hydraulic accumulator operability, along with experimental validation, demonstrated that direct accumulator charging, with the RO concentrate, to nearly the peak charging pressure can be achieved within a period of 30-40 s. Using the hydraulic accumulators that were self-charged via the pressurized RO concentrate stream, along with continuous delivery of UF backwash of RO concentrate (from the RO unit), enabled peak UF backwash flux that was up to a factor of 4.2 - 4.6 higher than the normal filtration flux. UF operation that combines direct continuous RO concentrate backwash with multiple consecutive backwash pulses was found to be more effective than with a single pulse, while inline coagulation further increased the UF performance. Self-adaptive triggering of UF backwash, whereby the number of consecutive pulses increased when a higher membrane fouling resistance was reached, was shown to be highly effective and enable stable UF operation over significant period over a wider range of water quality conditions and without the need for chemical cleaning. The present results suggest with the present UF-RO integration enhanced UF backwash can be achieved without sacrificing water productivity given the use of RO concentrate for backwash and the flexibility of being able to actuate multiple consecutive backwash pulses.

5 Online Fouling Monitoring and Characterization for Effective Operational Control of Ultrafiltration as Pretreatment for Seawater Desalination

5.1 Overview

The applicability of fouling indicators for real time assessment of the performance of UF pretreatment of seawater RO desalination was explored in a field study using an integrated seawater UF-RO plant. A set of online UF fouling indicators were determined to assess cycle-to-cycle filtration and backwash fouling and permeability recovery (or fouling resistance removal). The UF filtration period and fouling rate (*FR*), unbackwashed and post-backwash UF resistances (ΔR_{UB} and R_{PB}, respectively), and UF backwash efficiency (BW_{eff}) were determined in real-time for each filtration/backwash cycle over both short and long-term field tests. The fouling indictors provided real-time quantification of UF backwashability, unbackwashed UF fouling resistance and the rate of UF fouling.

Feed water quality and coagulant dose had a direct impact on both UF fouling rate (during the filtration period) and effectiveness of foulant removal by UF hydraulic backwash. Increasing the coagulant dose resulted in higher rate of cake formation, and in turn increased backwash efficiency. However, a maximum coagulant dose was observed beyond which backwash efficiency was not improved. Backwash effectiveness also increased with backwash flux and duration up to a threshold upper limit (for a given UF filtration flux and inline coagulant dose), but declined as the filtration periods increased above a threshold value. Field tests over periods during which feed water quality varied temporally (as indicated by turbidity and chlorophyll-*a* measurements) demonstrated that higher fouling rate as promoted by inline coagulation indeed led to more effective backwash and hence lower progressive rise in UF post-backwash resistance. The study results suggest that real-time UF fouling indicators based on UF filtration resistance metrics and backwash effectiveness can provide useful information for self-adaptive control for increased effectiveness of UF feed pretreatment for RO desalination.

5.2 Experimental

5.2.1 Integrated UF-RO System

The UF-RO seawater desalination system (**Fig. 5-1**) consisted of directly integrated UF and RO skids (i.e., without an intermediate UF or RO feed tank). The designed maximum system feed water capacity was 190.8 m^3/day (50,400 GPD) operating at a maximum RO unit recovery of 35% recovery (equivalent to desalted water production of 45.2 m^3/day (12,000 GPD)). Details of the integrated UF-RO system are available elsewhere [147]. Briefly, the UF skid comprised of an inline basket strainer (0.32 cm ID perforation, Hayward SB Simplex, Clemmons, NC), a 200µm self-cleaning microfilter (TAF-500, Amiad Corp., Mooresville, NC), and three inside-out polyethersulfone (PES) multi-bore hollow fiber membranes (0.02 µm pore size) UF modules (Dizzer 5000+, Inge, Greifenberg, Germany) arranged in parallel with each module having membrane surface area of 50 m^2.

Feed water to the UF modules was delivered by a feed pump (XT100 SS, 3.73 kW, Price Pump, Sonoma, CA) controlled by a variable-frequency drive (VFD) (VLT AQUA Drive FC202, Danfoss, Denmark). Inline coagulants dosing was achieved by direct injection into the UF feed stream (prior to the UF feed pump) via a metering pump (Grundfos, DDA 7.5-16, Bjerringbro, Denmark). UF module filtrate flow rates were monitored using magnetic flow meters (Signet 2551, George Fischer Signet, Inc. El Monte, CA) and pressure was monitored via sensors (AST4000, American Sensor Technologies, Mt. Olive, NJ) installed on the feed and filtrate sides of the UF modules. A turbidity meter (Signet 4150, Georg Fischer Signet LLC, El Monte, CA), fluorometer sensor (Turner Designs, Cyclops-7 2108, San Jose, CA), pH meter (Sensorex S8000CD, EM802/pH, Garden Grove, CA), and a temperature sensor (Signet 2350-3, George Fischer Signet LLC, El Monte, CA) were installed on the UF filtrate line. Banks of electrically actuated 2 and 3 way ball valves (Type 107, 2-ways, Georg Fischer LLC, Irvine, CA and TEBVA6-1 3-way, Plast-O-Matic Valves, Inc. Cedar Grove, NJ) enabled switching between filtration and backwash modes, and changing filtration/backwash directions (top or bottom) for the individual UF modules [171].

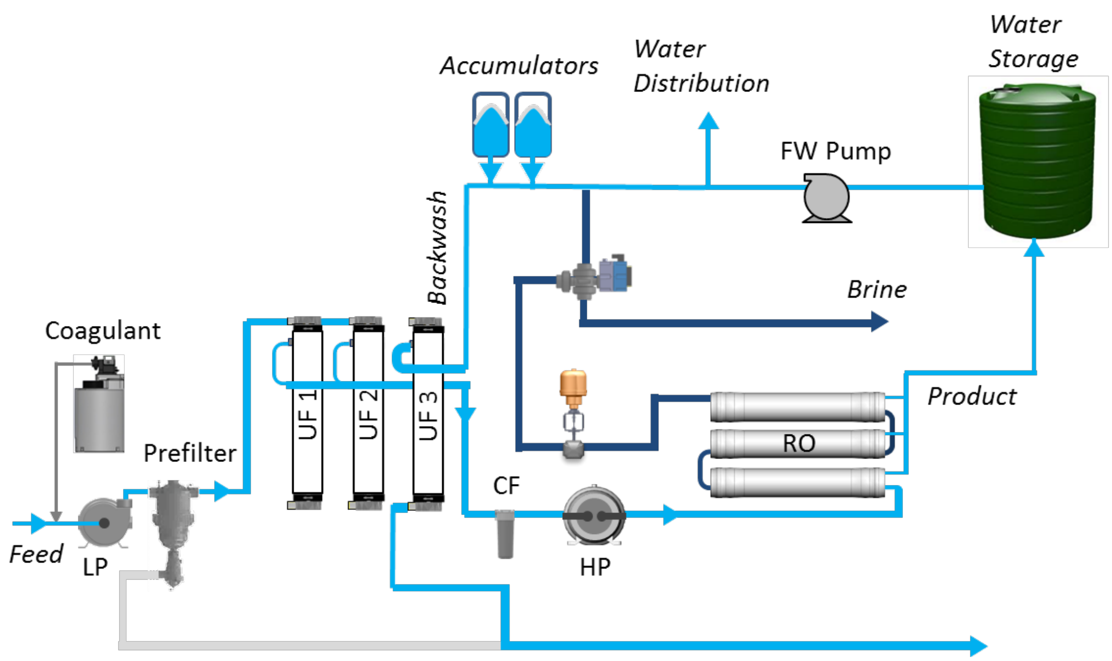

Figure 5-1 Schematic diagram of the UF-RO pilot system. (LP: low pressure feed pump, HP: high pressure positive displacement pump, CF: carbon filters for added RO protection).

The UF filtrate was delivered to the RO high pressure positive displacement feed pump (APP 10.2, Danfoss, Nordborg, Denmark) with a high efficiency motor (CEM4103T, 25 hp, TEFC, Baldor, Fort Smith, AR) and Variable Frequency Drive (VFD) control (VLT AQUA Drive FC 202, 22 kW, Danfoss, Nordborg, Denmark). The RO feed pump, with an outlet flow and pressure ranges of 66-170 L/min and 2-8 MPa, respectively, provided feed to three seawater (99.65% salt rejection) spiral-wound RO elements membranes (Dow Filmtec SW30HRLE-400, the Dow Chemical Company, Midland, MI) each housed in a separate pressure vessel arranged in series.

In the specialized arrangement of the integrated UF-RO system, the RO concentrate was available for direct backwash of the UF modules, through a continuous stream as well as via high flux pulse backwash using two 3L bladder type hydraulic accumulators (C111ND, Blacoh Fluid Control, Riverside, CA, USA) [174]. In addition, RO permeate was collected in a 1,136 L water storage tank with provision for diverting the permeate water for UF freshwater backwash using a centrifugal pump (CME5-4A, Grundfos, Denmark). Upon triggering of UF backwash, the UF membranes are taken offline sequentially and individually backwashed. It is noted that at all times at least two modules remain in filtration mode. In the above operational mode, a filtration and backwash sequence, which includes all three UF modules, is considered a complete UF filtration cycle.

5.2.2 Field study

The field study was conducted at the Naval Facilities Engineering and Expeditionary Warfare Center (NAVFAC-EXWC) at Port Hueneme, CA. Raw surface seawater was pumped directly from the port to a 7,571 L (2,000 gallon) holding tank (< 3h detention time), and used as feed to the UF-RO system. The range of intake water quality during the study is shown in **Table 5-1**. It is noted that in the above area algal bloom and red tide events are common during spring and summer seasons [175, 176]. It is emphasized that the feed water to the UF unit was not chlorinated and that UF backwash was without chemical additives.

Table 5-1 Range of seawater feed quality at field study location (2012-2015)

Feed water property/ quality parameters	Range
chlorophyll-*a*	12-400 (μg/L)
pH	7.5-8.2
Total Dissolved Solids (TDS)	33,440-36,800 mg/L
Total Organic Carbon (TOC)	0.7 -1.3 mg/L
Temperature	11.2-25.6 °C
Turbidity	1.1-19 NTU

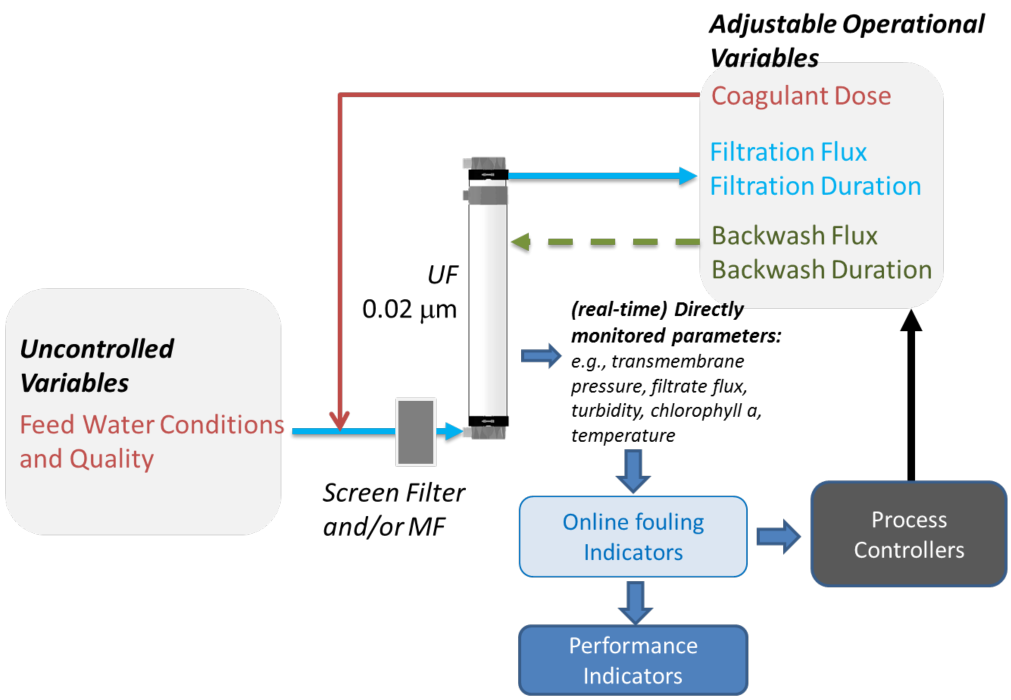

Figure 5-2 Schematic depiction of UF process variables that are uncontrolled and those that are adjustable for optimizing UF operation.

Effective UF operational control strategies require suitable fouling indicators that quantify UF performance and backwash effectiveness based on real-time monitoring of process parameters (target filtrate flux which in turns affects transmembrane pressure, feed water turbidity and chlorophyll-*a* and temperature). Moreover, such fouling indices should provide clear correlation with critical UF operational variables such as filtration duration, backwash duration, backwash flux and coagulant dose (**Fig. 5-2**). Accordingly, the present study proceeded along three sequential phases aimed at quantifying fouling indicators (**Section 5.2.3**). The first phase of the study focused on the effect of inline coagulation on the progression of UF fouling, filtration fouling rate and UF backwash performance. Two coagulants ($FeCl_3$ and ACH) were tested over a range of doses of 1.5 - 4.9 mg/l as Fe^{3+} and 2.8 - 25 mg/l as Al^{3+}, respectively, for fixed filtration duration for tests that consisted of least 64 filtration/backwash cycles. In the second phase, short term experiments were conducted, at fixed coagulant dose, to evaluate the impact of backwash flux, backwash duration and backwash frequency on UF performance. These tests were carried out over an operational period of 15 – 60 min, typically consisting of 12 filtration/backwash cycles. At the end of each of short duration tests, the UF modules were backwashed at a high flux (162 $L/m^2 \cdot h$, approximately 3.6 times the filtration flux) for two minutes, using RO permeate. The third phase focused on longer term (>240 h) field tests in which various fouling indicators were quantified to characterize UF filtration and backwash performance under temporally variable water quality conditions.

5.3 Online UF Fouling Characterization

5.3.1 Online fouling and performance indicators selection

UF pretreatment of RO feed water is generally carried out under constant filtration flux operation in a “dead-end” mode. The filtrate flux J_F (m/s) through the UF membrane is typically expressed as [177]:

$$J_F = \frac{\Delta P}{\mu R_t} \tag{5-1}$$

where μ is the feed water viscosity (Pa·s), ΔP is the transmembrane pressure drop (kPa), and R_t is the total membrane hydraulic resistance that is typically expressed by the resistance-in-series model [54].

$$R_t = R_m + R_{cake} + R_{irr} \tag{5-2}$$

in which R_m, R_{cake}, and R_{irr} are the clean membrane hydraulic, cake and irreversible resistances, respectively. Here R_{cake} refers to the foulant layer that can be removed by hydraulic backwash; this removable foulant portion is regarded as the cake layer that builds on the membrane surface. For constant flux operation, the UF membrane resistance increases with progressive fouling over the course of a filtration cycle (**Fig. 5-3**). When the UF membrane resistance reaches a prescribed threshold level, backwash is triggered to remove the foulant layer and thus recover the membrane permeability (**Fig. 5-3**). The UF foulant layer portion not removed (unbackwashed) in the backwash step may remain as "irreversible" fouling or may be removed to some degree in subsequent backwash cycles. Backwash effectiveness can thus be quantified by the degree of removal of the foulant layer as quantified by the reduction (or removal) of membrane resistance.

For a given filtration cycle n, the initial UF resistance ($R_{initial,n}$) (i.e., post-backwash resistance for cycle n-1), filtration duration (Δt_n) and final UF filtration resistance ($R_{final,n}$) are determined from the UF filtration resistance data. The UF fouling resistance increase for a given cycle n, $\Delta R_{T,n}$ (i.e., $R_{final,n}$ - $R_{initial,n-1}$) can be expressed as the sum of the resistance removed by the previous backwash period ($\Delta R_{BW,n}$=$R_{final,n}$ - $R_{initial,n}$) and the unbackwashed resistance (i.e., not removed) by UF backwash ($\Delta R_{UB,n}$=$R_{initial,n}$ - $R_{initial,n-1}$) (**Fig. 5-3**):

$$\Delta R_{\mathrm{T},n} = \Delta R_{UB,n} + \Delta R_{BW,n} \tag{5-3}$$

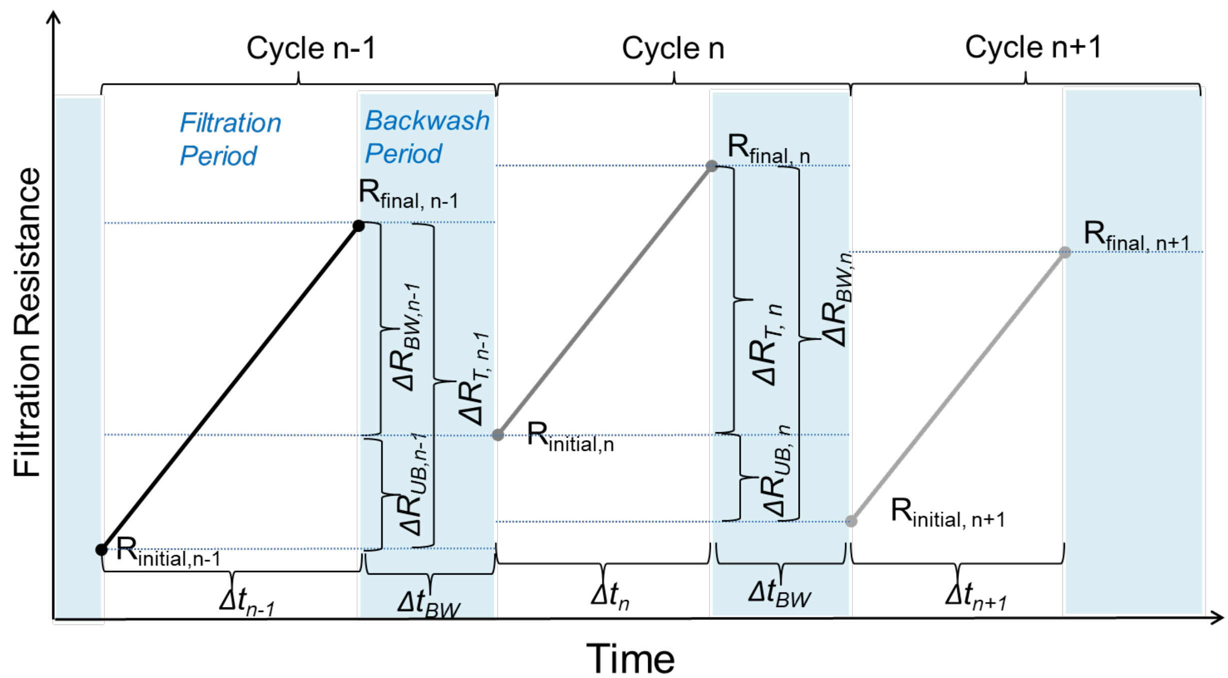

Figure 5-3 Illustration of filtration/backwash cycles. $R_{initial,n}$ and $R_{final,n}$ are the initial and final UF membrane resistances, respectively ($\Delta R_{T,n}$= $R_{final,n}$ - $R_{initial,n}$) for cycle *n* filtration duration of Δt_n, and $\Delta R_{UB,n}$ is the cycle *n* unbackwashed portion of the membrane fouling resistance buildup from cycle *n-1*. ($R_{initial,n}$ also represents the post-backwash resistance associated with cycle *n-1* and $\Delta R_{BW,n} = \Delta R_{T,n} + \Delta R_{UB,n}$).

The change in $\Delta R_{UB,n}$ with progressive filtration/backwash cycles is indicative of the effectiveness of foulant cake removal by backwash. In principle ΔR_{UB} can be negative (i.e., $\Delta R_{UB} >> R_{irr}$) which would be the case when the degree of foulant removal, in a given cycle, is higher relative to the previous cycle (e.g., due to improved water quality and environmental factors).

In characterizing UF filtration performance, the fouling rate for the given filtration cycle *n* (FR_n) is a fouling indicator for the filtration step,

$$FR_n = \frac{\Delta R_{T,n}}{\Delta t_n} \tag{5-4}$$

Recent work has demonstrated that rapid fouling, during the filtration step can be promoted by inline UF feed coagulant dosing. Coagulation promotes the formation of particle aggregates (or flocs) larger in size than the original smaller suspended solids which favors the formation of a foulant cake layer, while reducing the potential for membrane pore plugging. It is important to recognize that when conventional coagulation/sedimentation treatment is employed prior to UF filtration, FR_n may be higher or lower than UF treatment without coagulation. Moreover, unlike conventional coagulation/sedimentation, as shown in recent work, inline coagulation is effective in promoting a foulant cake layer that is more easily backwashed [161, 178], and provides a protective layer to reduce the likelihood of pore plugging. Moreover, the fouling rate, as quantified by FR_n, is expected to be higher for UF filtration with inline coagulant dosing relative to UF operation without coagulation [161, 179] .

The progression of UF fouling (as measured by post-backwash (*PB*) UF resistance for each cycle, i.e., $R_{PB,n}=R_{initial,n+1}$), over many filtration/backwash cycles, and the ability to reduce the rate of PB resistance increase relies on the ability to minimize the cycle-to-cycle unbackwashed membrane resistance ($\Delta R_{UB,n}$). Backwash efficiency ($BW_{eff,n}$) which here is defined as the percentage of removed resistance for a given cycle:

$$BW_{eff,n}(\%) = \frac{\Delta R_{BW,n}}{\Delta R_{\mathrm{T},n}} = 1 - \frac{\Delta R_{UB,n}}{FR_n \cdot \Delta t_n} \tag{5-5}$$

depends on both $\Delta R_{T,n}$ and $\Delta R_{UB,n}$. With progressive filtration/backwash cycles, the rise in post-backwash initial filtration resistance (R_{PB}) is given by:

$$R_{PB} = \sum_{n=0}^{N} (R_{PB,n-1} - R_{initial,n-1}) = \sum_{n=0}^{N} \Delta R_{UB,n} = R_{initial,N} - R_{initial,0} \tag{5-6}$$

where R_{PB}, which is indicative of the overall state of the UF membrane fouling, is the summation of the cycle-to-cycle UF unbackwashed resistance change, and $R_{initial,N}$ and $R_{initial,0}$ are the final post-backwash and initial UF membrane filtration resistances, respectively. The need for membrane CIP can be established based on a maximum allowable threshold R_{PB} for the

UF module (e.g., as per the manufacturer recommendation of the maximum recommended transmembrane pressure for a given filtration flux).

When UF backwash is with the RO concentrate the fraction of recovered UF filtrate (Y_{UF}) is complete (i.e., Y_{UF} =1). However, when the UF filtrate is stored and utilized for backwash, UF recovery for a given cycle n ($Y_{UF,n}$) is reduced to a level governed by the backwash flux and frequency as given by:

$$Y_{UF,n} = 1 - \left(\frac{J_{BW} \cdot \Delta t_{BW}}{2 \cdot J_F \cdot \Delta t_n} \right) \tag{5-7}$$

in which Δt_{BW} is the backwash time (h) and J_{BW} is the backwash flux (L/m^2·h), and where the total filtrate recovery at the end of N cycles ($Y_{UF,N}$) is given as:

$$Y_{UF,N} = 1 - \left(\frac{N \cdot J_{BW} \cdot \Delta t_{BW}}{2 \cdot \sum_{n=1}^{N} J_F \cdot \Delta t_n} \right) \tag{5-8}$$

Higher Y_{UF} can be achieved by maximizing filtrate production (e.g., higher filtration flux, reduced backwash frequency and system offline period) while minimizing backwash flux, duration and frequency. It is noted that in typical UF systems where UF filtrate is used for backwash UF recovery is reported to be in the range of 85-95%.

The utility of the different fouling metrics (FR_n, $\Delta R_{T,n}$, $\Delta R_{UB,n}$, BW_{eff} and R_{PB}) for control decisions regarding UF operation would clearly rely on establishing their correlation with UF operational performance and backwash efficiency as conceptualized in **Fig. 5-4**. The overall control objectives are to reduce the rate of PB resistance rise in order to lengthen the time (t_{cc}) before the need for CIP is reached (i.e., when the maximum allowed transmembrane pressure drop for the UF module (100 kPa) is reached), while also increasing the achievable UF filtrate recovery (Y_{UF} and t_{cc}). An informed UF operational decision would then require real-time determination of the degree by which the adjustable process variables can reduce the adverse change in the target fouling indicators.

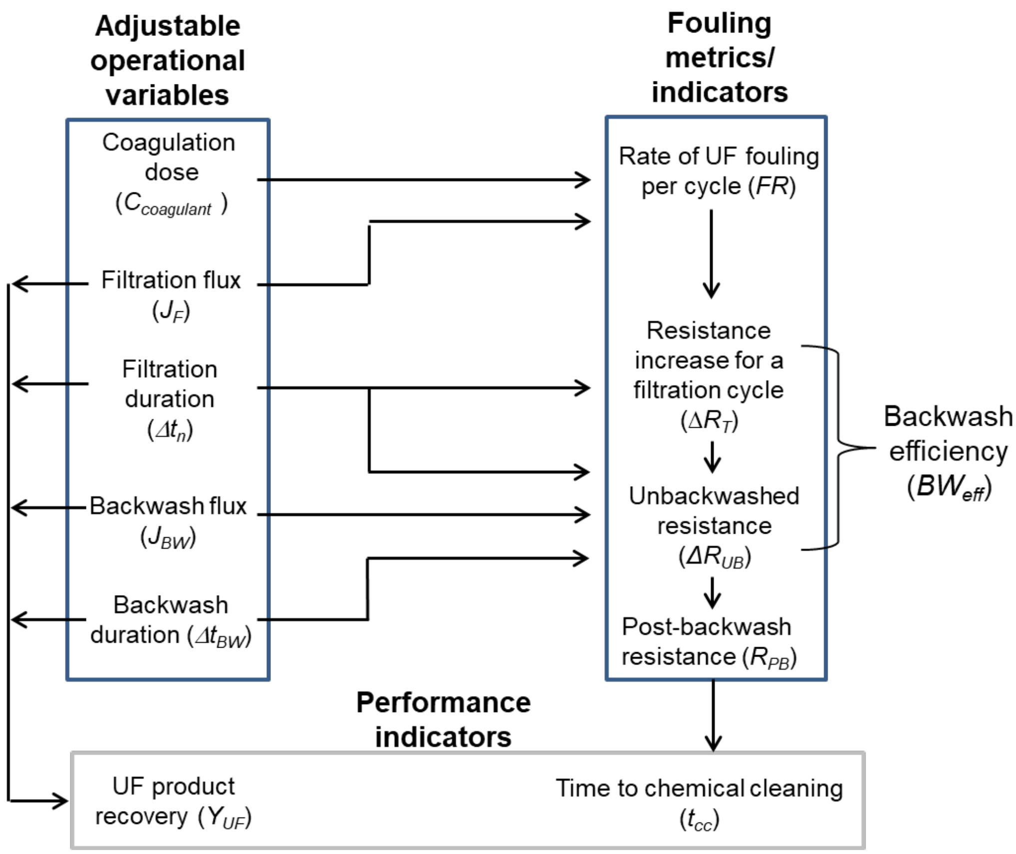

Figure 5-4 Causal relationship diagram of the links between UF adjustable operational variables and fouling indicators. Arrows from operational variables pointing toward a fouling or performance indicator indicate a direct cause-effect relationship.

5.3.2 Group averaged data analysis

Sensor data from field operation is affected by feed water quality and environmental conditions (e.g., feed water temperature), in addition to noise arising from natural fluctuation of sensor signals, actuators and pump operation. Therefore, a moving average was adapted for data processing over a minimum of 6 filtration/backwash cycles to quantify the average filtration period fouling rate $\langle FR \rangle_j$, unbackwashed resistance $\langle \Delta R_{UB} \rangle_j$, average resistance increase per filtration period $<\Delta R_{T,n}>$, and backwash efficiency $\left\langle BW_{eff} \right\rangle_j$, while the overall progression of post-backwash UF resistance $<R_{PB}>$ was assessed based on averaging over at least 6 cycles. A summary of the fouling indicators and their physical process implications is provided in **Table 5-2.**

Table 5-2 Summary of fouling indicators(a)

Online fouling indicators	Physical meaning	Cycle-to-cycle calculation (n^{th} cycle, over N cycles))	Averaged metric for jth segment (over N cycles)	Notes
Filtration period fouling rate (FR)	Rate of filtration resistance buildup (per cycle)	$FR_n = \frac{\Delta R_{T,n}}{\Delta t_n}$	$\left\langle FR \right\rangle_j$	Directly related to feed fouling potential
Backwash efficiency (BW_{eff})	Portion of filtration resistance removed	$BW_{eff,n} = \frac{\Delta R_{BW,n}}{\Delta R_{T,n}} = 1 - \frac{\Delta R_{UB,n}}{FR_n \cdot \Delta t_n}$	$\left\langle BW_{eff} \right\rangle_j$	Relative measurement of backwash efficiency
Unbackwashed resistance	Resistance not removed by backwash	$\Delta R_{UB,n} = \Delta R_{T,n} - \Delta R_{BW,n}$	$\left\langle \Delta R_{UB} \right\rangle_j$	Absolute measurement of initial resistance change per cycle
Post-backwash resistance	Current state of UF fouling	$R_{PB} = \sum_{n=0}^{N} (R_{ini,n} - R_{ini,n-1}) = \sum_{n=0}^{N} R_{PB,n}$	$\left\langle R_{PB} \right\rangle_j = \sum_{j=1}^{J} \left\langle R_{PB} \right\rangle_j$	Equivalent to change in initial resistance

(a) Fouling indictors were determined in real-time based on monitored process variables (**Section 5.3.1).**

5.4 Results & Discussion

5.4.1 Filtration resistance monitoring

In the operation of the UF system, membrane backwash was triggered by an online control system once the incremental UF resistance increase in a given filtration period, ΔR_T, exceeded a threshold value, as per the approach described previously [147]. The feed seawater filtration period for seawater pretreatment was typically of the order of 20 - 50 min, and the membrane filtration resistance (**Fig. 5-5**) increased linearly (i.e., constant rate of fouling) over this period. As illustrated in **Fig. 5-5,** the UF post-backwash resistance (i.e., the initial UF filtration period resistance) progressively increased with continual operation; however, the UF post-backwash resistance for a given cycle was also observed to decrease at times, relative to the previous cycle. Such a behavior should not be surprising since the membrane rate of fouling and the backwash effectiveness are governed by multiple factors including, for example, coagulation, filtration and backwash conditions, feed water chemistry quality and environmental conditions (e.g., temperature). The fact that post-backwash UF resistance can increase as well as decrease over the course of a system operation is critical to be able to ascertain in real time. Such information can then be utilized to implement proper feedback controls strategies not only with respect to backwash adjustment strategies (e.g., backwash duration and flux), but also with respect to real time optimization of coagulant dosing [161].

5.4.2 Effect of coagulants dose on filtration period fouling rate and UF backwash effectiveness

Inline coagulation increases floc size, thereby improving the effectiveness of particulate matter removal. At the same time, inline coagulation also leads to higher rate of membrane fouling via cake formation, while at the same time promoting increased backwash efficiency [161]. Therefore, in order to provide information needed for real-time coagulant dose optimization, it is necessary to establish the relationship between fouling indicators and coagulant dose.

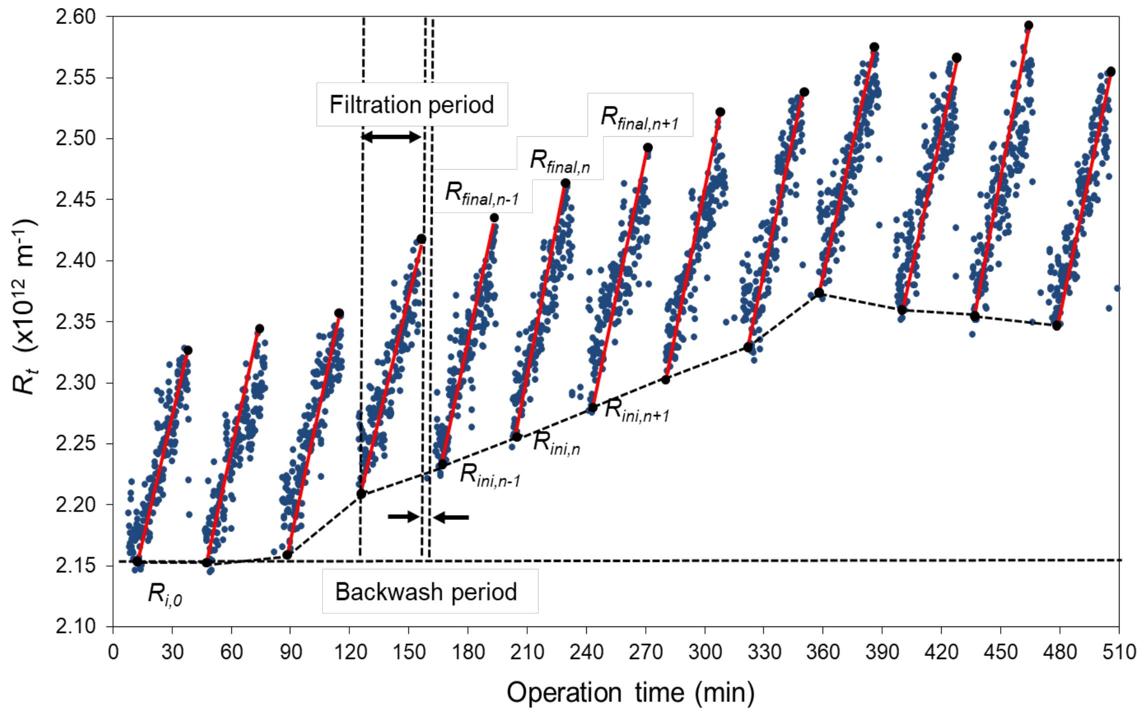

Figure 5-5 Illustration of UF operation displaying membrane resistance during multiple filtration/backwash cycles. The solid lines represent the fitted linear regression lines. $R_{i,o}$ is the initial UF resistance at the start of the run (0^{th} cycle), $R_{ini,n}$ and $R_{final,n}$ are the UF membrane resistances at the beginning and end of filtration cycle *n*. The dashed line traces the post-backwash resistance. UF operating conditions: Filtration flux 45.4 L/m^2·h for a duration of 29-30.4 min with inline $FeCl_3$ coagulant dosing of 2.20 mg/L Fe^{3+}, followed by 70 s backwash at a flux of 162 L/m^2·h. Feed turbidity and chlorophyll-*a* levels were in the range of 0.46-0.73 NTU and 67.2 -155 µg/L, respectively.

Indeed, based on a series of tests shown in **Fig. 5-6,** the average UF fouling rate in a filtration cycle (FR_n) clearly increases with increased coagulant dose. In this example, it is also evident that the coagulant $FeCl_3$ resulted in a higher fouling rate (by about a factor of 3.5) relative to ACH. A higher fouling rate and higher coagulant dose would lead to a greater foulant cake layer thickness, following the same linear rise as the fouling rate, as shown in the inset of **Fig. 5-6**; the latter is based on estimation derived from a cake formation model for constant flux operation [177] (**section 5.6.1**, **Supplementary Material**). With increased inline coagulant dose, membrane fouling is expected to shift toward the formation of a cake layer, which is not adhered to the surface, and can be backwashed more effectively than foulants that adsorb onto the membrane and/or plug its pores. Here it is noted that jar testing clearly showed that flocs formed using ACH were visually smaller and finer than the flocs formed by $FeCl_3$.

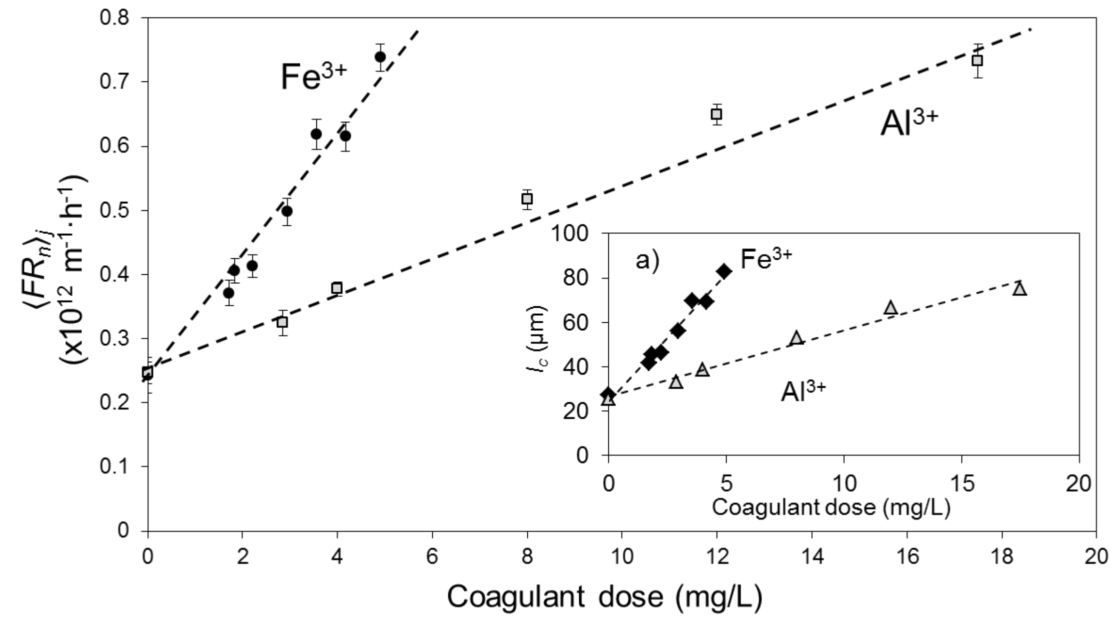

Figure 5-6 Dependence of UF membrane fouling rate (quantified as the rate of change in membrane filtration resistance, *FR*) during filtration on inline coagulant dose (using Fe^{3+} or Al^{3+}). UF operating conditions: Filtration flux of 45.4 L/m^2·h for 30 min followed by 70 s backwash at a flux of 162 L/m^2·h. The vertical error bars indicate standard deviation for the fouling rate averaged over 64 cycles. **The inset figure** shows the change in the UF fouling layer cake thickness (l_c) with coagulant dose for both Fe^{3+} and Al^{3+}.

The impact of inline coagulant feed dosing on backwash effectiveness was assessed by quantifying the post-backwash resistance, R_{PB} (averaged over a set of six filtration/backwash cycles) over a series of short-term tests over an operational period of ~ 1.3 days during which water quality did not change appreciably (**Fig. 5-7**). As expected, R_{PB} progressively increases with increasing cumulative number of filtration/backwash cycles. However, R_{PB} decreased significantly when coagulant dosing was introduced, implying greater backwash effectiveness at higher dose. For example, after 36 cycles, with 1.5 mg/L Fe^{3+} coagulant dosing, R_{PB} decreased by factor of 1.8 and further decreased, by a factor of 64 with coagulant dose of 4.9 mg/L. It is clear from **Fig. 7**, however, and consistent with previous work [161], that the benefit of inline coagulation reaches a level above which further coagulant decreases has little or no advantage in reducing R_{PB}. For example, after 36 cycles, as the coagulant was increased from 3.6 to 4.9 mg/L, the R_{PB} decreased by about 20%. A similar R_{PB} behavior was observed for the case of ACH dosing as detailed in the Supplementary Material (**Section 5.6.3**, **Supplementary Material, Figure 5-20**).

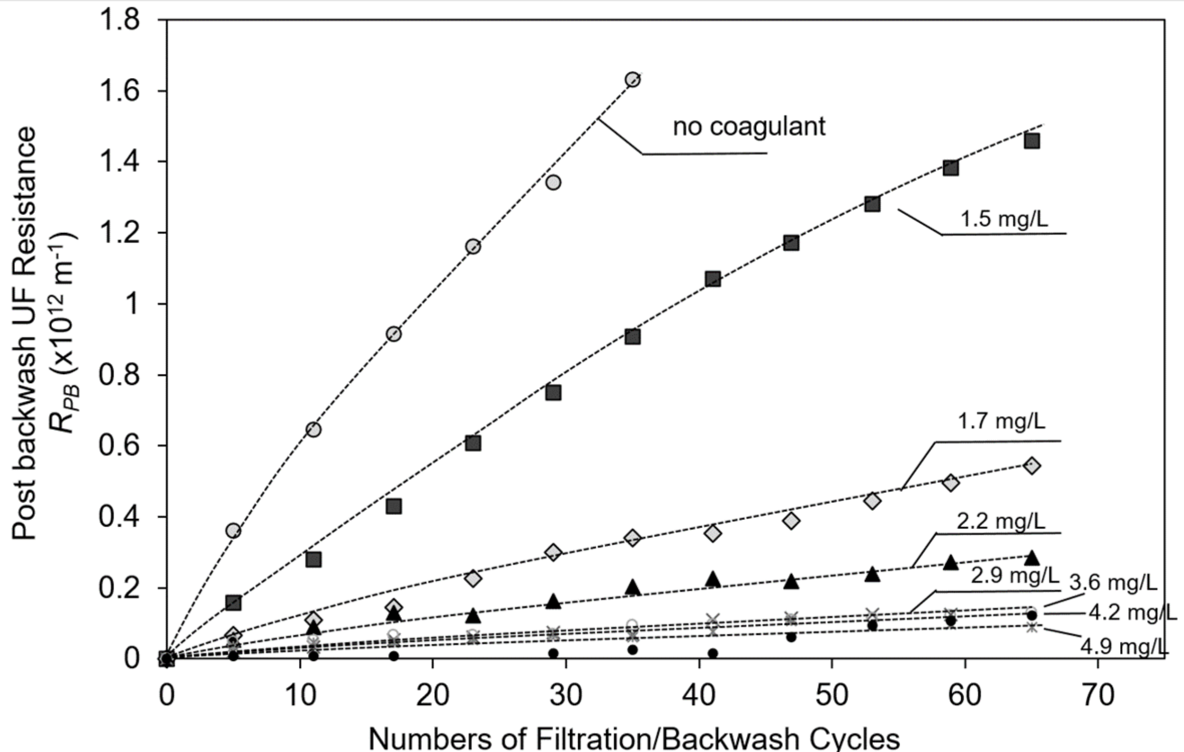

Figure 5-7 Assessment of post-backwash UF resistance for various Fe^{3+} coagulant doses. UF operating conditions: Filtration flux of 45.4 L/m^2·h with backwash triggering every 30 min (for a period of 70 sec) at a flux of 162 L/m^2·h. Feed turbidity during the 1.3 day experimental period was in the range of 0.45 – 1.32 NTU with chlorophyll-*a* being in the range of 32- 78 µg/L.

Over the course of UF operation it should be expected that R_{PB} will eventually increase up to a threshold that will require chemical cleaning in place (CIP) (**Section 5.3.1**). Accordingly, the operational period up to CIP requirement (Fig. 8) can be projected based on the slope of R_{PB} with respect to time (**Fig. 5-7**) past about 40 filtration/backwash cycles where CIP is required when the UF membrane filtration resistance reaches ~9.63 x10^{12} m^{-1} (calculated under fixed filtration flux and based on a maximum allowed transmembrane pressure drop across the UF, Section 3.1). Such an estimate, however, is only an approximation as it is calculated for on operation that is at the same conditions as for the above tests and with the same level of water quality as in the above tests. For example, as shown in **Fig. 5-8**, for the lowest overall fouling rate of 0.587 x10^9 $m^{-1}\cdot hr^{-1}$ at coagulant dose of 4.17 mg/L Fe^{3+} CIP would be required every 77 days. In contrast, with the ACH coagulant, even at a dose range of 12 - 25 µg/L, CIP would be required every 1-4 days. The above field tests suggest that $FeCl_3$ is a more effective coagulant in promoting higher fouling rate during filtration and correspondingly higher backwash effectiveness (i.e., lower remaining residual or unbackwashed UF resistance).

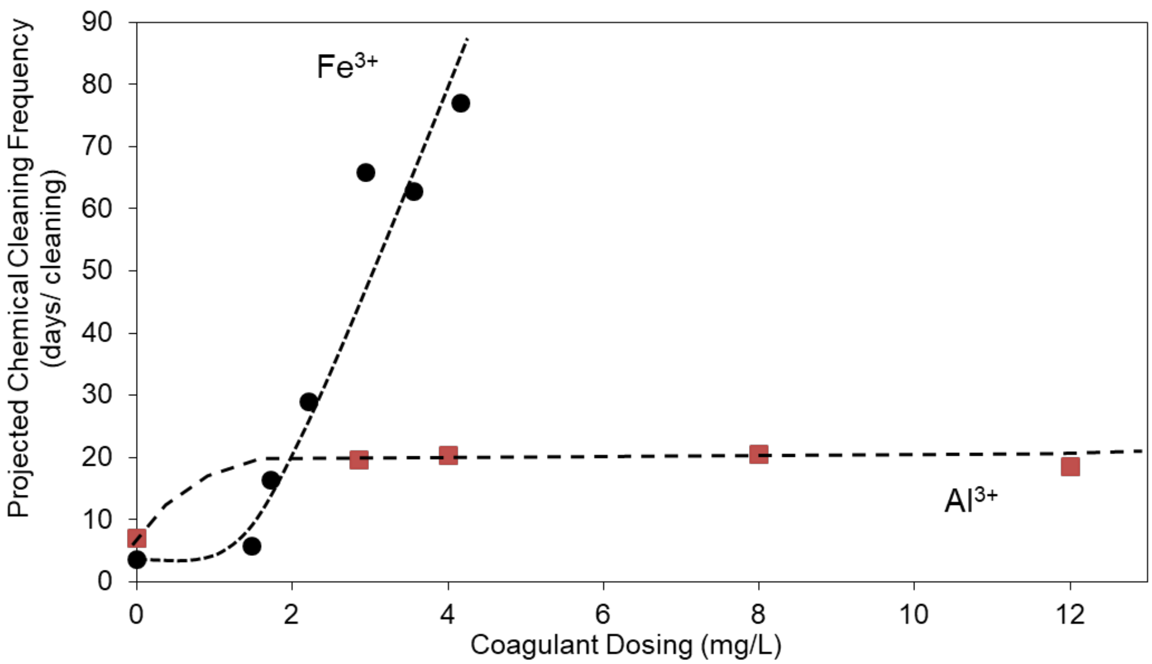

Figure 5-8 Projected chemical frequency (days per chemical cleaning) for two different coagulants ($FeCl^3$ and ACH). UF operating conditions: Filtration flux of 45.4 $L/m^2\cdot h$ with backwash triggered every 30 min, at a flux of 162 $L/m^2\cdot h$ for 70s duration. Initial (clean) UF membrane resistance: 4.76x10^{11} m^{-1}. Threshold (maximum allowable) UF membrane resistance that triggers needed chemical cleaning: 9.63 x10^{12} m^{-1}.

5.4.3 Effect of coagulants dose on UF backwash efficiency (BW_{eff})

A direct quantification of UF backwash efficiency, BW_{eff} (**Eq. 5-5**), can be illustrated by inspecting the behavior in ΔR_{UB} relative to total resistance increase per cycle (ΔR_T). As shown in **Fig 5-9**, the unbackwashed resistance decreases with increased coagulant dose which can also be viewed by the increased backwash efficiency (**Eq. 5-5,** averaged here over 64 cycles). It is postulated that at a higher rate of fouling (**Section 5.4.2**), which is facilitated increasing the coagulant dose, cake formation will be with larger flocs that are more easily removed. Indeed, as seen in **Fig. 5-9**, as the coagulant dose increases backwash efficiency correspondingly increases. For example, inline coagulation with $FeCl_3$ at 4.16 mg/L as Fe^{3+} would increase backwash efficiency to 99.7 % relative to 95% at coagulant dose of 1.7 mg/L as Fe^{3+} and 90% without coagulant dosing. Inline coagulation with ACH required higher dose to attain similar levels of backwash efficiencies. For example, to attain backwash efficiency of 97.9% ACH coagulant dose of 2.85 mg/L as Al^{3+} would be required, but a significantly higher dose of 12 mg/L would be needed to attain 99% efficiency.

As clearly seen in **Fig. 5-9,** there is an apparent threshold beyond which further increase in coagulant increase did lead to measurable backwash efficiency increase. This threshold was about 4.16 mg/L Fe^{3+} and 12 mg/L Al^{3+} for inline coagulation with $FeCl_3$ and ACH, respectively. Here it is important to state that overdosing should be avoided to avert coagulant passage to the RO elements. It is stressed that under conditions of temporally variable water feed quality the optimal coagulant dose will change. Therefore, both for achieving optimal UF operation and for reducing coagulant use, one would have to utilize a suitable coagulant dose controller, as demonstrated recently in [161].

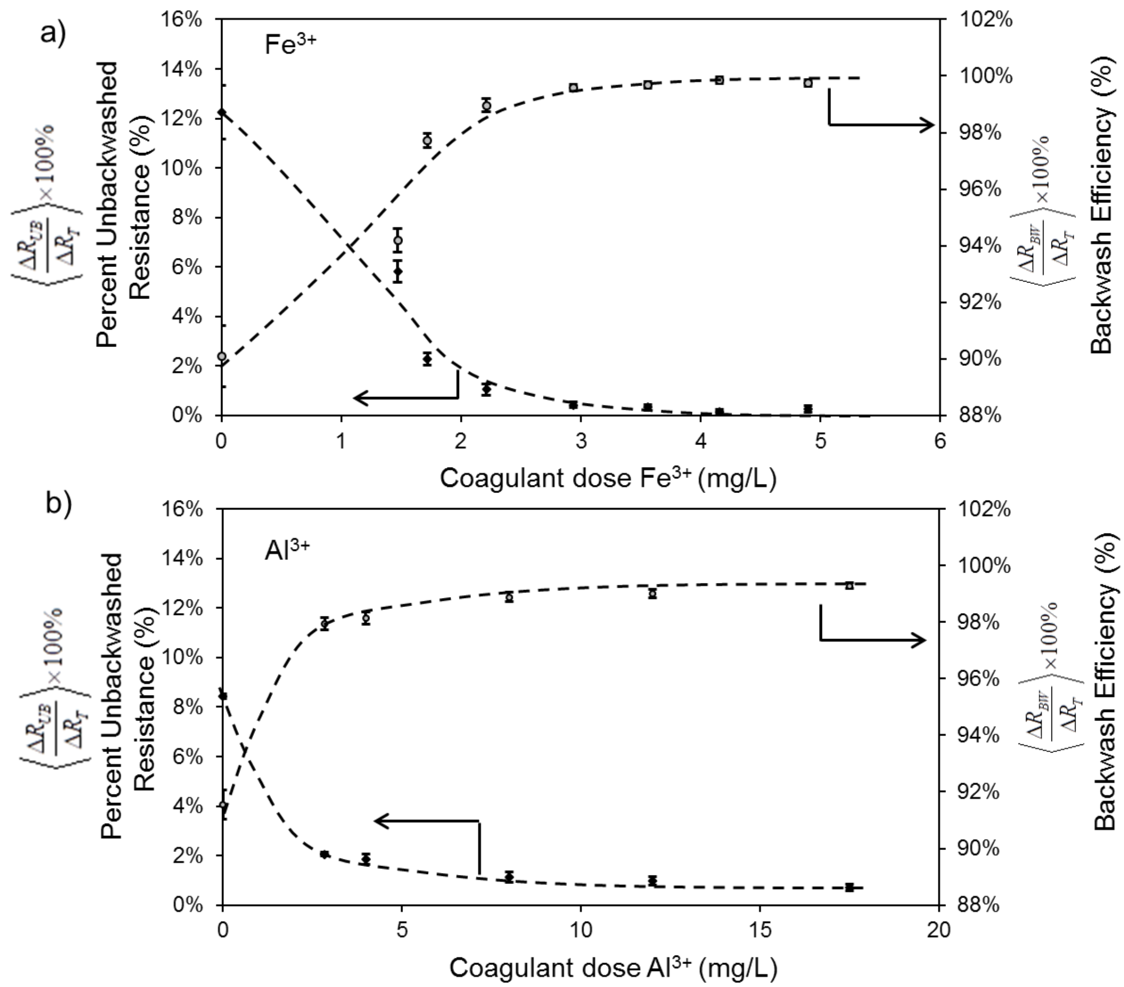

Figure 5-9 Impact of UF inline coagulation dose, for the coagulants $FeCl_3$ and ACH, on UF backwash efficiency (BW_{eff}). UF system was operated at filtration flux of 45.4 L/m^2·h for 30 min, followed by backwash at a flux of 162 L/m^2·h for 70 s.

Ultrafiltration along with inline coagulation promotes the formation of larger aggregates (or flocs) that lead to rapid membrane cake fouling (**Section 5.4.2**) which then renders backwash more effective. Accordingly, one should expect that with increased filtration cycle fouling rate (promoted by adjustment of the coagulant dose) the unbackwashed resistance (ΔR_{UB}) would decrease, thereby reducing the buildup of irreversible fouling. It is interesting to note that the trend is similar for both coagulants (**Fig. 5-10**) suggesting similar degree of cake formation for a filtration fouling rate. It is apparent that above a filtration period fouling rate threshold (FR~$0.4\text{x}10^{-12}$ $(\text{m}\cdot\text{h})^{-1}$ for the present case) the unbackwashed fouling resistance is no longer reduced with progressive filtration/backwash cycles. This behavior is expected given that there is a threshold coagulant dose (**Fig. 5-9**) above which the unbackwashed resistance (ΔR_{UB}) reaches its lowest value (i.e., maximum backwash efficiency) and given that the fouling rate varies linearly with coagulant dose (**Figs. 5-6**).

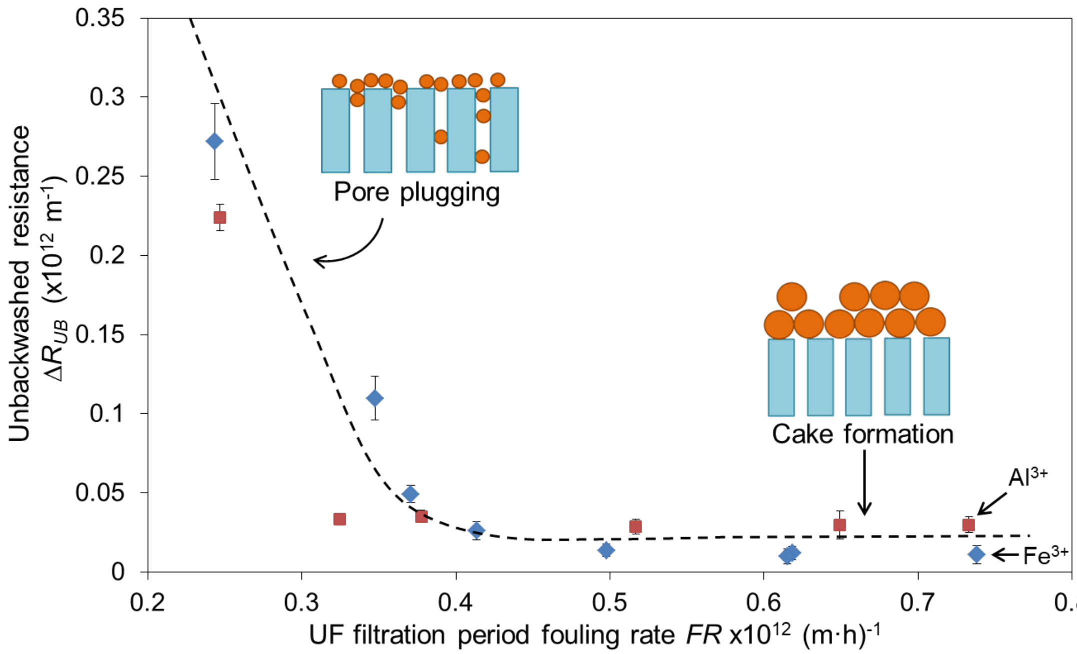

Figure 5-10 Variation of unbackwashed UF fouling resistance (ΔR_{UB}) with the UF filtration period fouling rate (FR) for the coagulants $FeCl_3$ and ACH over a dose ranges of 1.5 - 4.9 mg/l as Fe^{3+} (blue diamonds) and 2.8 - 25 mg/l Al^{3+} (red squares), respectively. UF operating conditions: Filtration flux of 45.4 L/m^2·h for 30 min, followed by backwash flux of 162 L/m^2·h for 70 s.

5.4.4 Effect of backwash conditions on UF backwash effectiveness (BW_{eff})

Backwash effectiveness is impacted by UF filtration and backwash conditions in addition to coagulant dose (**Section 5.4.3**). An illustration of the dependence of backwash effectiveness (average over 12 cycles) on filtration period length, backwash flux and duration is provided in **Fig. 5-11**, for UF operation at fixed $FeCl_3$ coagulant dose of 4.17 mg/L as Fe^{3+}. For a given filtration flux (36.9 L/m^2·h) and backwash flux and duration (70 s), backwash efficiency was essentially 100% until a threshold filtration period of 40 min was reached beyond which backwash effectiveness declined to nearly 82%. Backwash effectiveness decreased somewhat (by ~ 29%) as the filtration flux increased from ~ 33 to 42 $L/m^2{\cdot}h$. It is postulated that, over the above feasible range of filtration flux needed to maintain effective RO operation for the present plant, increased filtration flux was accompanying by a shorter convective residence time for effective inline coagulation and thus lower fouling rate and hence lower backwash effectiveness (see **Fig. 5-10** and **section 5.6.2**, **Supplementary Material**).

For a given filtration conditions, increasing the backwash flux increases backwash effectiveness up to a plateau after which there is little or no benefit in further increase in backwash flux (**Fig. 5-11b**). For example, upon increasing the backwash flux from 70 L/m^2h (about a factor of 1.9 greater than the filtration flux of 36.9 $L/m^2{\cdot}h$) by about 200% (or a factor of 3.8 higher than the filtration flux) BW_{eff} increased from 50% to 99.9%. For a given UF filtration flux and duration, the UF backwash efficiency can also be increased, for a given backwash flux, by lengthening the backwash duration (**Fig. 5-11c**). For example, for the current UF-RO system, upon increase the backwash duration, from 12 min to 80 min, backwash efficiency increased from about 78% to about 95%. It is noted that an upper limit is reached with respect to backwash duration beyond which there is no further improvements of backwash effectiveness.

5.4.5 Real-time monitoring of UF fouling indicators in seawater feed pre-treatment

A series of three UF operational field tests of 5-12 days in duration were undertaken in order to evaluate the fouling indicators under conditions during which water quality may vary to different extents (**Fig. 5-12**). In these field tests UF backwash was triggered based on the self-adaptive approach [147] described in **Section 5.3.1**.

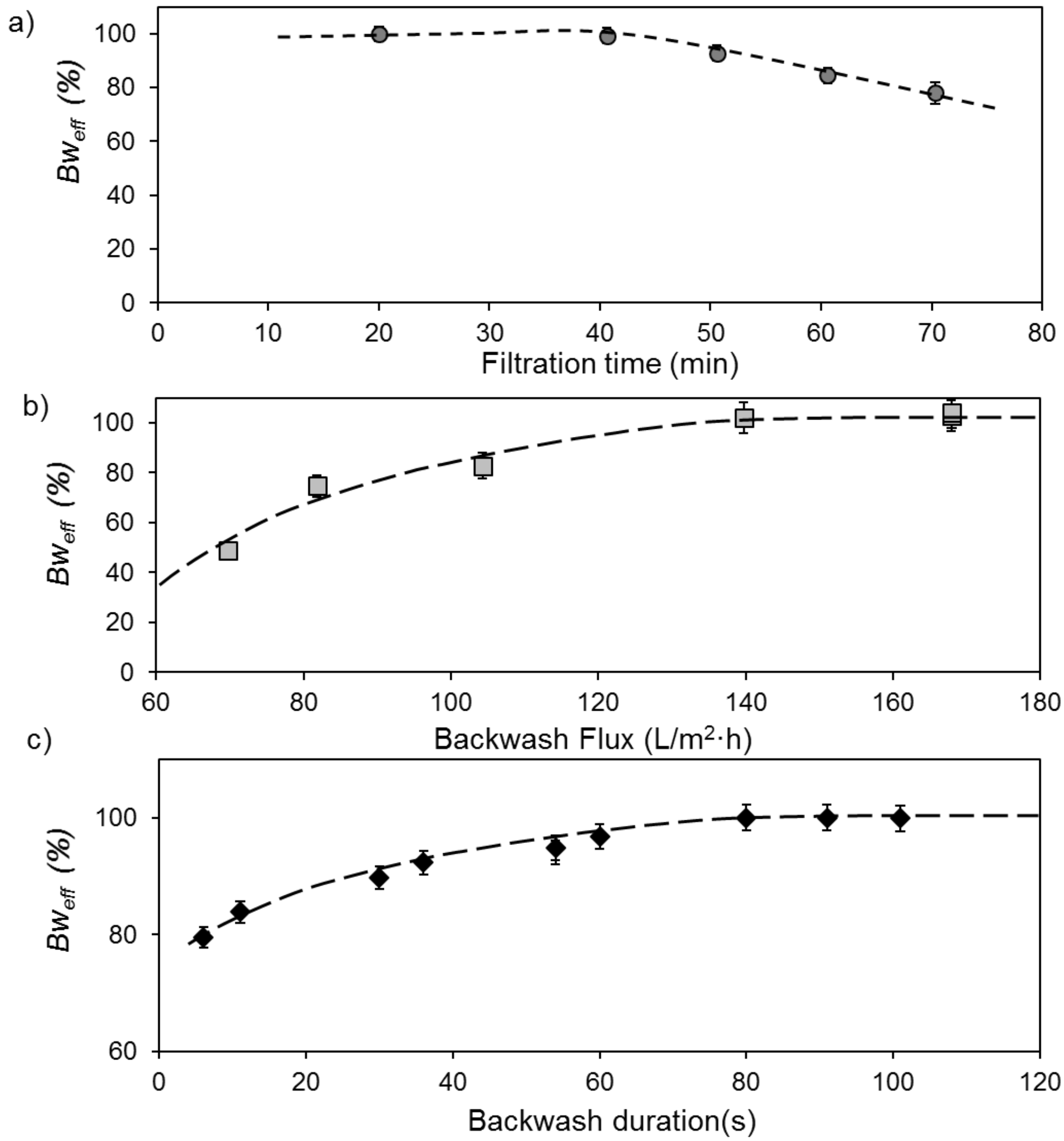

Figure 5-11 Dependence of backwash effectiveness on: a) filtration duration for operation at filtration flux of 36.9 $L/m^2 \cdot h$ and backwash flux of 162 $L/m^2 \cdot h$ of 70 s; b) backwash flux for UF operation at filtration flux of 36.9 $L/m^2 \cdot h$ for 30 min, followed by backwash for a period of 70 s; c) backwash duration for UF operation at filtration flux and period of 36.9 $L/m^2 \cdot h$ and 30 min, respectively, and backwash flux of 162 $L/m^2 \cdot h$. Note: All tests were conducted with inline $FeCl_3$ coagulant dosing of 4.17 mg/L as Fe^{3+}.

Field Test #1 was conducted over a period of 12 days of continuous UF-RO operation. The feed turbidity was in the range of 0.65- 4.9 NTU with chlorophyll-*a* in the UF feed and filtrate being in the range of 42 - 101 μg/L and 0.48 – 0.54 μg/L, respectively (**Fig. 5-12(a - c)**). During the above period, the average filtration duration was about 21 minutes with a total of 812 filtration/backwash cycles. For the above test period, the unbackwashed ($\langle \Delta R_{UB} \rangle$) and post-backwash resistance ($\langle R_{PB} \rangle$), and backwash efficiency ($\langle BW_{eff} \rangle$), and fouling rate (*FR*) all averaged over 24 cycles, are shown in **Figs. 5-13(a-d)**. During the first day of operation there was an initial period during which the residual unbackwashed resistance (**Fig. 5-13a**) increased during the first day and then after about 2 days of operation at about 0.030 ± 0.025 x10^{12} m^{-1}. The above trend is likely to have occurred due to foulant cake compaction and distribution of coagulant throughout the three UF modules (**Fig. 5-1**). The post-backwash UF resistance (**Fig. 5-13b**) increased with time due to progressive buildup of fouling resistance due to the accumulation of residual unbackwashed UF resistance (**Fig. 5-13a**). It is noted that the filtration period fouling rate (**Fig. 5-13c**) during the filtration periods was relatively constant (0.48 ± 0.07 x10^{12} $m^{-1}\cdot h^{-1}$) suggesting that the temporal fluctuations in feed quality did not lead to significant alteration of the severity of cycle-to-cycle membrane fouling rate, with the exception of the first day of rapid fouling. Given the above, it is not surprising that the UF backwash efficiency which was initially ~60% increased during the first two day of operation and thereafter remained relatively stable at $\langle BW_{eff} \rangle$=95.2% ±1.0% (**Fig. 5-13d**). Finally, it is noted that for the above operation, the post-backwash fouling rate (i.e., dR_{PB}/dt) for the UF system (**Fig. 5-13b**) was ~ 3.02 x 10^9 $m^{-1}\cdot h^{-1}$ which implies that CIP would have been required within 126 days.

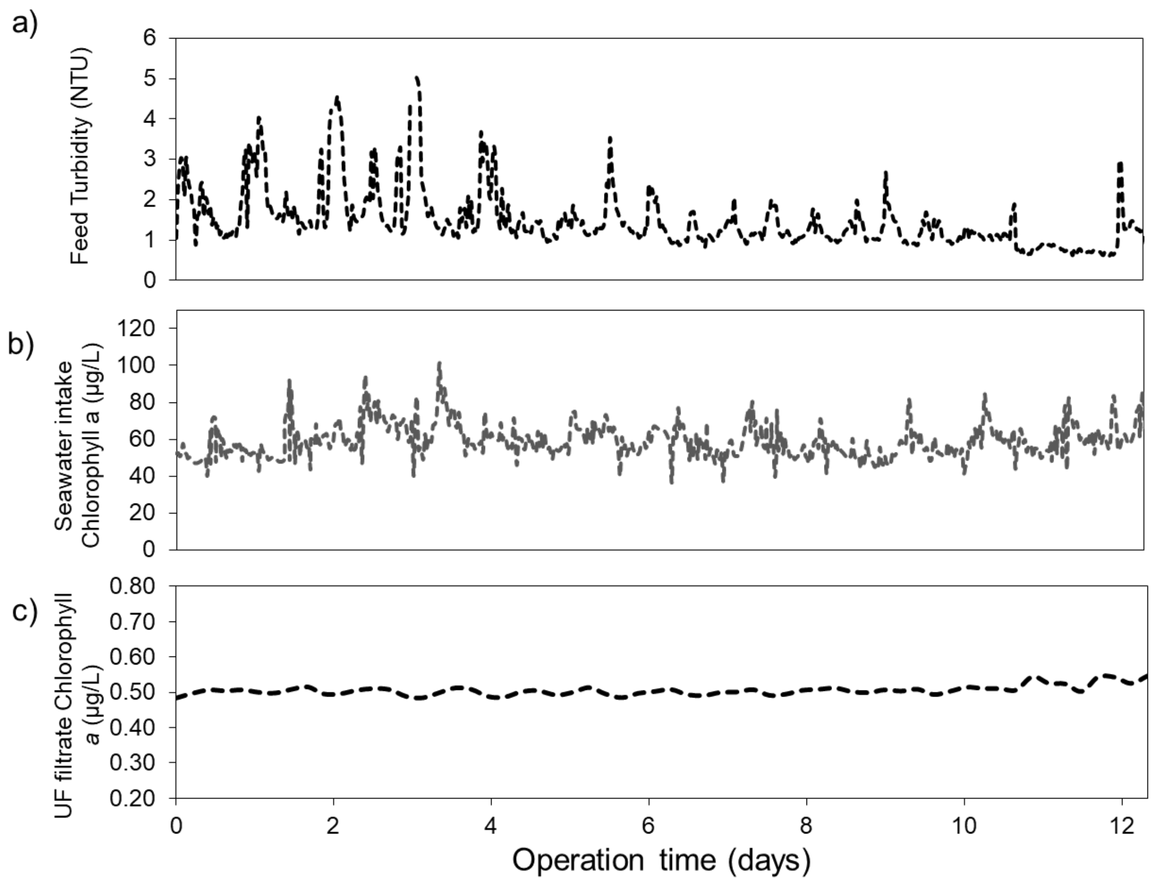

Figure 5-12 Water quality data during Test #1 over a period of 12 days (300 h). Feed turbidity: 1.46±0.05 NTU. Chlorophyll-*a,* feed: 59.7±0.73 µg/L, filtrate: 0.50±0.04 µg/L.

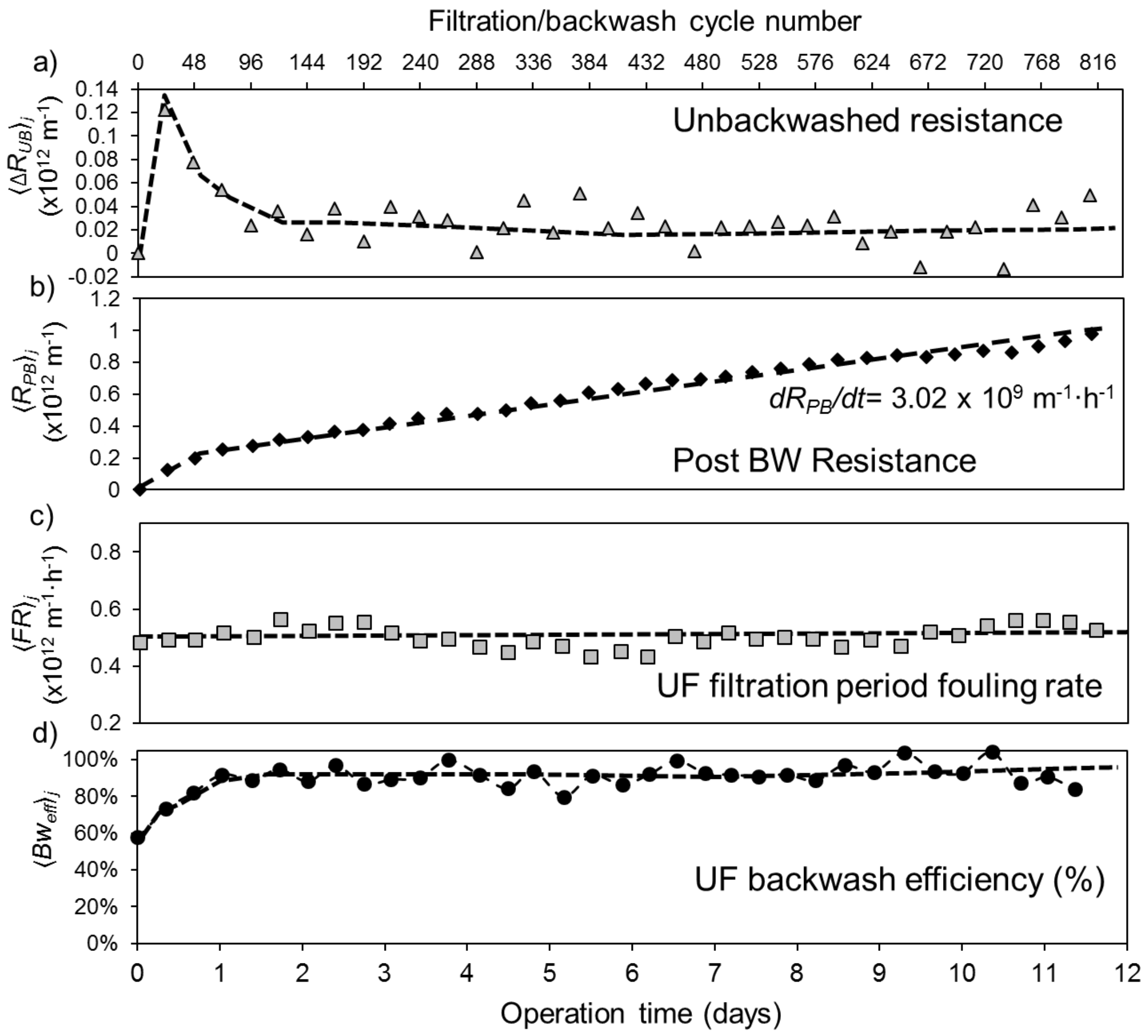

Figure 5-13 Variation of UF fouling indicators over a 12 day period during which water quality varied as given in **Fig. 5-12** (Test #1). UF operation was in self-adaptive mode of backwash triggering, whereby filtration duration was in the range of 29-42 min at a flux of 45.4 L/m^2·h with inline coagulant dosing of $FeCl_3$ of 4.12 mg/L Fe^{3+}, backwash flux was 162 L/m^2·h for a period of 70 s.

A follow-up field Test #2 was conducted over a period of about 5 days (consisting of UF operation of 482 filtration/backwash cycles). During the above period feed water turbidity was in the range of 1.25 - 3.24 NTU (**Fig. 5-14a**), and the UF feed and filtrate chlorophyll-*a* concentrations (**Fig. 5-14b,c**) were in the range of 20 - 127 µg/L and 0.41-0.66 µg/L, respectively. In this test the UF filtration and backwash fluxes were the same as in Test 1 with backwash also triggered in a self-adaptive mode (**Section 5.3.1**). In Test #2, as in Test #1, the unbackwashed UF resistance increased rapidly from an initial value of 0 m^{-1} to a maximum value of 0.74 $\times 10^{12}$ m^{-1} after an operational period of 6.5 hours (**Fig. 5-15a**), but then decreased to a value of ~0.079 $\times 10^{12}$ by day 3 with an apparent slight temporally decreasing slope (i.e., $d\langle \Delta R_{UB} \rangle / dt \approx -0.59\times10^{9}\,\mathrm{m^{-1}\cdot h^{-1}}$). Although the post-backwash resistance increased as expected during the initial 3 days (**Fig. 5-15b**), there was a slight decrease (~7.5%) from day 3 to day 5. This behavior should not be surprising since the filtration cycle fouling rate (**Fig. 5-15c**) increased monotonically from the initial value of ~0.55 $\times 10^{-12}$ $m^{-1}h^{-1}$ by a factor of 1.8 over the test period over the five day period.

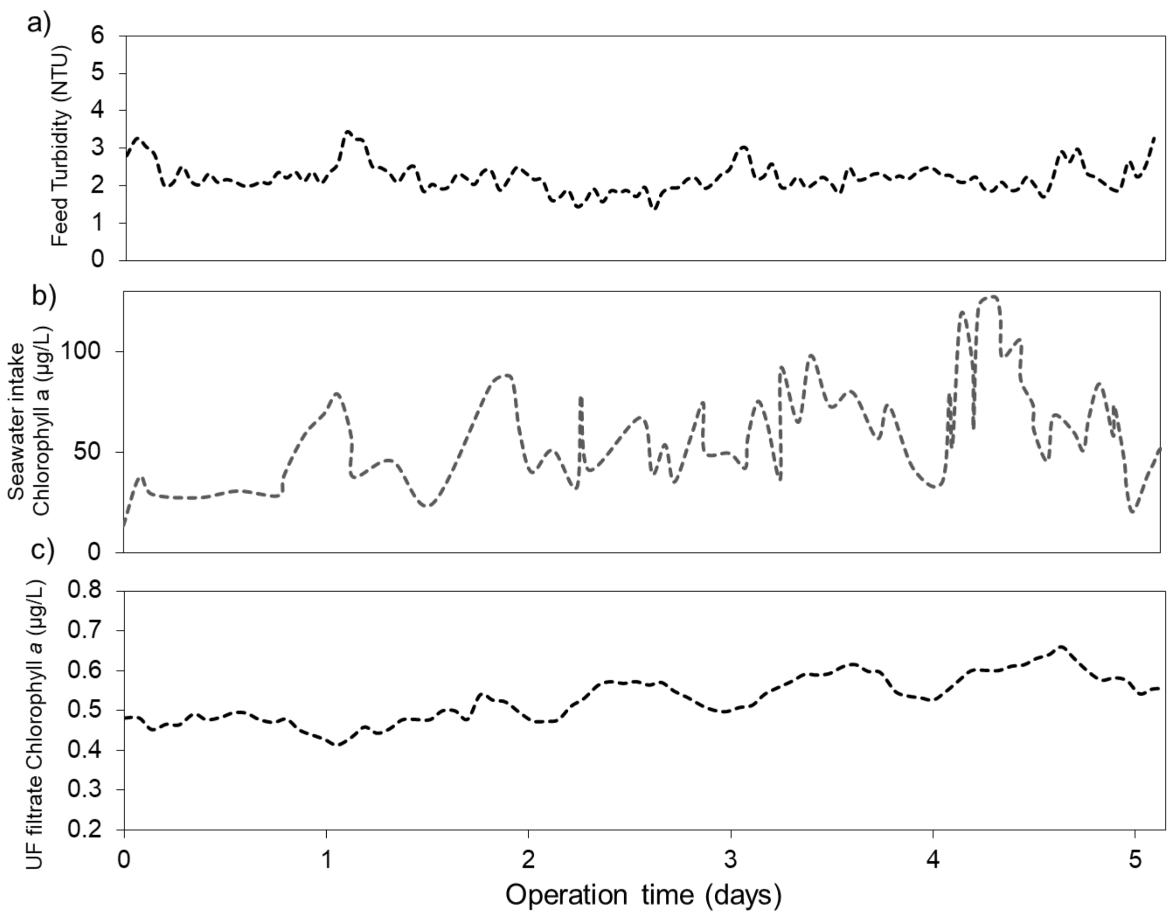

Figure 5-14 Feed water turbidity and chlorophyll a in the UF feed and filtrate for 25 hours (~ 5 days) of field Test #2. Feed turbidity: 2.22±0.07 NTU, feed and UF filtrate chlorophyll-a: 60.4±5.8 µg/L and 0.53±0.01 µg/L, respectively.

Given that the feed turbidity was relatively stable (1.25 - 3.24 NTU) (**Fig. 5-14a**), it is unlikely that particulate matter was responsible for the progressive increase in the filtration period fouling rate. This observation is consistent with the findings of other studies that turbidity measurements alone are insufficient for assessing the feed water fouling potential. We note, however, that the feed chlorophyll-*a* varied considerably (20 - 127 μg/L; **Fig. 5-14b**) and appeared to be elevated over the operational period of 40 to 120 hours. Chlorophyll-*a* implies the presence of algae which was likely the cause of higher filtration period fouling rate (**Fig. 5-15c**). However, for system operation under adaptive backwash control [147], at higher fouling rate in a filtration period triggered backwash at a higher frequency (**Section 5.6.6 Supplementary Materials, Figs. 5-23 - 5-24**) such that the UF filtration period decreased from 32.5 min to 25 min by the end of the test period. It is also noted that backwash efficiency is expected to increase with rising per cycle fouling rate, for operation under inline coagulant dosing (**Section 5.4.3**); this was indeed the case in this field Test showing that the backwash efficiency increased over the course of the field test from the initial value of 40% to about 99% (**Fig. 5-15d**).

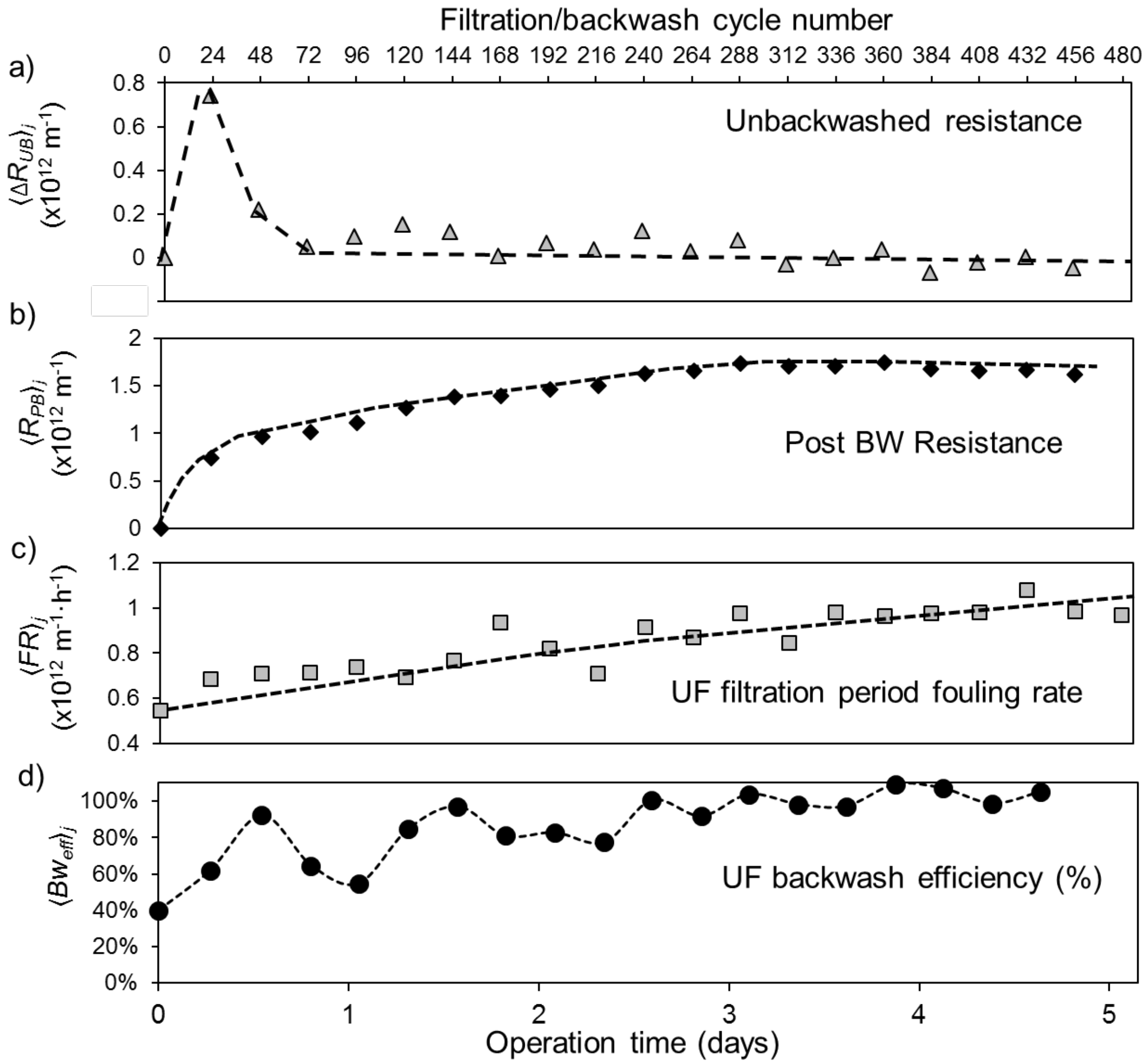

Figure 5-15 Variation of UF fouling indicators over the 125 hours (~ 5 days) of Test #2 during which water quality varied as given in **Fig. 5-14**. UF operation was in self-adaptive mode of backwash triggering (total of 479 filtration/backwash cycles), whereby filtration duration was in the range of 25-33 min at a flux of 45 L/m^2·h with inline coagulant dosing of $FeCl_3$ of 4.2 mg/L Fe^{3+}, backwash flux was 162 L/m^2·h for a period of 70 s.

Test #3 was conducted during a period in which there was a storm event that commenced in day 2 of the UF operation (about 53.5 hours after the test started). The feed water turbidity and chlorophyll-*a* data which were previously reported in [161] are reproduced in Fig. 16a. At day 4 of the 6.5 day test period both turbidity and chlorophyll-*a* spiked to values of about 15.3 NTU and 152 μg/L, respectively, which were significantly higher, by factors of 14.4 and 1.64, relative to the initial values at the beginning of the test period. Thus, Test #3 was a unique opportunity to evaluate the fouling indicators with respect to the observed UF performance under poor feed water quality conditions. Test #3, which was conducted under adaptive backwash triggering, was part of an earlier demonstration of UF operation with a coagulant dose controller as described in [161]. In this test the coagulant controller was activated (**Fig. 5-16(b-e)**) 62.4 hours after the beginning of the storm event (i.e., t=62.4 hours). Prior to the storm event the feed water turbidity level was < 1.0 NTU and chlorophyll-*a* was in the range of 80 - 100 µg/L (and ~0.64 µg/L in the UF filtrate, **Supplementary Information, Figure 5-25**), and where the filtration period fouling rate, $\langle FR \rangle$, was in the range of 0.45- 0.7 x10^{12} m^{-1}. The UF post-backwash resistance increased steadily, due to the progressive accumulation of unbackwashed UF resistance, rising to about 8% above the initial state during the storm. However, due to the increase in inline coagulant dose, the filtration period fouling rate increased enabling the backwash effectiveness to increase from the post-storm average of 80% ±7% to exceeding 100% during the storm. The latter behavior indicates that UF resistance removal was not only complete relative to the previous set of cycles, but that foulant that was not removed in previous cycles was also removed. The filtration period fouling rate stabilized after about day 5 (at ~ 1.51 $m^{-1}h^{-1}$) and the post-backwash UF resistance actually decreased which is consistent with both a high UF backwash efficiency and the improvement in feed quality. It is noted that throughout the field tests the UF filtrate turbidity was maintained at 0.03± 0.005 NTU (**Section 5.6.7, Supplementary Information, Figure 5-25**) and the RO unit, operating at a recovery level of 36%, produced permeate of salinity of 148 ± 13 mg/L total dissolved solids. The RO membrane elements did not reveal any signs of fouling and the permeability remained stable at 1.85± 0.137 x10^{-12} m/Pa·s.

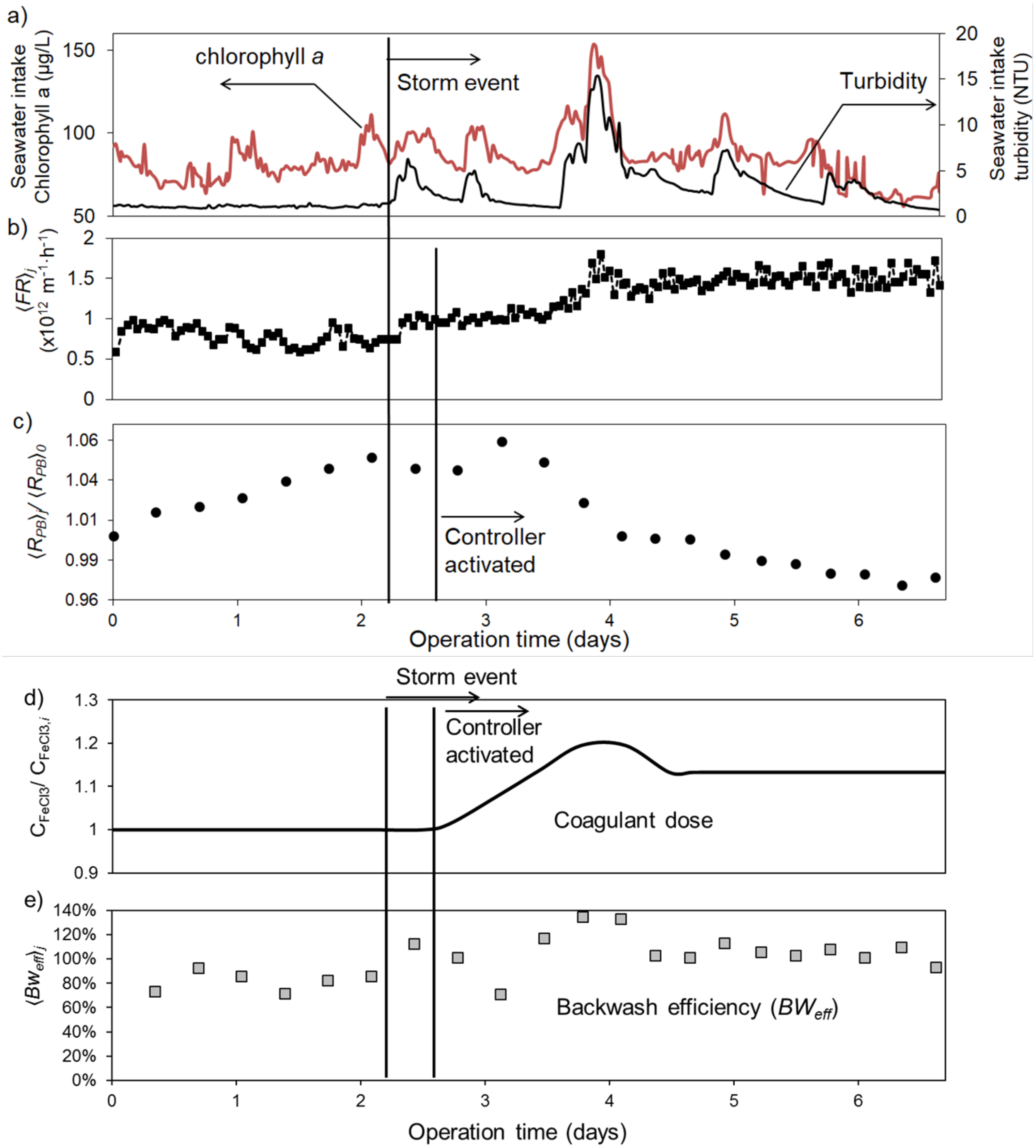

Figure 5-16 UF system fouling indicators during Test #3 in which a storm event was experienced (Fig. 15). UF operating conditions: Filtration flux of 45 $L/m^2 \cdot h$ with $FeCl_3$ inline coagulant dosing of 4.2 mg/L Fe^{3+}, with adaptive backwash (resulting in filtration periods of 25 – 45 min) at a flux of 162 $L/m^2 \cdot h$ for a period of 70 s.

5.5 Conclusions

Real-time monitoring of UF fouling behavior in the treatment of raw sweater feed for RO desalination was explored using fouling indicators that included filtration period fouling rate, unbackwashed and post-backwash resistances, as well as backwash efficiency. Field evaluation of the above parameters was carried out for sweater UF pretreatment of RO feed water. In a series of systematic short-term tests inline coagulation was sown to increase the rate of fouling which in turn reduced the unbackwashed resistance and increased backwash efficiency. $FeCl_3$ was a more effective coagulant relative to ACH in promoting higher backwash efficiency and thus projected to allow longer UF operation before requiring chemical cleaning. For a given UF operation at a given filtration flux and inline coagulant dose, backwash effectiveness increased with backwash flux and duration up to a threshold upper limit, but decreased for filtration periods above a threshold value. Backwash efficiency increased with coagulant dose, given the increase in the filtration period fouling rate, up to a threshold upper limit beyond which there was no further improvements in backwash efficiency. Field tests over periods of days, during which water quality was variable (with respect to monitored turbidity and chlorophyll-*a*), conclusively showed that increased fouling rate indeed resulted in higher backwash efficiency and thus a lower progressive increase of UF post-backwash resistance. The results of the current study suggest that real-time UF fouling indicators can provide useful insight regarding the UF operation and conceivably be utilized to guide and implement self-adaptive UF operational control for effective UF pretreatment.

5.6 Supplementary Material

5.6.1 Estimation of effective cake thickness (l_c) and UF resistance increase in a filtration cycle (ΔR_T)

The total UF filtration resistance can be expressed as the linear sum of the membrane (R_m), cake layer (R_{cake}) and irreversible fouling (R_{irr}) resistances to permeate flow, i.e., $R_T = R_m + R_{cake} + R_{irr}$ (Eq. 5-2), and where the cake resistance that result in UF filtration, R_{cake}, is related to the cake thickness as follows:

$$R_{cake} = \alpha \cdot l_c \tag{5-9}$$

in which l_c effective cake thickness and α (1/m^2) is the specific cake resistance that can be described by a form of Kozeny–Carman equation [57, 75, 180]:

$$\alpha = \frac{5 \cdot (1-\varepsilon_c)^2 \cdot \left(\frac{3}{a}\right)^2}{\varepsilon_c^{\ 3}} \tag{5-10}$$

where a is the radius of a cake particle and ε_c is the cake porosity calculated from,

$$\varepsilon_c = \frac{\rho_s - \rho_c}{\rho_s - \rho_w} \tag{5-11}$$

in which ρ_s , ρ_c and ρ_w are the densities (kg/m^3) of the cake particles (i.e., the dry coagulated particles in the case of UF with coagulant dosing), the cake layer and the seawater feed, respectively.

For UF modules of cylindrical hollow fibers in a multi-channel inside-out filtration configuration (as in the current study), the increase cake thickness (l_c) as a function of filtration time [177] can be expressed by the following differential equation,

$$\frac{dl_c}{dt} = \frac{C_b}{C_c - C_b} \cdot \frac{r_i}{r_i - l_c} \cdot J \tag{5-12}$$

in which C_c and C_b are the cake layer and particle concentrations (in the bulk) near the cake layer upper surface, J is the water filtrate flux, and r is the radial position within the fiber and r_i is the inner radius of the hollow fiber in the UF element. To a reasonable approximation the radius of the membrane fiber can be taken to be much greater than the cake thickness ($r_i >> l_c$), and hence Eq. (5-12) can be simplified as:

$$\frac{dl_c}{dt} = \frac{C_b}{C_c - C_b} \cdot J \tag{5-13}$$

The rate of change of cake resistance with time, FR, can then be obtained from

$$FR = \frac{dR_{cake}}{dt} == \alpha \frac{dl_c}{dt} = \frac{C_b}{C_c - C_b} J \cdot \alpha \tag{5-14}$$

and the cake thickness is obtained from the solution of Eq. (5-13), subject to the initial condition of $l_c(0) = 0$, to arrive at the following time-dependence of l_c,

$$l_c \approx \frac{C_b}{C_c - C_b} J \cdot t \tag{5-15}$$

It is noted that C_b can be estimated by rearranging Eq. (5-14) as follows:

$$C_b = \frac{C_c \cdot FR}{FR + J \cdot \alpha} \tag{5-16}$$

where FR can be determined experimentally for the given filtration period. The total UF filtration resistance, making use of Eq. (5-1), (5-2) and Eq. (5-15), can be expressed as,

$$R_T = \frac{\Delta P_o}{J \cdot \mu} + \frac{\Delta P_{irr}}{J \cdot \mu} + \frac{\alpha \cdot C_b}{C_c - C_b} \cdot J \cdot t \tag{5-17}$$

where ΔP_o and ΔP_{irr} are the contributions of membrane (clean) and irreversible fouling to the overall transmembrane pressure, respectively, the last term is the contribution of the cake layer to the total filtration resistance, and μ is the feed water viscosity.

In order to estimate the effective cake thickness (l_c) and UF resistance increase per filtration cycle (ΔR_T), the properties of the primary cake particles (i.e., $Fe(OH)_3$) were estimated from the published literatures [181-185] (a=~0.25 μm, ρ_s= 3120 kg/m^3 , ρ_w = 1025 kg/m^3, and ρ_c is assumed to vary linearly with ε_c in the range of 1045-2300 kg/m^3). The specific cake resistance (α) can be estimated using Eq. (5-10), Eq. (5-11), C_c can be estimated from $C_c = \rho_s (1- \varepsilon_c)$, C_b can be calculated using Eq. (5-16), and the effective cake thickness is estimated using Eq. (5-15). Finally, the total filtration resistance increase ($\Delta R_T = R_{final} - R_{initial}$) at a given inline coagulant dose, can be estimated from Eq. (5-9).

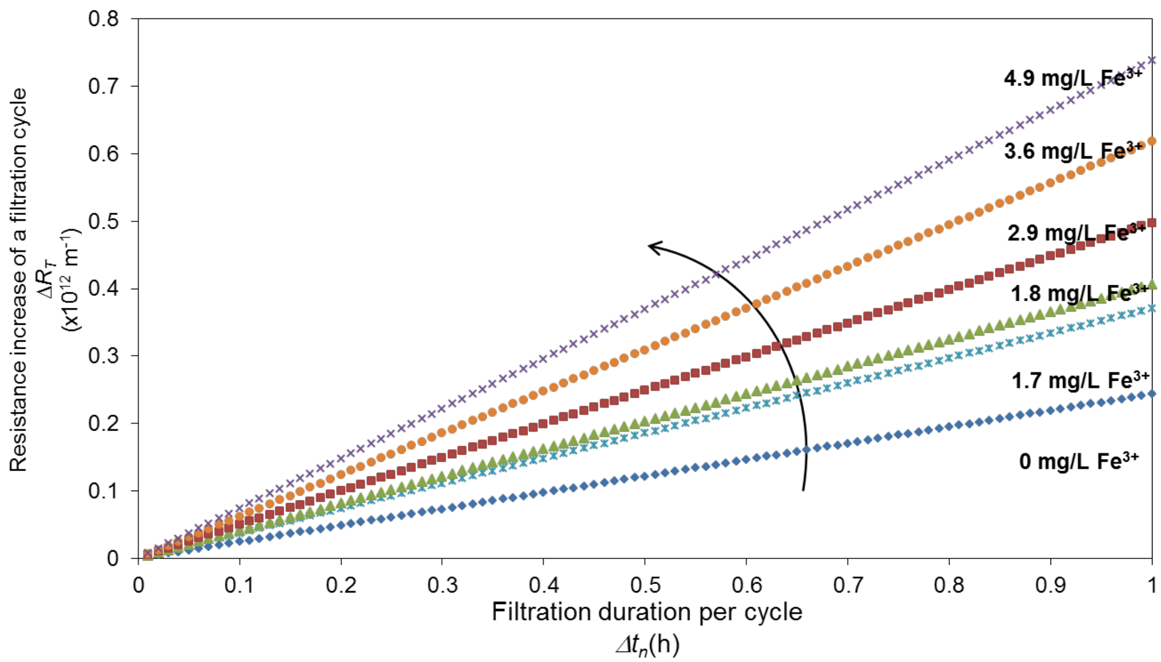

Figure 5-17 Projected effect of filtration duration (Δt_n) on filtration cycle resistance increase (ΔR_T) for various inline coagulant doses. UF operation: filtration flux of 45.4 L/m^2·h. Constant feed temperature of 25 ºC.

5.6.2 Effect of filtration flux on the fouling rate (FR) during the filtration period

The effect of filtration flux on the fouling rate in a given filtration period, *FR,* was investigated by a short-term experiments in which the filtration flux was varied (**Fig. 5-18**). The coagulant dose was kept constant during the filtration period by adjusting the coagulant inflow in proportion to the UF feed flow. As shown in **Fig. 5-19**, the rate of fouling in a given filtration cycle (*FR*) varied by only about 20% as filtration flux increased from 32.8 to 40.5 L/m^2·h (~23.5% increase). With inline coagulation, increased filtration flux which is achieved by a higher UF feed flow rate results in reduced residence time for inline coagulation and thus lower the effectiveness of flocculation and thus lower rate of cake buildup (see **Section 5.4.2**).

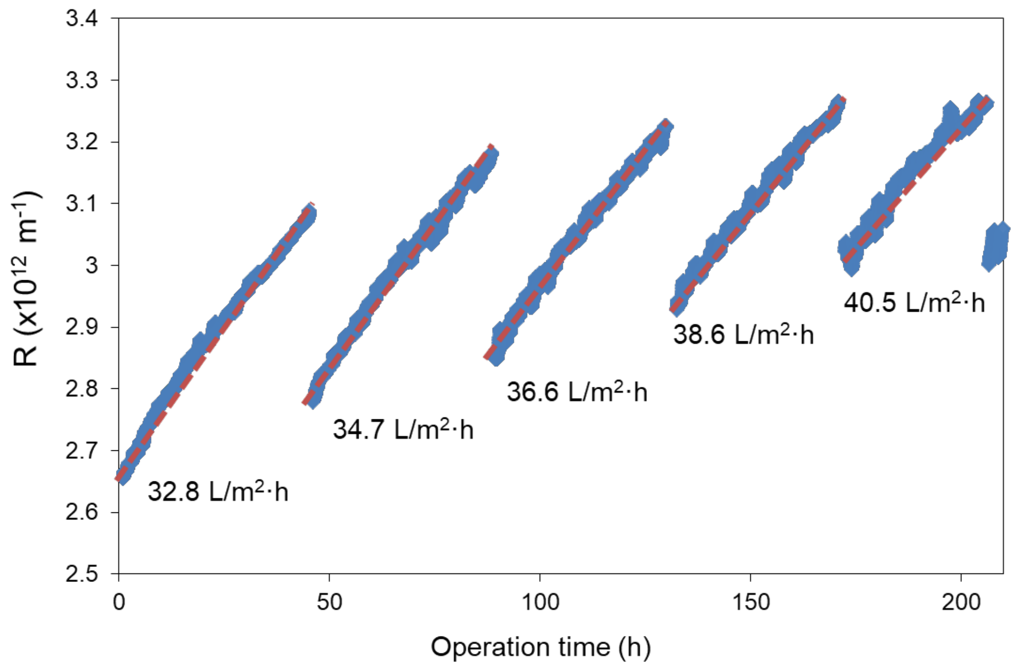

Figure 5-18 Illustration of UF resistance increase during single filtration periods at progressively increased UF filtration flux. The slopes of UF resistance increase with increased UF filtration flux. UF operating conditions: 42 min filtration time with inline $FeCl_3$ coagulant dose of 3.8 mg/L Fe^{3+}, backwash was set for 120 s at a flux of 162 L/m^2·h.

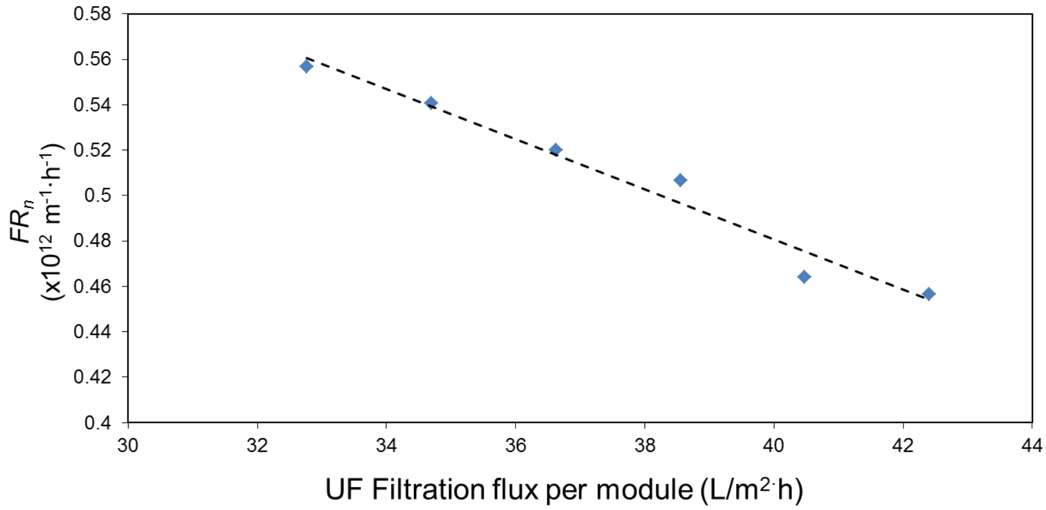

Figure 5-19 Effect of filtration flux on filtration period fouling rate (*FR*) as determined from the data presented in Fig B1. The fouling rate (as quantified by FR) decreases with increased filtration flux for the present operation with inline coagulation. UF operating conditions: 42 min filtration time with inline $FeCl_3$ coagulant dose of 3.8 mg/L Fe^{3+}, backwash was set for 120 s at a flux of 162 $L/m^2\cdot h$.

5.6.3 Post-backwash UF resistance for various ACH dose over a number of filtration cycles

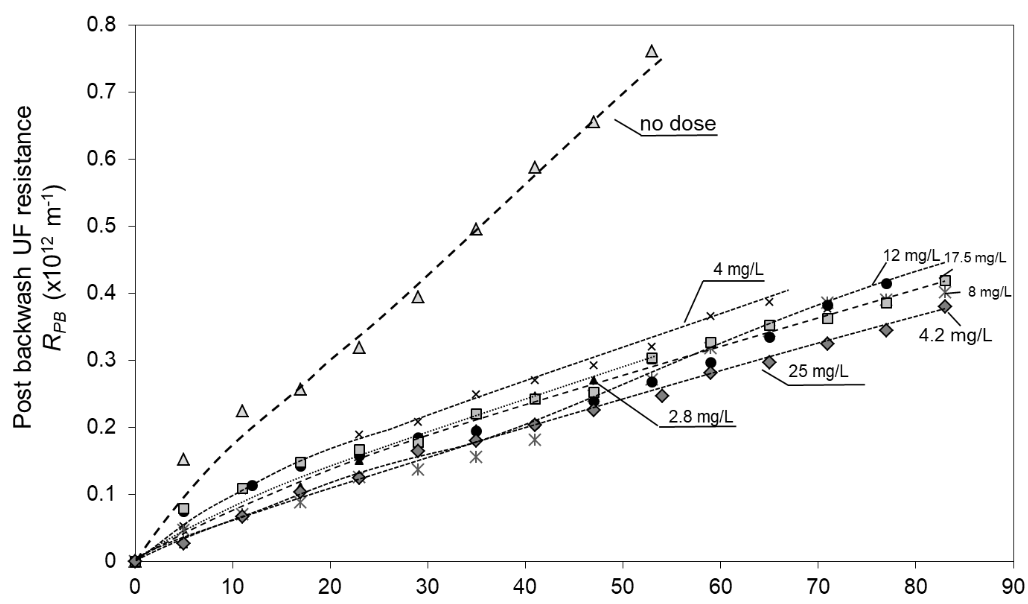

Figure 5-20 Post-backwash UF resistance increase with progressive filtration/backwash cycles for different levels of inline ACH coagulant dose (0- 25 mg/L as Al^{3+}). UF operating conditions: filtration flux of 45.4 $L/m^2\cdot h$ for 20 min at coagulant dose, backwash period of 70 s at a flux of 162 $L/m^2\cdot h$. Feed turbidity and chlorophyll *a* were in the range of 0.72 – 1.45 and 45-89 mg/L, respectively.

5.6.4 *Effect of backwash condition on unbackwashed resistance per cycle (ΔR_{UB}).*

UF backwash effectiveness of UF backwash, expressed in terms of the unbackwashed UF resistances (ΔR_{UB}) was evaluated with respect to filtration flux, duration and frequency. As shown in **Fig. 5-21, 1)**, ΔR_{UB} was essentially constant at ~0.011 $x10^{12}$ m^{-1} up to filtration time of ~ 40 min above which the unbackwashed UF resistance steadily increased reaching ~0.045 $x10^{12}$ m^{-1} (a 400% increase) at the filtration time of 70 min. Increased backwash flux (**Fig. 5-21, 2**)) reduced the unbackwashed UF resistance. The maximum effectiveness (in terms of lowering ΔR_{UB}) that was reached at a backwash flux of 140 $L/m^2 \cdot h$ at which ΔR_{UB} was 0.011 $x10^{12}$ m^{-1} (about a factor of 10 reduction in ΔR_{UB}) when the backwash flux was reduced by half. The duration of backwash was also critical as demonstrated in **Fig. 5-21, 3)**. For given operating conditions, as the backwash duration increased ΔR_{UB} declined (e.g., from a value of 9.08 $x10^{10}$ m^{-1} at backwash duration of 5s) to its lowest value (9.63 $x10^{9}$ m^{-1}) at backwash duration of 70 s beyond which there was essentially negligible improvement.

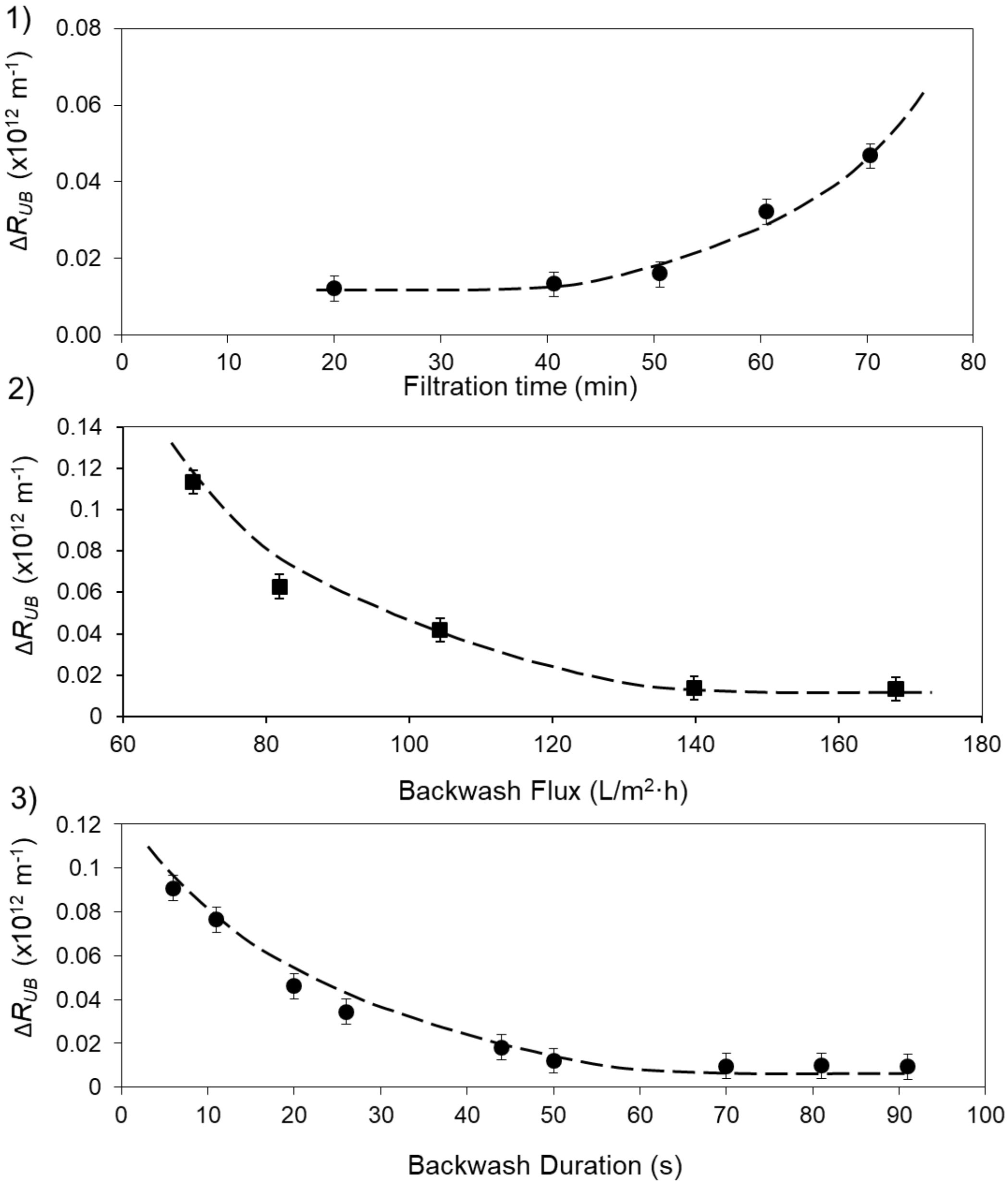

Figure 5-21 UF backwash performance quantified with respect to the unbackwashed resistance, ΔR_{UB}, as impacted by: (1) filtration time (filtration flux= 36.9 L/m^2·h, backwash flux= 162 L/m^2·h for 70 s); (2) backwash flux (filtration flux=36.9 L/m^2·h for 30 min, backwash flux duration of 70 s); and (3) backwash duration (filtration flux=36.9 L/m^2·h for 30 min, backwash flux=162 L/m^2·h). Inline $FeCl_3$ coagulant dose of 4.17 mg/L Fe^{3+} was applied in all cases.

5.6.5 *Appendix E: Dependence of Unbackwashed resistance (ΔR_{UB}) on coagulant dose*

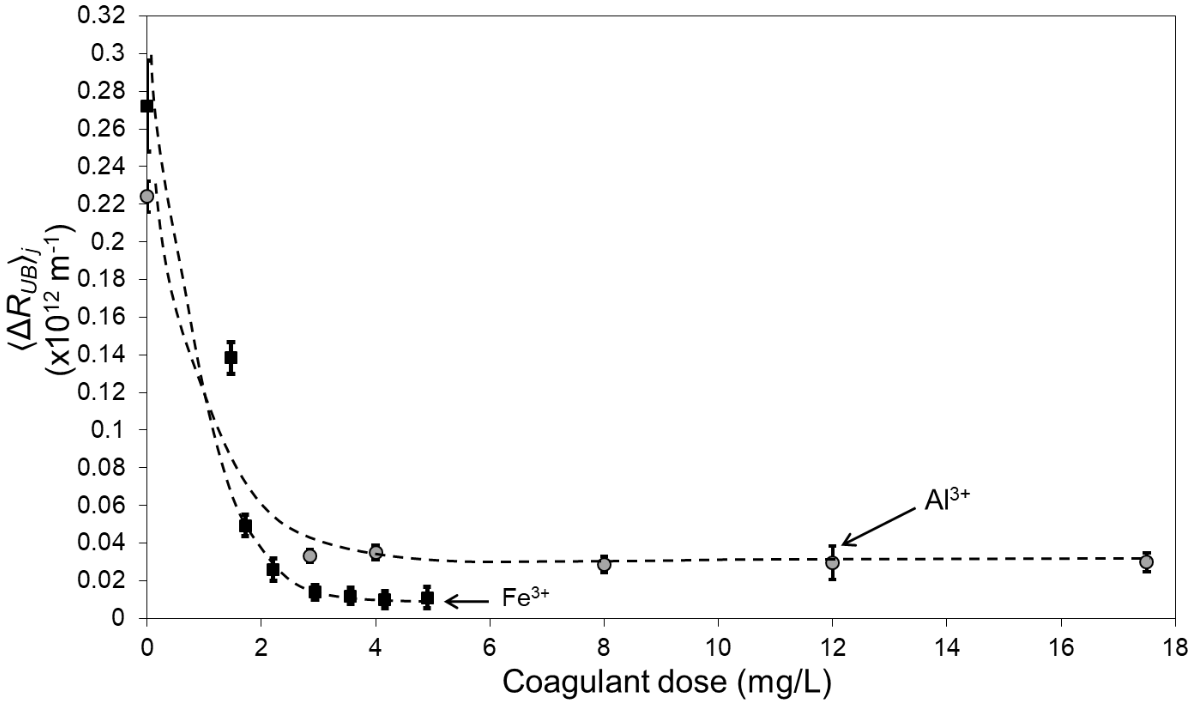

Figure 5-22 Dependence of unbackwashed UF resistance (averaged over 12 filtration/backwash cycles) on coagulant dose. UF operating conditions: filtration flux of 45.4 $L/m^2 \cdot h$ for 30 min, followed by backwash at a flux of 162 $L/m^2 \cdot h$ for 70s.

5.6.6 Appendix F: Comparison of filtration period Fouling rate with the frequency of backwash

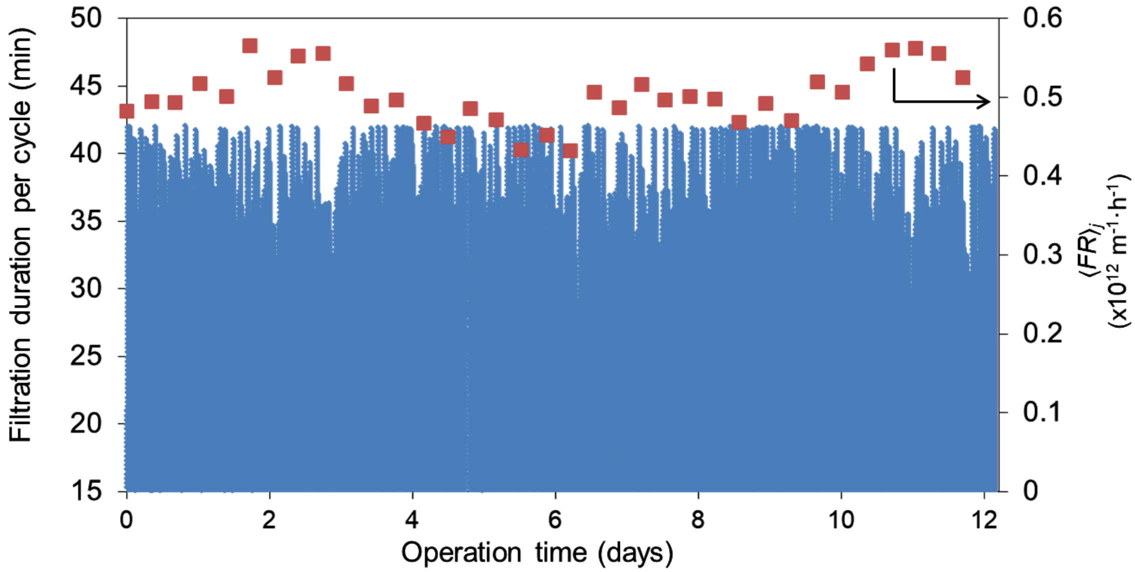

Figure 5-23 Comparison of filtration period fouling rate (averaged every 24 cycles, red square) with the filtration duration per cycle (or frequency of backwash, blue bar) for Test 1.

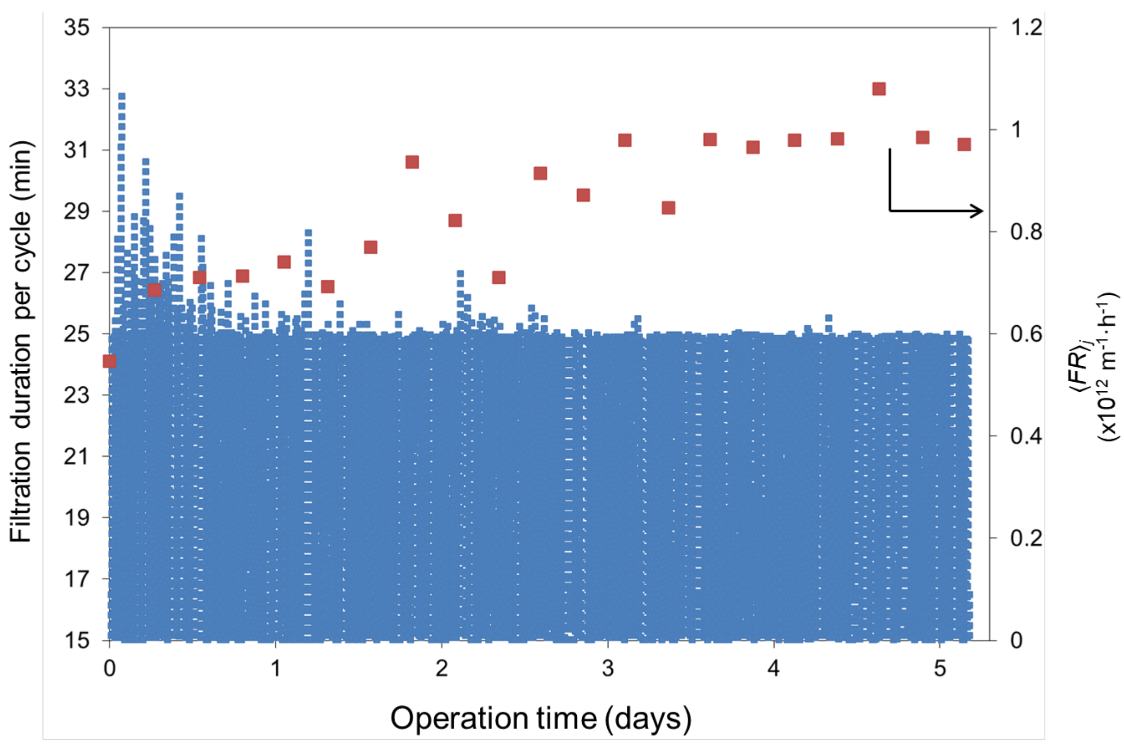

Figure 5-24. Comparison of filtration period fouling rate (averaged every 24 cycles, red square) with the filtration duration per cycle (or frequency of backwash, blue bar) for Test 2.

5.6.7 Real-time UF filtrate quality data and UF pre-filter fouling rate during storm event

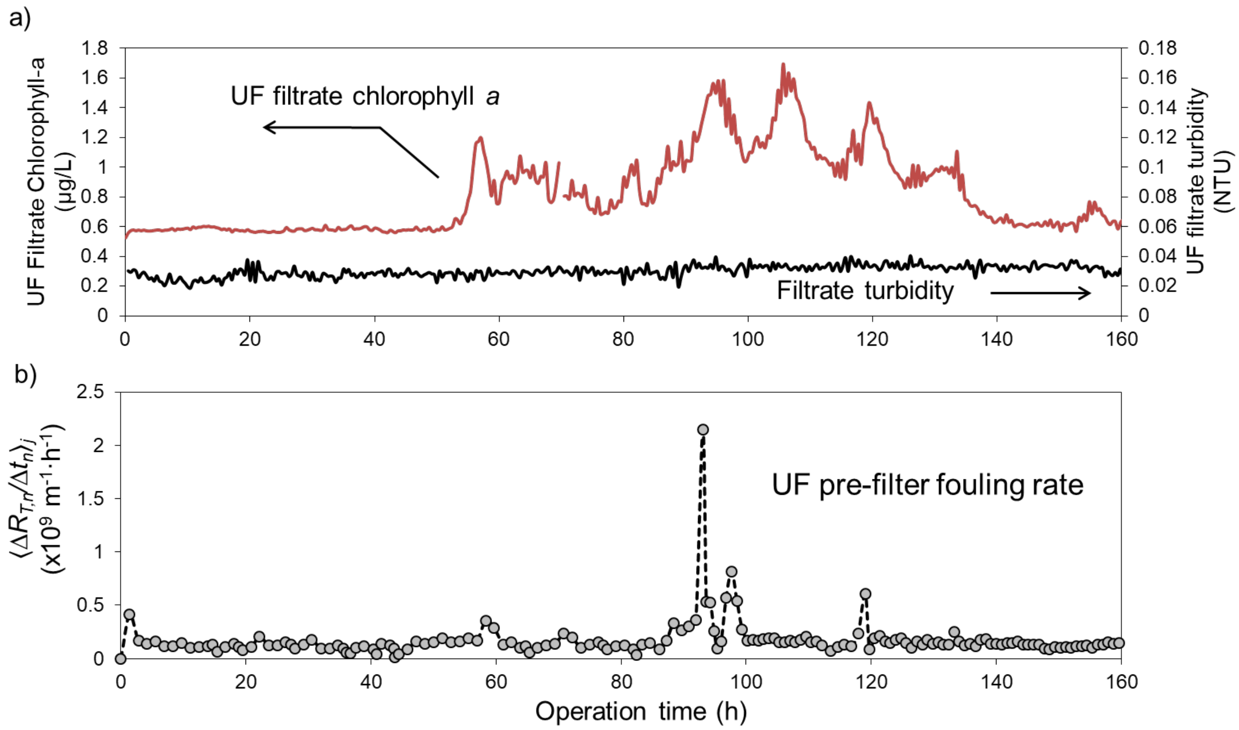

Figure 5-25 (a) UF filtrate turbidity and chlorophyll-*a* levels during Field Test #3 (Section 5.4.5), and (b) Fouling rate of the UF pre-filter (self-cleaning microfilter) (during field Test #3; Section 5.4.5) used as precautionary pretreatment prior to the UF unit for removal of large particles.

6 Demonstration of Adaptive Variable Coagulant Dosing Strategy in an Integrated UF-RO System

6.1 Overview

An adaptive variable inline coagulant dosing strategy (square wave dosing consisting of coagulation dose at a constant level, followed by dose reduction within each filtration period) was successfully demonstrated in a full-scale UF system as pretreatment for a seawater RO desalination system. Online UF fouling indicators were utilized for comparison of UF backwash effectiveness (in term of unbackwashed resistance) and post backwash resistance with and without coagulant dose (i.e., via inline dosing of $FeCl_3$). Short term experiments revealed that during the filtration period, it was necessary to ensure that the UF fouling rate per filtration cycle was kept in the optimal cake formation region via a precisely controlled initial coagulant dose followed by a second dose (determined to be at least 50% of the initial dose) to preserve a foulant cake layer that would enable effective UF backwash.

Coagulant dose set points (duration for initial continuous dose and percent reduction in second dosing step) were optimized based on fouling characteristics and monitored changes in real-time UF module chlorophyll-*a* retention. It was demonstrated that the dose reduction strategy in conjugation with self-adaptive backwash triggering (based on maximum allowable filtration resistance change per cycle, $\Delta R_{T,max}$) was effective in reducing both the required coagulant use and backwash frequency [147, 174]. It was also demonstrated that self-adaptive and thus variable coagulant dosing regiments could be effectively implemented via a coagulant controller [161], even when confronted with temporally variable feed water quality. The above approach enabled coagulant use reduction by more than 36%. In addition, field tests indicated that real-time chlorophyll-*a* measurements can serve to signal the condition of coagulant underdosing.

6.2 Experimental

6.2.1 Integrated Seawater UF-RO Pilot System

A simplified schematic of the experimental setup is provided in **Figure 6-1**. Detailed description of the UF-RO pilot system is provided in **Chapter 5**, **Section 5.2, Fig. 5-1**). The RO pretreatment system consisted of an inline basket strainer (0.32 cm ID screen perforation, Hayward SB Simplex, Clemmons, NC), a 200-micron self-cleaning screen strainer (TAF-500, Amiad Corp., Mooresville, NC), and three polyethersulfone (PES) multi-bore hollow fiber UF modules (Dizzer 5000+, Inge, Greifenberg, Germany) (0.02 μm pore size, inside-out filtration direction, surface area per module: 50 m^2) connected in parallel. In this part of the study two UF modules were kept in filtration mode at any given time [147, 174]. The UF modules were backwashed sequentially using RO concentrate or RO permeate. The RO feed pump (APP 10.2, Danfoss, Nordborg, Denmark), controlled by Variable Frequency Drive (VFD) (VLT AQUA Drive FC 202, 22 kW, Danfoss, Nordborg, Denmark) provided feed to three seawater spiral-wound RO elements membranes (Dow Filmtec SW30HRLE-400, Dow Chemical Company, Midland, MI) housed in separate pressure vessels and arranged in series (**Fig. 6-1**).

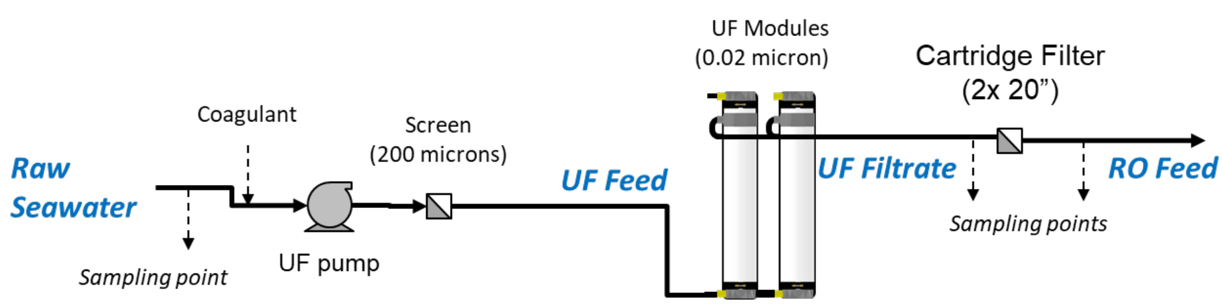

Figure 6-1 Simplified schematic diagram of the RO pretreatment system showing two UF modules in filtration mode.

Coagulant dosing was implemented by direct injection into the UF feed stream prior to the UF feed pump using a chemical metering pump (Grundfos, DDA 7.5-16, Bjerringbro, Denmark). A turbidity meter (Signet 4150, Georg Fischer Signet LLC, El Monte, CA) and a temperature sensor (Signet 2350-3, George Fischer Signet LLC, El Monte, CA) were installed on the UF filtrate line. An online fluorescence sensor (Turner Designs, Cyclops-7 2108, San Jose, CA) was installed on the UF filtrate line to detect chlorophyll-*a* concentration in the UF effluents (**Figure 6-1**) in order to detect passage of chlorophyll-*a* through the UF. The sensor output was averaged and normalized with respect to background signal and adjusted for the temperature in the sensor. A sampling tubing network was created to enable the switch sampling between UF feed (prior to coagulant dosage) and UF filtrate.

6.2.2 Field study

The feasibility of a coagulant dosing strategy that consisted of a step-wise dosing regiment was evaluated in a series of field tests using an integrated UF-RO seawater desalination system. All short-term and long-term UF-RO field experiments were conducted at the Naval Facilities Engineering and Expeditionary Warfare Center (NAVFAC-EXWC) at Port Hueneme, CA (Detailed information is provided in **Chapter 5, Section 5.2**). Three sets of preliminary short-term experiments were conducted to investigate the effects of various coagulant dose reduction strategies on UF filtration cycle fouling rate and backwash effectiveness. Two dose reduction strategies were evaluated: (a) an initial dose of a prescribed coagulant dose level and duration, and (b) regiment (a) followed by a secondary lower dose for the duration of the filtration period. The experimental conditions for the three experiments are summarized in **Table 6-1**. In addition, in selected field tests, the change in chlorophylls-*a* concentration in the UF filtrate stream was monitored to estimate the UF's ability to also reject chlorophylls-*a*. Each of the field tests were carried out for a fixed filtration duration that consisted of at least 8 filtration/backwash cycles (or 300-320 mins).

The implication of variable dosing in long-term pilot scale field tests was assessed via three long-term experiments (>120 hours). The first two tests were conducted over a period of 120 hours for the purpose of comparing UF fouling behavior and backwash effectiveness with and without a variable coagulant dosing strategy (aimed at reducing coagulant usage). UF backwash was triggered adaptively based on the maximum allowable filtration resistance change per cycle ($\Delta R_{T,max}$) [147]. The third test was conducted with the goal of demonstrating the benefit of integrating adaptive coagulant dosing and backwash frequency.

Table 6-1 Experimental conditions for short term coagulant reduction experiments

Experiment #	Initial dose (Fe^{3+} mg/L)	Initial dose duration (min)	Secondary dose (Fe^{3+} mg/L)	Secondary dose (% of initial dose)	Secondary dose duration (min)	Total filtration duration per cycle (min)
1	4.1	9	4.1	0%	19	28
	4.1	9	2.05	50%	19	28
	4.1	9	4.1	100%	19	28
	no coagulant	N/A	no coagulant	N/A	N/A	28
2	4.1	2	0	0%	28	30
	4.1	6	0	0%	24	30
	4.1	10	0	0%	20	30
	4.1	20	0	0%	10	30
	4.1	30	4.1	100%	0	30
	no coagulant	N/A	no coagulant	N/A	N/A	30
3	4.1	18	0	0%	18	36
	4.1	18	1.03	25%	18	36
	4.1	18	2.05	50%	18	36
	4.1	18	1.37	75%	18	36
	4.1	36	4.1	100%	18	36

6.3 Coagulant reduction strategy and online monitoring approach

6.3.1 Variable Inline Coagulant Dosing Strategy

In order to reduce the amount of coagulant use and avoid overdosing or underdoing, a "square wave" dosing strategy was evaluated. This approach is illustrated in **Figure 6-2**, where two filtration cycles (*n* and *n+1*) are separated by a backwash period. A constant initial dose is maintained during the filtration period for a given prescribed time, and in a subsequent period the dose is reduced for the remainder of the filtration cycle. The above approach was undertaken given the hypothesis that the formation of a fouling cake layer would be established at a constant administered dose serving as layer protecting the UF membrane from pore plugging and formation of an irreversibly adsorbed foulant layer. Once a cake layer is formed, the coagulant dose could be reduced to a level that is sufficient to maintain and even grow the cake layer.

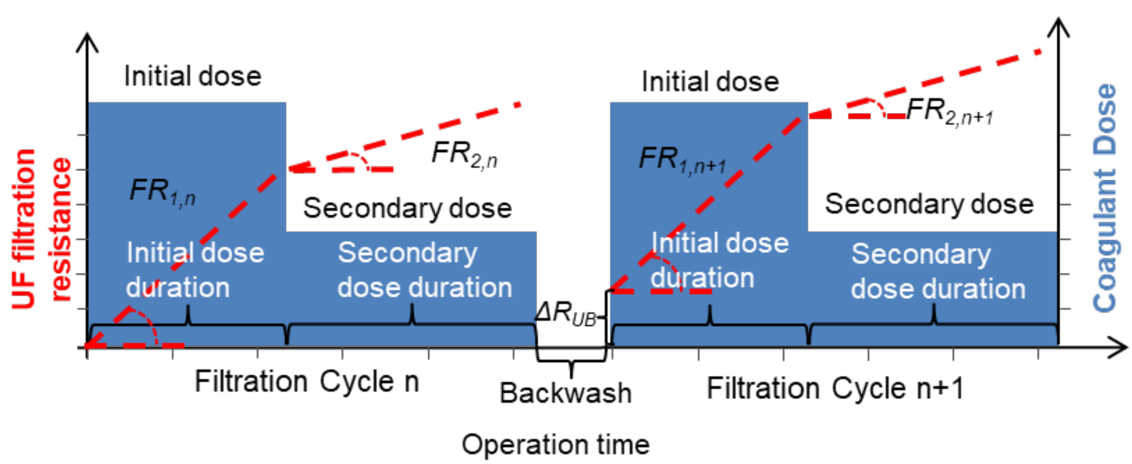

Figure 6-2. Illustration of inline coagulant variable dosing strategy and UF fouling metric. The solid bands represent the periods of the initial (i.e., primary) and secondary coagulant dosing. The dashed lines represent the trace of the UF filtration resistance for the shown cycles.

6.3.2 Metrics for Online UF Fouling Monitoring

The online UF fouling characterization method described in **Section 5.3** was utilized in order to determine the progression of fouling and backwash effectiveness. The total UF membrane resistance can be described as per the resistance-in-series model [85] as per Eq. 5.2 (i.e., $R_t = R_m + R_{cake} + R_{irr}$, where R_t is the total resistance, R_m is the clean membrane hydraulic resistance, R_{cake} is the foulant cake resistance, and R_{irr} is the hydraulically irreversible resistance). The total filtration resistance is expressed as,

$$R_t = \frac{\Delta P_0}{J \cdot \mu} + \frac{\Delta P_{irr}}{J \cdot \mu} + FR \cdot t \tag{6-2}$$

where ΔP_0 and ΔP_{irr} are the transmembrane pressure for pure water permeating through a clean membrane and the additional transmembrane pressure due to irreversible fouling, respectively, J is the filtration flux, μ is the viscosity of seawater and FR is the fouling rate for the given filtration period (i.e., the "slope" of the UF filtrate resistance curve).

As described in **Section 5.3**, the unbackwashable UF resistance (ΔR_{UB}, i.e., resistance not removed by UF backwash) and fouling rate for a given filtration cycle n (FR_n) can be used as metrics for online UF fouling monitoring. The hydraulically irreversible (unbackwashable) resistance (ΔR_{UB}) is defined as the change in UF initial resistance after a given hydraulic backwash period (as shown in **Figure 6-2**); it represents the remaining resistance on the membrane surface after a previous backwash step and indicated by the change in initial average resistance for each cycle. Tracking the accumulation or removal of ΔR_{UB} over the progression of filtration/backwash cycles (or post backwash "*PB*" UF resistance) provides the overall UF fouling trend. The rate of *PB* resistance rise can be used to project the time until the next CIP. As shown in **Figure 6-2**, $FR_{1,n}$ and $FR_{2,\ n}$ are the fouling rates for the initial and secondary fouling periods for the same filtration cycle n, respectively. It is noted that $FR_{2,n}$ may be positive or negative. In addition to the above UF fouling metrics, online measurements of chlorophyll-*a* concentration were used in the present work as an indicator of chlorophylls-*a* passage through the of UF membranes. The percent UF chlorophyll-*a* retention was quantified as:

$$R = \left(1 - \frac{C_p}{C_f}\right) X\ 100\% \qquad (6\text{-}3)$$

where C_f and C_p are the chlorophyll-*a* concentrations in the UF feed and filtrate, respectively.

Real time cycle-by-cycle analysis of the UF fouling rate and initial UF membrane resistance were achieved using a LabView based data analysis and logging software developed specifically for the present UF-RO system [147, 161]. The fouling metrics, ΔR_{UB} and FR, were calculated in real time from the UF performance data and averaged over several filtration cycles (~8-24) as described in **Section 5.3**.

6.4 Results & Discussion

6.4.1 Effects of coagulant dose reduction methods on UF filtration period fouling rate and backwash effectiveness

The objective of short-term experiment set #1 (Table 6-1) was to assess the effect on UF fouling behavior due to reduction of the second dosing step after a fixed initial constant dose. For each filtration cycle, the initial constant dose was for a 9 min duration (i.e., ~1/3 of the total filtration time per the 28 min cycle). The initial set dose of 4.1 mg/L Fe^{3+} was the optimal dose as determined in earlier work (**Section 5.4**). After 9 mins, the coagulant dose (i.e., secondary coagulant dosing period) was reduced to either 50% or 0% of the initial dose or kept at the initial dose level. The backwash conditions were set as per Tests 1-3 (**Table 6-1**).

Two filtration cycles of UF filtration resistance progression are shown in **Figure 6-3** with the average fouling rate FR_2 after the dose reduction shown in **Figure 6-4(a)**. For the constant full coagulant dose and no coagulant dose experiments, FR_2 was determined for the filtration period between 9 to 28 min. The highest FR was observed for UF operation at a constant coagulant dosing of 4.1 mg/L Fe^{3+} and no coagulant dose has the lowest FR. These results demonstrated that completely stopping the coagulant dose after 9 min in filtration will drastically change the filtration period fouling rate. The second filtration period FR_2 showed a negative slope of the filtration resistance-time curve and the UF filtration resistance decreased by ~90% and then stabilized at ~2.55 x10^{12}m^{-1} after 20 minutes of filtration. It is postulated that the above behavior is indicative of the need for continuous coagulant dosing in order to keep the concentration of agglomerated particles sufficiently large in the membrane feed channel and near the membrane surface. Cessation of coagulant dosing will reduce the growth of the cake layer and lead to disruption of the cake layer which would be reflected by a decrease in the membrane resistance during the filtration cycle.

As shown in **Fig. 6-4(b)**, the averaged results for 8 cycles of the full dose and 50% dose reduction in the last 2/3 of filtration period yield similar results ΔR_{UB} results, although the reduced dose case (1.12x10^{10} m^{-1}) was 1.37 times higher than the full dose one. The high ΔR_{UB} result suggested that the above dosing regiment is not optimal for long-term UF operation. It is noted that cessation of coagulant dosing ("no dose") after 9 min of continuous coagulant dosing resulted in the highest average ΔR_{UB} value (4.32x10^{10} m^{-1}) as is apparent after 8 cycles of filtration and backwash, which was about a factor of 4.2 higher than the case for full continuous dose (8.18x10^{9} m^{-1}), and 1.5 times higher than the "no dose" case (2.50x10^{10} m^{-1}). It noted that in a previous study it was established that without coagulant dosing, UF backwash of seawater RO feed operation was highly ineffective resulting in faster rate of accumulation of UF unbackwashed resistance[161].

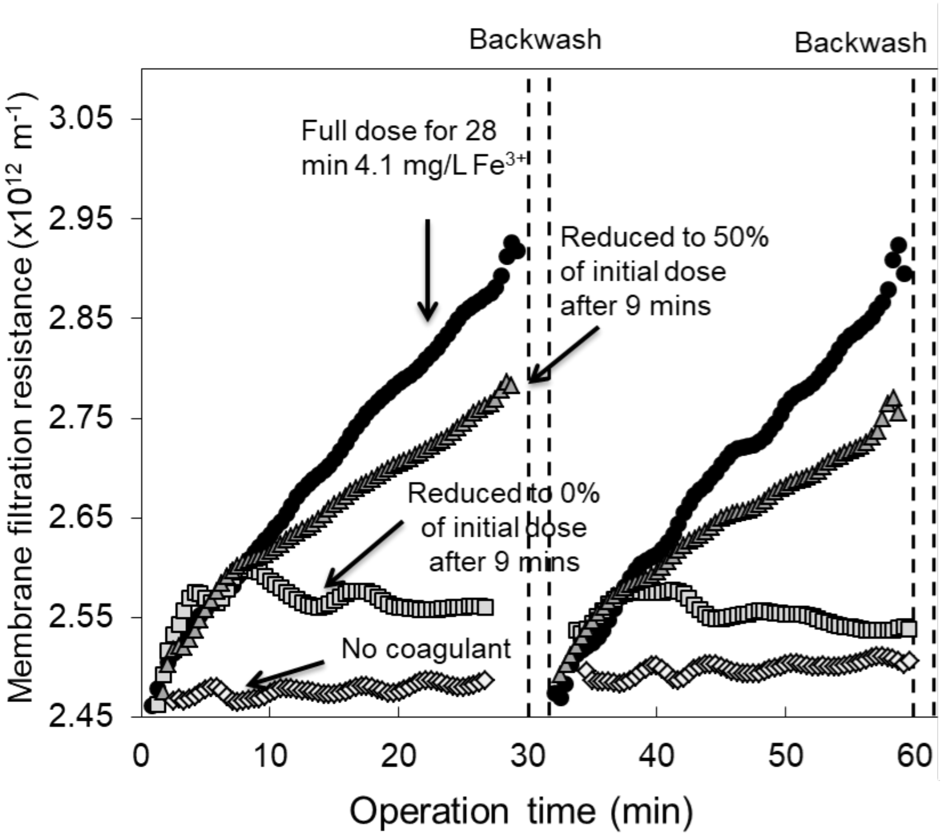

Figure 6-3 Short-term coagulant reduction experiment set #1 (**Table 6-1**). Membrane filtration resistance versus operation time for different dosing strategy: no coagulant, maintain the initial dose (4.1 mg/L Fe^{3+}) and duration (9 mins) and change the 2nd dose to 100% (constant dose), 50% and 0% (no dose) of the initial dose. Experimental conditions: filtration flux: 36.6 L/m^2·h backwash flux: 162 L/m^2·h and backwash duration: 60s, filtration duration per cycle: 28 min. Numbers of filtration/backwash cycles repeated: 8.

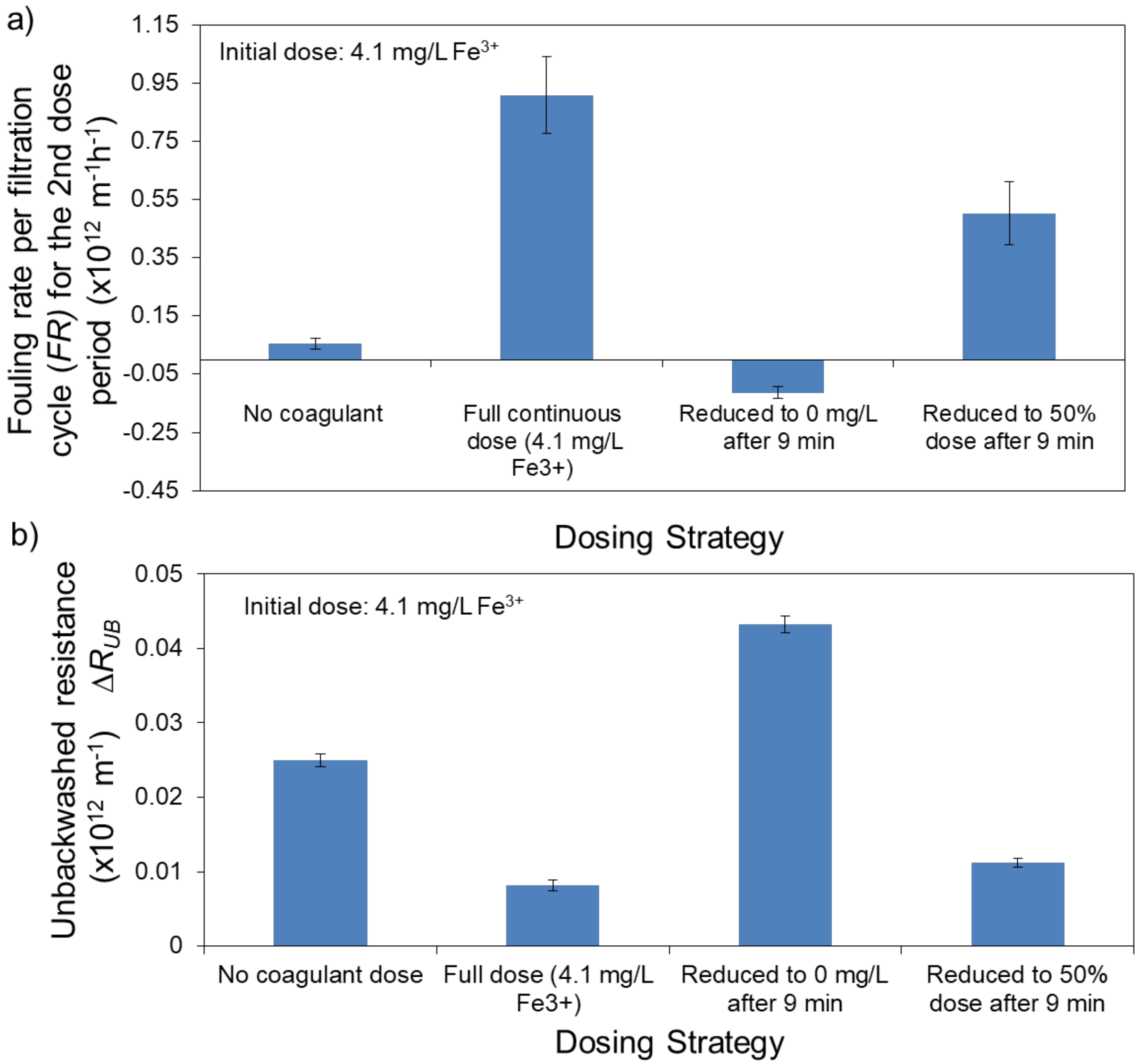

Figure 6-4 Short-term coagulant reduction experiment #1 (**Table 6-1**). a) Averaged fouling rate per filtration cycle (*FR)* for the 2nd dosing period and b) Averaged unbackwashed resistance ΔR_{UB} . Tests were conducted for four dosing strategies: (i) no coagulant dosing, (ii) coagulant dosing at a constant dose of 4.1 mg/L Fe^{3+}, (iii) coagulant dosing for a period of 9 mins followed by a filtration period without coagulant dosing, and (iv) filtration at coagulant dose of 4.1 mg/L Fe^{3+} for 9 min followed by dose reduction by 50%. Experimental conditions: filtration flux: 36.6 $L/m^2 \cdot h$ backwash flux: 162 $L/m^2 \cdot h$ and backwash duration: 60s, total filtration duration per cycle: 28 min. Numbers of filtration/backwash cycles repeated: 8.

In experiment #2, four initial dose durations were evaluated in order to determine the impact on UF fouling. In this test the following dosing regiments were evaluated: (a) coagulant dosing was terminated after operation at a constant dose of 4.1 mg/L Fe^{3+} for periods of 20 mins, 10 mins, 6 mins and 2 mins. It is noted that UF tests without coagulant dosing and with continuous dosing of 4.1 mg/L as Fe^{3+} were carried out as control experiments. The normalized filtration resistance (defined as R_t/R_0, where R_0 is the initial UF resistance at the beginning of the filtration cycle) in **Figure 6-5**. Similar to experiment #1 (**Fig. 6-3**), without coagulant dosing the ΔR_{UB} (1.76 x10^{10} m^{-1}) thus backwash is not optimal (**Fig. 6-6**), this is mostly likely due to pore plugging or adsorption fouling mechanism. The results demonstrated that coagulant dosing is necessary in order to attain reasonable UF backwash performance. As illustrated in **Fig. 6-6 (a),** cessation of coagulant dosing in the second dosing period led to a fouling rate (FR_2) that was negative, and lead to a "dissolution" of the cake layer (i.e., filtration resistance decrease). As shown in **Fig. 6-6 (a) and (b)**, FR_2 decreased proportionally with decreasing initial dose duration, and ΔR_{UB} increases proportionally with decreased initial dose duration. Although the apparent fouling rate in each filtration period was low without coagulant dosing, backwash operation was not optimal, resulting in high unbackwashed resistance after backwash, which would have led to the requirement of a significantly higher chemical cleaning frequency (Section 5.4.2).

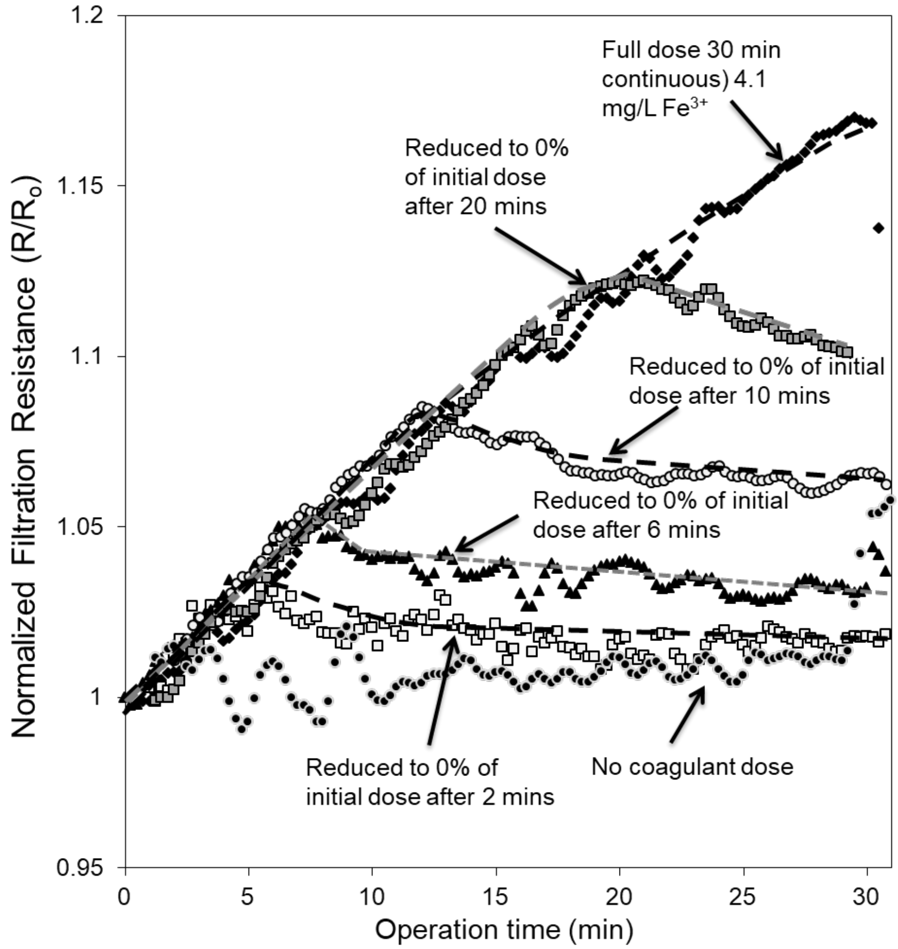

Figure 6-5. Filtration resistance for UF operation with coagulant reduction for the conditions of as Experiment #2 (**Table 6-1**). The coagulant dosing strategies were: (i) no coagulant dosing, (ii) maintaining a coagulant dose of 4.1 mg/L Fe^{3+} for periods of 30 min, and (iii) coagulant dosing of 4.1 mg/L Fe^{3+} for periods of 20 min, 10 min, 6 min, 2 min followed by cessation of coagulant dosing. Experimental conditions: filtration flux: 36.6 L/m^2·h, backwash flux: 162 L/m^2·h, and backwash duration: 60s, total filtration duration per cycle: 30 min. Numbers of filtration/backwash cycles repeated in experiment: 8. The first cycle is shown to clearly illustrate the filtration resistance trends.

It is hypothesized that the above observations of decreased filtration resistance post cessation of coagulant dosing could be the result of disruption of the cake layer on the membrane surface due to coagulant dislodging (or diffusion) from the pre-existing foulant cake leading to thinning of the cake layer as filtration time increases. Also, "sticky" biological foulant such as TEP will no longer be captured or "trapped" by the foulant cake on the membrane surface. Although the cake fouling resistance is lowered as the coagulant dose decreases, backwash is less effective (**Section 5.4.2)** due to the buildup of irreversible fouling on the membrane surface and its pores (**Section 5.4.2, Fig. 5-10).**

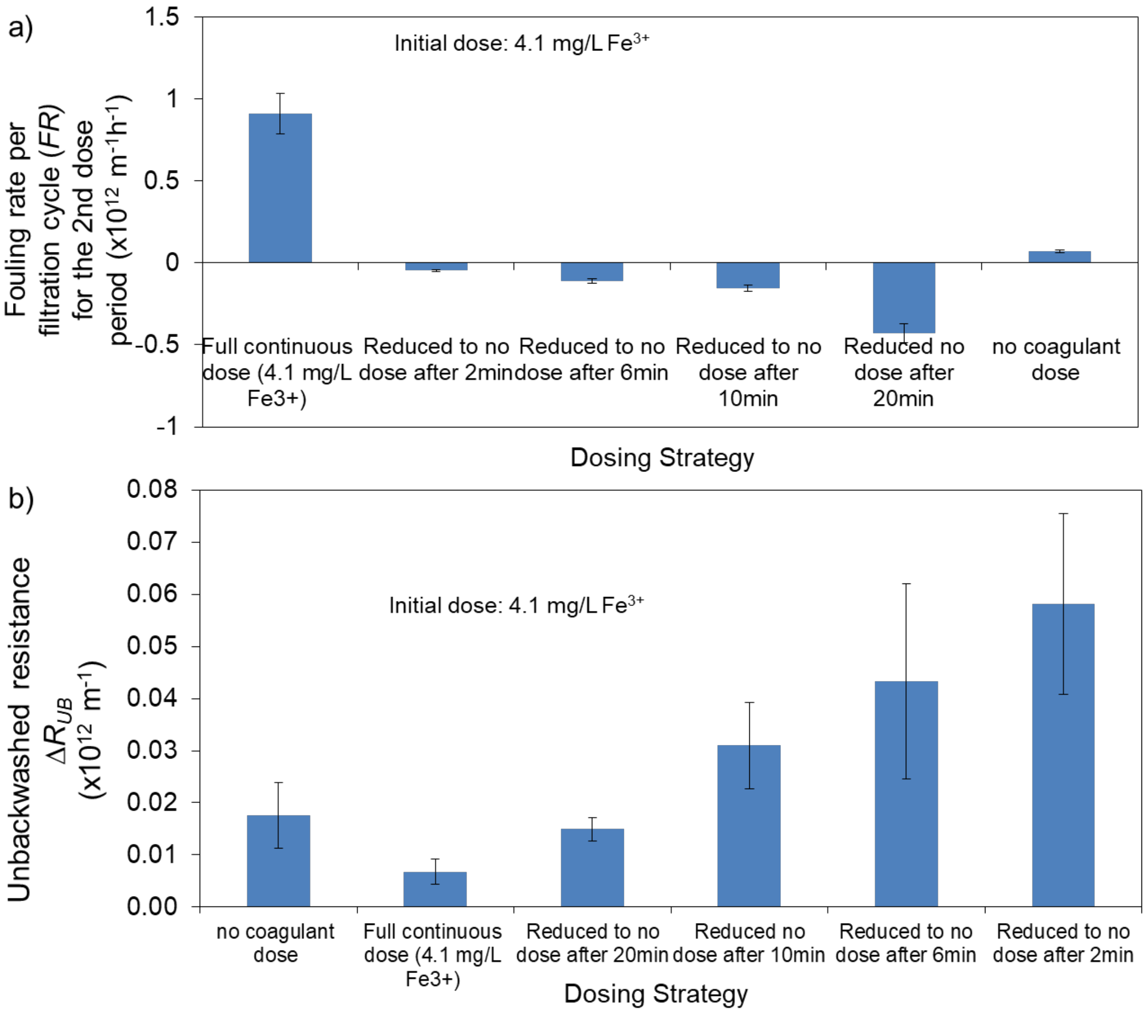

Figure 6-6 Short-term coagulant reduction Experiment #2 (**Table 6-1**). (a) Average fouling rate per filtration cycle (*FR)* for the 2nd dose period, and (b) Average unbackwashed resistance ΔR_{UB} under various dosing strategies: no coagulant dosing, maintaining a dose of 4.1 mg/L Fe^{3+} for 30 mins, 20 mins, 10 mins, 6 mins, 2 mins followed by transition to filtration without coagulant dosing. Experimental conditions: filtration flux: 36.6 $L/m^2{\cdot}h$, backwash flux: 162 $L/m^2{\cdot}h$, and backwash duration: 60 s, total filtration duration per cycle: 30 min. Numbers of filtration/backwash cycles averaged: 8.

The objective of Experiment #3 (Table 6-1) is to investigate the effect of the secondary dose with respect to the percent dose reduction. An initial dose of 4.1 mg/L Fe^{3+} for 18 mins, (50% of a full filtration duration), was maintained while the secondary dose of 100% (full constant dose), 75%, 50%, 25% and no dose were tested in five separate short term experiments (**Table 6-1**, **Figure 6-7**).

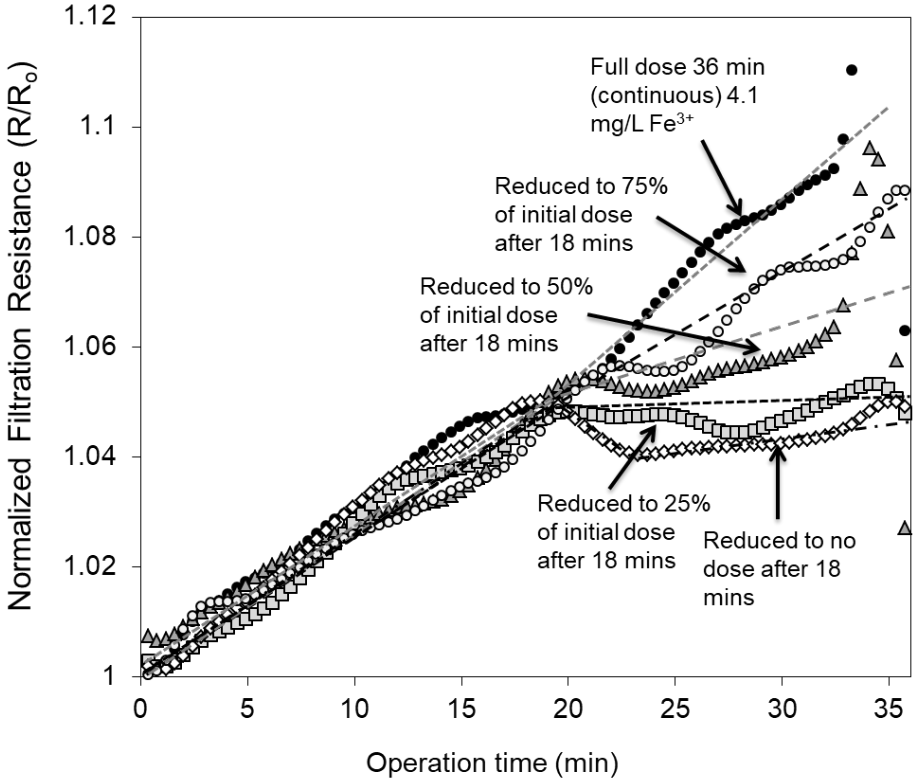

Figure 6-7 Short-term coagulant reduction Experiment #3 (**Table 6-1**). Normalized UF membrane filtration resistance versus operation time for various dosing strategy: no coagulant dosing, maintaining the initial dose of 4.1 mg/L Fe^{3+} for 18 minutes filtration duration and subsequently changing the dose in the 2nd portion of the filtration period to 100%, 75%, 50%, 25% or 0% of the initial dose. Experimental conditions: filtration flux: 36.6 $L/m^2{\cdot}h$, backwash flux: 162 $L/m^2{\cdot}h$, and backwash duration: 60s, total filtration duration per cycle: 36 min. 8 filtration/backwash cycles were repeated, the first filtration cycle is shown to clearly illustrate the filtration resistance trends.

As shown in **Fig. 6-8 a)**, the fouling rate for the second dose period (FR_2) decreased with decreasing secondary dose follow an apparent linear trend. For 50% dose reduction, FR_2 was about 0.366 times the FR_2 for the full continuous dose (0.41 $\times 10^{12}$ $m^{-1}h^{-1}$). **Figure 6-8 b)** showed the full dose, 50% and 75% resulted in similar ΔR_{UB} in 8 cycles, and dosing at least 50% of the initial dose for the second filtration period gave the lowest ΔR_{UB} resistance compared with the case of constant dosing coagulant. This corresponded to a 25% reduction in coagulant use compare with constant dosing. It is hypothesized the cake layer acts as a barrier to trap foulants in the feed water before it fouls the membrane. During filtration period, it is necessary to make sure the fouling is in the cake formation region via a precisely controlled coagulant dose and a second dose is needed to preserve the foulant cake. In addition, the cake layer need to "re-form" cake layer every cycle after backwash.

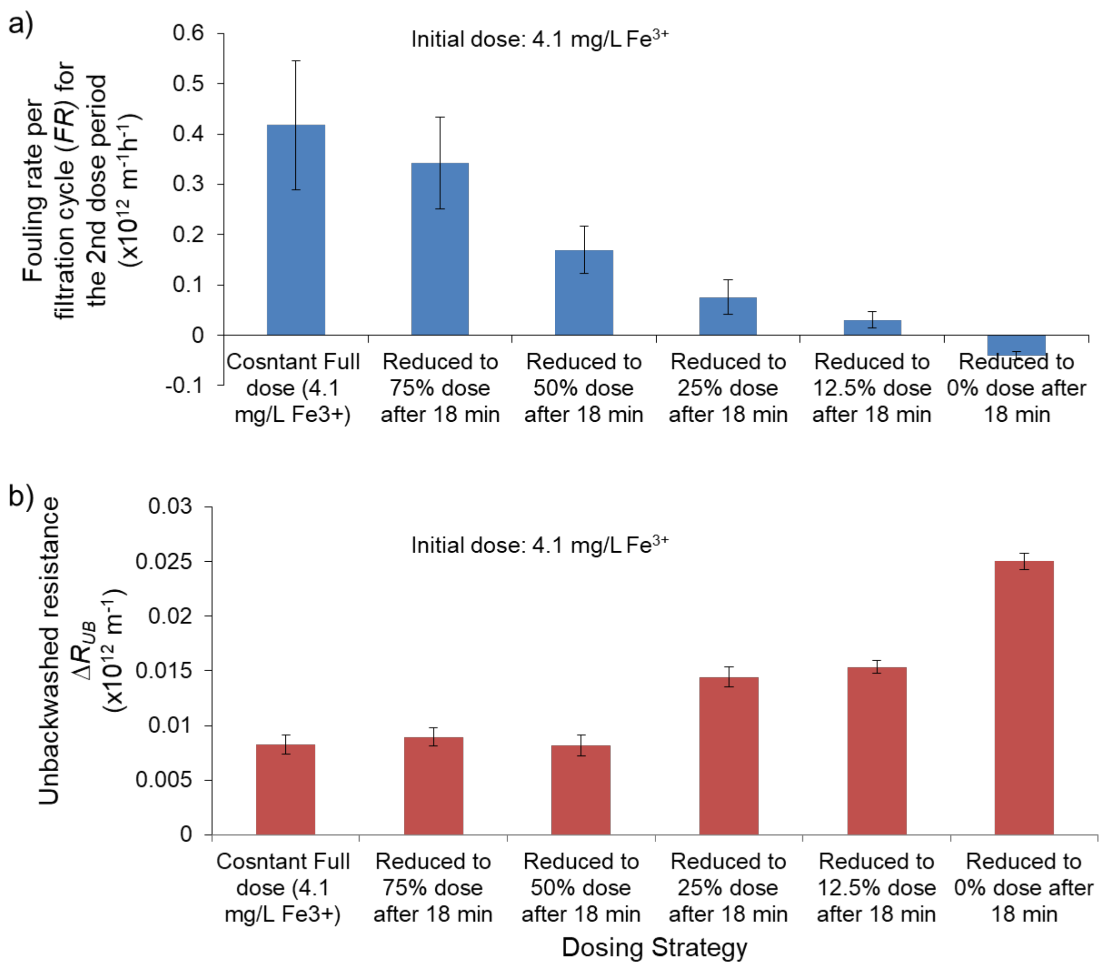

Figure 6-8 Short-term coagulant reduction Experiment #3 (**Table 6-1**). (a) Average fouling rate per filtration cycle (*FR)* for the 2nd dose period, and (b) Average unbackwashed resistance ΔR_{UB} under various dosing strategies: no coagulant dosing, maintaining the same initial dose (4.1 mg/L Fe^{3+}) for 18 minutes filtration duration followed by changing dose in the 2nd portion of the filtration period to 100%, 75%, 50%, 25%, 12.5% or 0% of the initial dose. Experimental conditions: filtration flux: 36.6 L/m^2·h, backwash flux: 162 L/m^2·h, and backwash duration: 60 s, total filtration duration per cycle: 36 min. The results as shown were average of 8 repeated cycles.

6.4.2 Short term effect of coagulant dose reduction methods on chlorophylls-a retention ability of UF module

In order to prevent coagulant underdosing condition during the proposed coagulant reduction period, it is necessary to quantify the effect of dose reduction methods on organic materials retention ability of the UF module. If a foulant cake is properly formed during filtration operation, the coagulant dose should be optimal, and the biological and organic materials passage through UF module should be consistent and low. In the current study, chlorophyll-*a* retention response for six dosing reduction strategy was compared. It was observed that after a step change in coagulant dose, the chlorophyll-*a* retention by the UF membrane (calculated using Eq.6-3) could change rapidly, typically within minutes.

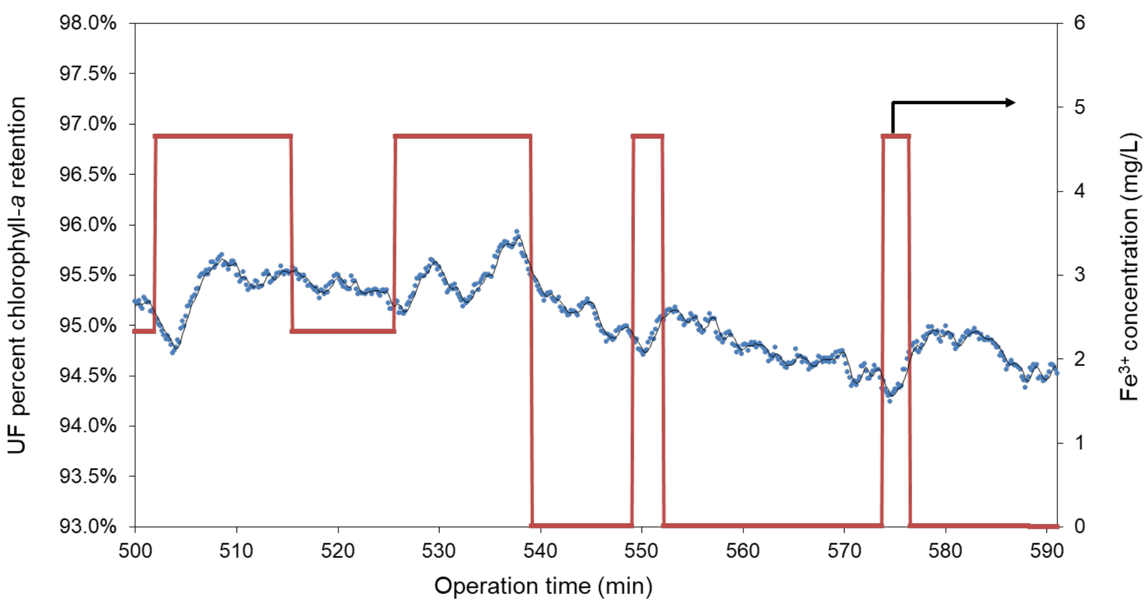

Figure 6-9 Example of percent UF chlorophylls-*a* retention during a short term coagulant reduction test. initial dose 4.6 mg/L as Fe^{3+}, initial dose duration: 18 min, secondary dose period: 50% of the initial dose. Initial dose duration: 3 min, secondary dose: no dose. Experimental conditions: filtration flux: 36.6 $L/m^2 \cdot h$, backwash flux: 162 $L/m^2 \cdot h$, and backwash duration: 60s, total filtration duration per cycle: 30 min.

An example is shown in **Fig. 6-9**, where UF filtrate concentration was measured in real-time by a chlorophyll-*a* fluorometer in UF filtrate steam while a dose reduction experiment take place. It is noted there are some fluctuation (±0.5%) in the chlorophyll-a measurement, this is primarily due to feed chlorophyll-*a* and temperature fluctuations. Between operation time of 515 to 525 mins, the coagulant dose was reduced in half and the percent UF chlorophylls-*a* retention remained constant. The coagulant dose was changed from 100% to 0% of the initial dose (4.7 mg/L) between operation time of 539 to 548 mins and 552 to 575 mins. At the same period chlorophyll-*a* concentration for the UF filtrate increased from 0.61 to 0.69 µg/L. As a result, chlorophylls-*a* retention decreased by 1.4% in about 30 min. The reverse trend was also observed when the dose was returned to its initial vale after the backwash. **Figure 6-10** shows a bar chart comparing the change in chlorophyll-*a* retention by the UF module for six separate dosing reduction set points. The results, which are the average of 4 repeated experiments, are very similar to the trends observed for unbackwashed resistance (ΔR_{UB}) obtained from short term test 1-3. In the latter experiments, the greatest chlorophyll-*a* passage occurred when coagulant dosing was terminated too early (2 min. of the total filtration time), resulting in 17.2% decrease in chlorophyll-*a* retention. When the coagulant was reduced by 50% or higher of the initial dose in the second portion of the filtration period, the change in UF chlorophyll-*a* retention was minimal (0.05-0.11%). As shown by the above result, chlorophyll-*a* monitoring in the UF filtrate enabled assessment of the effectiveness of dosing strategy for minimizing its passage.

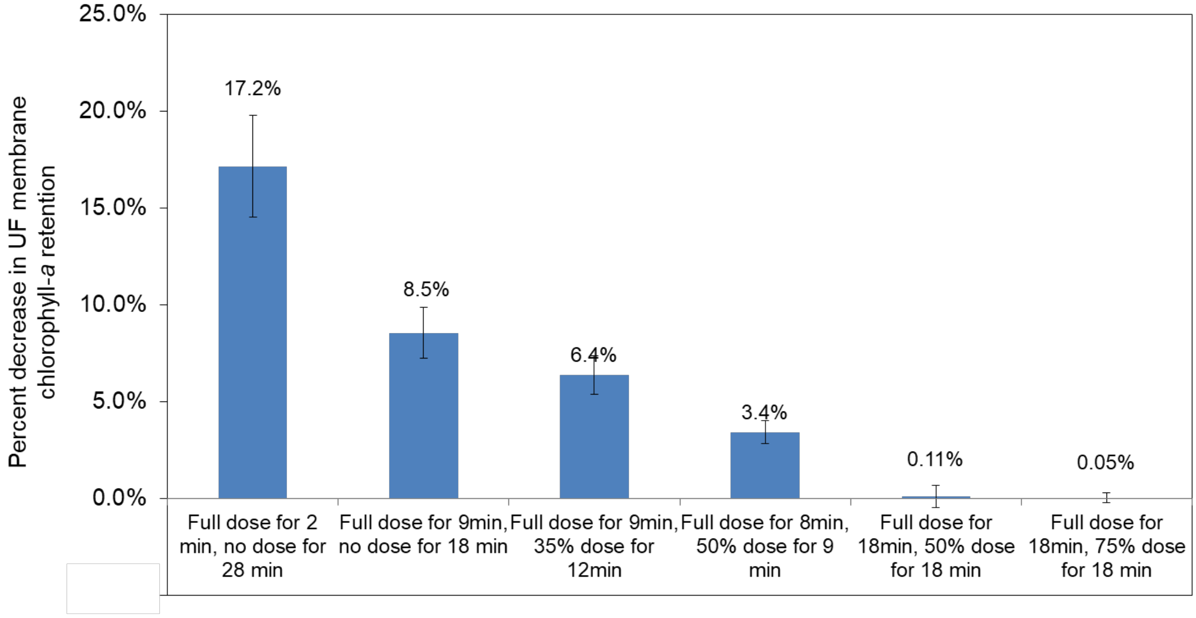

Figure 6-10 Change in UF chlorophylls-*a* retention in short-term coagulant dose reduction tests. Experimental conditions: filtration flux: 36.6 L/m^2·h, backwash flux: 162 L/m^2·h, backwash duration: 60s, filtration duration per cycle: 30 min. The results as shown were average of 4 repeated cycles.

6.4.3 Comparison of optimal dose reduction strategy with standard continuous dose in long term operation

In order to confirm the findings from the short-term experiments, two long term tests (about 120 h each) were carried out where the coagulant dose in long term experiment #1 was continues at a level of 4.17 mg/L Fe^{3+} and in long term experiment #2 a 50% dose reduction was set after an initial dosing period of 18 min. Both experiments were operated with self-adaptive backwash triggering control that enabled a flexible backwash frequency based on a maximum allowable resistance increase of 5.68x10^{11} m^{-1} per cycle [147, 174]. As shown in **Figure 6-11**, except for an initial peak of 0.27 x10^{12}m^{-1} during start up, the ΔR_{UB} trace was very similar for both runs, remaining consistently below 0.05 x10^{12}m^{-1} (dominated by cake formation). As a result, the post backwash resistance (R_{PB}) fouling progression profile was almost identical for both runs reaching about 1.2 x10^{12}m^{-1} at 120 hours (**Figure 6-12**).

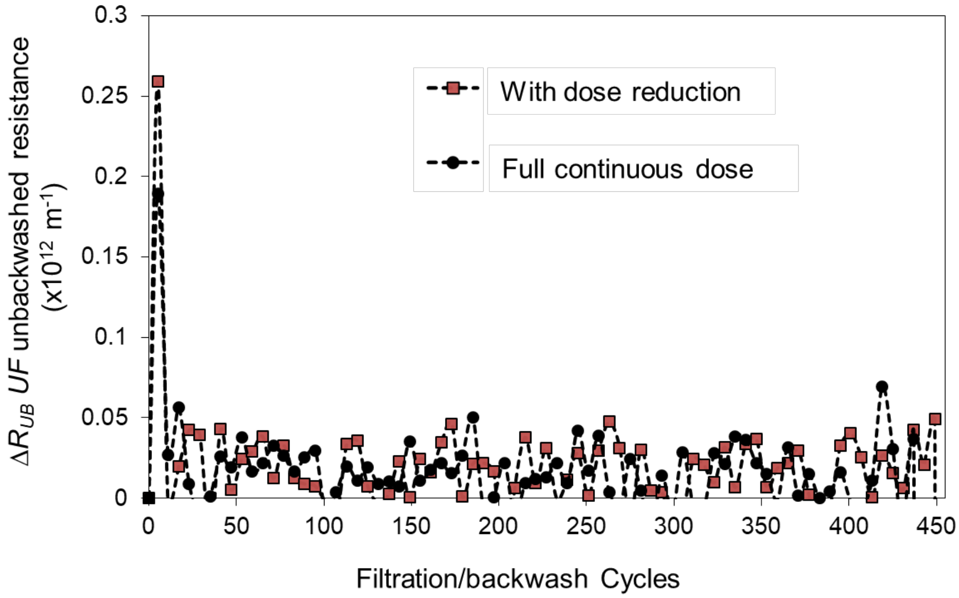

Figure 6-11 UF performance comparisons between full continuous dose (long term experiment #1) and with dose reduction (long term experiment #2). Average UF unbackwashed resistance (over every 6 filtration/backwash cycles) versus filtration/backwash cycles. Experimental conditions: filtration flux: 45.4 L/m^2·h backwash flux: 162 L/m^2·h and backwash duration: 70s, total filtration duration per cycle: 25-42 min. Numbers of filtration/backwash cycles: 446 (experiment #1) & 458 (experiment #2). Inline coagulant dose controller setting: Experiment 1: 4.17 mg/L as Fe^{3+} (constant dose), Experiment 2: initial dose 4.17 mg/L as Fe^{3+}, initial dose duration: 18 min, secondary dose: 50% of the initial dose.

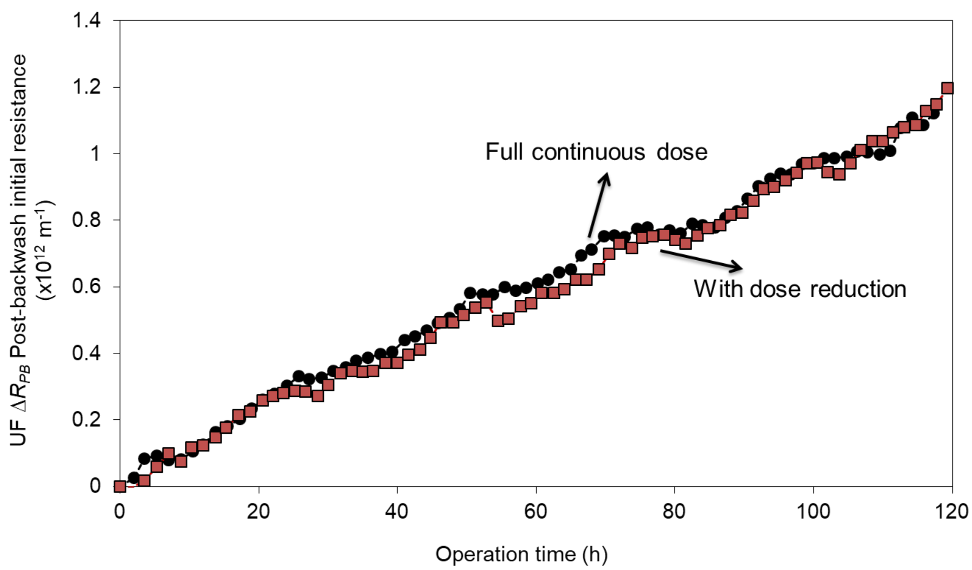

Figure 6-12 UF performance comparisons between long-term UF-RO seawater desalination test #1 and 2. UF post backwash resistance versus operation time. Experimental conditions: filtration flux: 45.4 L/m^2·h backwash flux: 162 L/m^2·h and backwash duration: 70s, total filtration duration per cycle: 25-42 min. Numbers of filtration/backwash cycles: 446 (experiment #1) & 458 (experiment #2). Inline coagulant dose controller setting: Experiment 1: 4.17 mg/L as Fe^{3+} (constant dose), Experiment 2: initial dose 4.17 mg/L as Fe^{3+}, initial dose duration: 18 min, secondary dose: 50% of the initial.

Figures 6-13a and **6-15a** show the UF module chlorophyll-*a* retention and coagulant dose for experiments #1 and #2. The experimental results confirmed that chlorophyll-*a* retention during constant dose experiment #1 were nearly identical at ~ 94.8% compared with step dose experiment #2. The fouling rate, *FR,* increased by about 145% in both runs due to feed water quality changes (**Figures 6-13b and 6-15b**). Integrated with the adaptive backwash triggering system, the filtration time per cycle (or backwash frequency) increased due to the dose reduction scheme. The final resistance at the end of the reduced dose filtration period was lower than for the continuous dose case; therefore, the second portion of the filtration period was extended under backwash controller. The average filtration duration for experiment #1 (full continuous dose) was 26.8 min and 31.5 min for experiment #2 (with dose reduction). Therefore, the overall filtrate production (i.e., reduce backwash frequency) was also increased. The total coagulant saving (compared with full continuous dose at 4.1 mg/L) with adaptive backwash triggering was 36% compared with 25% without adaptive backwash triggering.

The RO normalized permeability and salt rejection was also monitored and compared for both experiments in **Figure 6-14 and Figure 6-16**. No signs of RO permeability decline or change in salt rejection was observed for both experiments, the RO permeability was very stable at about 1.75 $\times 10^{-12}$ m/Pa·s and salt rejection at about 99.5%.

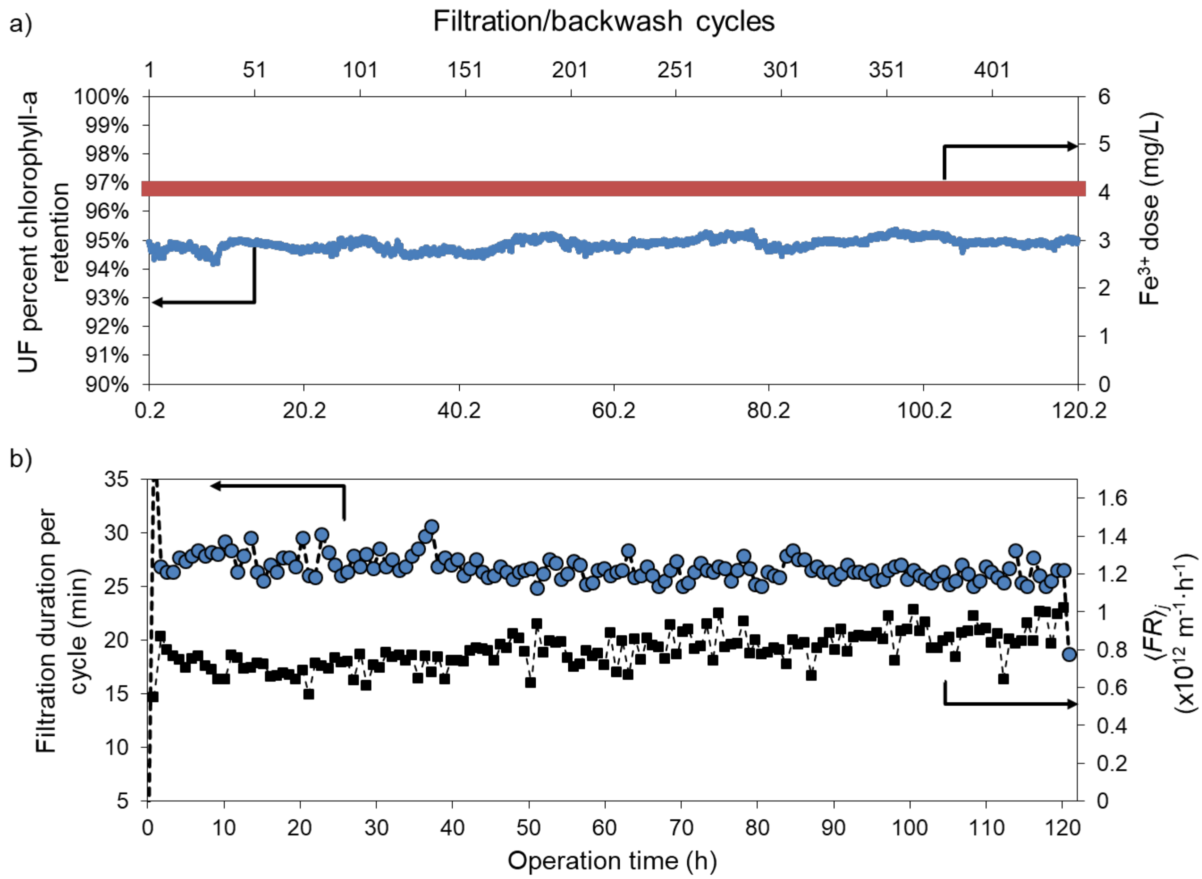

Figure 6-13 UF performance summary during long-term UF-RO seawater desalination test #1. (a) Percent chlorophyll-*a* retention by the UF module and coagulant dose during operation, and (b) Average UF filtration cycle duration and filtration period fouling rate (*FR*) versus operation time. Experimental conditions: filtration flux: 45.4 $L/m^2 \cdot h$ backwash flux: 162 $L/m^2 \cdot h$ and backwash duration: 70s, total filtration duration per cycle: 25-42 min. Numbers of filtration/backwash cycles: 446. Inline coagulant dose: 4.17 mg/L Fe^{3+}.

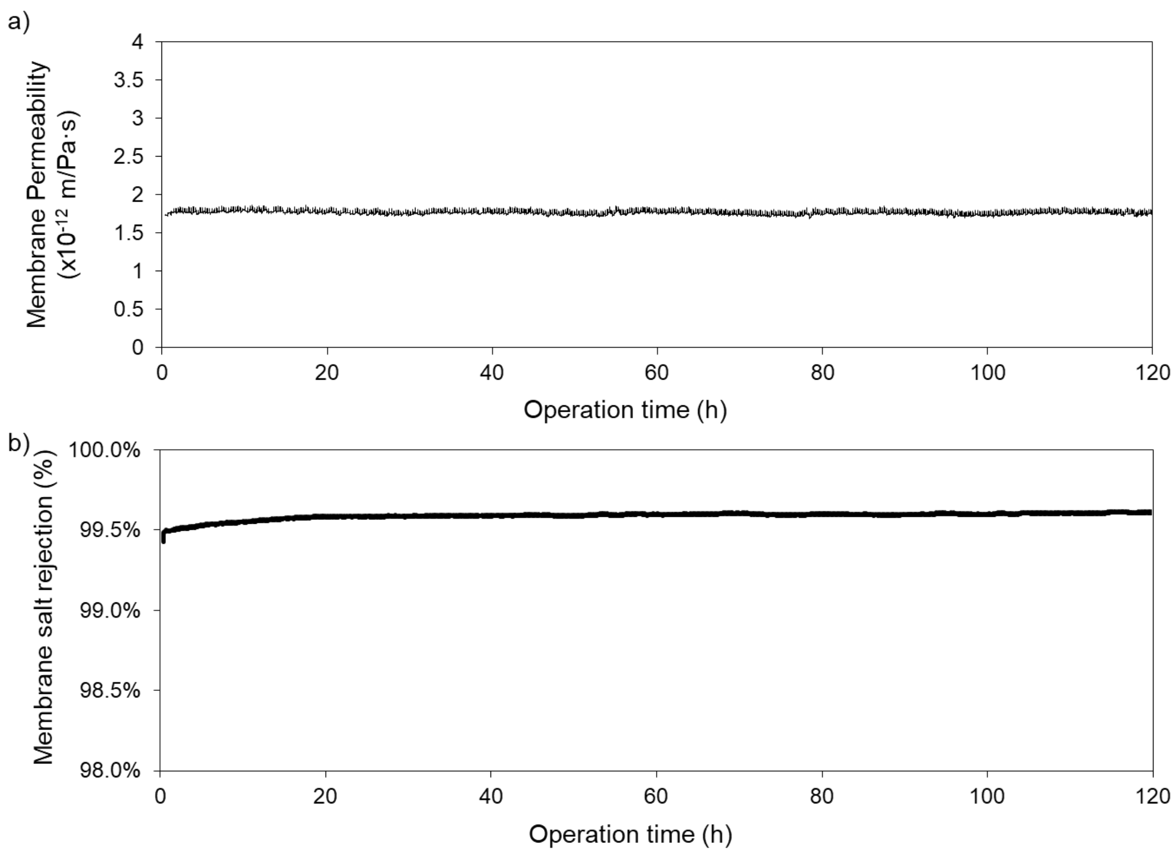

Figure 6-14 RO membrane permeability and normalized salt rejection during long-term UF-RO seawater desalination test #1. RO permeate flux: 12.3 L/(m^2·h), recovery:32%.

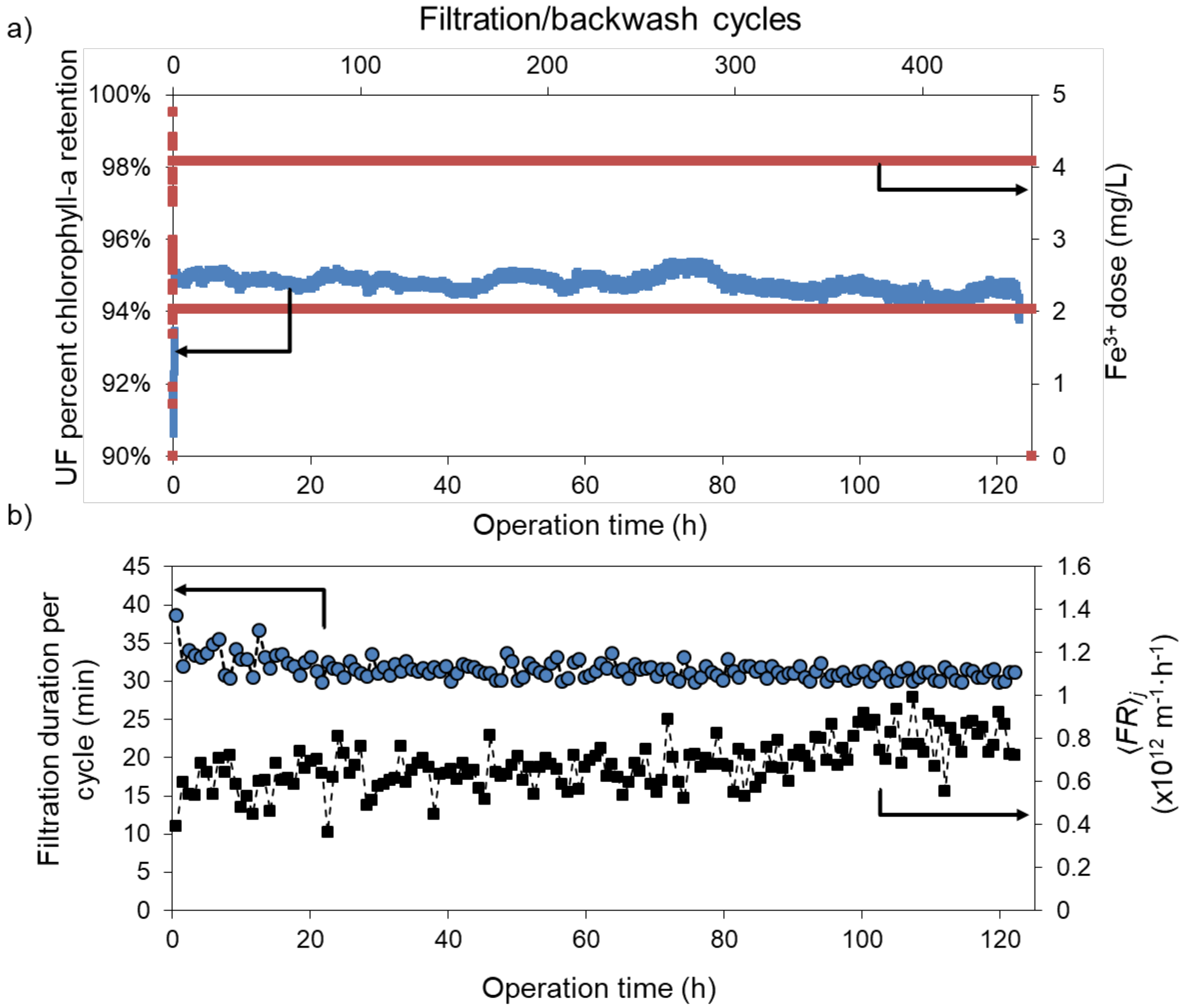

Figure 6-15 UF performance summary during long-term UF-RO seawater desalination test #2. (a) Percent chlorophyll-*a* retention of the UF module and coagulant dose, and (b) UF average filtration cycle duration and filtration period fouling rate (*FR*) versus operation time. Experimental conditions: filtration flux: 45.4 L/m^2·h backwash flux: 162 L/m^2·h and backwash duration: 70s, total filtration duration per cycle: 25-42 min. Numbers of filtration/backwash cycles: 458. Inline coagulant dose: initial dose 4.17 mg/L Fe^{3+}, initial dose duration: 18 min, secondary dose: 50% of the initial.

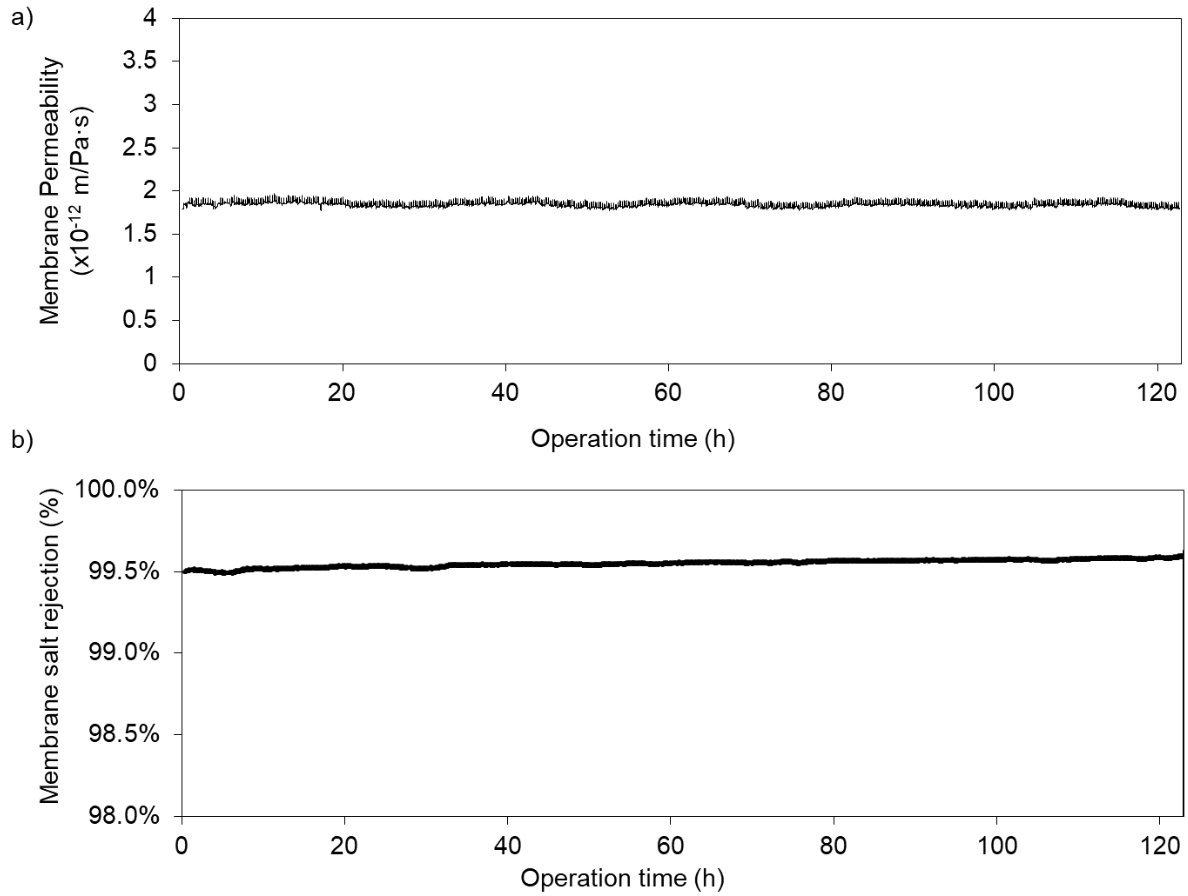

Figure 6-16 RO membrane permeability and normalized salt rejection during long-term UF-RO seawater desalination test #2. RO permeate flux: 12.3 L/(m^2·h), recovery:32%.

6.4.4 Demonstration of dose reduction strategy with self-adaptive coagulant controller and backwash triggering system

Given the encouraging results from long term experiment 1 and 2, an additional long term experiment (long term #3) was conducted with three controllers enabled: (i) adaptive coagulant dose controller, (ii) dose reduction controller, and (iii) self-adaptive backwashing triggering. The coagulant controller was described in a previous paper [161]. The benefits of step dosing strategy with respect to UF fouling control in conjugation with adaptive coagulant dosing was demonstrated for a run time of 130 hrs and a zoom-in coagulant dose controller view in action is provided in **Figure 6-17**.

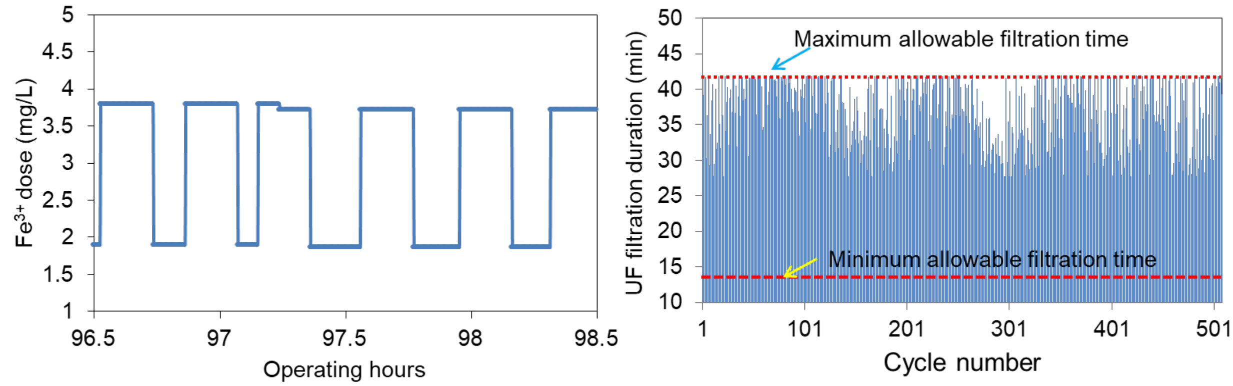

Figure 6-17 Left figure: closed-in view of the coagulant dose hehavior under both backwash triggering and coalgant dose controller. Inline coagulant dose controller setting: initial dose 3.47 mg/L Fe^{3+}, dose change amount per averaging window: 0.0686 mg/L Fe^{3+}, initial dose duration: 20 min, secondary dose: 50% of the initial. Right figure: UF filtration duration for individual cycle over during long-term UF-RO seawater desalination test #3.

The post backwash resistance profile for long-term experiment #3 was similar to long-term experiment 1 and 2, with the final post backwash resistance being about 1.16 x10^{12} m^{-1} (**Figure 6-18**). The ΔR_{UB} stabilized after about two days operation. The coagulant dose controller was active throughout the run during which the initial coagulant dose varied from 3.47 mg/L Fe^{3+} to 3.86 mg/L Fe^{3+} then back to 3.66 mg/L Fe^{3+} and the secondary dose varied from 1.74 mg/L Fe^{3+} to 1.93 mg/L Fe^{3+} then back to 1.83 mg/L Fe^{3+}. The dose change averaging window was every 24 cycles the dose change amount was 0.0686 mg/L Fe^{3+}.

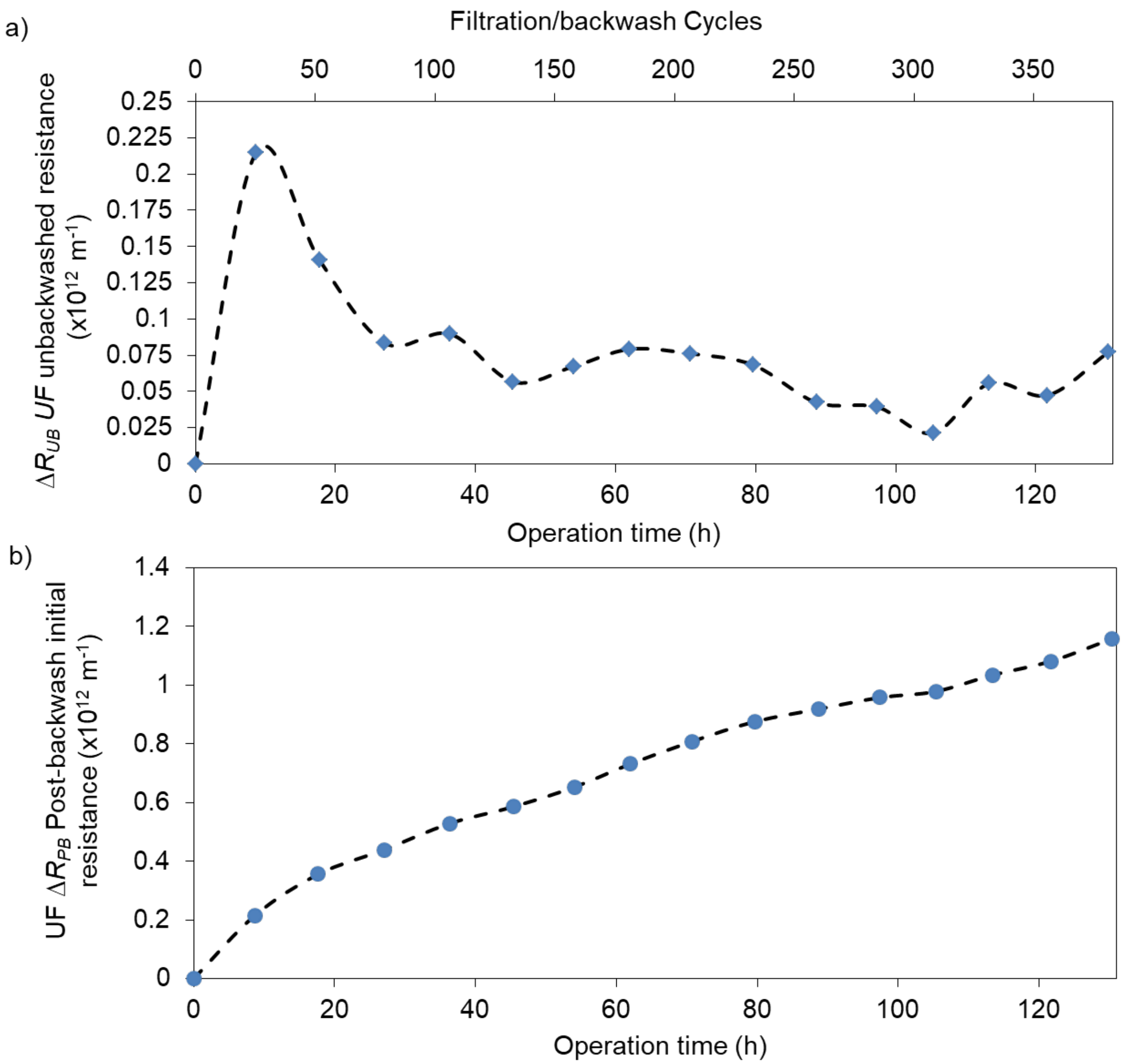

Figure 6-18 UF performance summary during long-term UF-RO seawater desalination test #3. (a) Average UF unbackwashed resistance (every 24 cycles) during operation, and (b) UF post backwash resistance versus operation time. Experimental conditions: filtration flux: 42.3 L/m^2·h backwash flux: 162 L/m^2·h and backwash duration: 75s, total filtration duration per cycle: 28-42 min. Numbers of filtration/backwash cycles: 358. Inline coagulant dose controller setting: initial dose 3.47 mg/L Fe^{3+}, dose change amount per averaging window: 0.0686 mg/L Fe^{3+}, initial dose duration: 20 min, secondary dose: 50% of the initial dose.

As shown in **Figure 6-19**, the *FR* (average *FR*: 0.53x10^{12} m^{-1}) increased slightly by about 5% over the period from 0 to 125 hours. Regulated by the backwash triggering controller, the average filtration duration was 37.1 min (range of filtration duration was 28-42 min). The step dosing strategy enabled prevention of chlorophyll-*a* passage through the UF module (i.e., ~

94.8% retention by the UF membrane). The above result for operation at constant dose as per experiment #3 was nearly identical with the finding from the long-term step dose experiments 1 and 2.

The RO normalized permeability and salt rejection data for long-term experiment 3 showed no RO permeability decline or change in salt rejection (**Figure 6-20**). The RO permeability was stable at about 1.85 x10^{-12} m/Pa·s and salt rejection at about 99.5%.

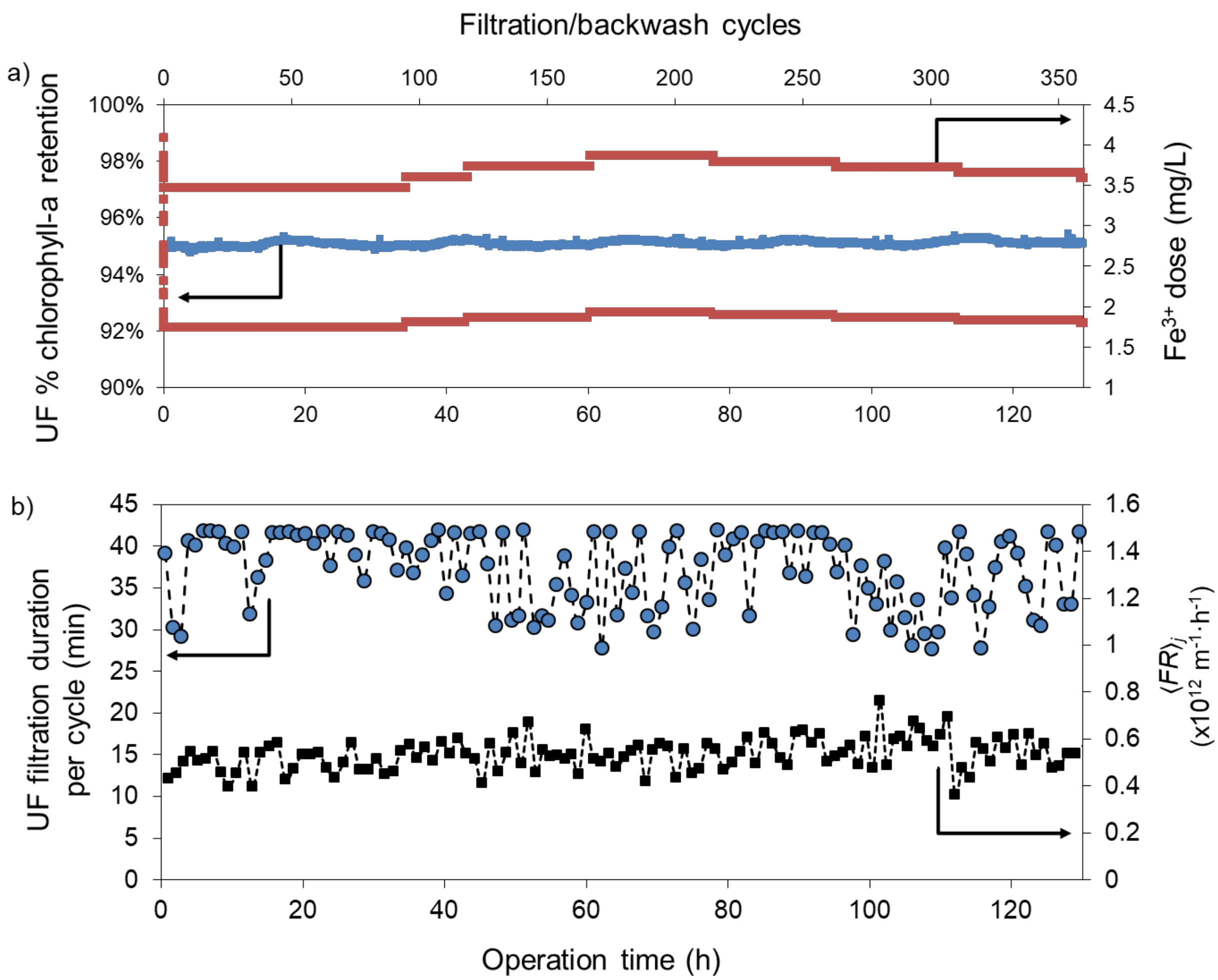

Figure 6-19 UF performance summary during long-term UF-RO seawater desalination test #3. (a) Percent chlorophyll-*a* retention of the UF module and coagulant dose during operation, and (b) UF average filtration cycle duration and filtration period fouling rate (*FR*) versus operation time. Experimental conditions: filtration flux: 42.3 L/m^2·h backwash flux: 162 L/m^2·h and backwash duration: 75s, total filtration duration per cycle: 28-42 min. Numbers of filtration/backwash cycles: 358. Inline coagulant dose controller setting: initial dose 3.47 mg/L Fe^{3+}, dose change amount per averaging window: 0.0686 mg/L Fe^{3+}, initial dose duration: 20 min, secondary dose: 50% of the initial dose.

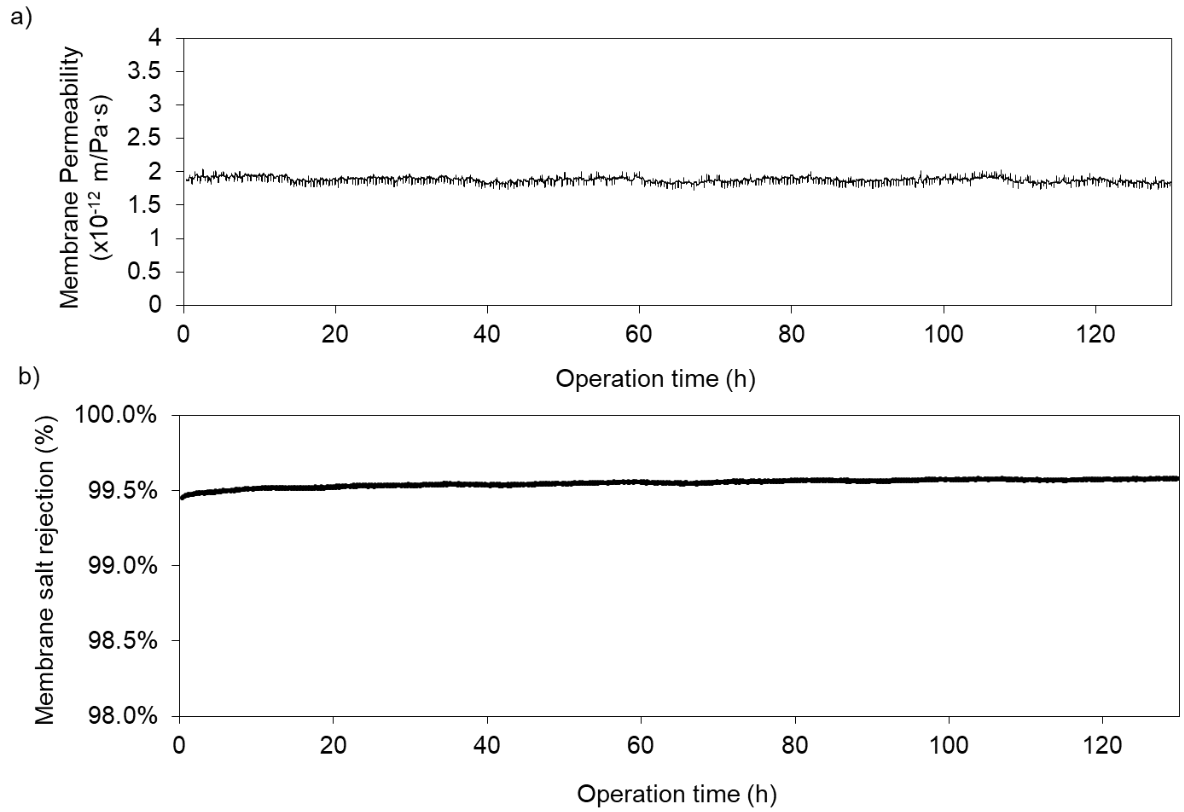

Figure 6-20 RO membrane permeability and normalized salt rejection during long-term UF-RO seawater desalination test #3. RO permeate flux: 12.3 l/(m^2·h), recovery: 32%.

6.4.5 Conclusions

The use of square wave variable inline coagulant dosing strategy was demonstrated in a series of short term and long term experiments as a viable mode of operation that can reduce coagulant use and also reduce chemical cleaning frequency. Short term experiments revealed that during filtration period, it is necessary to ensure that UF fouling is in the cake formation region as facilitated by coagulant dosing. Coagulant dose usage was reduced by operating with an initial dose that was reduced by 50% after a prescribed period during filtration. Such a coagulant dosing strategy enabled effective backwash and also ensured adequate chlorophyll-*a* retention by the UF membrane.

Appendix A: Advanced Pilot Membrane Platforms

The initial establishment of hardware/software solutions for model-based control, process monitoring, and operator decision support, as well as development of dynamic optimization model/algorithms for energy-optimal operation, was accomplished using the Compact and Modular Reverse Osmosis (CoMRO) platform developed at UCLA (Chapter 3) [22, 43, 47, 105, 169, 186, 187]. The CoMRO system (**Fig. A-1**) was constructed with the capability for feed capacity of up to 12,000 gallons per day. Process monitoring includes feed and permeate flow rate, conductivity, turbidity, temperature, and system pressures.

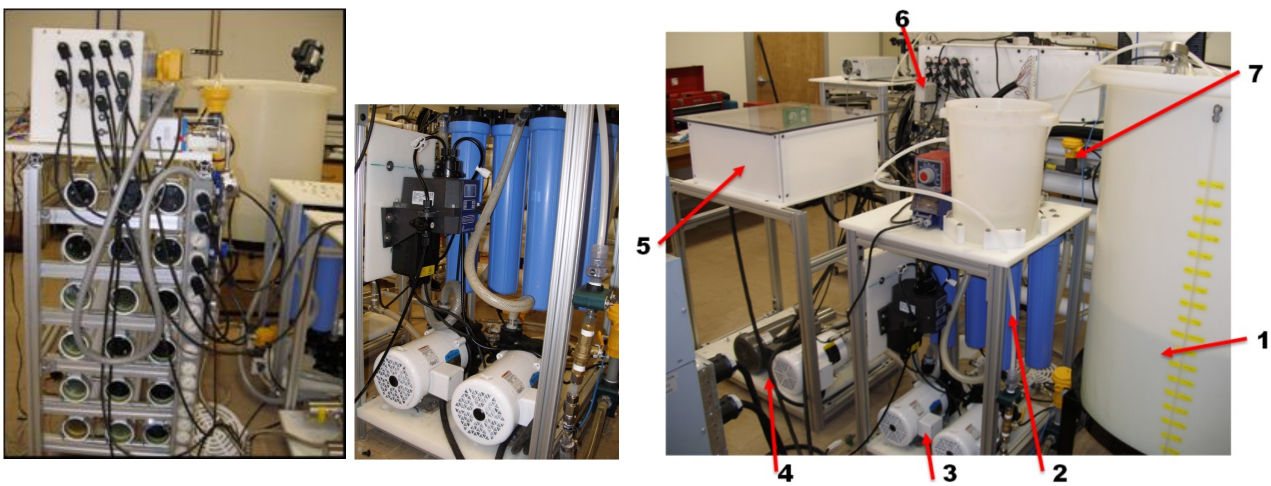

Figure A-1. CoMRO system showing (a) the RO pressure vessels module (left). The control box is on top of the RO module and measures 24"x12"x14" (it is self-standing and can be mounted where needed), (b) the high pressure pumps (can be mounted with the RO skid or as a separate platform), and (c) feed pumps and filtration system (middle). System permeate production capacity is up to ~6,000 gallons/day at 50% recovery. View of CoMRO system in laboratory setup (total recycle mode). 1) Feed tank, 2) Cartridge filters in pretreatment module, 3)Feed pump (low pressure), 4) High pressure pump, 5) Housing compartment for VFDs, 6) Actuated (retentate) valve for pressure control, 7) Retentate stream flow meter.

The second RO pilot system was built as a compact and modular RO system (referred to as CoM2RO) designed with feed water capacity of 35 GPM (50,400 GPD) and, with seawater as feed water, and with fresh water production capacity of 8.3 gpm (12,000 GPD) [188]. The system, consisting of UF and RO skids (**Fig. A-2, A-3**) with the UF skid having three ultrafiltration membrane modules that employ innovative hollow-fiber membranes. The UF system was designed to generate filtrate for the RO feed at a capacity of 12-18 gpm gallons per day per single module. It is an inside-out configuration employing periodic back flushing (typically 1 cycle per 20-60 minutes) and feed forward flushing to remove the UF foulant layer. The UF system was operated in a dead-end filtration mode or with a bleed stream. The pilot system was instrumented with the necessary actuated valves, pressure transducers, flow meters, and turbidity meter to provide information to the UF control system regarding the need for UF backwash, as well as to the RO control system to enable optimization of operating conditions. The RO feed line was fitted with a special cartridge filter in order to protect the RO membranes in the event of UF membrane integrity failure, as well as provide feed water "polishing" with regards to organics.

The CoM2RO system was outfitted with a number of sensors including flow, conductivity, pressure, pH, turbidity and temperature. Flow rate measurements were provided for the feed, concentrate, and permeate from individual RO modules or the overall system. Pressure sensors were positioned before the high pressure pumps (to detect low pressures that may lead to pump cavitation), before the first RO module, and after the last RO module. Conductivity sensors were located on the feed, retentate, and on the permeate stream. pH, turbidity, and temperature sensors were also installed for the feed stream, and a pH sensor was also installed on the permeate side.

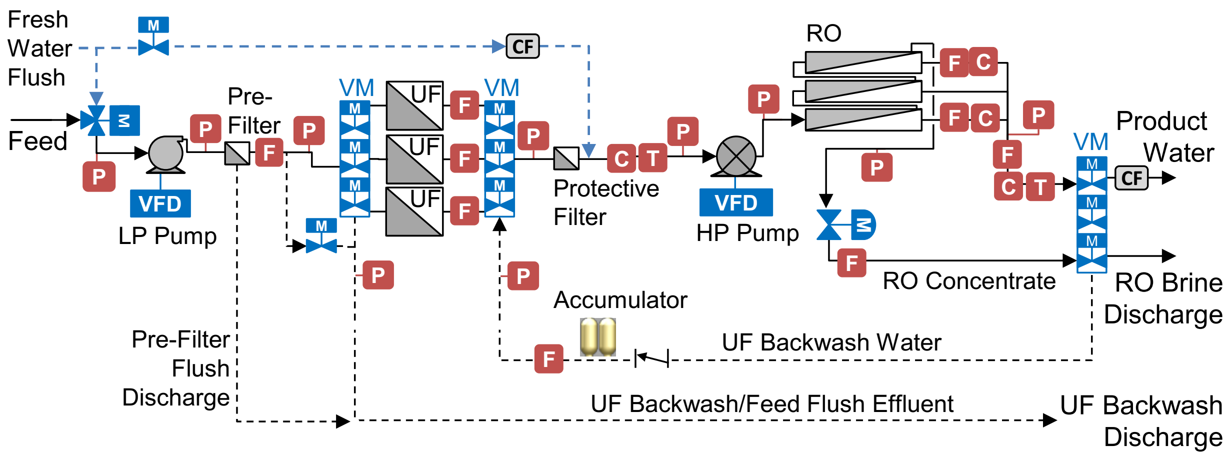

Figure A-2 UCLA CoM2RO system process layout depicting major system components, sensor, and actuators. P: pressure sensor, F: flow meter, T: temperature sensor, C: conductivity; VFD: variable frequency drive, VM: valve manifold, CF: carbon filter, M: electric-actuated motorized valves.

The CoM2RO system was constructed as a "one-touch" startup/shutdown, fully-automated stand-alone operation that is robust, without the need to manually adjust system parameters (e.g., UF backwashing frequency and duration, RO productivity) to cope with changing feed water conditions in naval shipboard deployment (littoral, open ocean, and coastal waters).

Figure A-3 A photo of CoM2RO system designed and constructed by UCLA WaTeR center deployed for costal seawater desalination.

Appendix B: Determination of Contaminant Removal by a Protective Active Filter Sheet at Different Coagulant Dose

B.1 Overview

The objectives of this part of the research were to assess the impact of inline coagulation on the passage of residual foulant material from the UF modules and the effectiveness of a protective nanoalumina adsorptive cartridge filter (rated at 0.7 μm mesh size) for capturing residual foulant material prior to the RO elements. Two cartridge filters (Ahlstrom Standard Disruptor) were installed in parallel after the UF membranes (on the UF filtrate line, **Figure B-1**). These filters were used to capture both nanoparticles and potentially dissolved organic matter (DOM) that may have passed through the UF module. The filters consisted of woven nanoalumina fibers (boehmite nanofibers) with a high adsorptive capacity of a wide range of dissolved organics.

B.2 Filtration experiments using filter sheets

In order to determine the effectiveness of the protective Disruptor cartridge filters in removing DOM and other contaminants, a series of filtration tests were conducted using the UF filtrate (pre-cartridge filters) or RO feed (post-cartridge filters) water as feed using a portable silt density index (SDI) system (Model: Y-SIMPLE SDI, Applied Membranes, Inc., Vista, CA) (**Figure B-2**). The nano-alumina adsorptive filter sheet was cut into a 47 mm diameter circular sheet and loaded into the flow cell of the SDI meter (**Figure B-1**). Each filtration test was carried out in real time when UF modules were in filtration mode. The UF filtrate or RO feed was filtered through the flow cell during the second cycle of a four cycle filtration/backwash experiments. The UF module average filtration flux and backwash fluxes were 36.9 LMH and 168 LMH, respectively, with the corresponding duration of filtration and backwash being 41 min and 2 min. During this study, each filtration test lasted about 15 min, and the filtration resistance of the filter sheet was calculated given the flow rate and inlet pressure measured by the SDI meter. The rate of filtration resistance increase for the filter sheet during the filtration test served to gauge the filtrate quality with and without the cartridge filter.

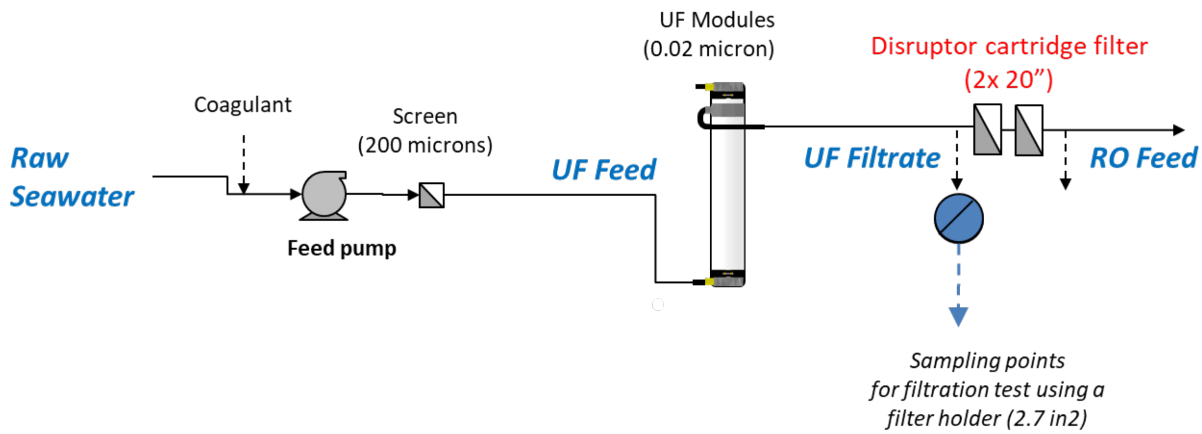

Figure B-1 Experimental setup for filter sheet contaminant removal filtration tests.

Figure B-3 shows the plots of filtration resistance of nano-alumina adsorptive filter versus filtration time for three different coagulant doses: 3.79 mg/L Fe^{3+}, 2.76 mg/L Fe^{3+}, and 0.347 mg/L Fe^{3+}. As shown in Figure B-3, the decrease in filtration resistance of the filter sheets for the UF filtrate, as determined for nano-alumina adsorptive filter sheet, with increasing coagulant dose suggests a decrease in the passage of residual material through the UF elements. This is consistent with the expectation that UF feed coagulation should improve UF rejection of materials <0.02 micron (e.g., organics). This result indicates that inline coagulation prior to UF reduces material passage through UF and the reduction is proportional to the coagulant dose level.

In a another set of experiments the nano-alumina adsorptive filter sheet was used to filter the UF filtrate and RO feed separately in order to assess the passage of UF residual foulants. **Figure B-4 and Figure B-5** shows that the overall filtration resistance of the filter sheet for RO feed is lower than the filtration resistance of the filter sheet for UF filtrate under inline coagulant dose of 2.76 mg/L and 4.10 mg/L of Fe^{3+}. The rise of filtration resistance upon filtration of the UF filtrates with the nanoalumina adsorptive filter sheets is indicative of residual passage of foulants through the UF elements to the RO feed even when UF feed coagulant dose was as high as 4.10 mg/L Fe^{3+}. **Figure B-6** shows that the difference of filtration resistance for the RO feed (post cartridge filter) was small at coagulant dose of 2.76 mg/L and 4.1 mg/L of Fe^{3+}. Compared with the results shows in **Figure B-4**, this suggests that the Disruptor cartridge filter was beneficial for the removal of residual materials that remained in the UF filtrate when coagulant dose was suboptimal.

In order to test the long term polishing capacity of the filter cartridges, the pressure drop across the filter cartridges was used as an indication of the foulant load onto the filter. **Figure B-7** shows the pressure drop progression across the cartridge filter comparing foulant passage of with inline coagulant dose of 2.76 mg/L and 4.1 mg/L Fe^{3+}. It is clear from the above results that the pressure drop rise for coagulant dosing of 4.1 mg/L Fe^{3+} was about 53.8% slower than for coagulant dosing at the level of 2.69 mg/L Fe^{3+}during the 120 hr UF operation period.

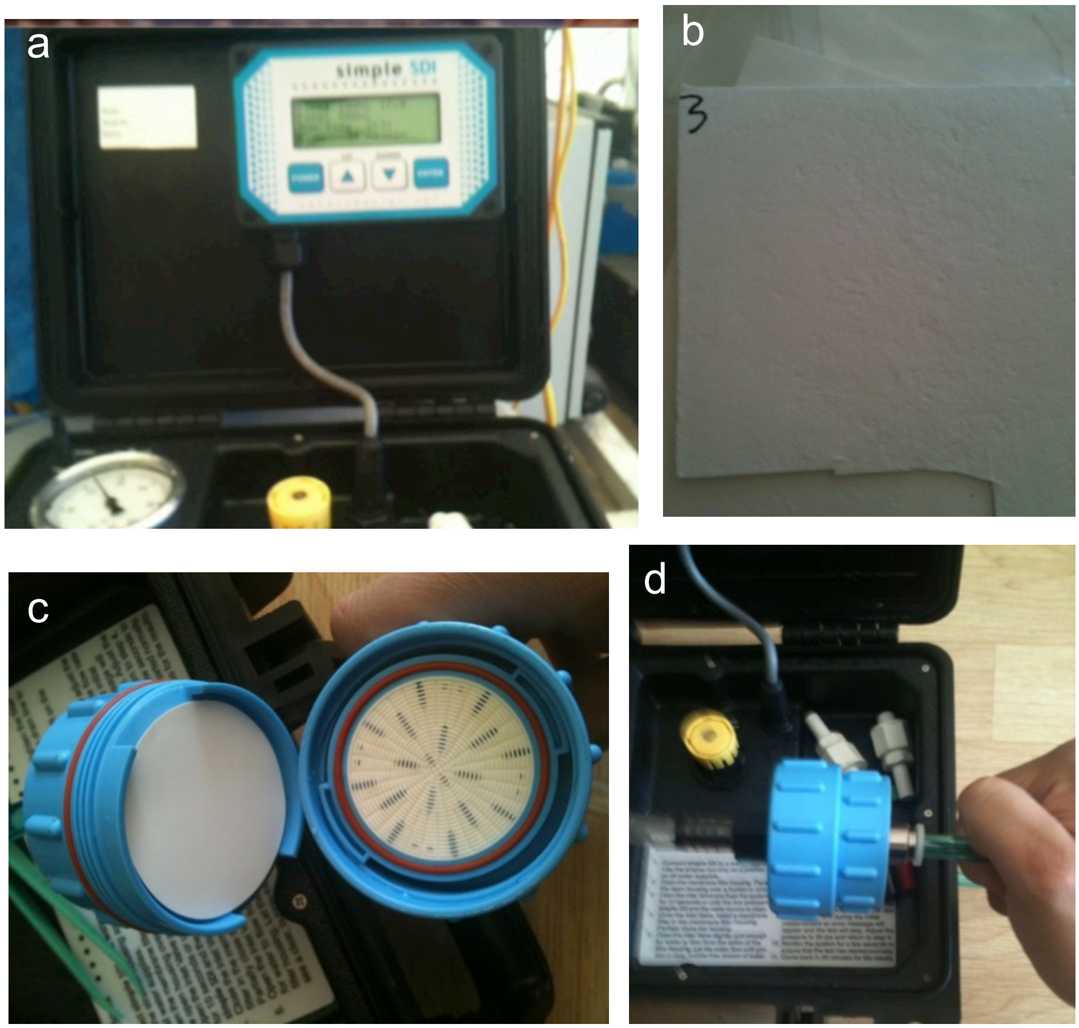

Figure B-2 (a) Simple SDI meter used in filtration test, (b) Nano-alumina adsorptive filter sheet, (c) Filter sheet inside filter holder (surface area: 2.7 in^2), and (d) Simple SDI meter during filtration test.

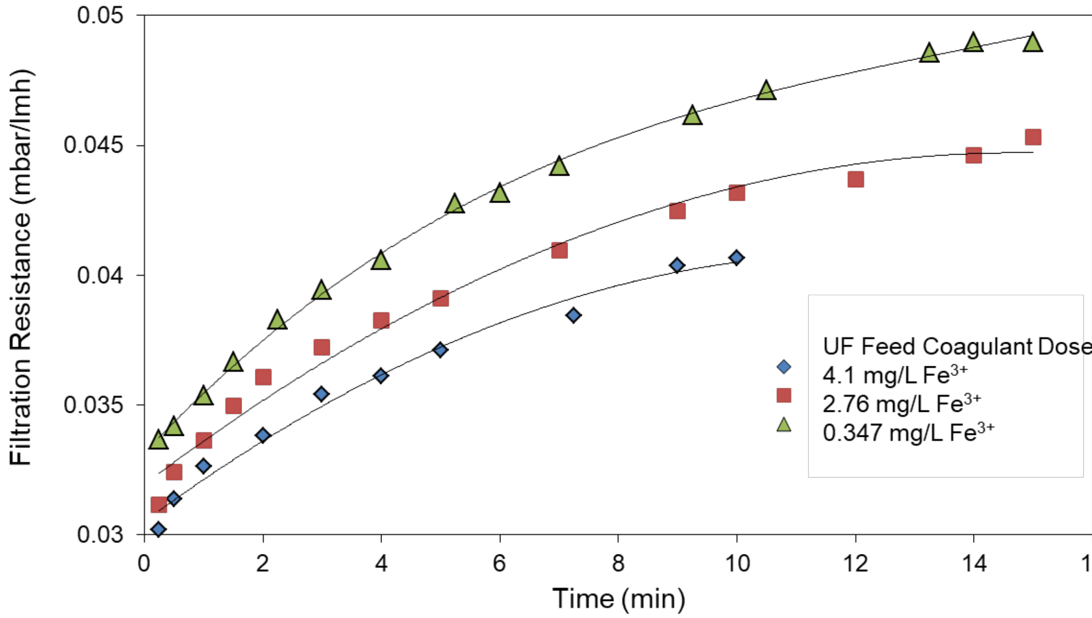

Figure B-3. UF filtrate samples were used to tests the Nano-alumina adsorptive filter sheet (in 2.7 in^2 small filter holder)

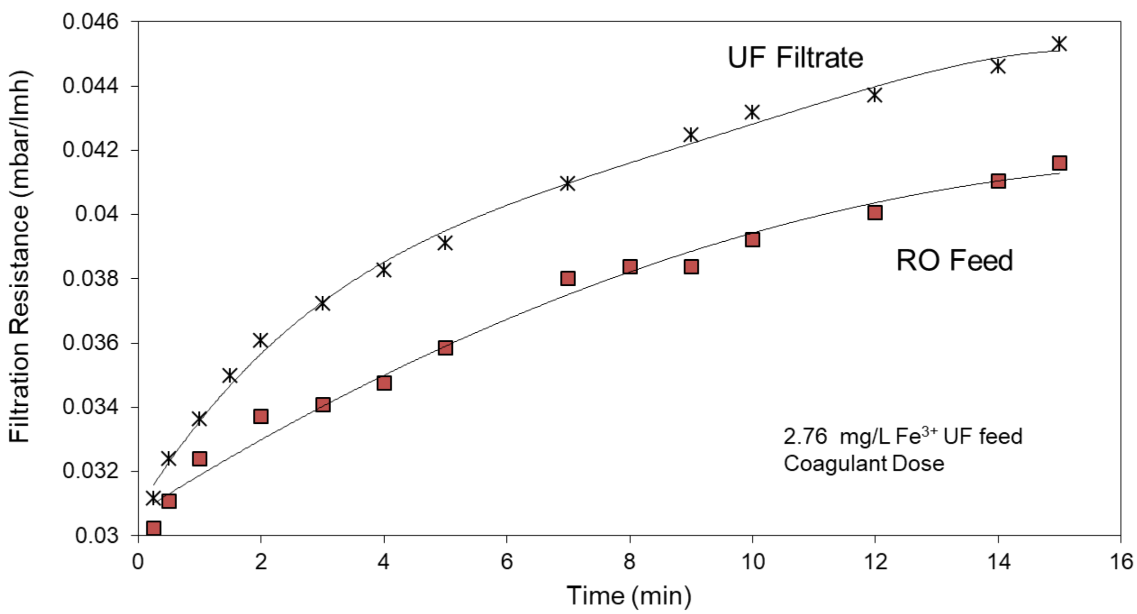

Figure B-4. Filtration of UF Filtrate (Pre-Cartridge) and RO Feed (Post-Cartridge) with Nano-alumina adsorptive filter sheet (Non-Laminated, 2.7 in^2)

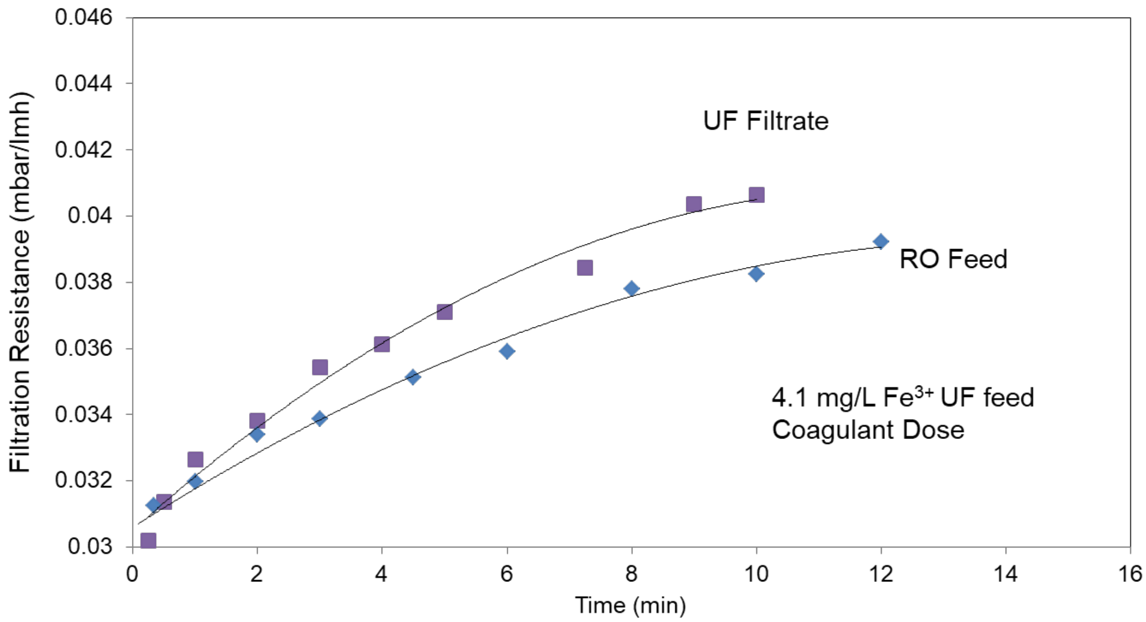

Figure B-5 Filtration of UF Filtrate (Pre-Cartridge) and RO Feed (Post-Cartridge) with Nano-alumina adsorptive filter sheet (Non-Laminated, 2.7 in^2)

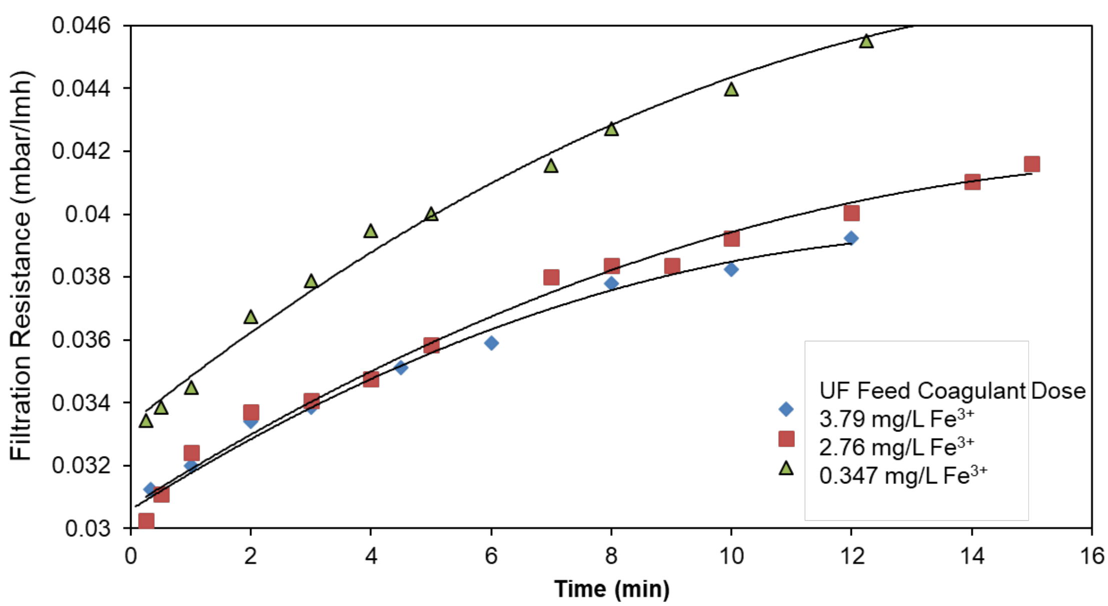

Figure B-6 Filtration of RO Feed (Post-Cartridge) with Nano-alumina adsorptive filter sheet (Non-Laminated, 2.7 in^2.

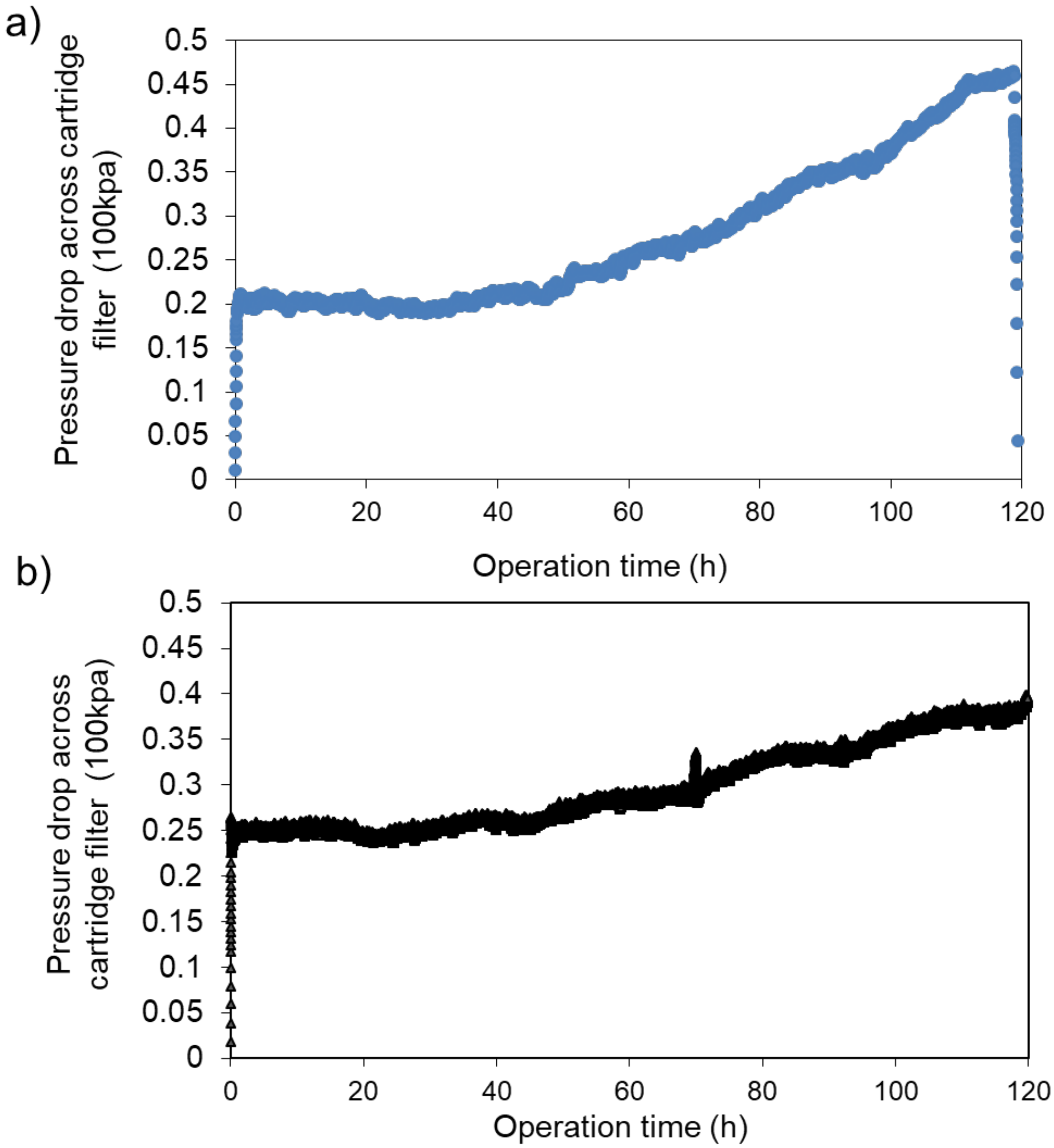

Figure B-7 Pressure drop across nano-alumina adsorptive cartridge filters during UF filtration tests with inline coagulant dosing of: (a) 2.76 mg/L Fe^{3+}, and (b) 4.1 mg/L Fe^{3+}. UF operating condition: UF module average filtration flux and backwash fluxes were 36.9 LMH and 168 LMH, respectively, with the corresponding duration of filtration and backwash being 41 min and 2 min.

B.3 Preliminary assessment of TEP passage through UF membrane via TEP detection (staining) experiments

In this part of the study, the potential passage of TEP through the UF (0.02 μm) membrane was quantified by filtering UF filtrate through a nano-alumina adsorptive filter (0.7 μm) at various coagulant dosages. Alcian Blue, which binds with negatively charged polysaccharide functional groups, was used to detect (via filter surface staining) the presence of organics deposition and may indicate the significance of any TEP. The blue/green color of the filter (due to staining by Alcian blue) is indicative of the presence of TEP. The experimental setup is shown in **Figure B-8**.

During each test, 200 ml of water sample was filtered through a 2'' diameter nano-alumina filter paper in a glass flask at low vacuum (<150 mmHg). After drying the filter (using the same vacuum filtration apparatus), 1 ml of 0.02% Alcian blue staining solution (Alcian Blue 8GX, certified, ACROS Organics, Waltham, MA, at pH = 2.5) was applied onto the filter. The solution was allowed to react with the surface deposits on the filter for about 4 seconds. Examination of the filter sheet surface after the filtration test was accomplished via an optical microscope (Dino-Lite AM4113T5X, AnMo Electronics Corporation, Taiwan) at different magnifications (90X, 500X).

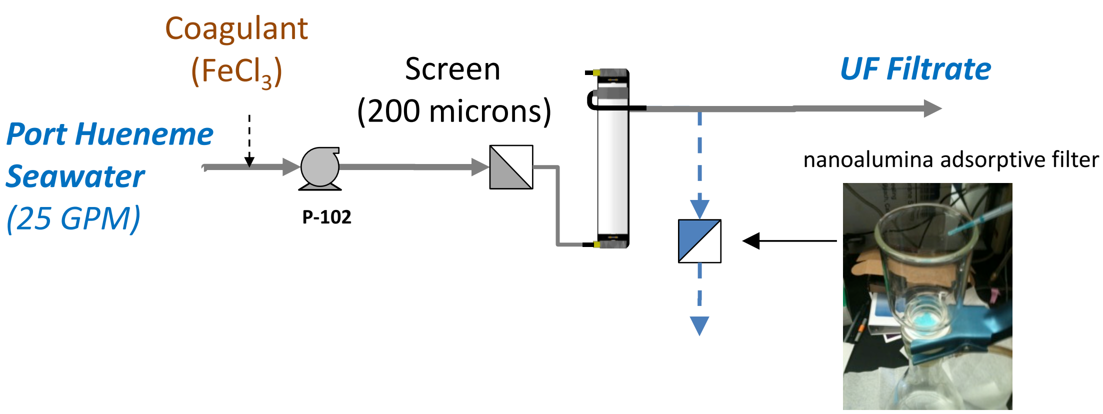

Figure B-8 Experimental setup for assessment of TEP passage through a UF element. Filtration in the adsorptive filter (bottom right) was via a vacuum filter setup (Glass filtration unit, insert on right)

Figure B-8-B-9 shows the photos, at 90X and 500X magnification, of the nanoalumina adsorptive filters after filtration tests with four different water samples. As expected, filtering seawater (UF feed) through the filter sheet resulted in the deepest blue color. The dark yellow spots on the filter were flocs formed by coagulant in the feed water (**Figure B-8**). Filtering DI water through the filter sheet resulted in the lightest blue on the filter (**Figure B-9**); this faint blue was probably due to blue dye pigments in the Alcian blue solution and not due to reaction with TEP. Filtration with UF filtrate with 2.9 mg/L of Fe^{3+} as inline coagulant (**Figure B-8**) yielded a lighter blue than UF filtrate without coagulant (**Figure B-9**) confirming the results from **Section B-2** that showed inline coagulation prior to UF reduces organic material (e.g., TEP) passage through the UF module. It is noted that although not done in this exploratory analysis study, it is possible to determine the intensity of the blue color quantitatively via spectroscopic means or via image analysis software and thus quantify the level of fouling potential of the water souce.

Scanning Electron Microscopy (SEM) images of the adsorptive filter sheets are shown in **Figure B-10** for clean and foulant covered sections of the fibrous filter. It is clear from the SEM image that colored section of the filter sheet were covered with foulants. The fibrous nature of the adsorptive filter provide a large surface area that contributed to adsorption of organic foulant. The Energy Dispersive X-ray Spectroscopy (EDX) of a foulant covered section of the fibrous filter, shown in **Figure B-11**, indicates EDX peaks corresponding to carbon and oxygen peaks (typically indicative of the presence of organic materials), silicon and aluminum, along with traces of magnesium, sodium, chloride, and iron.

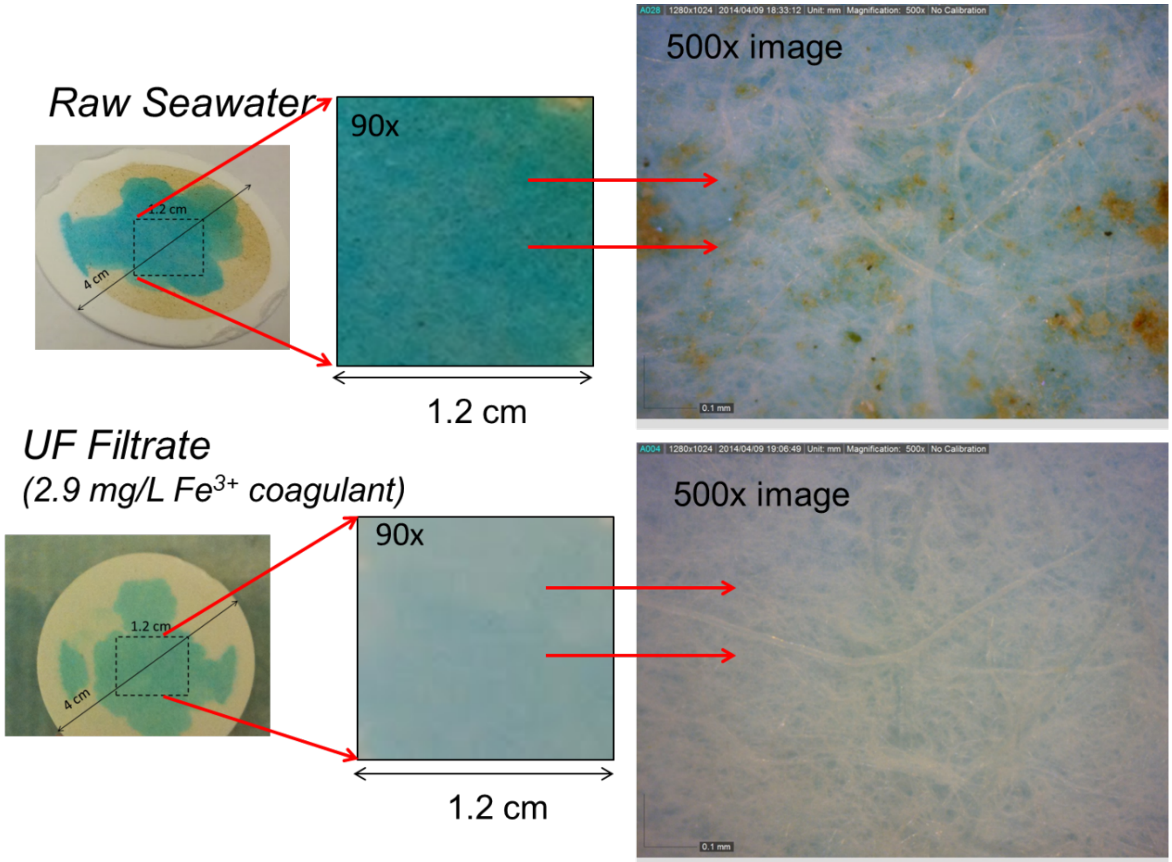

Figure B-9 Filter sheet surface after filtration test and Alcian blue staining viewed using a portable digital microscope at 1x, 90x, and 500x magnification. Top: Filtration of raw seawater (UF feed) Bottom: Filtration of UF filtrate with 2.9 mg/L Fe^{3+}.

B.4 Summary

With an optimal level of inline coagulant dosing of the feed to the UF elements TEP removal by UF module can be increased. The adsorptive cartridge filter provides the benefit of added level of removal of organics (especially TEP) from the UF filtrate. However, irrespective of UF operation mode and coagulant dose, the adsorptive cartridge filter only provides partial TEP removal from the UF filtrate.

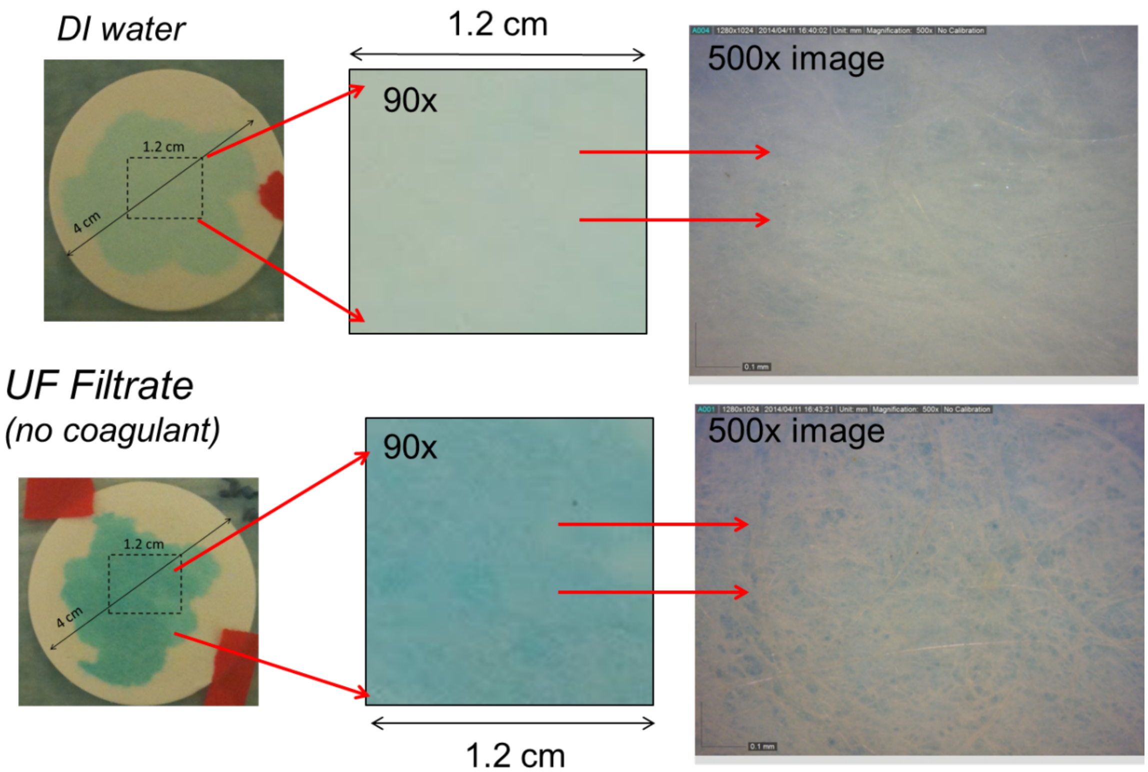

Figure B-10 Filter sheet surface after filtration test and Alcian blue staining viewed using a portable digital microscope at 1x, 90x, and 500x magnification. Top: Filtration with DI water. Bottom: Filtration using UF filtrate (without coagulant dosing).

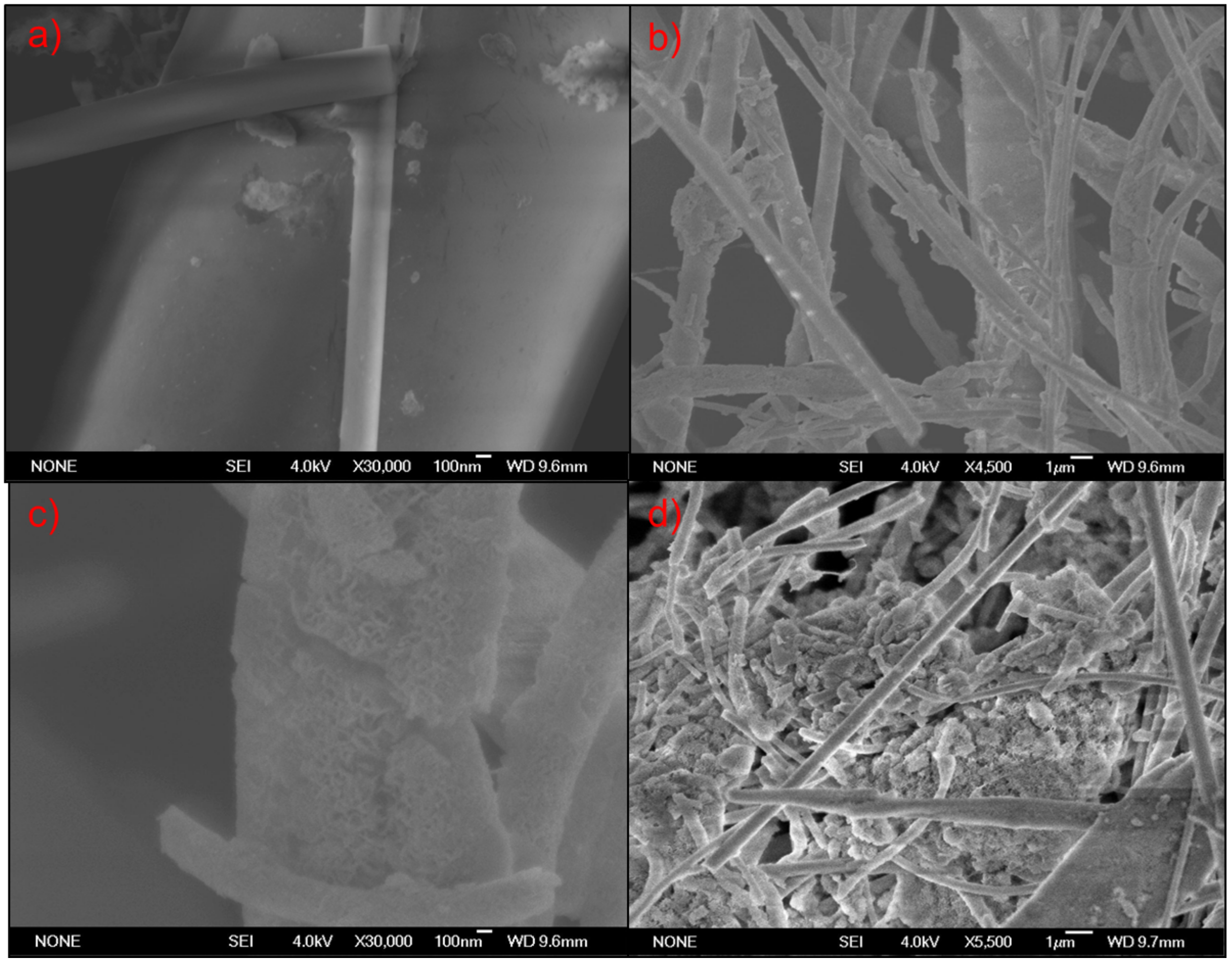

Figure B-11 SEM images of Nanoalumina adsorptive filter nanofibers. (a) Clean section of the fiber, 30,000x magnification, (b) Clean section of the fiber 4,500x magnification, (c) Foulant covered section of the fiber. 30,000x magnification, and (d) Foulant covered section of the fiber 5,500x magnification.

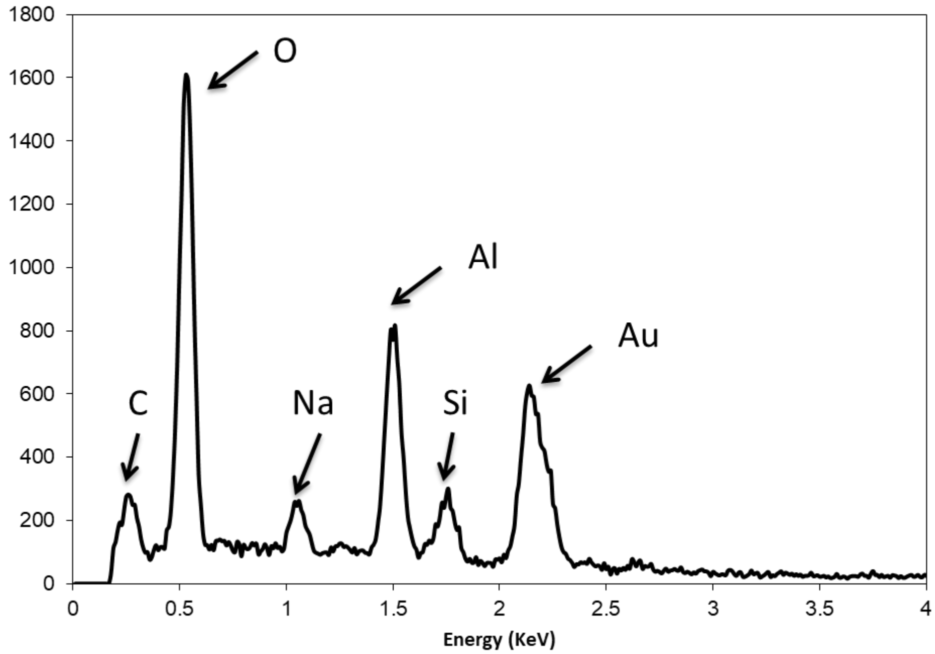

Figure B-12 Energy dispersive X-ray spectroscopy (EDX) result for stained portion of the adsorptive filter nanofiber.

Appendix C: Com2RO System Chemical Cleaning Protocol

1. Chemical checklist:

   Caustic solution: Use household bleach (CLOROX REGULAR-BLEACH) and technical grade NaOH pellets (MW 39.997 g/mol). In order to make 1 gallon of caustic + bleach solution (@ 100ppm free Chorine concentration in stream and pH 12)

   1) Add 3.3L of raw bleach into a container
   2) Add 485.4 mL of DI water to the bleach solution
   3) Slowly add 800g of NaOH pellets into the above solution, mix well. (avoid overheating of the solution).

   Citric acid solution: (MW 192.124 g/mol). To make 1 gallon of citric acid solution (@ pH 3.04 in stream)

   a) Add 1 gallon of DI water to a container
   b) Add 800g of citric acid powder (anhydrous) into the above solution, mix well.

2. Plumbing configuration:

1) Remove the metering pump (Grundfos Metering Pump 2 GPH, 4-20 mA, 190 strokes) along with the suction and outlet tubing from its connection to the chemical tank of the $FeCl_3$ solution.

2) Clean the suction and outlet tubing using tap water, change metering pump to 100% mode (full mode)

3) Remove metering pump (Walchem Metering Pump 1.8GPH PVC/Viton, 4-20 mA Input, 360 strokes) along with the suction and outlet tubing from its connection to the chemical tank of the NaOCl solution.

4) Feed flush the UF modules with seawater after system shutdown and the permeate water tank is filled completely with RO product water (300 gal.)

5) Connect the injection assembly of the metering pump to the injection point before the UF pump.

6) Connect the metering pump for the caustic solution and connect the injection assembly to the injection point after the UF pump.

7) Drain the UF system

a) Turn the manual ball valve for module drain and manual backwash drain valve to "switched on" position.

b) Open automated backwash valve

c) Open all feed and drain valves of the UF modules

d) Loosen the three-way actuated valve at the base of the UF modules, remove the valve to reveal the CIP outlet flange.

e) Connect the CIP outlet flexible hose the CIP outlet port and bring the hose to the chemical waste tank.

8) Turn UF filtrate and UF drain manual ball valves to CIP outlet direction. Divert both UF filtrate and drain to CIP outlet.

3. <u>Chemical cleaning procedure:</u>

Acidic cleaning:

1. Pump seawater through the UF system at 15 gpm. Configure the system to operate with only using one module at a time.
2. Start dose citric acid solution using metering pump @ 103.4 ml/min for 3 minutes. Alternate feed direction.
3. Check the UF filtrate pH at the UF filtrate sampling valve.
4. Dose acidic solution to the other UF modules.
5. Soak the UF module for 12-24 hrs.
6. Drain the UF system.
7. Fill and feed flush the UF system using seawater.

Caustic cleaning:

1. Pump fresh water through the UF system at 15 gpm. Configure the system to operate with only using one module at a time.
2. Start dose caustic acid solution using metering pump @ 360 spm for 3 minutes. Alternate feed direction.
3. Check the UF filtrate pH at the UF filtrate sampling valve.
4. Dose caustic solution to the other UF modules.
5. Soak the UF module for 12-24 hrs.
6. Add critic acid to UF modules
7. Drain the UF system.
8. Fill and feed flush the UF system using tap water.

Appendix D: Coagulant Dose Conversion

The relationship between F_{mp} (metering pump output flow rate (ml/h)), the RO pump flow rate (F_{RO_pump}) and the flow constant (FC) input to the metering pump (4-20 mA current input) was expressed as:

$$FC = F_{mp}\left[ml/h\right] \cdot \frac{39.33}{F_{RO\_pump}\left[gpm\right]} \tag{D-1}$$

$$F_{mp}\left[ml/h\right] = FC \cdot \frac{F_{RO\_pump}\left[gpm\right]}{39.33} \tag{D-2}$$

The concentration of $FeCl_3$ in a given stream is given by:

$$C_{FeCl_3} = \frac{FC \cdot C_{wt} \cdot SG}{6 \cdot 3.7854} \tag{D-3}$$

where C_{wt} is the wt % (weight percent) of $FeCl_3$ solution = 40.23 wt%, the specific gravity (SG) of $FeCl_3$ solution =1.424. The concentration of Fe^{3+} ions in stream is:

$$C_{Fe^{3+}} = \frac{C_{FeCl_3}}{(55.845 + 35.45 \times 3)} \tag{D-4}$$

where the denominator is the molecular weight of $FeCl_3$.

Using the above equations, the metering pump can be programmed to maintain different inline concentrations of $FeCl_3$ and ACH under different UF feed flow rates. As an example, **Table D-1** was generated for UF flow rate of 20 gpm (75.7 L/m)

Table D-1. Coagulant dose conversion table for ACH and $FeCl_3$ coagulants

Flow constant[a]	Concentration of Al^{3+} (mg/L) in feed stream	Concentration of $FeCl_3$ in feed stream (mg/L)	Coagulant metering pump flow rate (ml/min)[b]
13.54	10	23.98	261.0
16.24	12	28.76	313.0
18.34	13.5	32.48	353.5
20.30	15	35.95	391.2
27.06	20	47.93	521.5

(a) Eq. D-1 and D-2
(b) UF feed flow rate: 20 gpm, UF filtrate flux per module: 45.5 $L/m^2 \cdot h$, RO high pressure pump rpm: 800 rpm.

Appendix E: UF Operating Regions and Thresholds for Online Process Characterization

The impact of changes in field water quality will affect the optimal strategies of UF filtration and backwash. Therefore, it is convenient to categorize fouling indicators with respect to separate fouling regions and selected action thresholds. As an illustration, **Figures E1(a–d)** show four representative plots of fouling indicators and the thresholds that signify changes in fouling conditions.

In order to simplify the classification of fouling indicators, each indicator was assigned to a "low", "normal" and "high" regions according to the fouling indicators thresholds. In addition, the change in fouling indictors was described as "increasing", "steady", or "decreasing" according to the change in fouling indicators thresholds. This was done in order to elucidate the fouling trend. **Table E-1** summarizes the fouling indicators along with their corresponding thresholds.

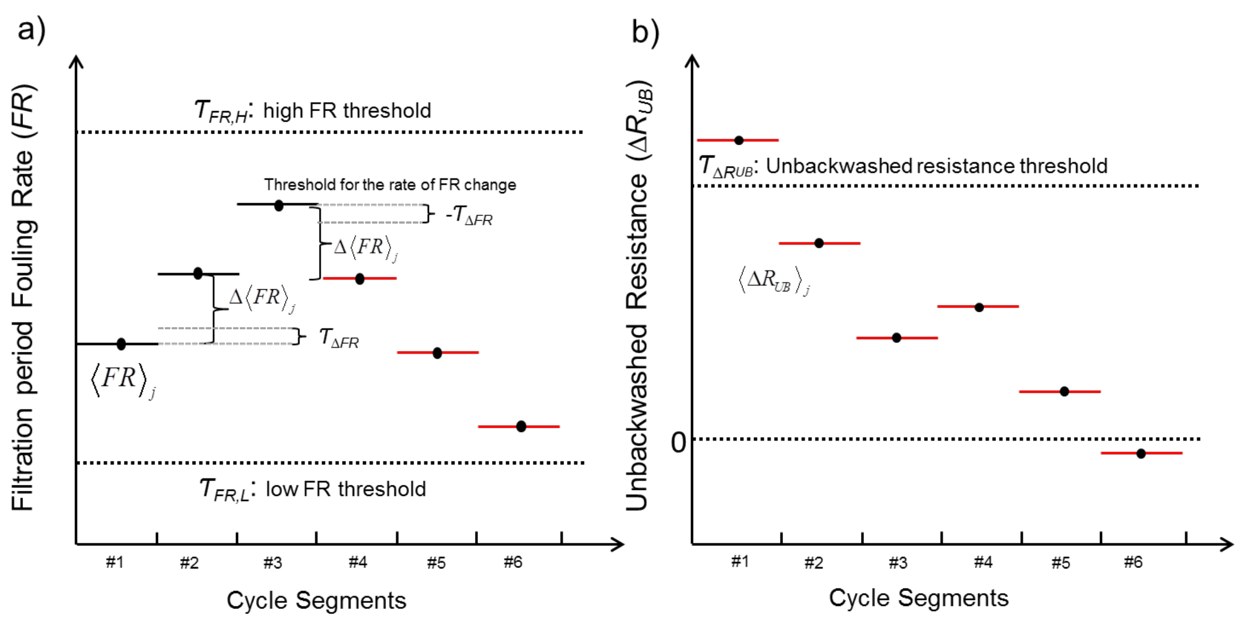

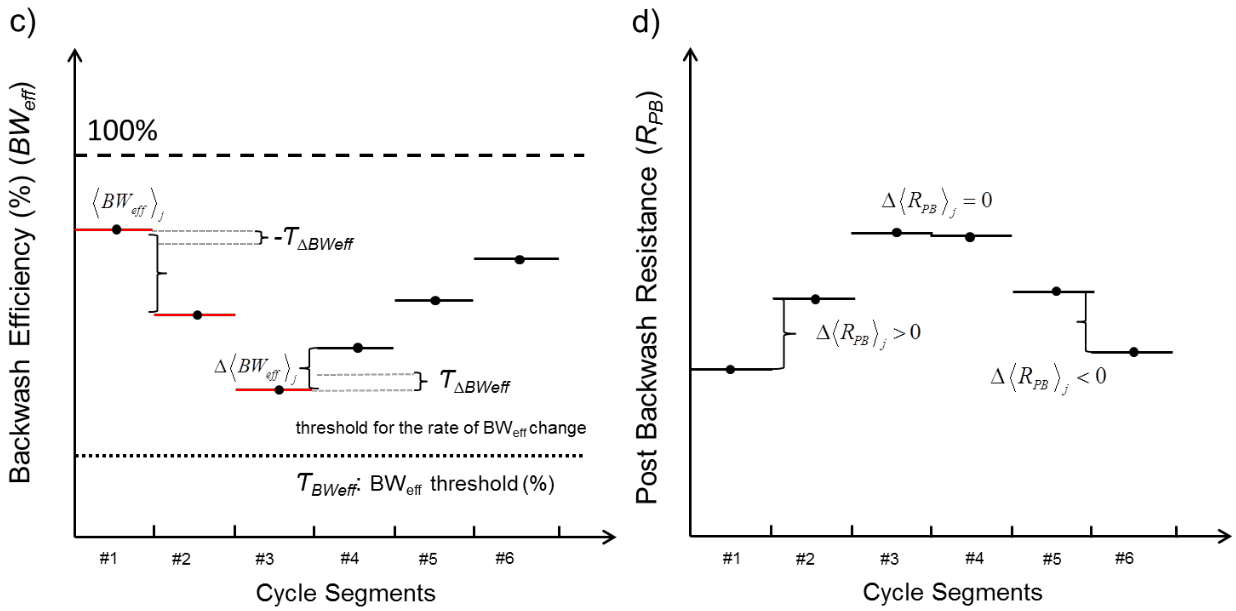

Figure E-1 Illustration of UF membrane fouling indicators and thresholds for changing in UF operational regions. Where $T_{\Delta FR}$ is threshold for the rate of FR change, $\Delta\langle FR\rangle_j$ is change in filtration period fouling rate. $T_{FR,H}$ and $T_{FR,L}$ is the high and low FR threshold, respectively. T_{RUBW} is the unbackwashed resistance threshold**,** $T_{\Delta BWeff}$ is rate of BW_{eff} change threshold, $\Delta\langle BW_{eff}\rangle_j$ is change in backwash efficiency, T_{BWeff} is BW_{eff} threshold, and $\Delta\langle R_{PB}\rangle_j$: change in accumulated unbackwashed resistance.

Figure E-1(a) shows an increasing trend (in the first 3 multi-cycle segments) and then a decreasing trend (4-6 multi-cycle segments) in the UF filtration fouling rate ($\langle FR\rangle_j$). In order to classify the filtration fouling rate, a high ($T_{FR,H}$) and a low ($T_{FR,L}$) thresholds for the filtration fouling rate were selected based on the maximum allowable resistance increase per cycle and filtration duration limitation. In addition, $\pm\ T_{\Delta FR}$ was defined as the threshold for the change (increase and decrease, receptively) in filtration fouling rate ($\Delta\langle FR\rangle_j$). For example, a $\Delta\langle FR\rangle_j$ greater than $T_{\Delta FR}$ indicates a real increase in $\langle FR\rangle_j$ (i.e. above normal fluctuation in $\langle FR\rangle_j$).

Three regions for $\langle \Delta R_{UB}\rangle_j$ are shown in **Figure E-1 (b),** where $T_{\Delta R}$ is the unbackwashed resistance threshold. For example, the normal $\langle \Delta R_{UB} \rangle_j$ region is between $T_{\Delta R}$ and 0. The three regions of UF backwash efficiency ($\langle BW_{eff}\rangle_j$) are defined by two thresholds. **Figure E-1(c)** shows a decreasing trend (in the first 3 multi-cycle segments) and then an increasing trend (4-6 multi-cycle segments) of backwash efficiency. T_{BWeff} was set as the threshold for low backwash efficiency and $<BW_{eff}>_j$ = 100% is the high backwash efficiency threshold. $T_{\Delta BWeff}$ is set as the backwash efficiency change threshold. For example, a negative $\Delta<BW_{eff}>_j$ more than - $T_{\Delta BWeff}$ would indicate a real decrease in $<BW_{eff}>_j$ (i.e. the change in backwash efficiency is below normal fluctuation).

The cumulative UBW resistance was categorized by determining the sign of the change in post backwash initial resistance ($\Delta<R_{PB}>_j$) for one multi-cycle segment as shown in as shown in **Figure E1(d)**. In particular, $\Delta<R_{PB}>_j > 0$ indicates increasing $<R_{PB}>_j$, $\Delta<R_{PB}>_j < 0$ indicates decreasing $<R_{PB}>_j$, and $<R_{PB}>_j \approx 0$ indicates steady or no change in $<R_{PB}>_j$.

Table E-1 UF membrane fouling indicators and thresholds that signify changes in UF operational regions

Category / Fouling indicators	Low	Normal	High
$<FR>_j$ filtration period fouling rate	$\langle FR\rangle_j < T_{FR,L}$	$T_{FR,L} \le \langle FR\rangle_j \le T_{FR,H}$	$\langle FR\rangle_j > T_{FR,H}$
$<\Delta R_{UB}>_j$ Unbackwashed Resistance	$\langle \Delta R_{UB}\rangle_j < 0$	$0 \le \langle \Delta R_{UB}\rangle_j \le T_{\Delta R}$	$\langle \Delta R_{UB}\rangle_j > T_{\Delta R}$
$<BW_{eff}>_j$ Backwash Efficiency	$\langle BW_{eff}\rangle_j < T_{BW_{eff}}$	$T_{BW_{eff}} \le \langle BW_{eff}\rangle_j \le 100\%$	$\langle BW_{eff}\rangle_j > 100\%$
Change in fouling indicators	Decreasing	Steady	Increasing
$\Delta<FR>_j$ Change in filtration period fouling rate	$\Delta\langle FR\rangle_j < T_{\Delta FR}$	$-T_{\Delta FR} \le \Delta\langle FR\rangle_j \le \mathrm{T}_{\Delta FR}$	$\Delta\langle FR\rangle_j > T_{\Delta FR}$
$\Delta<BW_{eff}>_j$ Change in Backwash Efficiency	$\Delta\langle BW_{eff}\rangle_j \le T_{\Delta BW_{eff}}$	$-T_{\Delta BW_{eff}} \le \Delta\langle BW_{eff}\rangle_j \le T_{\Delta BW_{eff}}$	$\Delta\langle BW_{eff}\rangle_j \ge T_{\Delta BW_{eff}}$
$\Delta<R_{PB}>_j$ Post backwash initial resistance	$\Delta\langle R_{PB}\rangle_j < 0$	$\Delta\langle R_{PB}\rangle_j \approx 0$	$\Delta\langle R_{PB}\rangle_j > 0$

Appendix F: Application of Utilizing Online UF Fouling Characterization under Different UF Operational Regions

Short term characterization tests and a long term UF experiment were conducted to establish the appropriate thresholds and operational regions for the development and application of UF fouling indictors. UF membrane fouling indicators thresholds are summarized in **Tables F-1 and F-2**. In all experiments $\Delta R_{T,n}$ serve as the trigger for adaptive backwash operation (Section 4.4.2).

The upper and lower thresholds ($\varepsilon_{FR,L}$ and $\varepsilon_{FR,H}$) for the filtration fouling rate were based on a filtration duration range of 20 – 42 minutes as determined from short-term experiments and the maximum allowable resistance increase per cycle. The maximum allowable change ($\Delta R_{f,n}$) in resistance per filtration cycle was set to 0.284 $x10^{12}$ m^{-1}. The normal operation range was determined to be in the range of 0.41 - 0.85$x10^{12}$ m^{-1}.

When FR for a particular filtration period was below 0.410 $x10^{12}$ m^{-1}, the UF module filtered until the maximum filtration time of 42 min was reached which and resulted in $\Delta R_{T,n}$ decline below the maximum allowable threshold. An increasing ΔR_{UB} for a cycle with a low FR will further decrease the BW_{eff}. On the other hand, if FR for a particular filtration period was above 0.850 $x10^{12}$ m^{-1}, UF filtration was continued until the minimum filtration time of 20 min and resulted in $\Delta R_{T,n}$ that exceeded the maximum allowable change for that cycle.

The threshold for the change in filtration fouling rate ($\varepsilon_{\Delta FR}$) was estimated from the standard deviation of the change of fouling rate over a period of time during which feed water quality was mostly time invariant. Any change smaller than the above threshold implied that the change was sufficiently small to be considered "steady". Similarly, the lower bound threshold for the backwash efficiency (ε_{BWeff}) was selected as 90%; this conservative choice was selected since, as shown in **Section 5.4.2, Figure 5-9**, the range of backwash efficiency was mostly in the range of 90-100%. The upper bound was conveniently set as 100% $BW_{eff,}$ which signifies complete removal of previously formed foulant layer from the last filtration period.

The threshold for the change in backwash efficiency ($\varepsilon_{\Delta BWeff}$) was estimated from the standard deviation of the change in backwash efficiency over a period of time during which feed water quality was essentially time invariant. Any change smaller than this value implies that the change is sufficiently small for the operation to be considered stable. The threshold for Unbackwashed Resistance (ε_{RUBW}) were determined based on short term inline coagulation experiments as shown in **Section 5.4.2, Figure 5-10**. This conservative choice was selected since, as shown in **Figure 5-10**, the range of $<R_{UBW}>$ was in the range of 0.02-0.05 x10^{12} m^{-1}. A described in **Table F-1**, as R_{UBW} for a given decreases, a high FR will further increase BW_{eff}. If R_{UBW} for the cycle decreases below zero, BW_{eff} will be above 100% indicating that previously unbackwashed resistance has been removed in the last backwash step.

Table F-1 Typical fouling indicators for different UF operational regions

Cases	$<FR>_j$ filtration period fouling rate	$\Delta<FR>_j$ Change in filtration period fouling rate	$<R_{UBW}>_j$ Unbackwashed Resistance	$<BW_{eff}>_j$ Backwash Efficiency	$\Delta<BW_{eff}>_j$ Change in Backwash Efficiency	$\Delta<R_{UBW,T}>_j$ Change in Cumulative Unbackwashed Resistance	Status of operation

1	Normal	Steady	Normal	Normal	Steady	Increasing	Stable operation
2	Normal to High	Increasing	Low – Normal	Normal	Increasing	Steady	Effective backwash
3	High to Normal	Decreasing	Low	High	Increasing	Decreasing	Removing previously UBW resistance
4	Low to Normal	Decreasing	High	Low	Decreasing	Increasing	Coagulant dose inadequate
5	Normal to High	Increasing	Low	High	Increasing	Decreasing	Removing previous UBW resistance
6	Normal	Steady	High	Low	Steady	Increasing	Inadequate backwash flux and/or duration

Note: UBW – unbackwashed

Table F-2 UF membrane fouling indicators thresholds

Thresholds	Symbols	Values based on experimental values
Filtration period fouling rate (low)	$\varepsilon_{FR,L}^{(a)}$	0.41×10^{12} $m^{-1} \cdot h^{-1}$
Filtration period fouling rate (high)	$\varepsilon_{FR,H}^{(b)}$	0.85×10^{12} $m^{-1} \cdot h^{-1}$
Change in filtration period fouling rate	$\varepsilon_{\Delta FR}^{(c)}$	0.036×10^{12} $m^{-1} \cdot h^{-1}$
Unbackwashed Resistance	$\varepsilon_{RUBW}^{(d)}$	0.050×10^{12} m^{-1}
Backwash Efficiency	$\varepsilon_{BWeff}^{(d)}$	90%
Change in backwash efficiency	$\varepsilon_{\Delta BWeff}^{(f)}$	4.8%

(a) Lower threshold for filtration fouling rate
(b) Upper threshold for filtration fouling rate
(c) Threshold for the change in filtration fouling rate
(d) Threshold for unbackwashed resistance
(e) Threshold for backwash efficiency
(f) Threshold for change in backwash efficiency

Appendix G: Monitoring of long term self-adaptive operation of UF system with autonomous backwash triggering and a coagulant controller for real time dose optimization

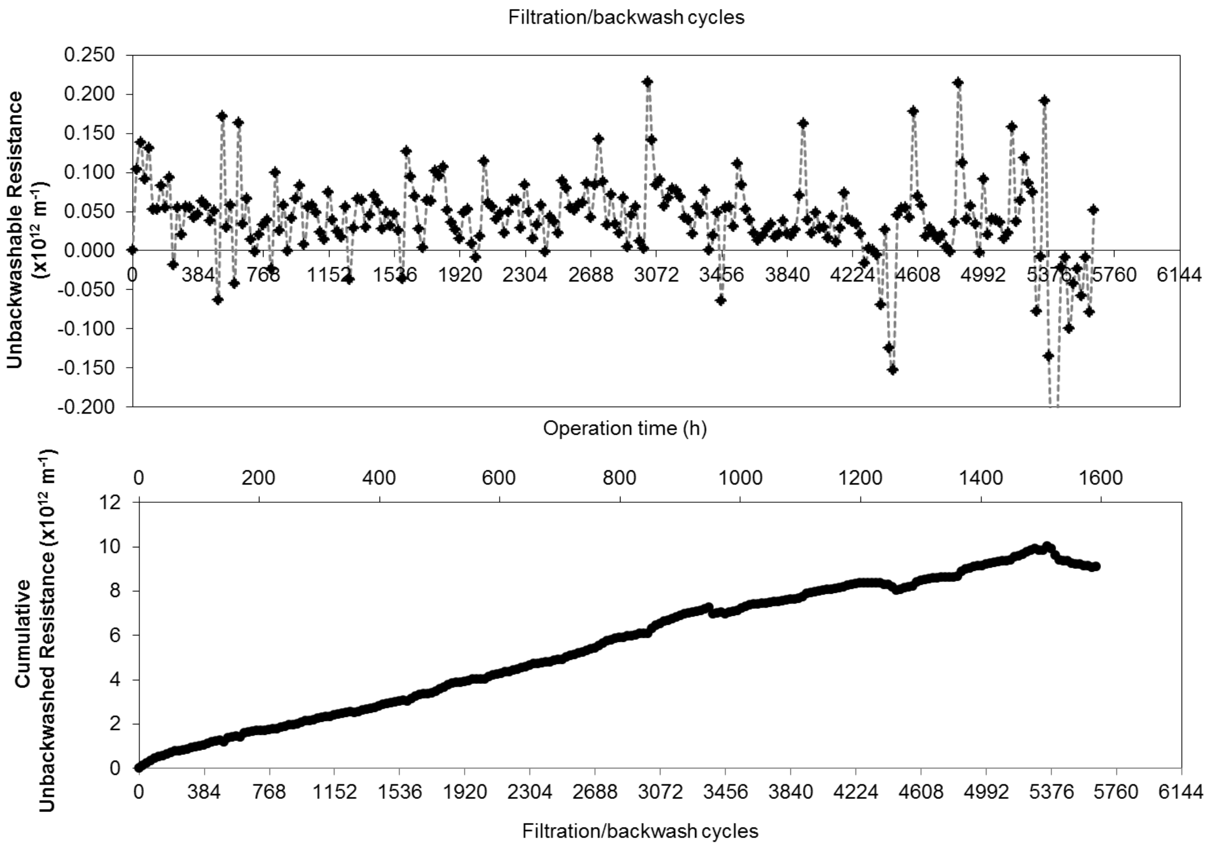

Figure G-1 Long term unbackwashed resistance (ΔR_{UB}) and post backwash resistance (R_{PB}) (i.e., cumulative unbackwashed resistance) tracking.

7 References

[1] S. Vigneswaran, P.J. Smith, N. Huu Hao, R. Ben-Aim, N. Hung, A new approach to backwash initiation in membrane systems, Journal of Membrane Science, 278 (2006) 381-389389.

[2] V. Bonnelye, L. Guey, J. Del Castillo, UF/MF as RO pre-treatment: the real benefit, Desalination, 222 (2008) 59-65.

[3] Y. Yun, S. Lee Nuang, B. Herulah, V. Chen, A.G. Fane, Effects of operating conditions on submerged hollow fibre membrane systems used as pre-treatment for seawater reverse osmosis, Journal of Membrane Science, 365 (2010) 78-8888.

[4] C. Fritzmann, J. Lowenberg, T. Wintgens, T. Melin, State-of-the-art of reverse osmosis desalination, Desalination, 216 (2007) 1-76.

[5] N. Alexandratos, J. Bruinsma, World agriculture towards 2030/2050: the 2012 revision, in, ESA Working paper Rome, FAO, 2012.

[6] S. Gray, R. Semiat, M. Duke, A. Rahardianto, Y. Cohen, 4.04 - Seawater Use and Desalination Technology A2 - Wilderer, Peter, in: Treatise on Water Science, Elsevier, Oxford, 2011, pp. 73-109.

[7] M.M. Mekonnen, A.Y. Hoekstra, Four billion people facing severe water scarcity, Science advances, 2 (2016) e1500323.

[8] Energy Report - Crude Oil - Texas Comptroller of Public Accounts, in, Office of the Texas Comptroller, 2013.

[9] A.H. Zhu, P.D. Christofides, Y. Cohen, On RO membrane and energy costs and associated incentives for future enhancements of membrane permeability, Journal of Membrane Science, 344 (2009) 1-5; ibid, Corrigendum - 346 (2009) 2361.

[10] L. Cheng, M. Hoerling, A. AghaKouchak, B. Livneh, X.-W. Quan, J. Eischeid, How Has Human-Induced Climate Change Affected California Drought Risk?, Journal of Climate, 29 (2016) 111-120.

[11] A. Escriva-Bou, B. Gray, S. Green, T. Harter, R. Howitt, D. MacEwan, J. Medellín-Azuara, P. Moyle, N. Seavy, Water Stress and a Changing San Joaquin Valley, (2017).

[12] J. Mount, E. Hanak, C. Chappelle, B. Colby, R. Frank, G. Gartrell, B. Gray, D. Kenney, J. Lund, P. Moyle, Improving the Federal Response to Western Drought: Five Areas for Reform, California Journal of Politics and Policy, 8 (2016) 0_1.

[13] U.S.D.o.t.I.U.S.G. Survey, Thermoelectric Power Water Use, in: H. Perlman (Ed.), https://water.usgs.gov/edu/wupt.html, 2005, pp. Thermoelectric Power Water Use.

[14] Will Water Constrain Our Energy Future?, in, 2017 The World Bank Group, 2014.

[15] D. Gille, W. Czolkoss, Desalination and the EnvironmentUltrafiltration with multi-bore membranes as seawater pre-treatment, Desalination, 182 (2005) 301-307.

[16] R. Singh, Chapter 1 - Introduction to Membrane Technology, in: Membrane Technology and Engineering for Water Purification (Second Edition), Butterworth-Heinemann, Oxford, 2015, pp. 1-80.

[17] A.G. Fane, C.J.D. Fell, A REVIEW OF FOULING AND FOULING CONTROL IN ULTRAFILTRATION, Desalination, 62 (1987) 117-136.

[18] Filmtec Reverse Osmosis Membranes Technical Manuals - Dow Water & Process Solutions, in, 2011.

[19] K.N. Bourgeous, J.L. Darby, G. Tchobanoglous, Ultrafiltration of wastewater: Effects of particles, mode of operation, and backwash effectiveness, Water Research, 35 (2001) 77-90.

[20] R. Field, Fundamentals of Fouling, in: Membrane Technology, Wiley-VCH Verlag GmbH & Co. KGaA, 2010, pp. 1-23.

[21] S. Madaeni, S. Samieirad, Chemical cleaning of reverse osmosis membrane fouled by wastewater, Desalination, 257 (2010) 80-86.

[22] M. Uchymiak, E. Lyster, J. Glater, Y. Cohen, Kinetics of gypsum crystal growth on a reverse osmosis membrane, Journal of Membrane Science, 314 (2008) 163-172.

[23] D. Hasson, R. Semiat, D. Bramson, M. Busch, B. Limoni-Relis, Suppression of CaCO3 scale deposition by anti-scalants, Desalination, 118 (1998) 285-296.

[24] R. Semiat, I. Sutzkover, D. Hasson, Characterization of the effectiveness of silica anti-scalants, Desalination, 159 (2003) 11-19.

[25] W.-Y. Shih, J. Gao, A. Rahardianto, J. Glater, Y. Cohen, C.J. Gabelich, Ranking of antiscalant performance for gypsum scale suppression in the presence of residual aluminum, Desalination, 196 (2006) 280-292.

[26] M. Uchymiak, A.R. Bartman, N. Daltrophe, M. Weissman, J. Gilron, P.D. Christofides, W.J. Kaiser, Y. Cohen, Brackish water reverse osmosis (BWRO) operation in feed flow reversal mode using an ex situ scale observation detector (EXSOD), Journal of Membrane Science, 341 (2009) 60-66.

[27] N. Pomerantz, Y. Ladizhansky, E. Korin, M. Waisman, N. Daltrophe, J. Gilron, Prevention of scaling of reverse osmosis membranes by "zeroing" the elapsed nucleation time. Part I. Calcium sulfate, Industrial & Engineering Chemistry Research, 45 (2006) 2008-2016.

[28] D.F. Halpern, J. McArdle, B. Antrim, UF pretreatment for SWRO: pilot studies, Desalination, 182 (2005) 323-332.

[29] A. Bennett, 50th Anniversary: Desalination: 50 years of progress, Filtration + Separation, 50 (2013) 32-39.

[30] S. Lattemann, M. Kennedy, J. Schippers, G. Amy, Chapter 2 Global Desalination Situation, 2010.

[31] M. Wilf, EFFECT OF NEW GENERATION OF LOW PRESSURE, HIGH SALT REJECTION
MEMBRANES ON POWER CONSUMPTION OF RO SYSTEMS, in, 2010.

[32] N. Ahmad, R.E. Baddour, A review of sources, effects, disposal methods, and regulations of brine into marine environments, Ocean & coastal management, 87 (2014) 1-7.

[33] J. Morillo, J. Usero, D. Rosado, H. El Bakouri, A. Riaza, F.-J. Bernaola, Comparative study of brine management technologies for desalination plants, Desalination, 336 (2014) 32-49.

[34] X, Reverse Osmosis Membrane Inside a Pressure Vessel, in, Lower Colorado Regional Office, U.S. Bureau of Reclamation, Boulder City NV 2012, pp. Reverse Osmosis Membrane Inside a Pressure Vessel.

[35] I. Sutzkover, D. Hasson, R. Semiat, Simple technique for measuring the concentration polarization level in a reverse osmosis system, Desalination, 131 (2000) 117-127.

[36] G. Belfort, R.H. Davis, A.L. Zydney, THE BEHAVIOR OF SUSPENSIONS AND MACROMOLECULAR SOLUTIONS IN CROSS-FLOW MICROFILTRATION, Journal of Membrane Science, 96 (1994) 1-58.

[37] V. Gekas, B. Hallström, Mass transfer in the membrane concentration polarization layer under turbulent cross flow : I. Critical literature review and adaptation of existing sherwood correlations to membrane operations, Journal of Membrane Science, 30 (1987) 153-170.

[38] B.C. McCool, A. Rahardianto, J. Faria, K. Kovac, D. Lara, Y. Cohen, Feasibility of reverse osmosis desalination of brackish agricultural drainage water in the San Joaquin Valley, Desalination, 261 (2010) 240-250.

[39] A. Rahardianto, W.Y. Shih, R.W. Lee, Y. Cohen, Diagnostic characterization of gypsum scale formation and control in RO membrane desalination of brackish water, Journal of Membrane Science, 279 (2006) 655-668.

[40] M. Elimelech, W.A. Phillip, The Future of Seawater Desalination: Energy, Technology, and the Environment, Science, 333 (2011) 712-717.

[41] P.K. Park, C.H. Lee, S.J. Choi, K.H. Choo, S.H. Kim, C.H. Yoon, Effect of the removal of DOMs on the performance of a coagulation-UF membrane system for drinking water production, Desalination, 145 (2002) 237-245.

[42] M. Wilf, Future of the osmotic processes, Desalination and Water Treatment, 15 292-298.

[43] A.R. Bartman, P.D. Christofides, Y. Cohen, Nonlinear Model-Based Control of an Experimental Reverse-Osmosis Water Desalination System, Industrial & Engineering Chemistry Research, 48 (2009) 6126-6136.

[44] A. Joss, C. Baenninger, P. Foa, S. Koepke, M. Krauss, C.S. McArdell, K. Rottermann, Y.S. Wei, A. Zapata, H. Siegrist, Water reuse: > 90% water yield in MBR/RO through concentrate recycling and CO2 addition as scaling control, Water Research, 45 (2011) 6141-6151.

[45] E. Lyster, M.M. Kim, J. Au, Y. Cohen, A method for evaluating antiscalant retardation of crystal nucleation and growth on RO membranes, Journal of Membrane Science, 364 122-131.

[46] M. Uchymiak, A. Rahardianto, E. Lyster, J. Glater, Y. Cohen, A novel RO ex situ scale observation detector (EXSOD) for mineral scale characterization and early detection, Journal of Membrane Science, 291 (2007) 86-95.

[47] J. Thompson, A. Rahardianto, H. Gu, M. Uchymiak, A. Bartman, M. Hedrick, D. Lara, J. Cooper, J. Faria, P.D. Christofides, Y. Cohen, Rapid field assessment of RO desalination of brackish agricultural drainage water, Water Research, 47 (2013) 2649-2660.

[48] A. Matin, Z. Khan, S.M.J. Zaidi, M.C. Boyce, Biofouling in reverse osmosis membranes for seawater desalination: Phenomena and prevention, Desalination, 281 (2011) 1-16.

[49] J.S. Vrouwenvelder, C. Picioreanu, J.C. Kruithof, M.C.M. van Loosdrecht, Biofouling in spiral wound membrane systems: Three-dimensional CFD model based evaluation of experimental data, Journal of Membrane Science, 346 (2010) 71-85.

[50] A. Brehant, V. Bonnelye, M. Perez, Comparison of MF/UF pretreatment with conventional filtration prior to RO membranes for surface seawater desalination, Desalination, 144 (2002) 353-360.

[51] H. Huang, N. Lee, T. Young, A. Gary, J.C. Lozier, J.G. Jacangelo, Natural organic matter fouling of low-pressure, hollow-fiber membranes: Effects of NOM source and hydrodynamic conditions, Water Research, 41 (2007) 3823-3832.

[52] K.A. Bu-Rashid, W. Czolkoss, Pilot Tests of Multibore UF Membrane at Addur SWRO Desalination Plant, Bahrain, Desalination, 203 (2007) 229-242.

[53] C.P. Huang, J.L. Lin, W.S. Lee, J.R. Pan, B.Q. Zhao, Effect of coagulation mechanism on membrane permeability in coagulation-assisted microfiltration for spent filter backwash water recycling, Colloids and Surfaces a-Physicochemical and Engineering Aspects, 378 (2011) 72-78.

[54] J.D. Lee, S.H. Lee, M.H. Jo, P.K. Park, C.H. Lee, J.W. Kwak, Effect of coagulation conditions on membrane filtration characteristics in coagulation-microfiltration process for water treatment, Environmental Science & Technology, 34 (2000) 3780-3788.

[55] K. Listiarini, D.D. Sun, J.O. Leckie, Organic fouling of nanofiltration membranes: Evaluating the effects of humic acid, calcium, alum coagulant and their combinations on the specific cake resistance, Journal of Membrane Science, 332 (2009) 56-62.

[56] E. Ofir, Y. Oren, A. Adin, Comparing pretreatment by iron of electro-flocculation and chemical flocculation, Desalination, 204 (2007) 87-93.

[57] S.A.A. Tabatabai, M.D. Kennedy, G.L. Amy, J.C. Schippers, Optimizing inline coagulation to reduce chemical consumption in MF/UF systems, Desalination and Water Treatment, 6 (2009) 94-101.

[58] L. Ravina, Moramarco, N. , Everything you want to know about Coagulation & Flocculation.... in, Zeta-Meter, Inc., Staunton, Virginia, April 1993.

[59] S.D. Diaz, L.V. Pena, E.G. Cabrera, M.M. Soto, L.M.V. Cabezas, L.R.B. Sanchez, Effect of previous coagulation in direct ultrafiltration of primary settled municipal wastewater, Desalination, 304 (2012) 41-48.

[60] R. Schurer, A. Janssen, L. Villacorte, M. Kennedy, Performance of ultrafiltration and coagulation in an UF-RO seawater desalination demonstration plant, Desalination and Water Treatment, 42 (2012) 57-64.

[61] Y. Soffer, R. Ben Aim, A. Adin, Membrane fouling and selectivity mechanisms in effluent ultrafiltration coupled with flocculation, Water Science and Technology, 51 (2005) 123-134.

[62] F. Fu, Q. Wang, Removal of heavy metal ions from wastewaters: A review, Journal of Environmental Management, 92 (2011) 407-418.

[63] S. Lopus, P. Bachand, A. Heyvaert, I. Werner, S. Teh, J. Reuter, Potential toxicity concerns from chemical coagulation treatment of stormwater in the Tahoe basin, California, USA, Ecotoxicology and environmental safety, 72 (2009) 1933-1941.

[64] T. Berman, R. Mizrahi, C.G. Dosoretz, Transparent exopolymer particles (TEP): A critical factor in aquatic biofilm initiation and fouling on filtration membranes, Desalination, 276 (2011) 184-190.

[65] V. Discart, M.R. Bilad, S. Van Nevel, N. Boon, J. Cromphout, I.F.J. Vankelecom, Role of transparent exopolymer particles on membrane fouling in a full-scale ultrafiltration plant: Feed parameter analysis and membrane autopsy, Bioresource Technology, 173 (2014) 67-74.

[66] I.M. El-Azizi, A. Schmalenberger, R. Komlenic, R.G.J. Edyvean, Study of a depth filter (Disruptor (TM)) for the novel application of reducing SWRO membrane fouling, Desalination and Water Treatment, 29 (2011) 20-28.

[67] E. Friedler, I. Katz, C.G. Dosoretz, Chlorination and coagulation as pretreatments for greywater desalination, Desalination, 222 (2008) 38-49.

[68] L. Henthome, B. Boysen, State-of-the-art of reverse osmosis desalination pretreatment, Desalination, 356 (2015) 129-139.

[69] S. Van Nevel, T. Hennebel, K. De Beuf, G. Du Laing, W. Verstraete, N. Boon, Transparent exopolymer particle removal in different drinking water production centers, Water Research, 46 (2012) 3603-3611.

[70] L.O. Villacorte, M.D. Kennedy, G.L. Amy, J.C. Schippers, The fate of Transparent Exopolymer Particles (TEP) in integrated membrane systems: Removal through pre-treatment processes and deposition on reverse osmosis membranes, Water Research, 43 (2009) 5039-5052.

[71] E. Heiderscheidt, T. Leiviskä, B. Kløve, Coagulation of humic waters for diffused pollution control and the influence of coagulant type on DOC fractions removed, Journal of environmental management, 181 (2016) 883-893.

[72] A. Matilainen, M. Vepsäläinen, M. Sillanpää, Natural organic matter removal by coagulation during drinking water treatment: a review, Advances in colloid and interface science, 159 (2010) 189-197.

[73] P. Harmant, P. Aimar, Coagulation of colloids retained by porous wall, Aiche Journal, 42 (1996) 3523-3532.

[74] S. Delgado Diaz, L. Vera Peña, E. González Cabrera, M. Martínez Soto, L.M. Vera Cabezas, L.R. Bravo Sánchez, Effect of previous coagulation in direct ultrafiltration of primary settled municipal wastewater, Desalination, 304 (2012) 41-48.

[75] S. Delgado, F. Diaz, L. Vera, R. Diaz, S. Elmaleh, Modelling hollow-fibre ultrafiltration of biologically treated wastewater with and without gas sparging, Journal of Membrane Science, 228 (2004) 55-63.

[76] A. Alhadidi, A.J.B. Kemperman, B. Blankert, J.C. Schippers, M. Wessling, W.G.J. van der Meer, Silt Density Index and Modified Fouling Index relation, and effect of pressure, temperature and membrane resistance, Desalination, 273 (2011) 48-56.

[77] A. Alhadidi, A.J.B. Kemperman, R. Schurer, J.C. Schippers, M. Wessling, W.G.J. van der Meer, Using SDI, SDI+ and MFI to evaluate fouling in a UF/RO desalination pilot plant, Desalination, 285 (2012) 153-162.

[78] S.F.E. Boerlage, M. Kennedy, Z. Tarawneh, R. De Faber, J.C. Schippers, Development of the MFI-UF in constant flux filtration, Desalination, 161 (2004) 103-113.

[79] S.F.E. Boerlage, M.D. Kennedy, M.R. Dickson, D.E.Y. El-Hodali, J.C. Schippers, The modified fouling index using ultrafiltration membranes (MFI-UF): characterisation, filtration mechanisms and proposed reference membrane, Journal of Membrane Science, 197 (2002) 1-21.

[80] K. Hong, S. Lee, S. Choi, Y. Yu, S. Hong, H. Moon, J. Sohn, J. Yang, Assessment of various membrane fouling indexes under seawater conditions, Desalination, 247 (2009) 247-259.

[81] H. Huang, T.A. Young, J.G. Jacangelo, Unified membrane fouling index for low pressure membrane filtration of natural waters: Principles and methodology, Environmental Science & Technology, 42 (2008) 714-720.

[82] R.M. Rachman, N. Ghaffour, F. Wali, G.L. Amy, Assessment of silt density index (SDI) as fouling propensity parameter in reverse osmosis (RO) desalination systems, Desalination and Water Treatment, 51 (2013) 1091-1103.

[83] S.G. Salinas-Rodriguez, G.L. Amy, J.C. Schippers, M.D. Kennedy, The Modified Fouling Index Ultrafiltration constant flux for assessing particulate/colloidal fouling of RO systems, Desalination, 365 (2015) 79-91.

[84] M. Zupancic, D. Novak, J. Diaci, I. Golobic, An evaluation of industrial ultrafiltration systems for surface water using fouling indices as a performance indicator, Desalination, 344 (2014) 321-328.

[85] A. Massé, O. Arab, V. Séchet, P. Jaouen, M. Pontié, N.-E. Sabiri, S. Plantier, Performances of dead-end ultrafiltration of seawater: From the filtration and backwash efficiencies to the membrane fouling mechanisms, Separation and Purification Technology, 156, Part 2 (2015) 512-521.

[86] S. Jeong, S. Vigneswaran, Practical use of standard pore blocking index as an indicator of biofouling potential in seawater desalination, Desalination, 365 (2015) 8-14.

[87] K. Chinu, S. Vigneswaran, L. Erdei, H.K. Shon, J. Kandasamy, H.H. Ngo, Comparison of fouling indices in assessing pre-treatment for seawater reverse osmosis, Desalination and Water Treatment, 18 (2010) 187-191.

[88] Y.C. Woo, J.J. Lee, L.D. Tijing, H.K. Shon, M. Yao, H.-S. Kim, Characteristics of membrane fouling by consecutive chemical cleaning in pressurized ultrafiltration as pre-treatment of seawater desalination, Desalination, 369 (2015) 51-61.

[89] S.A. Alizadeh Tabatabai, J.C. Schippers, M.D. Kennedy, Effect of coagulation on fouling potential and removal of algal organic matter in ultrafiltration pretreatment to seawater reverse osmosis, Water Research, 59 (2014) 283-294.

[90] C.-H. Wei, S. Laborie, R. Ben Aim, G. Amy, Full utilization of silt density index (SDI) measurements for seawater pre-treatment, Journal of Membrane Science, 405 (2012) 212-218.

[91] H.K. Shon, S.H. Kim, S. Vigneswaran, R. Ben Aim, S. Lee, J. Cho, Physicochemical pretreatment of seawater: fouling reduction and membrane characterization, Desalination, 238 (2009) 10-21.

[92] A. Resosudarmo, Y. Ye, P. Le-Clech, V. Chen, Analysis of UF membrane fouling mechanisms caused by organic interactions in seawater, Water Research, 47 (2013) 911-921.

[93] S.Q. Huang, N. Voutchkov, S.C. Jiang, Investigation of environmental influences on membrane biofouling in a Southern California desalination pilot plant, Desalination, 319 (2013) 1-9.

[94] Y. Liu, X. Li, Y. Yang, S. Liang, Fouling control of PAC/UF process for treating algal-rich water, Desalination, 355 (2015) 75-82.

[95] Y. Zhang, J. Tian, J. Nan, S. Gao, H. Liang, M. Wang, G. Li, Effect of PAC addition on immersed ultrafiltration for the treatment of algal-rich water, Journal of Hazardous Materials, 186 (2011) 1415-1424.

[96] A. Jezowska, A. Bottino, G. Capannelli, C. Fabbri, G. Migliorini, Ultrafiltration as direct pre-treatment of seawater - a case study, Desalination, 245 (2009) 723-729.

[97] R. Schurer, A. Tabatabai, L. Villacorte, J.C. Schippers, M.D. Kennedy, Three years operational experience with ultrafiltration as SWRO pre-treatment during algal bloom, Desalination and Water Treatment, 51 (2013) 1034-1042.

[98] K. Glucina, A. Alvarez, J.M. Laîné, Membranes in Drinking and Industrial Water ProductionAssessment of an integrated membrane system for surface water treatment, Desalination, 132 (2000) 73-82.

[99] S. Jeong, F. Nateghi, T.V. Nguyen, S. Vigneswaran, T.A. Tu, Pretreatment for seawater desalination by flocculation: Performance of modified poly ferric silicate (PFSi-delta) and ferric chloride as flocculants, Desalination, 283 (2011) 106-110.

[100] K. Kimura, K. Tanaka, Y. Watanabe, Microfiltration of different surface waters with/without coagulation: Clear correlations between membrane fouling and hydrophilic biopolymers, Water Research, 49 (2014) 434-443.

[101] P. Lipp, M. Witte, G. Baldauf, A.A. Povorov, Membranes in Drinking and Industrial Water ProductionTreatment of reservoir water with a backwashable MF/UF spiral wound membrane, Desalination, 179 (2005) 83-94.

[102] A.H. Nguyen, J.E. Tobiason, K.J. Howe, Fouling indices for low pressure hollow fiber membrane performance assessment, Water Research, 45 (2011) 2627-2637.

[103] W.-Y. Shih, A. Rahardianto, R.-W. Lee, Y. Cohen, Morphometric characterization of calcium sulfate dihydrate (gypsum) scale on reverse osmosis membranes, Journal of Membrane Science, 252 (2005) 253-263.

[104] A. Rahardianto, B.C. McCool, Y. Cohen, Reverse osmosis desalting of inland brackish water of high gypsum scaling propensity: kinetics and mitigation of membrane mineral scaling, Environmental science & technology, 42 (2008) 4292-4297.

[105] A.R. Bartman, E. Lyster, R. Rallo, P.D. Christofides, Y. Cohen, Mineral scale monitoring for reverse osmosis desalination via real-time membrane surface image analysis, Desalination, 273 (2011) 64-71.

[106] N. Avraham, C. Dosoretz, R. Semiat, Osmotic backwash process in RO membranes, Desalination, 199 (2006) 387-389.

[107] G.Z. Ramon, T.-V. Nguyen, E.M.V. Hoek, Osmosis-assisted cleaning of organic-fouled seawater RO membranes, Chemical Engineering Journal, 218 (2013) 173-182.

[108] J. Gilron, M. Waisman, N. Daltrophe, N. Pomerantz, M. Milman, I. Ladizhansky, E. Korin, Prevention of precipitation fouling in NF/RO by reverse flow operation, Desalination, 199 (2006) 29-30.

[109] E. Lyster, J. Au, R. Rallo, F. Giralt, Y. Cohen, Coupled 3-D hydrodynamics and mass transfer analysis of mineral scaling-induced flux decline in a laboratory plate-and-frame reverse osmosis membrane module, Journal of Membrane Science, 339 (2009) 39-48.

[110] J.-J. Qin, M.H. Oo, K.A. Kekre, B. Liberman, Development of novel backwash cleaning technique for reverse osmosis in reclamation of secondary effluent, Journal of Membrane Science, 346 (2009) 8-14.

[111] W.J.C. van de Ven, I.G.M. Pünt, A. Zwijnenburg, A.J.B. Kemperman, W.G.J. van der Meer, M. Wessling, Hollow fiber ultrafiltration: The concept of partial backwashing, Journal of Membrane Science, 320 (2008) 319-324.

[112] E.P. Jacobs, S.M. Bradshaw, J.P. Botes, V.L. Pillay, Reverse-pressure back-flush in pilot scale, dead-end ultrafiltration of surface water, Journal of Membrane Science, 252 (2005) 51-63.

[113] M. Kennedy, S.-M. Kim, I. Mutenyo, L. Broens, J. Schippers, Intermittent crossflushing of hollow fiber ultrafiltration systems, Desalination, 118 (1998) 175-187.

[114] J.P. Chen, S.L. Kim, Y. Ting, Optimization of membrane physical and chemical cleaning by a statistically designed approach, Journal of Membrane Science, 219 (2003) 27-45.

[115] B.-z. Dong, Y. Chen, N.-y. Gao, J.-c. Fan, Effect of coagulation pretreatment on the fouling of ultrafiltration membrane, Journal of Environmental Sciences, 19 (2007) 278-283.

[116] P. Glueckstern, M. Priel, M. Wilf, Field evaluation of capillary UF technology as a pretreatment for large seawater RO systems, Desalination, 147 (2002) 55-62.

[117] J.D. Zhang, S.M. Gao, H.M. Zeng, F. Zhang, C.Z. Li, Y.W. Liu, D.K. Fu, C.S. Ye, Pilot testing of two inside-out UF modules prior to RO for high-turbidity seawater desalination, Desalination, 196 (2006) 66-75.

[118] X. Zheng, S. Plume, M. Ernst, J.P. Croue, M. Jekel, In-line coagulation prior to UF of treated domestic wastewater - foulants removal, fouling control and phosphorus removal, Journal of Membrane Science, 403 (2012) 129-139.

[119] E. Zondervan, B. Blankert, B.H.L. Betlem, B. Roffel, Development of a multi-objective coagulation system for long-term fouling control in dead-end ultrafiltration, Journal of Membrane Science, 325 (2008) 823-830.

[120] P.S. Goh, T. Matsuura, A.F. Ismail, N. Hilal, Recent trends in membranes and membrane processes for desalination, Desalination, 391 (2016) 43-60.

[121] K. Katsoufidou, S.G. Yiantsios, A.J. Karabelas, Experimental study of ultrafiltration membrane fouling by sodium alginate and flux recovery by backwashing, Journal of Membrane Science, 300 (2007) 137-146.

[122] J. Kim, F.A. DiGiano, Fouling models for low-pressure membrane systems, Separation and Purification Technology, 68 (2009) 293-304.

[123] P.J. Remize, C. Guigui, C. Cabassud, Evaluation of backwash efficiency, definition of remaining fouling and characterisation of its contribution in irreversible fouling: Case of drinking water production by air-assisted ultra-filtration, Journal of Membrane Science, 355 (2010) 104-111.

[124] S. Li, S.G.J. Heijman, J.C. van Dijk, A pilot-scale study of backwashing ultrafiltration membrane with demineralized water, Journal of Water Supply Research and Technology-Aqua, 59 (2010) 128-133.

[125] S. Li, S.G.J. Heijman, J. Verberk, J.C. van Dijk, Influence of Ca and Na ions in backwash water on ultrafiltration fouling control, Desalination, 250 (2010) 861-864.

[126] A.E. Pagana, S.D. Sklari, E.S. Kikkinides, V.T. Zaspalis, Microporous ceramic membrane technology for the removal of arsenic and chromium ions from contaminated water, Microporous and Mesoporous Materials, 110 (2008) 150-156.

[127] C.S. Parnham, R.H. Davis, Protein recovery from bacterial cell debris using crossflow microfiltration with backpulsing, Journal of Membrane Science, 118 (1996) 259-268.

[128] V.G.J. Rodgers, R.E. Sparks, Effects of solution properties on polarization redevelopment and flux in pressure pulsed ultrafiltration, Journal of Membrane Science, 78 (1993) 163-180.

[129] X. Shi, G. Tal, N.P. Hankins, V. Gitis, Fouling and cleaning of ultrafiltration membranes: A review, Journal of Water Process Engineering, 1 (2014) 121-138.

[130] R.K. Lalrinsanga, N.B. Bejgam, S. Ganguly, Effect of pressure pulsing on concentration boundary layer over membrane-a numerical investigation, Asia-Pacific Journal of Chemical Engineering, 8 (2013) 519-526.

[131] S. Redkar, V. Kuberkar, R.H. Davis, Modeling of concentration polarization and depolarization with high-frequency backpulsing, Journal of Membrane Science, 121 (1996) 229-242.

[132] E. Drioli, A. Criscuoli, F. Macedonio, Membrane-based Desalination: An Integrated Approach (MEDINA), Iwa Publishing, 2011.

[133] N. Hilal, O.O. Ogunbiyi, N.J. Miles, R. Nigmatullin, Methods Employed for Control of Fouling in MF and UF Membranes: A Comprehensive Review, Separation Science and Technology, 40 (2005) 1957-2005.

[134] H. Ma, C.N. Bowman, R.H. Davis, Membrane fouling reduction by backpulsing and surface modification, Journal of Membrane Science, 173 (2000) 191-200.

[135] S.G. Redkar, R.H. Davis, Cross-flow microfiltration with high-frequency reverse filtration, AIChE Journal, 41 (1995) 501-508.

[136] I. Wenten, D. Koenhen, H. Roesink, A. Rasmussen, G. Jonsson, The Backshock Process: A novel backflush technique in microfiltration, Proceedings of Engineering of Membrane Processes, II Environmental Applications, Ciocco, Italy, (1994).

[137] I.G. Wenten, Mechanisms and control of fouling in crossflow microfiltration, Filtration & Separation, 32 (1995) 252-253.

[138] M. Lee, Z. Wu, K. Li, 2 - Advances in ceramic membranes for water treatment, in: A. Basile, A.C.K. Rastogi (Eds.) Advances in Membrane Technologies for Water Treatment, Woodhead Publishing, Oxford, 2015, pp. 43-82.

[139] U. Rhyner, R. Mai, H. Leibold, S.M.A. Biollaz, Model of back pressure pulses generated by coupled pressure pulse (CPP) technology, Biomass and Bioenergy, 68 (2014) 175-184.

[140] R. Sondhi, R. Bhave, Role of backpulsing in fouling minimization in crossflow filtration with ceramic membranes, Journal of Membrane Science, 186 (2001) 41-52.

[141] W.D. Mores, C.N. Bowman, R.H. Davis, Theoretical and experimental flux maximization by optimization of backpulsing, Journal of Membrane Science, 165 (2000) 225-236.

[142] V.G.J. Rodgers, R.E. Sparks, Effect of transmembrane pressure pulsing on concentration polarization, Journal of Membrane Science, 68 (1992) 149-168.

[143] C.R. Gillham, P.J. Fryer, A.P.M. Hasting, D.I. Wilson, Enhanced cleaning of whey protein soils using pulsed flows, Journal of Food Engineering, 46 (2000) 199-209.

[144] P. Mikulasek, J. Cakl, P. Pospisil, P. Dolecek, The use of flux enhancement methods for high flux cross-flow membrane microfiltration systems, Chemical and biochemical engineering quarterly, 14 (2000) 117-123.

[145] Microfiltration and Ultrafiltration: Principles and Applications, Taylor & Francis, 1996.

[146] I. Koyuncu, R. Sengur, T. Turken, S. Guclu, M.E. Pasaoglu, 3 - Advances in water treatment by microfiltration, ultrafiltration, and nanofiltration, in: A. Basile, A.C.K. Rastogi (Eds.) Advances in Membrane Technologies for Water Treatment, Woodhead Publishing, Oxford, 2015, pp. 83-128.

[147] L.X. Gao, A. Rahardianto, H. Gu, P.D. Christofides, Y. Cohen, Novel design and operational control of integrated ultrafiltration - Reverse osmosis system with RO concentrate backwash, Desalination, 382 (2016) 43-52.

[148] D.R. McGowan, Pressurized backflush system US 6562246 B2, 13 May, 2003 in: U.S.P. Office (Ed.), , US, 2003.

[149] T.M. Schneidewend, Point of Use Filtration System with Backwash, Pub. No.: US 2014/0251905 A1, 11 September 2014 in: U.S.P. Office (Ed.), US, 2014.

[150] Z. Shaowu, Z. Jun, H. Jiang, H. Zhijun, Research on the pressure fluctuation of ceramic filter backwash, in: System Science, Engineering Design and Manufacturing Informatization (ICSEM), 2011 International Conference on, 2011, pp. 47-50.

[151] M. Xu, G. Chen, J. Ni, Y. Liu, Modeling and Analysis of a Semiactive Power-Assisted Unit Based on Hydraulic Accumulator, Advances in Mechanical Engineering, 5 (2013) 894576.

[152] A. Pourmovahed, S. Baum, F. Fronczak, N. Beachley, Experimental evaluation of hydraulic accumulator efficiency with andwithout elastomeric foam, Journal of Propulsion and Power, 4 (1988) 185-192.

[153] D. McGowan, Size Press & White Water Filtration Using the Pulse Purge™ Backwash System, in: ANNUAL MEETING-PULP AND PAPER TECHNICAL ASSOCIATION OF CANADA, Pulp and Paper Technical Association of Canada; 1999, 2001, pp. A19-A22.

[154] S. Mamèic, M. Bogdevièius, Simulation of dynamic processes in hydraulic accumulators, Transport, 25 (2010) 215-221.

[155] C. Regula, E. Carretier, Y. Wyart, G. Gésan-Guiziou, A. Vincent, D. Boudot, P. Moulin, Chemical cleaning/disinfection and ageing of organic UF membranes: A review, Water Research, 56 (2014) 325-365.

[156] A. Jezowska, A. Bottino, G. Capannelli, C. Fabbri, G. Migliorini, Ultrafiltration as direct pre-treatment of seawater – a case study, Desalination, 245 (2009) 723-729.

[157] J.B.a.W. Marquardt, Model-based control of MF/UF filtration processes: pilot plant implementation and results, Water Science & Technology, 59 (2009) 1713–1720

[158] P.J. Smith, S. Vigneswaran, H.H. Ngo, R. Ben-Aim, H. Nguyen, A new approach to backwash initiation in membrane systems, Journal of Membrane Science, 278 (2006) 381-389.

[159] P.J. Smith, S. Vigneswaran, H.H. Ngo, R. Ben-Aim, H. Nguyen, Design of a generic control system for optimising back flush durations in a submerged membrane hybrid reactor, Journal of Membrane Science, 255 (2005) 99-106.

[160] B. Blankert, B.H.L. Betlem, B. Roffel, Development of a control system for in-line coagulation in an ultrafiltration process, Journal of Membrane Science, 301 (2007) 39-45.

[161] L.X. Gao, H. Gu, A. Rahardianto, P.D. Christofides, Y. Cohen, Self-adaptive cycle-to-cycle control of in-line coagulant dosing in ultrafiltration for pre-treatment of reverse osmosis feed water, Desalination, 401 (2017) 22-31.

[162] Practical Guidelines for the analysis of Seawater CRC press Institute of Ocean Sciences, Sidney, British Columbia, Canada 2009.

[163] L.O. Villacorte, M.D. Kennedy, G.L. Amy, J.C. Schippers, Measuring transparent exopolymer particles (TEP) as indicator of the (bio) fouling potential of RO feed water, Desalination and Water Treatment, 5 (2009) 207-212.

[164] S.K. Hong, P. Krishna, C. Hobbs, D.H. Kim, J.W. Cho, Variations in backwash efficiency during colloidal filtration of hollow-fiber microfiltration membranes, Desalination, 173 (2005) 257-268.

[165] A.R. Bartman, A.H. Zhu, P.D. Christofides, Y. Cohen, Minimizing energy consumption in reverse osmosis membrane desalination using optimization-based control, Journal of Process Control, 20 1261-1269.

[166] ROSA (Reverse Osmosis System Analysis) design software in, Dow Water Solutions, 2010.

[167] Filmtec Reverse Osmosis Membranes Technical Manuals in, Dow Water Solutions, 2009.

[168] Technical Manual Ultrafiltration, in, inge GmbH 2010.

[169] A.R. Bartman, C.W. McFall, P.D. Christofides, Y. Cohen, Model-predictive control of feed flow reversal in a reverse osmosis desalination process, Journal of Process Control, 19 (2009) 433-442.

[170] L. Gao, A. Rahardianto, H. Gu, P.D. Christofides, Y. Cohen, Energy-Optimal Control of RO Desalination, Industrial & Engineering Chemistry Research, 53 (2014) 7409-7420.

[171] Y. Cohen, P.D. Christofides, A. Rahardianto, A.R. Bartman, A. Zhu, H. Gu, L.X. Gao, Apparatus, system and method for integrated filtration and reverse osmosis desalination, in, Google Patents, 2014.

[172] M. Rabie, Fluid power engineering, McGraw Hill Professional, 2009.

[173] D.A. Pease, J.J. Pippenger, Basic fluid power, Pearson College Division, 1987.

[174] H. Gu, A. Rahardianto, L.X. Gao, P.D. Christofides, Y. Cohen, Ultrafiltration with self-generated RO concentrate pulse backwash in a novel integrated seawater desalination UF-RO system, Journal of Membrane Science, 520 (2016) 111-119.

[175] D.M. Anderson, J.M. Burkholder, W.P. Cochlan, P.M. Glibert, C.J. Gobler, C.A. Heil, R.M. Kudela, M.L. Parsons, J.J. Rensel, D.W. Townsend, Harmful algal blooms and

eutrophication: examining linkages from selected coastal regions of the United States, Harmful Algae, 8 (2008) 39-53.

[176] R.A. Horner, D.L. Garrison, F.G. Plumley, Harmful algal blooms and red tide problems on the US west coast, Limnology and Oceanography, 42 (1997) 1076-1088.

[177] G. Belfort, R.H. Davis, A.L. Zydney, The behavior of suspensions and macromolecular solutions in crossflow microfiltration, Journal of Membrane Science, 96 (1994) 1-58.

[178] S.A.A. Tabatabai, J.C. Schippers, M.D. Kennedy, Effect of coagulation on fouling potential and removal of algal organic matter in ultrafiltration pretreatment to seawater reverse osmosis, Water Research, 59 (2014) 283-294.

[179] M. Yao, J. Nan, T. Chen, D. Zhan, Q. Li, Z. Wang, H. Li, Influence of flocs breakage process on membrane fouling in coagulation/ultrafiltration process—Effect of additional coagulant of poly-aluminum chloride and polyacrylamide, Journal of Membrane Science, 491 (2015) 63-72.

[180] S.A. Lee, A.G. Fane, R. Amal, T.D. Waite, The Effect of Floc Size and Structure on Specific Cake Resistance and Compressibility in Dead-End Microfiltration, Separation Science and Technology, 38 (2003) 869-887.

[181] A. Bagga, S. Chellam, D.A. Clifford, Evaluation of iron chemical coagulation and electrocoagulation pretreatment for surface water microfiltration, Journal of Membrane Science, 309 (2008) 82-93.

[182] M. Li, J. Lu, B. Heijman, L. Rietveld, Effect of cake layer characteristics on fouling control in long time filtration without backwash for submerged ceramic MF membrane in surface water treatment, Delft University of Technology, Delft, The Netherlands, (2012).

[183] W.Z. Yu, N. Graham, H.J. Liu, J.H. Qu, Comparison of FeCl3 and alum pre-treatment on UF membrane fouling, Chemical Engineering Journal, 234 (2013) 158-165.

[184] P. Gebbie, Using polyaluminium coagulants in water treatment, in: Proc. 64th AWIEO Conference, 2001.

[185] P. Gebbie, A dummy's guide to coagulants, in: Proc. of the 68th Annual Water Industry Engineers and Operators' Conference, 7th and 8th September, Bendigo, Australia, 2005.

[186] X. Pascual, H. Gu, A.R. Bartman, A. Zhu, A. Rahardianto, J. Giralt, R. Rallo, P.D. Christofides, Y. Cohen, Data-driven models of steady state and transient operations of spiral-wound RO plant, Desalination, 316 (2013) 154-161.

[187] X. Pascual, H. Gu, A. Bartman, A. Zhu, A. Rahardianto, J. Giralt, R. Rallo, P.D. Christofides, Y. Cohen, Fault Detection and Isolation in a Spiral-Wound Reverse Osmosis (RO) Desalination Plant, Industrial & Engineering Chemistry Research, 53 (2014) 3257-3271.

[188] Y. Cohen, et al., Integrated Ultrafiltration and Reverse Osmosis Process and System, in: Patent USSN 61/382 (Ed.), 2011.